



THE HONG KONG
POLYTECHNIC UNIVERSITY

香港理工大學

Pao Yue-kong Library

包玉剛圖書館

Copyright Undertaking

This thesis is protected by copyright, with all rights reserved.

By reading and using the thesis, the reader understands and agrees to the following terms:

1. The reader will abide by the rules and legal ordinances governing copyright regarding the use of the thesis.
2. The reader will use the thesis for the purpose of research or private study only and not for distribution or further reproduction or any other purpose.
3. The reader agrees to indemnify and hold the University harmless from and against any loss, damage, cost, liability or expenses arising from copyright infringement or unauthorized usage.

IMPORTANT

If you have reasons to believe that any materials in this thesis are deemed not suitable to be distributed in this form, or a copyright owner having difficulty with the material being included in our database, please contact lbsys@polyu.edu.hk providing details. The Library will look into your claim and consider taking remedial action upon receipt of the written requests.

Pao Yue-kong Library, The Hong Kong Polytechnic University, Hung Hom, Kowloon, Hong Kong

<http://www.lib.polyu.edu.hk>

**A CHICK VITREOUS PROTEOME DATABASE
AND DIFFERENTIAL VITREOUS PROTEIN
EXPRESSIONS DURING MYOPIA
DEVELOPMENT**

CHEUNG KA WAI

PhD

The Hong Kong Polytechnic University

2023

The Hong Kong Polytechnic University
School of Optometry

**A Chick Vitreous Proteome Database and
Differential Vitreous Protein Expressions during
Myopia Development**

CHEUNG KA WAI

**A thesis submitted in partial fulfilment of the
requirements for the degree of Doctor of
Philosophy**

SEPT 2020

CERTIFICATE OF ORIGINALITY

I hereby declare that this thesis is my own work and that, to the best of my knowledge and belief, it reproduces no material previously published or written, nor material that has been accepted for the award of any other degree or diploma, except where due acknowledgment has been made in the text.

_____ (Signed)

CHEUNG KA WAI (Name of student)

15TH March 2022 (Date)

Abstract

Myopia is the most common refractive error, estimated to affect half the world's population by 2050. High myopia increases the risk of more complicated ocular diseases, which could eventually lead to total blindness. Although multiple factors have been associated with myopia, the exact mechanism of myopia onset or progression is still yet to be identified. Vitreous humor (VH) is a transparent gelatin-like substance that takes up two-thirds of the eyeball and alters the most during eye elongation, covering normal growth and abnormal growth periods such as myopia. As myopia can be seen as an excess growth of the eyeball, quantitative proteomics on the normal ocular growth period and the myopia progression period in the VH could provide new insights into understanding its progression mechanism in the early stages of myopia.

Specific characteristics of the VH, such as being highly hydrated (making the sample more diluted in terms of protein content), and the gel-like elasticity properties, hampered the advancement in ocular proteomics studies with the use of VH. Therefore, a series of optimization studies aiming at the tissue extraction process and mass spectrometry acquisition, data analysis, and processing were conducted in earlier chapters of this thesis. Vitreous homogenized in a 1:1 ratio [v/v, tissue protein extraction reagent (T-PER), lysis buffer: vol] homogenization method was found to yield the optimal protein concentration (0.2 $\mu\text{g}/\mu\text{l}$) while maintaining a reasonable sample volume for downstream analysis. Acetone precipitation (100%) was found to be the best precipitation for the in-solution protocol, with digested peptides cleaned up using the solid phase extraction (SPE) column. With the use of high-pH fractionation, a loading quantity of 1 μg VH peptides with a 90 mins liquid chromatography (LC) gradient was injected into the mass spectrometer for data analysis for optimal results.

Using a next-generation mass spectrometry label-free data-independent acquisition (DIA) method or termed Sequential Window Acquisition of all Theoretical Mass Spectra (SWATH-MS), relative protein changes in vitreous during the normal growth period (7, 14, 21, and 28 days old) in the chick model were identified and

quantified. This was followed by protein confirmation using a novel high-resolution multiple reaction monitoring (MRM^{HR}) mass spectrometry using separate batches of animals. The average changes in the refraction showed a reduction in diopter (D), from a hyperopic state on Day 7 to a nearly emmetropic state on Day 28, where both eyes at each time point remained the same (≥ 0.05 , paired T-test, $n=6$ at each time point) and the vitreous chamber depth (VCD) were found to be significantly elongated ($P < 0.05$, paired T-test, $n=6$ at each time point) during the growth period. Using a highly sensitive nanoLC-ESI-MS/MS system, this study was able to identify a total of 1576 non-redundant proteins (22987 distinct peptides) at 1% FDR without the need for fractionation or protein depletion, making it the most comprehensive chick vitreous protein library covering the emmetropization period (from day 7 across today 28), while 159 proteins were found as “core vitreous proteins”. The top abundance proteins identified were Serum albumin (ALB), reelin (RELN), fibronectin, tenascin, and Ovotransferrin. With stringent filtering criteria set as fold change (FC) cut off threshold at ≥ 1.5 or ≤ 0.7 folds, differential expression in the same direction from both eyes and each identified protein must have at least 2 quantifiable peptides, 27 proteins were found up-regulated, and 37 proteins were found down-regulated across all time points compared to the baseline at day 7. Targeted MRM^{HR} MS further confirmed proteins such as cadherins (CDH), neurocan (NCAM), and reelin (RELN), which are known to be related to structural and growth-related pathways for the first time, providing novel evidence on which might be key molecules involved in the overall ocular elongation mechanism in the chicks.

Next, myopia progression was studied using the monocular Lens-Induced Myopia (LIM) chick model. -10D lens was attached to a random eye of each chick for 3 days (LIM3) and 7 days (LIM7) to induce myopia progression., Significant LIM was successfully introduced for short-term (LIM3) and long-term (LIM7) old chicks ($n=7$ for each time point). The refraction of LIM3 treated eye indicated that the eyes were not fully compensated to the -10D lens, but significant differences were found in Rx compared to the controlled eyes. The eyes further compensated and had an average change in refraction up to -11.61 ± 0.90 D in LIM7 eyes while the change in refraction in controlled eyes remained at -0.46 ± 0.96 D. Furthermore,

the VCD changed significantly during this phase (for both LIIM3 and LIM7 with biometric parameters from A-Scan showing that the eyes were able to respond to hyperopic defocus and compensated to the lens introduced successfully. Using the high-pH fractionation technique for constructing a specific ion library for SWATH-MS acquisition data extraction, a total of 1242 proteins (15181 distinct peptides) were identified using the shorter 90 mins MS running gradient as the protein library. With an FC cut off at ≥ 1.5 or ≤ 0.7 and $p \leq 0.05$, unpaired T-test, >1 peptide per protein: For myopia LIM3 study using SWATH-MS analysis, a total of 8 down-regulated proteins were found differentially expressed. The extracellular matrix (ECM) proteins such as Inter-alpha-Trypsin inhibitor heavy chain 3 (ITIH3) indicated a possible breakdown in the VH structural integrity. Also, neuropeptides such as Vasoactive intestinal polypeptide (VIP) and Corticotropin-releasing factor-binding protein (CRHBP) suggested a transfer of molecules from the neurons for multiple functions including oxidative stress which might take part in myopia. For the LIM7 experimental group, a total of 23 proteins were found differentially expressed (10 up and 13 down-regulated), with several upregulated proteins found to be related to $\alpha 2$ -macroglobulin (A2M) and were responsible for inflammation/immune responses. These differential expressed proteins (DEPs) were again mostly neuroproteins that could be leaked from the neighboring tissues, indicating chances of biofluids exchange between the vitreous and its neighboring tissues.

VIP was found to be significantly down-regulated in both LIM groups (LIM3 FC: -0.67, $P= 0.004$ and LIM7 FC: -0.70, $P= 0.0012$, $n= 7$ at each time point). Its expression was previously found reduced in FDM animal myopia studies and its suggested to be involved in circadian rhythm. The down-regulation of VIP was further validated with the targeted multiple reaction monitoring (MRM^{HR}) approach in LIM3 ($n= 5$) and LIM7 ($n= 6$) using another batch of animals. However, VIP was not detected in the VH in qPCR studies of LIM3 and LIM7, where else a down-regulation of VIP gene expression was found in both time points in the retina (LIM3 FC: 0.665 ± 0.267 , $P= 0.046$, and LIM7 FC: 0.696 ± 0.117 , $P= 0.02$, $n= 4$ at both time points). This further suggested that VIP could be transferred from neighboring tissues close to the VH during axial elongation in LIM and FDM.

Along with the other novel candidate proteins obtained using SWATH-MS from this study, a list of potential candidates from the VH under normal growth and myopia progression may serve as potential therapeutic targets to be tested in animal trials to further solidify the understanding of the mechanical of myopia.

List of presentations and publications

Posters and presentations

1. **Cheung, K. W.** (2022) A chick vitreous proteome database and differential vitreous protein expressions during myopia development using SWATH-based quantitative proteomics. Oral presentation at the 3rd ABCT Research Postgraduate Symposium in the Biology Discipline, August 2022, Hong Kong
2. **Cheung, K. W.,** Sze, Y. H., Li, K. K., & Lam, C. (2019). Efficient sample preparation of human tears proteomic workflow using S-TrapTM. Poster session presented at 18th Human Proteome Organization World Congress (HUPO), Sept 2019, Adelaide, Australia.
3. Zheng, H., **CHEUNG, K. W., Jimmy,** Li, K. K., Tang, X., To, C. H., Tse, D., & Lam, T. C. (2018). Relative protein quantification in lens-induced chick retina by iTRAQ-based proteomics approach. Poster session presented at the Association of Research in Vision and Ophthalmology (ARVO), May 2018, Hawaii, USA.
4. **CHEUNG, K. W., Jimmy,** Bian, J., Yu, F., Li, K. K., To, C. H., Zhou, L., & Lam, T. C. (2018). Comprehensive proteomic study of chick vitreous during normal growth. Poster session presented at the Association of Research in Vision and Ophthalmology (ARVO), May 2018, Hawaii, USA.
5. **Cheung, J. K. W.** (2017) SWATH MS based quantification of chick vitreous proteins during normal eye growth. Speaker presented in Sciex user meeting, November 2017, Hong Kong.
6. **Cheung, J. K. W.** (2017) A label-free proteomic analysis of chick vitreous during normal growth. Speaker presented at International Conference of Vision and Eye Research (iCover), May 2017, Hong Kong.

7. **Cheung, J.**, Shan, S., Li, K., To, C., & Lam, T. C. (2016). Comparison of fixed sequential windowed acquisition of all theoretical fragment ion mass spectra (SWATH) windows for normal chick vitreous proteome. Poster session presented at 15th Human Proteome Organization World Congress (HUPO), Sept 2016, Taipei.

Publications

1. Shan, S. W., Wang, P. F., **Cheung, J. K. W.**, Yu, F., Zheng, H., Luo, S., Yip, S. P., To, C. H., & Lam, T. C. (2022). Transcriptional profiling of the chick retina identifies down-regulation of VIP and UTS2B genes during early lens-induced myopia [10.1039/D1MO00407G]. *Molecular Omics*.
<https://doi.org/10.1039/D1MO00407G>
2. Tse, J. S., Lam, T. C., **Cheung, J. K.**, Sze, Y. H., Wong, T. K., & Chan, H. H. (2020). Data on assessment of safety and tear proteome change in response to orthokeratology lens - Insight from integrating clinical data and next generation proteomics. *Data Brief*, 29, 105186. <https://doi.org/10.1016/j.dib.2020.105186>
3. **Cheung, J. K.-W.**, Bian, J., Sze, Y.-H., So, Y.-K., Chow, W.-Y., Woo, C., Wong, M. T.-K., Li, K.-K., & Lam, T. C. (2021). Human tear proteome dataset in response to daily wear of water gradient contact lens using SWATH-MS approach. *Data in Brief*, 36, 107120.
<https://doi.org/https://doi.org/10.1016/j.dib.2021.107120>
4. Kang, B. S., Lam, T. C., **Cheung, J. K.-w.**, Li, K. K., & Kee, C.-s. (2021). Corneal proteome and differentially expressed corneal proteins in highly myopic chicks using a label-free SWATH-MS quantification approach. *Scientific Reports*, 11(1), 5495. <https://doi.org/10.1038/s41598-021-84904-4>
5. Sze, Y. H., Zhao, Q., **Cheung, J. K. W.**, Li, K. K., Tse, D. Y. Y., To, C. H., & Lam, T. C. (2021). High-pH reversed-phase fractionated neural retina

proteome of normal growing C57BL/6 mouse. *Sci Data*, 8(1), 27. <https://doi.org/10.1038/s41597-021-00813-1>

6. **Cheung, J. K.**, Li, K. K., Zhou, L., To, C. H., & Lam, T. C. (2020). Data on protein changes of chick vitreous during normal eye growth using data-independent acquisition (SWATH-MS). *Data Brief*, 30, 105576. <https://doi.org/10.1016/j.dib.2020.105576>
7. Tse, J. S., Lam, T. C., **Cheung, J. K.**, Sze, Y. H., Wong, T. K., & Chan, H. H. (2020). Data on assessment of safety and tear proteome change in response to orthokeratology lens - Insight from integrating clinical data and next generation proteomics. *Data Brief*, 29, 105186. <https://doi.org/10.1016/j.dib.2020.105186>
8. Zhu, Y., Bian, J., Lu, D., Wang, Q., Gong, B., Li, K. K., Yu, F., **Cheung, J. K.**, Ji, X., Zhang, H., Du, B., Nian, H., To, C. H., Wei, R., & Lam, T. C. (2020). Combined retinal proteome datasets in response to atropine treatment using iTRAQ and SWATH-MS based proteomics approaches in guinea pig myopia model. *Data Brief*, 33, 106526. <https://doi.org/10.1016/j.dib.2020.106526>
9. Kang, B. S., Lam, T. C., **Cheung, J. K.**, Li, K. K., & Kee, C. S. (2019). Data on corneal proteome and differentially expressed corneal proteins in highly myopic chicks using a data independent quantification approach. *Data Brief*, 26, 104478. <https://doi.org/10.1016/j.dib.2019.104478>
10. Yu, F. J., Lam, T. C., Liu, L. Q., Chun, R. K., **Cheung, J. K.**, Li, K. K., & To, C. H. (2017). Isotope-coded protein label based quantitative proteomic analysis reveals significant up-regulation of apolipoprotein A1 and ovotransferrin in the myopic chick vitreous. *Sci Rep*, 7(1), 12649. <https://doi.org/10.1038/s41598-017-12650-7>

Awards

1. **Cheung, K. W.** (2022) A chick vitreous proteome database and differential vitreous protein expressions during myopia development using SWATH-based

quantitative proteomics. 3rd ABCT Research Postgraduate Symposium in the
Biology Discipline 2022. Best oral presentation award.

Acknowledgments

I want to show my deepest appreciation to my supervisor, Dr. Thomas Chuen Lam, and Professor Chi Ho To for all the tremendous support and guidance throughout my Ph.D. study. Moving into a new area completely different from my previous field was a tough and gratifying challenge that greatly benefited my personal growth.

I want to thank you, my parents, for supporting me without a doubt in my wildest dream of pursuing further study beyond the master's degree in the research field. With all the emotional support and, of course, the financial support, so that I could focus entirely on my study.

There will always be a special place for you in my heart KHK; with all the support you have given me, seeing both of us grow and reach where we are now is the best scenery I could ever wish for. Thank you, HWH, for listening to me mumble all day and night. I wouldn't have made it to the end without your support.

I would also like to thank all my lab mates for going through all the ups and downs together in the lab, especially my teammates: Dr. Feng Juan Yu, Dr. Jing Fang Bian, Mr. Ying Hon Sze, and Mr. King Kit Li as well as Dr. Sze Wan Shan and Dr. Hoi Lam Li for all the support provided in and outside the lab.

The bravest thing I have done so far in my life, and yes, I am finally here looking at it.

Table of Contents

ABSTRACT	I
LIST OF PRESENTATIONS AND PUBLICATIONS	V
ACKNOWLEDGMENTS	IX
TABLE OF CONTENTS	X
LIST OF FIGURES AND TABLES	XIII
LIST OF FIGURES	XIII
LIST OF TABLES	XXV
LIST OF ABBREVIATIONS	XXVI
CHAPTER 1. LITERATURE REVIEW	1
1.1 MYOPIA	1
1.1.1 Epidemiology of myopia	1
1.1.2 Myopia management, interventions, and research	6
1.2 VITREOUS- AN OVERVIEW	10
1.2.1 The physical location of the vitreous	11
1.2.2 Composition of the vitreous	13
1.2.3 Vitreous- the missing gap?	17
1.3 INTRODUCTION TO PROTEOMICS	19
1.3.1 Information-dependent acquisition (IDA)	20
1.3.2 Data-independent acquisition (DIA)- SWATH-MS	21
1.3.3 Targeted proteomics	22
1.3.4 Proteomic applications in eye research	24
1.4 RESEARCH GAPS	27
1.5 STUDY OBJECTIVES OF THE PRESENT STUDY	27
CHAPTER 2. ANIMAL MODEL AND GENERAL EXPERIMENTAL SETUP FOR PROTEOMICS	28
2.1 GENERAL ANIMAL HANDLING AND BIOMETRIC MEASUREMENTS	28
2.1.1 Eggs	28
2.1.2 Chicks raising condition	29
2.1.3 Chick model setup (Normal and Lens-induced myopia)	30
2.1.4 Biometric measurements	30
2.2 VITREOUS HUMOR (VH) TISSUE PROTEIN AND PEPTIDE EXTRACTION	32
2.2.1 Vitreous collection	32
2.2.2 Homogenization of vitreous	34
2.2.3 Protein concentration determination	35
2.2.4 Reduction and alkylation	36
2.2.5 Precipitation of proteins	36
2.2.6 Trypsin digestion	36
2.2.7 Peptide cleanup	37
2.2.8 High-pH peptide fractionation	38
2.3 IDENTIFICATION AND QUANTITATION OF PROTEINS BY SWATH-BASED LABEL-FREE PROTEOMICS	39
2.3.1 LC-MS/MS settings	39

2.3.2	MS data analysis.....	42
2.3.3	High-resolution multiple reaction monitoring (MRM ^{HR}) confirmation	42
CHAPTER 3. OPTIMIZATION OF VITREOUS PROTEOMIC PROTOCOLS.....		44
3.1	VITREOUS SAMPLE PREPARATION.....	45
3.1.1	Homogenization methods of chick vitreous protein extraction ..	45
3.1.2	Protein precipitation (Acetone vs. TCA/Acetone/ methanol- chloroform)	56
3.1.3	Cleanup method (SPE (HLB) /ZipTip /Spin column).....	65
3.2	MS OPTIMIZATION	76
3.2.1	Vitreous sample loading quantity in information-dependent acquisition (IDA) mode.....	76
3.2.2	Vitreous protein repeatability under information-dependent acquisition (IDA) mode.....	81
3.2.3	HPLC fractionation	86
3.2.4	Gradient time (90 vs. 155 mins)	95
3.2.5	High-pH fractionation	99
3.3	SWATH-MS OPTIMIZATION	107
3.3.1	Sequential Windowed Acquisition of All Theoretical Fragment Ion Mass Spectra (SWATH-MS) windows size comparison	107
3.3.2	IDA and SWATH-MS comparison in protein quantitation.....	113
3.3.3	Fold change cut-off determination for SWATH	117
CHAPTER 4. IN-DEPTH PROTEOMIC ANALYSIS OF INTER-AND INTRA-OCULAR DIFFERENCES IN NORMAL GROWING CHICK VITREOUS USING SWATH QUANTITATION		124
4.1	INTRODUCTION	124
4.2	METHODS AND MATERIALS	125
4.3	RESULTS.....	127
4.4	DISCUSSION.....	134
4.5	CONCLUSION.....	136
CHAPTER 5. CHANGES IN CHICK VITREOUS PROTEOMES DURING NORMAL EYE GROWTH		137
5.1	INTRODUCTION	137
5.2	METHODS AND MATERIALS	140
5.3	RESULTS.....	143
5.4	DISCUSSION.....	155
5.5	CONCLUSION.....	160
CHAPTER 6. VITREOUS: MYOPIA STUDY – LENS INDUCED MYOPIA (LIM)		161
6.1	INTRODUCTION	161
6.2	METHODS AND MATERIALS	162
6.3	RESULTS.....	164
6.4	DISCUSSION.....	173
6.5	CONCLUSION.....	180

CHAPTER 7. PROTEIN VALIDATION USING HIGH-RESOLUTION MULTIPLE-REACTION MONITORING (MRM^{HR}) AND QUANTITATIVE PCR APPROACH	182
7.1 INTRODUCTION	182
7.2 METHODS AND MATERIALS	183
7.3 RESULTS.....	187
7.4 DISCUSSION.....	194
7.5 CONCLUSION.....	198
CHAPTER 8. SUMMARY AND CONCLUSION	200
REFERENCE	202
APPENDICES	I

List of figures and tables

List of figures

Figure 1.1 Illustration of how light enters the eye parallel to the optic axis is focused: on the retina (emmetropia) and in front of the retina (myopia). The light will be corrected using convex (lens-induced myopic defocus) and concave (lens-induced hyperopic defocus) lenses. Figure modified from Carr and Stell, 1995.	1
Figure 1.2 The global prediction of myopia prevalence from 2000 to 2050; Figure adapted from B. A. Holden et al., 2016.	3
Figure 1.3 The Vitreous anatomy inside the eyeball; Figure adapted from Le Goff and Bishop, 2008.	12
Figure 1.4 Vitreous composition with the meshwork containing hyaluronan and collagen fibrils; Figure adapted from Le Goff and Bishop, 2008.	15
Figure 1.5 The overall vitreous meshwork with hyaluronan filling up between the collagen fibrils. Figure adapted from Halfter et al., 2005.	15
Figure 1.6 The workflow of peak selection for an initial full scan, IDA: where a certain intensity threshold must be reached for MS/MS fragmentation, and IDA: where all are fragmented. Figure modified from J. Guo and Huan, 2020.	22
Figure 1.7 (A) The precursor ions are selected by the instrument based on abundance. (B) All the precursor ions within a selected mass range are selected in DIA mode for fragmentation and analysis. (C) Only a selection of precursor ions is selected for fragmentation and analyzed for a more targeted approach. Figure modified from A. Hu et al., 2016.	24
Figure 1.8 The number of proteins found in various proteomics studies of the human eye. Figure adapted from Ahmad et al., 2018.	25
Figure 2.1 An overview of vitreous proteomics workflow used in this study, from chick vitreous collection to data analysis using MS.	28
Figure 2.2 Chicken breeding equipment and lighting setups. (A) Eggs were placed in the large egg incubator with temperature and humidity controls for 21 days. Each stack of egg holders was allowed to rock up	

and down to ensure airflow. (B) Eggs were transferred into a smaller hatcher under the same environmental condition for chicks to hatch. (C) Breeding room with stainless steel brooders under a 12/12 dark/ light cycle with an average luminance of 500 lux at the center of the cage and automatically controlled temperature environment.30

Figure 2.3 Normal and lens-induced myopia (LIM) chickens along with A-Scan and refractive error measurements equipment. (A) Normal growing white leghorn chicks at 3 days post-hatch. (B) -10D PMMA lens attached to one side of the eye of the chick's eye using a velcro ring. (C) A-Scan Ultrasound system setup connected with an adjustable pump system. (D) A-Scan ultrasound peaks for ocular component diameter measurement showing the cornea, lens, retina, choroid, and sclera thickness (E) Refractive measurements using streak retinoscopy with trial lens bars.....32

Figure 2.4 (A) The eyeball was transferred to ice-cold PBS and the removal of excess muscles and blood. (B) Hemisecting the eyeball equatorially into the anterior part showing the lens on the left and the posterior part showing the vitreous, pecten oculi, and the retina. (C) Pushing the vitreous out of the posterior eyeball using a pair of tweezers while keeping the retina intact. (D) Removal of the vitreous to the RPE/retina layer, while having the pecten oculi visible inside the vitreous. (E) Remains of liquid vitreous after the collection of the main vitreous body, which were also collected using a pipette. (F) Clean extracted vitreous body, free from blood or extra surrounding tissues such as the retina...34

Figure 2.5 (A) Two milliliter homogenization tubes with 1.4mm + 2.8mm ceramic (zirconium oxide) beads used in the vitreous sample homogenization process. (B) Two tubes on the left: after homogenization of vitreous; Two tubes on the right: before homogenization of vitreous (with T-PER lysis buffer).....35

Figure 2.6 Oasis ® C18 HLB column (1 cc/10 mg) inserted into the Visiprep™ SPE manifold system (12 ports) for peptide clean-up step. ...38

Figure 2.7 Gradient profiles for (A) long (155 minutes total) and (B) short (90 minutes total) LC/MS running time. Mobile phase A was a mixture of

0.1% FA (v/v), 5% ACN (v/v) in water, and mobile phase B contains 0.1% FA (v/v), 98% ACN (v/v) in water.	40
Figure 2.8 (A) A general extracted-ion chromatogram (XIC) of a vitreous IDA (blue), and SWATH (purple) under a 90 mins run. (B) A variable SWATH-MS windows calculation (100 windows) chromatogram of vitreous.	41
Figure 3.1 Tissue homogenization methods (metallic bead with the homogenizer and water-bath sonicator) with different lysis buffer volume ratios.	46
Figure 3.2 (A) The use of foil to determine the location of the sonicator inside the water bath (before and after 2 mins of turning on). (B) The location of where samples were placed for each set of homogenization with sonicator water bath experiments was determined by the foil test. (C) The monitoring of temperature changes with water bath sonicator on for 10 mins.	49
Figure 3.3 (A) The total sample volume after each homogenizing method (Homogenizer with metal bead in chamber and water bath sonicator) for each lysis buffer ratio group. (B) The protein concentration was measured after each homogenizing method for each lysis buffer ratio group. (C) The total protein amount after each homogenizing method for each lysis buffer ratio group. Statistical analysis was analyzed by one-way analysis of variance (ANOVA) with a significance level of 0.05, and an unpaired T-test was applied when comparing individual groups (*P ≤ 0.05, **P ≤ 0.01, and *** P ≤ 0.001, total n= 18).	52
Figure 3.4 Seven individual age-matched chicks vitreous were collected. Samples were individually homogenized using T-PER lysis buffer and reduced and alkylated. These were then pooled together and split into 9 parts of equal amounts of 20 µg. Three precipitation methods (Chloroform/ methanol, 100% Acetone, and 10% TCA/Acetone, n= 3 each) were tested, the protein precipitant was re-dissolved in a buffer, and protein concentration was compared.	57
Figure 3.5 Seven age-matched chicks vitreous were pooled together for reduction and alkylation. The protein concentration was determined	

using protein assay kit, and equal amounts (20 µg) of vitreous proteins (n= 3 in each group) underwent three different precipitation methods: 100% Acetone precipitation, Acetone with the addition of different concentrations of NaCl (10mM and 30mM). The protein concentration was determined again with protein assay for recovery yield calculation after re-dissolving in a buffer consisting of 1M Urea in 25mM NH₄HCO₃.....58

Figure 3.6 (A) The protein concentration (µg/µl) after precipitation (n= 3 from each condition). B) Overall protein recovery (%) for three precipitation methods. One-way ANOVA testing was performed with a significant level set at 0.05, Tukey post hoc test (P≤ 0.05, *=0.05, **=0.01, and *=0.00, n= 3 for each condition).61**

Figure 3.7 (A) The protein concentration (µg/µl) after each precipitation method (100% Acetone, Acetone+ 10mM NaCl, and Acetone+ 30mM NaCl). (B) Overall protein recovery (%) for three precipitation methods. One-way ANOVA testing with a significant level set at 0.05, (n= 3), Tukey post hoc test (P≤ 0.05, *=0.05, **=0.01, and *=0.00, n= 3 for each condition).....62**

Figure 3.8 Pooled trypsin-digested vitreous was split into 9 equal parts (5 µg each) and went through each type of cleanup method (n= 3 for each method: C-18 spin column, SPE HLB cartridge, and ZipTip). Samples were vacuum dried and re-dissolved in equal amounts of 0.1% FA. The peptide concentration was measured for peptide recovery (%) and was injected into MS for protein analysis.66

Figure 3.9 (A) The average protein concentration (µg/µl) was measured after each cleanup method. One-way ANOVA, significant different setting as 0.05, n= 3. (B) The average peptide recovery (%) from the three types of cleanup methods. One-way ANOVA, significantly different setting as 0.05, n= 3. (C) The number of proteins identified at 1% FDR for each clean-up method. (D) Venn diagram showing the overlapping and individual proteins obtained from the IDA experiment at 1% FDR.....70

Figure 3.10 Gravy index score (average hydrophobicity and hydrophilicity) of vitreous proteins under three clean-up methods. Hydrophobicity

scores below 0 are more likely to be hydrophilic proteins, whereas above 0 are more likely to be hydrophobic proteins. (ZipTip: Orange, HLB SPE cartridge: Blue, and C-18 spin column: Green).....72

Figure 3.11 Age-matched vitreous samples were collected (n= 3) and digested. These were then pooled together, and the peptide concentration was measured using a peptide assay kit. Digested peptides were then diluted into 3 groups: 0.5 µg, 1 µg, and 2 µg (n= 3) for quantity injection determination into the MS in IDA mode (2 injections for each condition).77

Figure 3.12 (A) Proteins and (B) peptides identified from three injections quantity (0.5 µg, 1 µg, and 2 µg) at 1 % FDR (2 technical replicates for each injection amount group. (C) Venn diagram showing the number of proteins identified (from combined search) overlapped from each group.79

Figure 3.13 (A) The number of proteins identified at 1% FDR from all technical replicates. The black bar indicates the total distinct proteins found from injections; the white bar indicates the number of overlapped proteins. (1) shows the number of proteins identified from only 1 injection, while (1-2) indicates 2 injections were added together, (1-3) indicates 3 injections, (1-4) indicates 4 injections, and (1-5) indicated all 5 injections. (B) The increase in distinct proteins from when each technical replicate was added together (%). (C) The decrease in overlapping proteins from searching when each technical replicate was added together (%).83

Figure 3.14 A pooled sample of ~140 µg digested vitreous for the unfractionated sample and the fractionation workflow using HPLC fractionation with a reversed-phase (RP) strong cation-exchange SCX column. The sample was separated into 21 parts, and the peptide concentration for each part was measured using a peptide assay kit. These parts (Parts 1-12 and Parts 13-21) were then further combined based on the peptide concentration for loading into the MS under IDA mode.87

Figure 3.15 The total peptide amount (μg) of each fraction (1- 21). Fractions without bars indicated the concentration was too low for detection.90

Figure 3.16 The number of (A) proteins and (B) distinct peptides identified at 1% FDR for fraction (1-12), (13-21), fractionated combined (combined search of 1-12 and 13-21 parts) and unfractionated groups.91

Figure 3.17 (A) The % of proteins identified (1% FDR) in the number of fractions (either only found in 1 or found in 2 fractions). Blue indicates the % proteins that were found in only one fraction [Either in Fraction (1-12 or 13-21)]. Orange indicates % of proteins that were found in both fractions. (B) The number of proteins identified in Fraction (1-12) and Fraction (13-21). (C) The number of proteins identified in fractionated combined (combine search of fraction 1-12 and 13-21) and unfractionated group.92

Figure 3.18 Running settings of two MS gradients. (A) standard long (155mins) gradient (B) A shorter (90mins) gradient. Solvent A contained 2% ACN, 0.1% FA, and Solvent B contained 98% ACN, 0.1% FA.96

Figure 3.19 The number of (A) proteins and (B) distinct peptides identified in vitreous from 90 mins and 155 mins gradient at 1% FDR (C) The number of proteins found in each and overlapped from two gradient settings.97

Figure 3.20 Three separate batches of chicks (n= 14 vitreous pooled for each set, total n= 42) were homogenized and digested. Unfractionated and high-pH fractionated (Fraction A: 12.5% ACN in 0.1% TEA and Fraction B: 50% ACN in 0.1% TEA) samples were injected with two technical IDA injections each.101

Figure 3.21 The number of proteins identified at 1% FDR in three sets (1, 2, and 3) of vitreous digest (n= 14 chick vitreous for each set). Solid black bars resemble proteins that were identified from a combined search of two fractions (Fraction A: 12.5% ACN in 0.1% TEA and Fraction B: 50% ACN in 0.1% TEA), and white bars resemble the proteins that were from the unfractionated group.102

Figure 3.22 The % of proteins that were identified at 1% FDR in fractionated, unfractionated and common overlaps in three sets (1,2

and3). Blue indicates the proteins that were found overlapped from high-pH fractionated and unfractionated samples. Orange indicates % of proteins that were only found in fractionated samples. Grey indicates % of proteins that were only found in unfractionated samples.....103

Figure 3.23 The % of proteins identified (1% FDR) in the number of fractions (either only found in 1 or found in 2 fractions) in three sets (1,2 and 3). Blue indicates the % proteins that were found in only one fraction (Either in Fraction A or B). Orange indicates % of proteins that were found in both fractions.104

Figure 3.24 A proteome was firstly generated under IDA mode, and four SWATH window settings were used for comparison (15Da, 20Da, 25Da, and variable windows 100).108

Figure 3.25 (A) The proteins and (B) peptides quantified (at 1%FDR) using various SWATH window size settings (25Da, 20Da, 15Da, and variable windows 100). Three retention time window settings (5, 10, and 15 mins) were compared during PeakView processing. (C) The cumulative frequency (%) at 20%CV under 3 PeakView retention time settings (5, 10, and 15 mins) for various SWATH window size settings (15Da, 20Da, 25Da, and variable windows 100).110

Figure 3.26 Same amount (1 µg) of digested vitreous was loaded into the MS under IDA and SWATH-MS mode with three technical replicates for each mode. Three injections of IDA were combined searched for the generation of a protein ion library. SWATH-MS data were then loaded onto the library for protein quantitation.114

Figure 3.27 (A) The number of identified proteins in each IDA technical replicate (T1, 2, and 3) (B) The number of overlapped proteins (white bars) found from all three technical replicates (under IDA or SWATH-MS mode). Black bars indicate the total distinct proteins in each mode.115

Figure 3.28 The pooled vitreous lysate was split into 3 equal parts: A, B, and C for sample preparation and digestion. An ion library was generated from a combined search of the 3 IDA injections. Then the SWATH injections from the 3 groups were loaded onto the ion library and

quantified. Ratios from each group were calculated to determine the Fold Change cutoff.....	118
Figure 3.29 The normal distribution curve of raw values and adjusted values for the three SWATH comparison groups, with and without Most-likely-ratio (MLR) method for normalization.....	121
Figure 4.1 The workflow for quantification of proteins between the Right (OD) and the Left (OS) eyes in two separate batches of chicks (Set A: n= 8 and Set B: n= 7) using SWATH quantification workflow. Individual samples from both sets were pooled into their respective group, and 2 technical injections under IDA mode were done and were combined searched as their respective ion library. DIA (SWATH) injections were done in duplicates on each individual sample from OD and OS groups in both sets. Obtained spectra were processed in PeakView and exported using MarkerView for statistical analysis.....	125
Figure 4.2 The intra and interocular comparison method. Obtained data for OD and OS were compared within each animal (Intra, shown in orange lines). For interocular comparison, the OD was compared to the OS from a different animal (Inter, shown in green lines) for each animal in each set.	126
Figure 4.3 The change in refractive error (D) in OD and OS for Intra (left bar) and inter (right bar) ocular comparison for both sets (n= 8 for set A and n= 7 for set B, Error bars = Mean \pm SD).....	128
Figure 4.4 The change in ocular components in length (mm) in OD and OS for intra and interocular comparison for both sets (n= 8 for set A and n= 7 for set B, Error bars = Mean \pm SD) from A-scan for (A) set A and (B) set B. ACD: anterior chamber depth, LT: lens thickness. VCD: vitreous chamber depth, AXL: axial length from the front of the cornea to the front of the retina	129
Figure 4.5 The average difference in protein concentration ($\mu\text{g}/\mu\text{l}$) of lysed vitreous (T-PER, 1:1 w/v ratio) from the right eye (OD) and the left (OS) for intra and interocular comparison (set A, n= 8 and set B, n= 7, Error bars = Mean \pm SD).....	130

Figure 4.6 Intra (OD/OS FC of the same animal) and interocular (OD/OS FC of different animals) comparison of (A) set A and (B) set B in terms of protein fold change acquired from SWATH quantitation. *p ≤0.05, ns: not significant, unpaired T-test (set A, n= 8 and set B, n= 7, Error bars = Mean ± SD).131

Figure 4.7 Scatter plots of protein intensities acquired from SWATH quantitation. Typical intraocular protein intensities comparison between the OD and OS vitreous of the same animal for (A) set A and (B) set B. Typical interocular protein intensities comparison between the OD and OS vitreous of different animals for (C) set A and (D) set B. (A much higher + C intercept indicating a higher rate of false up-regulation). ..132

Figure 5.1 The SWATH-MS experimental workflow of normal growth (emmetropization) period. Chick vitreous samples were collected at Day7, 14, 21, and 28 (a total of 24, n= 6 at each time point). These were then pooled into the right eye (OD) and left eye (OS) for sample preparation. IDA injections were performed on each of the samples with 3 SWATH injections for quantification. The ion library was generated from the combined search of all the IDA injections. Acquired data were then exported for data analysis software.140

Figure 5.2 Average changes of refractive error of the right eye (OD) and left eye (OS) as compared to the baseline (D4) during different time points of normal growth: n= 6 at each time point. *P ≤=0.05 and **P ≤=0.01, one-way ANOVA. No significant differences were found between OD and OS at all time points for Rx.144

Figure 5.3 Average changes of ocular components of the right eye (OD) and left eye (OS) during different time points of normal growth: (A) ACD: anterior chamber depth, (B) LT: lens thickness. (C) VCD: vitreous chamber depth, (D) AXL: from the front of the cornea to the front of the retina), n= 6 at each time point. *p ≤ 0.05, **P ≤=0.01 *p ≤=0.001, one-way ANOVA. No significant differences were found between OD and OS at all time points for ACD, LT, VCD, and AXL.....145**

Figure 5.4 Average protein concentration of homogenized vitreous, n= 6 at each time point. *p ≤ 0.05, **P ≤ 0.01 *p ≤ 0.001, paired T-test between eyes and one-way ANOVA for multiple time points.146**

Figure 5.5 Gene ontology (GO) classifications of proteins from combined search proteins of normal growing chick vitreous. (A) Biological process (B) Molecular function (C) Cellular components using PANTHER.147

Figure 5.6 (A) The number of proteins identified at 1% FDR at each time point (individually searched of the pooled sample). (B) The Comparison between the combined library and 8 individual libraries; Traditional shotgun proteomics (8 individual injections, individually searched) and combined searched library (8 injections combinedly searched). The total unique proteins (peptides) identified from all 8 individual injections, and a combined search were 1988 and 1576, respectively. The total overlapping unique proteins found across all 8 injections in IDA and DIA mode were 542 and 1456, respectively.148

Figure 5.7 The number of proteins found differentially expressed from each time point using the combined ion library. The FC ratio was calculated by comparing it to the baseline (D7). The fold change calculation filter was set as ≥1.5 or ≤0.7 FC, same direction for both eyes.150

Figure 5.8 Heatmap showing DEPs in normal eye growth period (Day 7, 14, 21, and 28). Dark red indicates a more positive value (i.e., up-regulated proteins), and yellow indicates a more negative value (i.e., down-regulated proteins).151

Figure 5.9 STRING analysis on commonly differential expressed proteins (DEPs) across all the time point. The color represents Red- cell adhesion; Blue- nervous system development; Purple: Cell adhesion molecules pathway; Yellow: Lysosome pathway; Pink- ECM-receptor interaction pathway; Green Serum albumin family. Grey: co-expressed proteins.154

Figure 6.1 Schematic workflow of quantitative discovery proteomics in myopic lens-induced (LIM_T) eyes vs control eyes (LIM_C). Seven vitreous lysates from 7 chicks (7 treated and 7 control eyes) were included. Three micrograms of sample digest from individual samples

from both groups (LIM3 and LIM7) were subjected to high-pH fractionation, and 5 µg remained as the unfractionated pool. The three pools (LIM3, LIM7, and unfractionated pool) were injected into the MS with two technical replicates to establish the proteome library under IDA. One microgram of digested proteins from each individual sample in two technical replicates was analyzed under SWATH-MS mode. Protein identification was performed using ProteinPilot, and quantification with PeakView and MarkerView software. Identified proteins were then analyzed further with online bioinformatic analysis tools.....162

Figure 6.2 Average changes of refractive error during (A) -10D LIM for 3 days and (B) -10D LIM for 7 days compared to the control eyes (n= 7 at each time points, *p ≤ 0.05, **P ≤ =0.01 *p ≤ =0.001, unpaired T-test. Error bars= Mean ±SD).....165**

Figure 6.3 Average changes of ocular components during (A & B) -10D LIM for 3 days and (C & D) -10D for 7 days compared to the control eyes. ACD: anterior chamber depth, LT: lens thickness, VCD: vitreous chamber depth, AXL: from the front of the cornea to the front of the retina (n= 7 at each time point. *p ≤ 0.05, **P ≤ =0.01 *p ≤ =0.001, unpaired T-test, Error bars= Mean ±SD).....166**

Figure 6.4 Protein concentration of chick vitreous in 1:1 T-PER buffer ratio for (A) -10D LIM 3 days and (B) -10D 7 days between the treated and control eyes. (n= 7 at each time points, ns= not significant, unpaired T-test, Error bars= Mean ±SD).....167

Figure 6.5 (A) Volcano plot displaying the statistical p-value with the magnitude of fold change between lens-induced myopia for 3 days (LIM3) vs. fellow eye control. The non-axial vertical dashed lines denote a fold change, of ± 0.58 Log2 unit (i.e., ± 1.5 fold change) whereas the non-axial horizontal dashed line denotes 1.30 -Log10 p-value (i.e., p = 0.05), which is the significance threshold prior to logarithmic transformation. A total of 8 DEPs out of 1242 proteins were found to be differentially expressed (Blue: down-regulated). (B) Heatmap showing DEPs in LIM3 study. Dark red indicates a more positive value (i.e., up-

regulated proteins), and yellow indicates a more negative value (i.e., down-regulated proteins).....169

Figure 6.6 (A) Volcano plot displaying the statistical p-value with the magnitude of fold change between lens-induced myopia for 7 days (LIM7) vs. fellow eye control. The non-axial vertical dashed lines denote a fold change of $\pm 0.58 \text{ Log}_2$ unit (i.e., ± 1.5 fold change), whereas the non-axial horizontal dashed line denotes $1.30 -\text{Log}_{10}$ p-value (i.e., $p = 0.05$), which is the significance threshold prior to logarithmic transformation. A total of 23 DEPs out of 1242 proteins were found to be differentially expressed (Blue: down-regulated). **(B)** Heatmap showing DEPs in LIM7 study. Dark red indicates a more positive value (i.e., up-regulated proteins) and yellow indicates a more negative value (i.e., down-regulated proteins).....173

Figure 7.1 The fold change of proteins validated in MRMHR experiments in normal growth study (D7 and D14), $n= 4$, $*p <0.05$; $***p <0.01$, T-test. Error bars= Mean \pm SD. Normalized with GAPDH.....189

Figure 7.2 The fold change of proteins validated in MRM^{HR} experiments in myopia study (LIM3), $n= 4$, ns= not significant, $***p <0.01$, T-test. Error bars= Mean \pm SD.....190

Figure 7.3 The fold change of protein validated in MRM^{HR} experiments in myopia study (LIM7), ($*p <0.05$, unpaired T-test. Error bars= Mean \pm SD, $n= 6$).....191

Figure 7.4 Chick retina VIP expression normalized to GAPDH at Lens-induced myopia (LIM) for (A) 3 and (B) 7 days, $n= 4$ at each time point ($*p <0.05$; $***p <0.01$, unpaired T-test. Error bars= Mean \pm SD).193

List of tables

Table 3.1 Top 10 vitreous proteins found overlapped from all three clean-up methods at 1% FDR.....	71
Table 3.2 Number of proteins and distinct peptides identified at 1% FDR for 5 repeated injections (T1 -T5) of the vitreous digest.....	82
Table 3.3 Average adjusted fold change (FC) calculated from all SWATH-MS injections (with and without MLR normalization)	121
Table 4.1 The number of DEPs found intra and interocular comparisons using SWATH quantitation (set A, n= 8 and set B, n= 7). An FC cutoff filter ($FC \geq 1.5$ or ≤ 0.70) was applied to reduce false-positive results....	133
Table 5.1 Growth-related differentially expressed proteins (DEPs) found across all time points (14, 21, and 28). The fold change (FC) was calculated against the baseline (Day 7), FC cut off ≥ 1.5 or ≤ 0.7, and both eyes have to be in the same FC direction. Red: up-regulated proteins, Blue: down-regulated proteins.....	152
Table 6.1 DEPs found in LIM3 using SWATH-MS, n= 7, unpaired T-test, FC cut off ≥ 1.5 or ≤ 0.7 and $p \leq 0.05$. Blue: down-regulated proteins.....	168
Table 6.2 DEPs found in LIM7 using SWATH-MS, n= 7, unpaired T-test, FC cut off ≥ 1.5 or ≤ 0.7 and $p \leq 0.05$. Red: up-regulated proteins, Blue: down-regulated proteins.....	170
Table 7.1 The peptides and transition identified and selected in GAPDH as the internal standard for the MRM^{HR} experiments (A) Normal growth study, (B) Myopia study (LIM3), and (C) Myopia study (LIM7).....	185
Table 7.2 FC of GAPDH acquired from SWATH-MS compared to MRM^{HR} in their respective experiment study.	187
Table 7.3 The fold change of DEPs in SWATH-MS and MRM^{HR} experiments in myopia study (LIM3), n= 5.	190
Table 7.4 The fold change of DEPs in SWATH-MS and MRM^{HR} experiments in myopia study (LIM7), n= 6.	192

List of abbreviations

ABS	Absorbance
ACN	Acetonitrile
AMD	Age- related macular degeneration
NH ₄ HCO ₃	Ammonium bicarbonate
ACD	Anterior chamber depth
AXL	Axial length
BSA	Bovine serum albumin
CS	Chondroitin sulfate
DIA	Data independent acquisition
°C	Degree in Celsius
DEPs	Differentiated expressed proteins
D	Diopter
ECM	Extracellular matrix
FDR	False discovery rate
FA	Formic acid
GAGs	Glycosylated proteins- glycosaminoglycans
HS	Heparan sulfate
HPLC	High-performance liquid chromatography
MRM ^{HR}	High-resolution multiple reaction monitoring
HA	Hyaluronic acid
HLB	Hydrophilic-lipophilic balanced
IDA	Information-dependent acquisition
LIH	Lens-induced hyperopia
LIM	Lens-induced myopia
m/z	Mass to charge ratio
MRM	Multiple reaction monitoring
PBS	Phosphate-buffered saline
PCR	Polymerase chain reaction
PMMA	Polymethyl methacrylate
PVD	Posterior vitreous detachment
qPCR	Quantitative polymerase chain reaction
RT-qPCR	Quantitative reverse transcription PCR

RD	Retinal detachment
RPE	Retinal pigment epithelium
RP	Reversed-phase
	Sequential window acquisition of all theoretical Mass
SWATH-MS	Spectra
S/N	Signal-to-noise ratio
SRM	Single reaction monitoring
SDC	Sodium deoxycholate
SDS	Sodium dodecyl sulfate
SPE	Solid-phase extraction
S.E.	Spherical equivalent
SCX	Strong cation exchange
T-PER	Tissue protein extraction reagent
TFA	Trifluoroacetic acid
2-DE	Two-dimensional gel electrophoresis
Uniprot	Universal protein resource
VCD	Vitreous chamber depth
VH	Vitreous humor
VIP	Vasoactive intestinal peptide

Chapter 1. Literature review

1.1 Myopia

1.1.1 Epidemiology of myopia

1.1.1.1 Definition of myopia

Myopia is a common refractive error that can be defined qualitatively where parallel light rays are focused in front of the retina where ocular accommodation is relaxed (Flitcroft et al., 2019). Myopia is measured quantitatively in units of diopters (D) and can be defined as a condition in which the spherical equivalent (S.E.) refractive error of an eye is ≤ -0.50 D when accommodation is relaxed (Carr & Stell, 1995) (shown in Figure 1.1). It can be further categorized into low myopia: ≤ -0.50 D and > -6.00 D and high myopia: ≤ -6.00 D when accommodation is relaxed (Flitcroft et al., 2019).

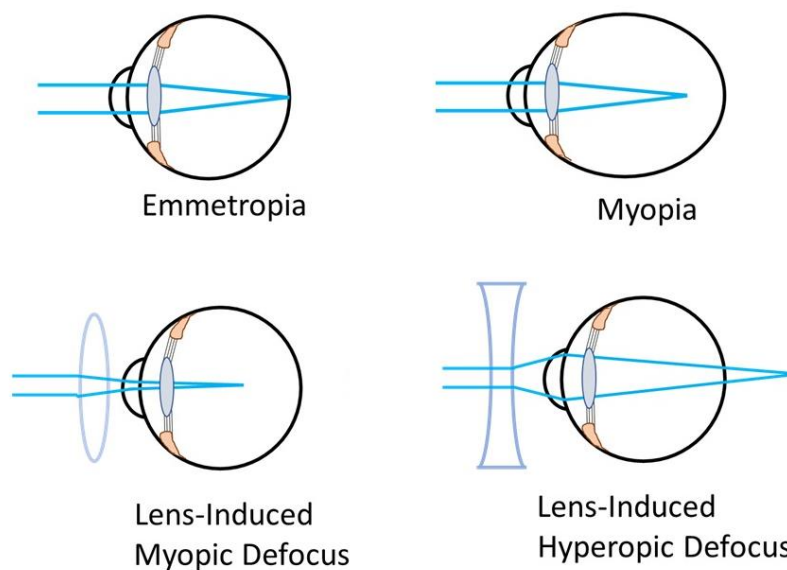


Figure 1.1 Illustration of how light enters the eye parallel to the optic axis is focused: on the retina (emmetropia) and in front of the retina (myopia). The light will be corrected using convex (lens-induced myopic defocus) and concave (lens-induced hyperopic defocus) lenses. Figure modified from Carr and Stell, 1995.

1.1.1.2 Myopia: Global concern

Myopia is a global concern as it currently affects more than 22% (1.4 billion) of the world's population, making it the most prevalent eye disorder worldwide. This figure has been predicted to rise, where almost 50% of the world's population will have myopia by 2050 (Figure 1.2), while 10% could be accounted for as high myopes (Holden et al., 2016). This number is expected to rise further if no treatments are to be discovered which paves the way for more serious ocular conditions that could result in total visual loss such as retinal detachment (Saw et al., 2005) and posterior vitreous detachment (PVD) (Akiba, 1993). Although myopia is at epidemic proportions worldwide, the highest prevalence rates are observed in urban areas of East and Southeast Asia (Dolgin, 2015; C. W. Pan et al., 2012; Wu et al., 2016) such as China [China (>90%), Singapore(>80%) (Koh et al., 2014) and Taiwan (>80%) (Lin et al., 1999)]. In contrast, populations diagnosed with myopia in western countries such as the USA was much lower, only around 25% from 1971 to 1972, but this number rose to 41% in 1999-2004, and the overall prevalence of myopia is expected to increase in the future (Vitale et al., 2009). With the prevalence of myopia being on the rise, the chances of high myopia also increase. Among the overall myopia population, almost 24% were classed as having high myopia (Lin et al., 2001; Tan et al., 2005; Zhou et al., 2007), which further increases the chances of sight-threatening complications.

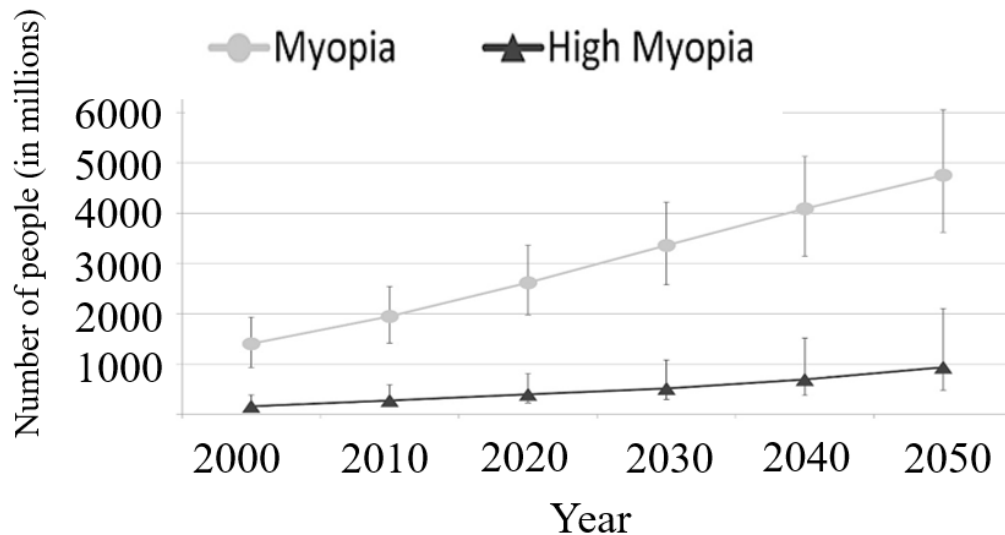


Figure 1.2 The global prediction of myopia prevalence from 2000 to 2050; Figure adapted from B. A. Holden et al., 2016.

1.1.1.3 Risk factors of myopia

It has been suggested that myopia could be affected by multi-factors such as environmental (Foster & Jiang, 2014; Rahi et al., 2011) and genetic (Morgan & Rose, 2005). However, the fundamental mechanism of this refractive disorder's initial cause and development is still poorly understood, which urges a solution in prevention and treatment.

Environmental factors contribute via visual guidance through the visual system, which affects the growth of the eye (Wallman & Winawer, 2004), of which one of the strongest and most replicated environmental risk factors is associated with education conditions (Mirshahi et al., 2014; Morgan & Rose, 2005). The same group conducted a cross-sectional study on young Australian children indicating that those children who spend more time in close-up environments without spending time outdoors have a higher chance of becoming myopic compared to children who go to a school infrequently (C.-W. Pan et al., 2012). Multiple studies also concluded that the prevalence of myopia was increased in those children who either had more involvement in classes and schools (Czepita et al., 2008; Mutti et al., 2002) or had better grades (Czepita et al., 2008).

Furthermore, higher myopia prevalence was found in industrialized areas compared to more remote areas (Saw et al., 2001; Uzma et al., 2009). However, in contrast, the role of near work duration and working distance has also been deemed less critical (Mutti & Zadnik, 2009); hence the exact mechanism of myopia with these links is still unclear. Time spent outdoors is another environmental factor that is important in the development of myopia (Rose et al., 2008; Xiong et al., 2017) and could have a protective effect on slowing down the myopia progression due to the stimulation of dopamine (French et al., 2013).

Genetics is another major risk factor for myopia, with several studies looking at the myopia progression based on different ethnicity across the same environment in the UK (Rudnicka et al., 2010), USA (Luong et al., 2020). While this provided some evidence, environmental factors mentioned earlier should also be considered regarding the prevalence in different ethnicities (Ip et al., 2007; Rudnicka et al., 2016). Another link is parental myopia, where various studies across various ethnic groups have indicated that the risk of children having myopia is greater among parents that are myopes (Edwards, 1998; Liang et al., 2004; Xiang et al., 2012). Many genes have been found to be associated with myopia: Lumican (LUM) affects collagen fibrillogenesis, leading to the reformation of the sclera, and there is a significant association between LUM to high myopia (Lin, Kung, et al., 2010; Lin, Wan, et al., 2010; Zhang et al., 2009). Paired box 6 (PAX6) and its variants had been associated with playing a potential role in controlling eye development in high myopia (Kanemaki et al., 2015; Tang et al., 2014), but contradictive results were also found (Mutti et al., 2007), or rather the fact that it has little effect on low myopia groups only (Tang et al., 2018). Transforming growth factor-beta 1 (TGFB1) is present in the extracellular matrix (ECM) of the sclera, and having a significant association with high myopia (Lin et al., 2006; Zha et al., 2009). Another protease that mediates the sclera biomechanical strength is Matrix metalloproteinases (MMPs) such as MMP2 (Gong et al., 2013; Zhao et al., 2018) and MMP3 (Liang et al., 2006), which were found up-regulated in high myopic patients.

1.1.1.4 Complications of myopia

Myopic eyes are clinically presented as the elongation of the eyeball, with VCD changing the most during this phase. This change is also well recognized across different species such as chicks (Seltner & Sivak, 1987; Wallman & Adams, 1987; Wallman et al., 1981; Wallman et al., 1978), tree shrews (Sherman et al., 1977) and monkeys (Bradley et al., 1999; Qiao-Grider et al., 2007). However, this disease's underlying mechanism or pathogenesis is still unclear and seldom explored. With the alarming increase in myopia prevalence, myopia-associated/lead ocular complications such as cataracts (Lim et al., 1999), glaucoma (Chen et al., 2012), and posterior vitreous detachment (Akiba, 1993) increase the chances of leading to a severe reduction in vision loss or total blindness (Cedrone et al., 2006; Xu et al., 2006). Peripheral retinal degeneration and lattice degeneration are just some of the complications that could arise from myopia with an increase in the axial length of the eyeball. Reports have shown a positive correlation between the increasing axial length with lattice degeneration and retinal holes in 19 to 25 years old in Asian eyes (Chen et al., 2018). As a result, myopes are more susceptible (can be 20x higher) to retinal detachment than emmetropes (Pierro et al., 1992). Due to sclera thinning, posterior staphyloma is also much more common in high myopia adults (more than 23%). Due to the increase in axial length, the possibility of the liquefaction of vitreous in high myopia eyes occurs earlier, posing a severe threat that could lead to blindness compared to normal subjects(Akiba, 1993),

1.1.1.5 Burdens of myopia

Typical myopia management, such as glasses and contact lenses needed for individuals, will start to pile up the economic burden and social problems (Smith et al., 2009), which could be up to 202 billion USD annually. If the disorder worsens, related treatment costs will be expected to be much higher and put more pressure on individuals. Furthermore, other complications, such as loss of productivity and independence, will lead to an overall reduction in the quality of life (Smith et al., 2009). The combined costs of productivity and social security worldwide due to the burden of visual impairment caused by uncorrected myopia have exceeded 670 billion USD and are expected to rise to 1.7 trillion USD by 2050 (Holy et al., 2019).

On the social side, although it has not been a frequent complication of the matter, multiple studies have indicated peer pressure and the fear of discrimination (Gogate et al., 2013) are potential barriers to spectacles in primary school children (Aldebasi, 2013) or even if the spectacles were provided for free in older ages (Holguin et al., 2006; Keay et al., 2010; Odedra et al., 2008). Furthermore, consequences such as poorer academic scores, injuries, and impairment could impact the patient even more than they should.

1.1.2 Myopia management, interventions, and research

1.1.2.1 Spectacles/ optics

The refractive error associated with myopia has been corrected with spectacle lenses for centuries and later with contact lenses, which are still being improved for better biocompatibility and modalities. By adding a concave lens with correct adjustment in front of the cornea, light is focused correctly on the retina. Even though optical management mainly provides a temporary solution to correcting the disorder, this traditional method remains the most widely used solution in dealing with this eye disorder. In the last few decades, it has now been possible to reshape the patient's cornea through surgical procedures such as Laser in situ keratomileuses (LASIK) (Lindstrom et al., 1997). LASIK (Guell & Muller, 1996) utilizes laser (long term) to reshape the cornea, allowing light to travel and focus correctly on the retina. Small incision lenticule extraction (SMILE) (Sekundo et al., 2011) showed a high success rate in correcting myopia by using a small opening in the cornea similar to LASIK in reshaping the cornea allowing light to travel and to focus correctly onto the retina. Other non-surgical processes like orthokeratology (OrthoK) utilize a contact lens to alter the cornea's shape, allowing the light to focus correctly on the retina, correcting the refractive error (Cho & Cheung, 2012; Lui & Edwards, 2000). More recently, Defocus Incorporated Multiple Segments (DIMS) spectacle lenses have been a breakthrough in myopia control regimen shown to retard myopia progression in children with daily wear (Lam et al., 2020). This technology utilizes simultaneous

defocus rings on the lens, allowing the focal plane on the retina for myopia correction while the other myopic defoci act upon the different areas of the retina, such as peripheral sites. Based on this theory, newer contact lenses are now commercially available for controlling myopia progression (Chamberlain et al., 2019). Although with recent advances regarding the use of spectacles in myopia control, most of these are still seen as temporary solutions in managing refractive error. Myopia progression is still not prevented or reverted, as myopia is not directly cured without fully understanding the core mechanism of myopia (Wildsoet et al., 2019).

1.1.2.2 Pharmacological solutions

Efforts have also been turning towards pharmacological solutions in developing anti-myopia drugs in the form of eye drops such as atropine, pirenzepine, and 7-methylxanthine (7-mx) which have shown promising results in controlling and slowing the progression of myopia. **Atropine** is a nonselective muscarinic antagonist and is commonly used as a cycloplegic and mydriatic drug in ophthalmic practice (Rengstorff & Doughty, 1982). A lot of interest was drawn into this drug since the discovery of its potential effect on myopia progression in earlier studies (Bedrossian, 1979; Young, 1965), but the exact mechanism of how the drug suppresses myopia is still yet to be determined. Several clinical trials have been tested to see the effect of different concentrations of atropine to be used on myopia (Chua et al., 2006; Tong et al., 2009), and 0.01% of atropine was found to be an optimal concentration to use for myopia control (Chia et al., 2014) which were further confirmed in a 5-year follow up study (Chia et al., 2016). **Pirenzepine** is a muscarinic receptor antagonist which was found to inhibit the development of experimental myopia (lens-induced myopia (LIM) and form deprived myopia (FDM), which will be discussed in later Chapters) in animal studies such as tree shrew (Cottrill & McBrien, 1996), monkey (Tigges et al., 1999). In clinical trials, 2% pirenzepine was found to show suppression effects in myopic children (Siatkowski et al., 2008). **7-methylxanthine (7-mx)** is a nonselective adenosine receptor antagonist (Beach et al., 1985) which has shown a reduction in collagen

content in sclera associated with myopia axial elongation in rabbits (Trier et al., 1999) and myopic human children (Trier et al., 2008).

Although these drugs show potential effects as pharmacological options for myopia control, the mechanisms of these drugs are still unknown. Furthermore, common side effects such as dry eyes (Leo & Young, 2011), accommodative difficulties (Stacher et al., 1982), increased aberrations, and photophobia (Chiang et al., 2001) and in the combination of the concerns in safety profile in long-term slowed down the utilization of these drugs to be accepted widely in the community (Tkatchenko & Tkatchenko, 2019).

On top of that, it is challenging to provide a solution as the actual pathophysiology of myopia remains where a better understanding is needed to provide much more effective and targeted treatment in precision medicine in the prevention of myopia as it has become a leading health concern to be dealt with (Morgan et al., 2012).

1.1.2.3 Myopia animal models

The underlying mechanism of myopia progression is poorly understood; therefore, it is difficult to provide targeted treatments for myopia treatment effectively. To understand the underlying mechanism of myopia, several animal models were established in an attempt to see the myopia progression by a degree of myopia induction. The tree shrew (Sherman et al., 1977) and monkeys (Wiesel & Raviola, 1977) were one of the earlier models that have long been used in ocular research having advantages such as the composition of the sclera is similar to humans which are single-layered and as mammals which are closer to humans and their eye growth can compensate to defocus during a specific period. However, the complexity of handling and breeding made this model more challenging. The avian chick model has been well-established in ocular research (Holden et al., 1988; Schaeffel et al., 1988; Wallman & Adams, 1987; Wallman et al., 1981) due to the large eyeball size as well as the fast-natural growth of chicks made it a preferable choice for a lot of ocular studies and will be discussed below. Other animal models such as guinea pig (Howlett & McFadden, 2006), zebrafish (Collery et al., 2014), and mice (Barathi et

al., 2008; Tejedor & de la Villa, 2003) have also been successfully developed for ocular research to resemble the human eye refractive development.

There are two main methods of introducing myopia in animal models (Morgan et al., 2013): Lens-induced myopia (LIM) is where a negative lens is placed in front of the eye, inducing a blurred and hyperopic defocus environment for the eye. It can be seen as a closed-loop condition as the eye covered with the lens will compensate for the lens power and cause induced myopia with eyeball elongation (Sebag, 2014). Form deprivation myopia (FDM) is where a diffuser is applied in front of the eyeball, which will cause the eye to have no clear focal points. Therefore, the eyeball will elongate without proper focusing and can be seen as an open-loop condition.

With that in mind, the chick (*Gallus gallus domesticus*) model has been used extensively in myopia research (Megaw et al., 1997; Schaeffel et al., 1988; Troilo & Wallman, 1991; Wallman & Adams, 1987; Wallman et al., 1981). The complete genome of the chick (*Gallus gallus*) also allows more in-depth proteogenomics studies. It is widely seen as a suitable candidate due to its many advantages: A relatively large eyeball size (8- 14 mm) (Waldvogel, 1990), a fast growth rate (about 100 μ m per day), high availability (eggs), the cheap cost to operate and maintain (house facilities and equipment) as well as its ability for accommodation (around 17 D)(Schaeffel & Howland, 1987). However, as the chicken is a non-mammalian animal, there are some differences in the humans eye, such as the lack of fovea, differences in scleral composition (with a much higher % of cartilage) as well as the accommodation mechanism (cornea)(Glasser & Howland, 1995). It has been demonstrated that the chick's eye can emmetropize during growth, resembling the human eye growth, but at a much faster rate (Troilo & Wallman, 1991; Wallman et al., 1981). Furthermore, a growing chick eye can compensate for the introduction of an optical lens (Lens- induced myopia) by adjusting to the power of the lens (Schaeffel et al., 1988) as well as the use of form- deprived lens (FDM) in the change of optics degrading the retinal image without the need of the removal of the optic nerve (Troilo et al., 1987; Wildsoet & Pettigrew, 1988). With these advantages

in mind, the chick model remains ideal for studying molecular mechanisms and drug effects for myopia control.

Several possible myopia-related biomarkers were identified using these animal models: The gene Early growth response protein 1 (Egr-1/ ZENK) was found to be upregulated in myopic defocus and downregulated in hyperopic defocus in the chick retina. (Bitzer & Schaeffel, 2002; Brand et al., 2005; Fischer et al., 1999). Glucagon, which can be found in the amacrine cells, was also an inhibitor of myopia in chicks (Buck et al., 2004). Recent studies have shown that dopamine levels are affected by the retinal image brightness and the contrast of the retinal image (Feldkaemper et al., 1999). The dopamine content was dropped during the development of FDM, and its agonists may play a role in inhibiting myopia (Stone et al., 1989). It was also proposed that bright light inhibits myopia progression as it could be partially suppressed in FDM and LIM chick models (Ashby et al., 2009; Cohen et al., 2012). Vasoactive intestinal peptide (VIP) showed a positive correlation with the increase in vitreous chamber depth (Tkatchenko et al., 2006) in chicks, and its receptor (VIPR2) levels were altered in chick retina and choroid during FDM (Liu et al., 2005). While most of these studies were focused on the retina, and its neighboring tissue, the vitreous remained less studied due to its highly hydrated nature (where 99% of it is water). This however, raised an interest as the vitreous chamber depth (VCD) is one of the main contributors in myopia progression and advancements in analytic techniques (such as the more sensitive proteomic approaches) offered the possibility of revealing more understanding in this tissue and will be discussed in details in the next few Chapters.

1.2 Vitreous- An overview

During myopia progression, VCD changes the most during eyeball elongation. The vitreous will catch up to the elongation progress while maintaining homeostasis within the eye. However, sight-threatening complications such as posterior vitreous detachment (PVD) (Akiba, 1993) as well as retinal detachment (Alimanović-Halilović, 2008; Devin et al., 2011; Sasoh et al., 2000; Williams & Hammond,

2019) could arise if the eyeball elongates too much as the vitreous on the side starts to detach.

Vitreous has been traditionally labeled mainly for its contribution to providing ocular clarity as well as the maintenance of the shape of the eyeball. It comprises 98-99.7% water, while the remaining 1% includes hyaluronic acid, organic salts, and soluble and insoluble proteins (collagen- mainly type 2) firmly attached to the vitreous base and around the optic disc.

Physically being a transparent gel-like liquid, little attention was paid to the vitreous as it is also easily removed from surgical procedures like vitrectomy without surgical complications to ocular health (Bishop, 2000; Foulds, 1987). However, complete removal of the vitreous will cause other problems, such as the collapse of the eyeball and reduced ability in homeostasis. Its role in the exchange of molecules to its neighboring tissues and the structural support indicates the vitreous to be a necessary part of the eyeball. Furthermore, due to its location within the eyeball, the vitreous has been an ideal location for loading drugs towards the posterior side of the eyeball, allowing drugs to reach the macula and retina.

1.2.1 The physical location of the vitreous

The vitreous is a transparent gel-like tissue bound anteriorly by the lens and ciliary body and posteriorly to the retina (Figure 1.3). The vitreous is a vascular structure that fills up the space of the eyeball (Fishman, 1990; J, 1989; Le Goff & Bishop, 2008). It takes up to 80% of the total volume of the eyeball having around 4 mL and about 16.5 mm in axial length in a healthy emmetropic adult eye. There are several places where the vitreous is attached and are mainly basement membranes, such as the pars plana of the ciliary body and the inner limiting membrane of the retina, where others have the weakest attachment to retinal vessels. The vitreous attaches the strongest at the anterior part at the vitreous base and the posterior side to the edge of the optic disc and the macula lutea. The hyaloid layer/ membrane is the layer where the vitreous lies in contact with the surrounding. Anteriorly, the anterior hyaloid membrane over the vitreous body near the ora Serrata, lies in contact with pars plana, ciliary body, ciliary zonules, and post-lens capsule. This

membrane connects with other intraocular structures by following fine ligaments of the hyalociliary zonules. The hyaloideocapsular ligament of weiger / Retrolental ligament is another place to which the vitreous is firmly attached. This is a circular adhesion at the lens's posterior capsule. However, this strong adhesion will slowly reduce with age.

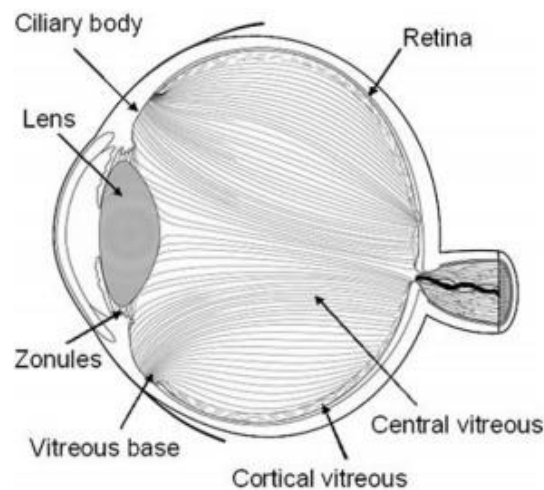


Figure 1.3 The Vitreous anatomy inside the eyeball; Figure adapted from Le Goff and Bishop, 2008.

The vitreous base lies within the posterior side of the pars plana and adjacent to the anterior side of the ora Serrata, and it is denser than the vitreous cortex (Balazs EA, 1972; BP, 1981).

Posteriorly, the membrane layer extends from the vitreous base up to the optic disc, where the posterior hyaloid layer lies in contact with the internal limiting membrane of the retina. At these sites, the vitreous fibers and the basement membrane of the non-pigmented epithelium of the ciliary body made a strong connection for vitreous adhesion. The membrane at the interfaces varies in thickness, and it is the thickest around the macula than the parts around it (Foos, 1972).

The cortical vitreous (vitreous cortex) forms the outer side of the vitreous in the peripheral zone (0.2- 0.3mm in width in humans). It resembles around 2% of total vitreous and consists mainly of Type II collagen fibrils forming a condensed

fibrillar structure. These strong collagen fibrils run parallel and perpendicularly toward the retinal surface providing viscosity, elasticity, and tensile strength for the vitreous. This is also the location for cell synthesis, as the metabolic center for hyalocytes (90%) and fibrocytes & glial cells (10%).

The central vitreous (vitreous core) forms the major part of the vitreous body. It has a less fibrillar structure than cortical vitreous, and it is cell-free with a meager amount of hyalocytes, with the hyaloid canal passing by in the middle. The central vitreous is in a complete gel shape at birth due to the high level of collagen composition (no liquid is found at <4 years of age in humans). The gel volume is stable until age 40, when it begins to steadily decline throughout the remainder of life, slowly losing its elastic properties due to liquidation of the vitreous (Balazs, 1993).

Reports have shown that around 98% of vitreous's content is water (Ali & Bettelheim, 1984), while the rests are proteins and salts. In humans, the protein concentration ranges from 0.5 to 1 mg/ml. This indicates that although the water content is high, the proteins within are variable and complex. Early studies of protein investigation in vitreous contain around 60-80% serum albumin using electrophoresis (Cagianut & Wunderly, 1953), while others are iron-binding related proteins (Van Bockxmeer et al., 1983), such as transferrin which is found in rabbit studies (Laicine & Haddad, 1994).

1.2.2 Composition of the vitreous

1.2.2.1 Collagen

Collagen is the main fibrillar protein inside the vitreous, with a concentration of around 100 µg/ ml in humans. The collagen content/ amount in the vitreous doesn't change throughout the lifespan (Bishop et al., 1994). These fibers are responsible for maintaining structural integrity by supporting the vitreous shape. Various collagen types are co-assembled into heterotypic collagen fibrils, forming a non-crosslinked random network with a triple-helical polypeptide chains (alpha chains)

configuration. Type II collagen is the primary collagen type in the vitreous (60-75%) (Bishop et al., 1994), offering its strength in the vitreous and giving it elasticity- gel-like properties when arranged in staggering arrays. The rest are Type IX collagen (up to 25%) (Bos et al., 2001), and the core of the fibrils is made up of Type V/XI collagen (10-25%) (Bos et al., 2001). Type II collagen is found coated around core fibers, forming the core fibrils bundles of chondroitin sulfate glycosaminoglycan chains of type IX collagen. The distribution of collagen type II is not equal in the eye: the highest level is at the vitreous base, where the collagens are synthesized, and decreases towards the central medullary vitreous. Then the amount is increased again in the posterior vitreous cortex adjacent to the retina. The overall amount of collagen is not regenerated and remains more or less constant after prenatal development. As collagen provides the structural integrity of the vitreous, losing it will turn the vitreous into a viscous liquid.

1.2.2.2 Hyaluronic acid/ Hyaluronan

Hyaluronic acid (HA) was first isolated from the vitreous in the 1930s by L.Meyer and J. W. Palmer (Meyer & Palmer). The stabilized hydrated HA and collagen network prevents the movement of molecules, and the highest concentration of HA is found in the posterior vitreous cortex (Snowden et al., 1982). Inside the vitreous, HA forms a meshwork with the collagen fibrils in a randomly assigned fashion (Sebag & Balazs, 1989). Hyalocytes produce HA, a polysaccharide known as a glycosaminoglycan (GAG), are compounds made up of repeating disaccharide units (sugar). The content of HA is found unevenly distributed throughout the vitreous, where it has its highest concentration in the posterior cortical gel. HA has a very high affinity for water and an enormous size for the hydrated molecule. Figure 1.4 shows HA's chemical structure and its repeating units.

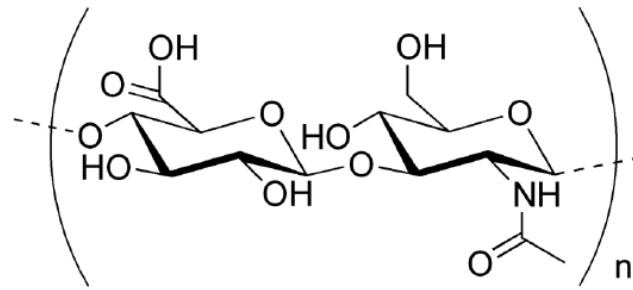


Figure 1.4 Vitreous composition with the meshwork containing hyaluronan and collagen fibrils; Figure adapted from Le Goff and Bishop, 2008.

The networks of collagen and hyaluronan meshwork are found inside the vitreous, while collagen fibrils offer the gel state and tensile strength (shown in Figure 1.5). Hyaluronan fills up the space between these fibers and swelling for the inflation of the gel, giving it a gel-like status (Halfter et al., 2005).

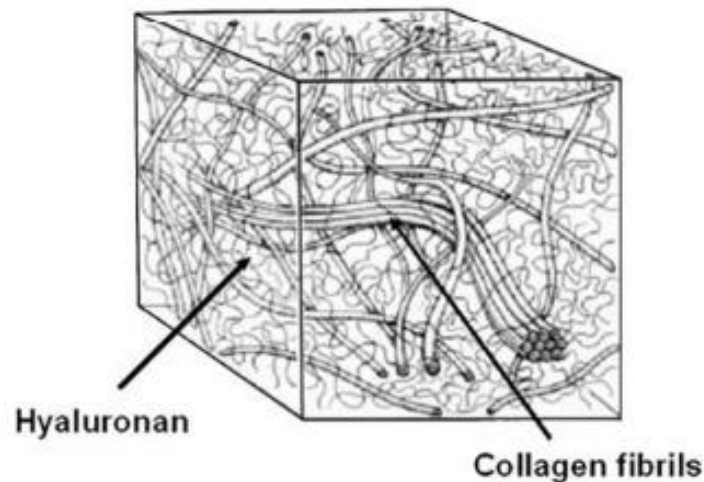


Figure 1.5 The overall vitreous meshwork with hyaluronan filling up between the collagen fibrils. Figure adapted from Halfter et al., 2005.

1.2.2.3 Proteoglycans and glycosaminoglycan

As mentioned earlier, HA is a type of glycosaminoglycan (GAGs). Other glycosylated proteins- can be found inside the vitreous, covalently attached to the core proteins. With HA being the main GAGs in the vitreous, the others can be found in a small amount. Chondroitin sulfate (CS) is an extracellular matrix component that includes versican and collagen type IX (Theocharis et al., 2008), which carries multiple CS chains and binds to HA. Another is Heparan sulfate (HS), which includes Agrin- a major component of basement membranes found between collagen fibrils and presented during development. The level declines rapidly in the adult stage (Halfter et al., 2005).

1.2.2.4 Opticin

Opticin is an extracellular matrix glycoprotein with leucine-rich proteins that bind to collagen to regulate fibril morphology and organization. It attaches to type II collagen, filling these collagen fibrils' space and bringing CS and HS together. It has been shown that opticin could regulate growth factors during development in an 8-day-old chick embryo (Sanders et al., 2003) by binding to HS and CS (Hindson et al., 2005).

Apart from these proteins identified, several metabolites such as glucose, ascorbic acid, fatty acids, and prostaglandins were also found in the vitreous, showing their active role in metabolism around the surrounding tissues. As vitreous is kept within the compacted space, this has the advantages in therapeutic as it will prolong the therapeutic effects in certain ocular disease treatments such as AMD, but this also causes other problems. The breakdown in the blood-ocular barrier will lead to inflammatory cytokines and angiogenic factors being stored in the vitreous and will remain in the vitreous, commonly seen in vitreous hemorrhage in which surgery is required for the removal of blood. The gel structure promotes angiogenic factors such as VEGF for neovascularization and the high ascorbic acid content maintain a low level of oxygen (in normal conditions), preventing oxidative stress, which has been seen to lower oxygen tension in both retina and lens after vitrectomy predisposes to cataract formation (Holekamp et al., 2005). The gel-like

characteristics are mainly due to HA and elastic characteristics from the combination of collagen + HA. This visco-elastic property can absorb energy rapidly and release it slowly, protecting the retina from shock and head injuries.

1.2.3 Vitreous- the missing gap?

Studying the proteomics of the vitreous is vital as the VCD is the main contributor during myopia progression in the axial length elongation, affecting the refractive error (Pickett-Seltner et al., 1988; Wallman & Adams, 1987). Additionally, its location close to other tissues and its inert properties provided an ideal candidate for a compartment for potential drugoffload for therapeutic device/ drugdelivery strategies, as this offers a much higher dissociating rate than just eyedrops alone.

Studying the vitreous proteome allows us to understand the mechanism underneath the myopia progression since previous studies of the vitreous proteome indicate that a large number of structural proteins were presented within the highly hydrated tissue. Furthermore, other proteins provide a wide range of functions, such as oxidative stress regulation, energy metabolism, and immune functions (Skeie et al., 2015). Technical challenges such as the difficulty in the detection of lower abundant proteins in a very dilute tissue (99% of water) as well as the small magnitude of differential proteins found under myopia progression (Yu et al., 2017), studies of myopia progression aiming specifically towards the vitreous are still scarce. Our group was among the first to utilize mass spectrometry (MS) as a diagnostic tool for looking at the vitreous under this ocular complication (Yu et al., 2017), suggesting that it was apparent that the vitreous is more bioactive than what we initially believed. As to our knowledge now, in recent myopia studies related to the vitreous, a comprehensive library has not been completed or established, nor have the attempts to quantify myopia biomarkers in depth. This project employs a next-generation proteomics platform with a combination of high-speed nano-liquid chromatography-mass spectrometry (LC/MS) in an attempt to produce a most comprehensive chick vitreous proteome as well as the quantification of differentially expressed proteins covering the normal and lens-induced chick

myopia (LIM) model in the combination of protein validation using multiple reaction monitoring (MRM) techniques.

1.3 Introduction to proteomics

Amino acids (AA) are the building blocks of life that build up into biological molecules called proteins. Proteins are responsible for many functions, including maintaining structural integrity, cellular activity, signaling between cells, regulatory functions, and many more, all of which are essential functions of life (Timp & Timp, 2020). A proteome is “the entire protein complement expressed by the genome in an organism or a cell type” (Wilkins et al., 1996), where a unique proteome can be presentable from each species. And based on this, the term proteomics is referred to be the study of the proteome (Tyers & Mann, 2003) which can be applied to a wide range of fields. Proteomics studies aim to see the dynamic changes of the protein cascade, analyzing the protein changes at a specific time frame, with the specific changes of the target (treatment) compared to its normal conditions. Mass spectrometry has long been used in the analytical industry to separate, analyze, and purify a compound mixture. With the advancements throughout time, modern mass spectrometer nowadays has a much high resolution and sensitivity compared to older generation MS, allowing accurate comparison and analysis of samples in a short period. Furthermore in pharmaceutical areas also for the development of drug candidates and signaling proteins, and mainly in the discovery of identification and quantification of proteins in different disease models for possible disease treatments (Amiri-Dashatan et al., 2018; Geyer et al., 2017).

Most common and the majority of proteomic studies are the bottom-up method, where proteins are lysed or digested into peptides using enzymes such as trypsin/Ly-c (Chait, 2006; Hughes et al., 2010; Nesvizhskii & Aebersold, 2005) to cleave into short segments at the C-terminal of peptide bonds at lysine and arginine (Olsen et al., 2004). These digested peptides are then ionized, and these ions are separated according to their mass/ charge ratio (m/z) for ion detection using a mass spectrometer. Peptide fingerprints will be produced as a result that would be used to correlate into known proteins using search databases such as Mascot or Sequest (Resing & Ahn, 2005). However, as multiple peptides are digested, it might be challenging for the distinguishment of identical masses of AAs that are produced when database searching (Resing & Ahn, 2005). Seeking to tackle these problems, top-down proteomics on the other hand introduce whole protein analysis to detect

the whole protein sequence or scaffold (Catherman et al., 2014; Siuti & Kelleher, 2007). Top-down analysis requires the intact protein ions by electrospray ionization (ESI) into a gas phase for disassociation in the mass spectrometer, resulting in protein and fragment ions. It has advantages in PTM and isoform determination, but limitations such as hard for fractionation as it is in the ionization in the gas phase. Furthermore, the high cost of equipment hampers the implementation of large-scale processing as well as the long processing times from dissociation techniques such as Electron-transfer dissociation (ETD), resulting in a lower throughput in comparison to the bottom-up approach (Gregorich et al., 2014). The bottom-up approach will be used throughout this thesis and will be discussed in detail in the next Chapter.

1.3.1 Information-dependent acquisition (IDA)

Information-dependent acquisition (IDA) is a common data acquisition method of shotgun proteomics (bottom-up proteomics technique) in the identification of proteins and complex peptides mixtures in proteomic studies, where samples are ionized and put through into the mass spectrometer (Link et al., 1999; Yates, 1998, 2004). Based on the mass-to-charge (m/z) ratio, the detector was then able to detect the intensities during the mass range and period. From the initial time-of-flight (TOF)/MS scan, ionized species of the precursor ion with high intensity (over the threshold set by the user) will then be fragmented by the collision energy, selecting for isolation tandem mass analysis (MS/MS) scans for the determination of the peptide sequences. This method is widely used in proteomic studies because it can scan through the sample to produce a “full” spectrum of information. However, due to how only ions with high intensity are selected, it could create problems as it could be covering some of the less abundant ones due to the limited scan rates.

Using the IDA workflow, digested peptides are introduced into the MS by 2 common ionization methods: **Matrix-assisted laser desorption/ionization laser (MALDI)**, where samples are firstly mixed and dissolved in a matrix on the probe surface and a laser such as nitrogen UV light (337 nm) will be used to strike the matrix on the surface (Karas & Hillenkamp, 1988; Tanaka et al., 1988). With the

matrix absorbing the heat energy, parts of the matrix will then be heated up and vaporized (carrying the sample). This will convert into the gas phase to be ionized and then be separated by a TOF analyzer. Another ionization method is liquid chromatography (LC) coupled with **electrospray ionization (ESI)**. Where peptides are carried in a liquid phase, they will travel through a strong electric field, with a capillary tube into an ion spray for ionization. This produces highly charged (positive or negative) droplets. The Evaporation of droplets turns the ions into the gas phase via the ESI method, for the molecular weight of the precursors to be profiled by the MS (Fenn et al., 1989).

Ions are analyzed by their mass-to-charge ratio (m/z) and intensity, where tandem mass spectrometry picks the highest abundance for fragmentation. When the intensity/ abundance of these fragments reaches a certain threshold, tandem mass MS or MS/MS will be triggered, and a second fragmentation will occur in tandem for spectra collection. Acquired data are then analyzed with a database search which assembles peptides into corresponding proteins (Zhang et al., 2013). The peptide abundance from IDA acquired data are usually measured quantitatively using spectral count and ion signal intensity (Zhu et al., 2010), but due to the lack of reproducibility (~ 75% in two IDA runs, and will be reduced the more IDA injections are included) from how IDA works on fragment selection (Choi et al., 2008; Kapp et al., 2005; Liu et al., 2004; Tabb et al., 2010; van Midwoud et al., 2007), data-independent acquisition (DIA) was looked into to overcome these limitations, which will be discussed next.

1.3.2 Data-independent acquisition (DIA)- SWATH-MS

As mentioned earlier, IDA triggers MS/MS based on the intensity threshold. On the contrary, DIA collects data Independently from the previous scans, therefore collecting all peptide fragments ignoring the intensity threshold (Chapman et al., 2014). Sequential Window Acquisition of all THEoretical Mass Spectra (SWATH) acquisition is a label-free method that allows the possibility of protein quantitation (Gillet et al., 2012). A 25 Da precursor window or variable size m/z windows are set to scan across a mass range of interest, passing the ions into the collision cell

for the entire liquid chromatography separation. Ions are then fragmented and analyzed by the TOF analyzer. Because of this small window scanning throughout the spectrum, a very fast scanning time will be needed. This method is data-independent (DIA) since it does not need to rely on the precursor ion as the whole spectrum is scanned throughout the duration (Guo & Huan, 2020). Peak selection of full scan, IDA, and DIA are shown in Figure 1.6. As multiple windows were applied throughout the mass range, fragmented ions in the given window will be more easily associated with their precursor ion, and more specific MS and MS/MS spectra will be obtained. However, the data acquired from SWATH-MS mode will require a known database (from IDA mode) for spectra matching and processing, therefore, a comprehensive database will be needed for possible protein quantitation using this method.

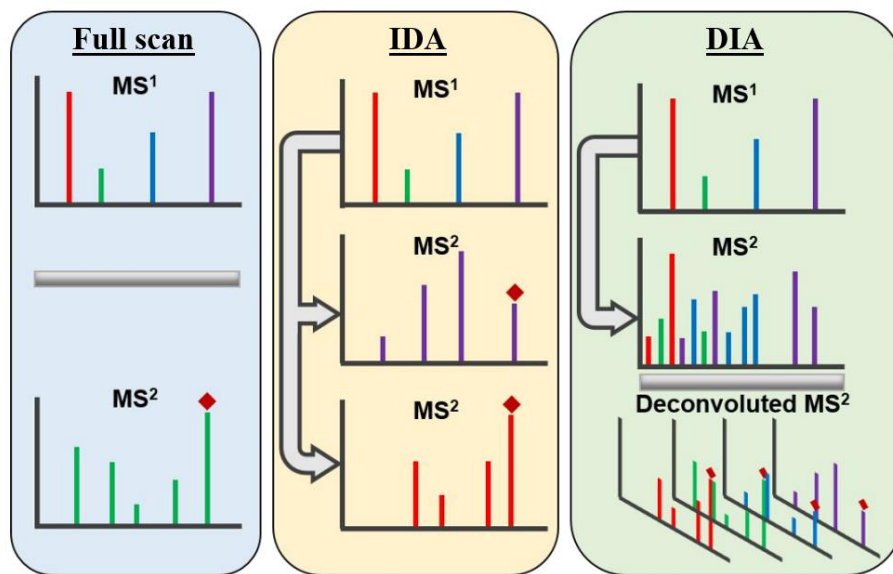


Figure 1.6 The workflow of peak selection for an initial full scan, IDA: where a certain intensity threshold must be reached for MS/MS fragmentation, and IDA: where all are fragmented. Figure modified from J. Guo and Huan, 2020.

1.3.3 Targeted proteomics

While the discovery approach taken using IDA/ DIA maximized the chances for protein numbers, this approach lacked the power of detecting or quantitating lower

abundance proteins. With a high chance that the proteins or peptides of interest are often low abundant, confirmation or validation of these proteins remains difficult due to the limitations of the traditional IDA method (Picotti et al., 2013; Shi et al., 2016; van Bentum & Selbach, 2021) on how MS/MS are selected basing on the intensity threshold.

In contrast to the discovery approach, single/multiple reaction monitoring (SRM/MRM) and parallel reaction monitoring (PRM) are more targeted methods in proteomics. This targeted approach has been used in proteomics for the validation of specific peptides, which offers a more sensitive and specific quantitation approach (Alex Hu et al., 2016; Kondrat et al., 1978; Vidova & Spacil, 2017) in the validation of specific peptides. In contrast to the traditional shotgun proteomics, the MRM targeted approach targets specific peptides by selecting the precursor mass of the known peptide for tandem MS/MS fragmentation (Figure 1.7). For a successful MRM run, a predesigned transition list from the peptides of the target protein must be obtained, and the first quadrupole (Q1) of the MS will be able to select and transfer the precursor ions for fragmentation in the second quadrupole (Q2). The fragmented ion (product ion) will then be transferred to the third quadrupole (Q3), which will only detect ions with the specific predefined m/z, which ensures specificity. This allowed specific peptides to be identified within the selected time frame while ignoring all the other peptides for fragmentations, therefore allowing a longer dwell time, resulting in a higher signal-to-noise ratio (S/N) for more precise differentiation of peaks. Similar to SRM/MRM, the high-resolution multiple reaction monitoring (MRM^{HR}) utilizes the SWATH-MS mode which offers rapid and reliable results in a target acquisition mode on a quadrupole-time of flight instrument (Q-TOF) while requiring a much lower volume/concentration of samples needed with the nanoLC (Montemurro et al., 2020; Sze Wan Shan et al., 2018).

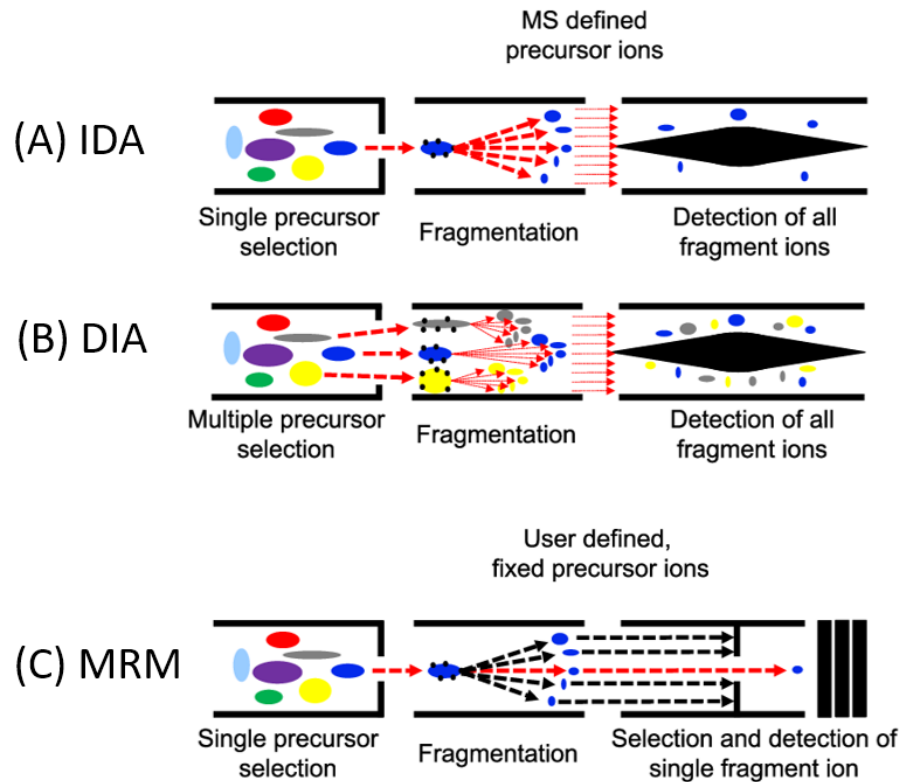


Figure 1.7 (A) The precursor ions are selected by the instrument based on abundance. (B) All the precursor ions within a selected mass range are selected in DIA mode for fragmentation and analysis. (C) Only a selection of precursor ions is selected for fragmentation and analyzed for a more targeted approach. Figure modified from A. Hu et al., 2016.

1.3.4 Proteomic applications in eye research

Limitation in the traditional way of proteomics with the use of 2-DE based in the discovery of a comprehensive system, hampers early studies in the field of ocular research as this technique poses a lot of disadvantages. These includes the limited ability in dealing with a high dynamic range of proteins, and often only high abundant proteins can be identified while covering up the low abundant proteins (most often with the use of Coomassie Brilliant Blue (Skeie & Mahajan, 2011)), as well as the high time-consuming process, hampering the number of proteins to be identified in the use of ocular tissues. Proteomic-based research began to gain popularity in the ocular research field enabling numerous potential biomarkers to

be identified in several ocular diseases such as myopia (Bertrand et al., 2006; Yu et al., 2017), diabetic retinopathy (Gao et al., 2008; Kim et al., 2007; Loukovaara et al., 2015), and diabetic macular edema (Ouchi et al., 2005). And with recent efforts in the Human Eye Proteome Project, identified proteins from different tissues within the human eye (Figure 1.8) have now been grouped and updated constantly (Ahmad et al., 2018)

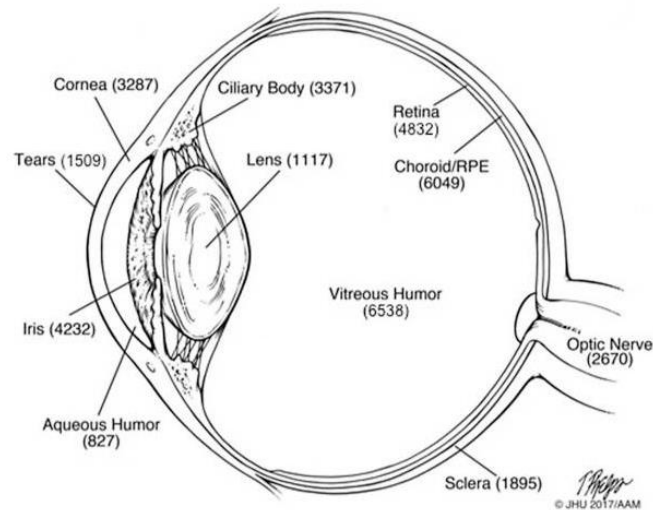


Figure 1.8 The number of proteins found in various proteomics studies of the human eye. Figure adapted from Ahmad et al., 2018.

Most proteomics studies on the vitreous have been done on proliferative diabetic retinopathy (PDR), as this is often the case for patients that undergo surgery, where the vitreous was often taken out (Steely & Clark, 2000). Vitreous transferrin was one of the earliest proteins to be identified within the vitreous using the proteomics approach (Laicine & Haddad, 1994) since it is one of the most abundant proteins in the vitreous. Yamane et al. demonstrated the ability to identify vitreous proteins in proliferative diabetic retinopathy and idiopathic macular hole using 2-D gel separation with the combination of ESI and MALDI, showing over 141 proteins (Yamane et al., 2003). The same group identified 463 proteins from idiopathic macular hole patients with the use of silver-stained 2D gels (Yamane et al., 2003), 28 proteins from diabetic macular edema (DME), and non-DME patients using SYPRO-RUBY-stained 2D-gel (Ouchi et al., 2005). Ouchi et al. used 2D gel electrophoresis and were able to identify the differentially expressed ApoA-1 and

pigment epithelial-derived factor (PEDF) in the vitreous of diabetic macular edema (DME) patients compared to normal counterparts (Ouchi et al., 2005). Skeie et al. isolated each part of the vitreous and studied the unique protein profiles by using one-dimensional (1D) sodium dodecyl sulfate-polyacrylamide gel electrophoresis (SDS-PAGE) (Skeie & Mahajan, 2011). As technology advances, the introduction of nano-LC/MS and MALDI-MS allowed a more precise separation of the peptides to be identified with MS. Kim et al. managed to identify 531 proteins from proliferative diabetic retinopathy and nondiabetic patients with the help of immunoaffinity subtraction (Kim et al., 2007). Hernández, C et al. quantified differentially expressed proteins in VH of PDR patients compared to non-diabetic subjects, identifying 8 up-regulated proteins including ApoA1 and ZAG using 2D fluorescence difference gel electrophoresis (DIGE) (Hernández et al., 2010). With the help of fractionation methods (SCX, SDS-PAGE), Murthy et al. identified over 1000 proteins in the vitreous making it one of the most completed human vitreous proteomes to date (Murthy, Goel, Subbannayya, Jacob, Murthy, Manda, Patil, Sharma, Sahasrabudhe, Parashar, Nair, Krishna, Prasad Ts, et al., 2014). Several myopia studies have been looked at, including FDM and LIM in chicks (Lam et al., 2007; Yu et al., 2020) and in the monkey. However, published research on vitreous specifically looking into myopia is still scarce. Our group was one of the first to quantify DEPs such as APOA-1 using isotope-coded protein label (ICPL) in the vitreous with the LIM chick model (Yu et al., 2017).

1.4 Research gaps

Vitreous humor (VH) is a transparent gelatin-like substance that takes up two-thirds of the eyeball and alters the most during eye elongation, covering normal growth and abnormal growth periods such as myopia. As myopia can be seen as an excess growth of the eyeball, quantitative proteomics on the normal ocular growth period and the myopia progression period in the VH could provide new insights into understanding its progression mechanism in the early stages of myopia. VH being highly hydrated (making the sample more diluted in terms of protein content), and the gel-like elasticity properties made it more challenging, hampered the advancement in ocular proteomics studies with the VH using conventional proteomic techniques such as the top- down 2D gel electrophoresis. With the more robust and sensitive SWATH-MS-based proteomics workflow, a more global and comprehensive analysis of the VH and the identification and quantification of growth and myopia-related biomarkers during myopia progression while using less sample consumption with high sensitivity. The biomarkers identified in this study may allow more understanding of the mechanism of myopia progression and provide novel pharmaceutical approaches for tackling this highly prevalent refractive error.

1.5 Study objectives of the present study

1. Establishment of the LIM chick model and optimization of the vitreous sample preparations and label-free proteomic workflow for SWATH-MS.
2. Generation of a comprehensive normal growth chick vitreous proteome during emmetropization and the use of SWATH-MS for protein quantitation.
3. Identification and quantitation of differential protein changes during myopia progression using established chick LIM model and SWATH-MS workflow.
4. Validation of selected differential expressed proteins (DEPs) identified from the previous studies using the MRM^{HR} approach and qPCR.

Chapter 2. Animal model and general experimental setup for proteomics

The general proteomics workflow used in this study is shown in Figure 2.1, and the details of each step will be shown in this chapter.

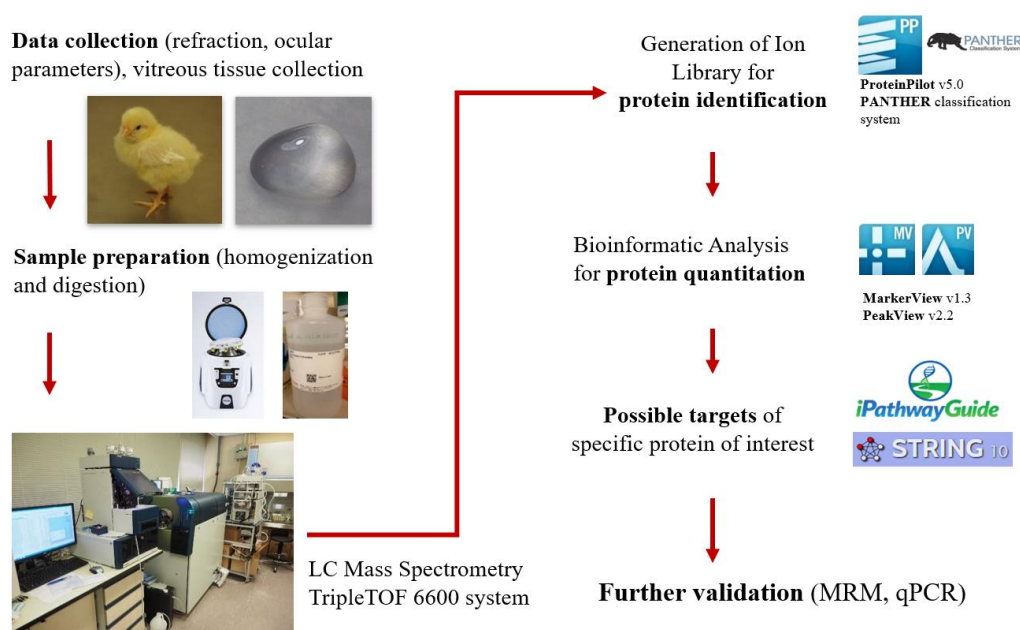


Figure 2.1 An overview of vitreous proteomics workflow used in this study, from chick vitreous collection to data analysis using MS.

2.1 General animal handling and biometric measurements

2.1.1 Eggs

SPF white leghorn chick eggs were ordered from Jinan poultry CO., LTD, China, and incubated locally in the centralized animal facilities (CAF) at the Hong Kong Polytechnic University. Eggs were placed in a large egg incubator (ELYE-3, Onelye, China) for 21 days with an average temperature of 36.6 °C and a humidity of 68 g.kg⁻¹ while rocking up and downwards on the holder. After 21 days, the eggs were moved to a smaller egg hatcher (EH-96H, Onelye, China) under the same

temperature and humidity conditions for 1 week for eggs to hatch (shown in Figure 2.2 A and B).

2.1.2 Chicks raising condition

Newly born white leghorn chicks at 3 days of age were raised in-house in stainless steel brooders under a 12/12 dark/ light cycle with an average luminance of 500 lux at the center of the cage inside the breeding room with an automatically controlled temperature environment of an average temperature of 25.8 °C and a humidity level of 41.8% during the housing period (shown in Figure 2.2 C). All chicks were given *ad libitum* access to food and water. Handling and operations throughout the experiment were in compliance with the ARVO statement for the Use of Animals in Ophthalmic and Vision Research and approved by the Hong Kong Polytechnic university animal subjects ethics sub-committee (ASESC).



Figure 2.2 Chicken breeding equipment and lighting setups. (A) Eggs were placed in the large egg incubator with temperature and humidity controls for 21 days. Each stack of egg holders was allowed to rock up and down to ensure airflow. (B) Eggs were transferred into a smaller hatcher under the same environmental condition for chicks to hatch. (C) Breeding room with stainless steel brooders under a 12/12 dark/ light cycle with an average luminance of 500 lux at the center of the cage and automatically controlled temperature environment.

2.1.3 Chick model setup (Normal and Lens-induced myopia)

For normal growth study, chicks were raised in housing conditions mentioned above for up to 28 days without any lenses (shown in Figure 2.3 A). For myopia studies (lens-induced myopia model, LIM), chicks were raised to 7 days old and then induced to ametropia by a negative (-10D) lens made from polymethyl methacrylate (PMMA). The lens was attached to a random eye of the chick according to the during of different studies (LIM3: 3 days and LIM7: 7 days). A velcro ring lens back (15 mm in diameter) was glued on the fur to the area around the eye using epoxy resin a day before lens induction. Then the -10D lens was mounted to a google frame with a base curve of 6.7mm and an optical zone of 11 mm in diameter, shown in Figure 2.3 B. Lenses were cleaned every day to prevent dirt from getting onto the lens, which could affect the vision of the chick.

2.1.4 Biometric measurements

Measurements of ocular growth and weight were taken at set time points at each measurement date. Tissue was used to wrap around the chick for containment. An A-Scan ultrasound system (5073PR, Olympus, Japan) coupled with a 30 MHz probe (PZ25-025-R1.00, Panametrics, USA) and an adjustable pump system (505u, Watson Marlow, UK) was used to measure ocular components for ocular growth measurements shown in Figure 2.3 C. Saline was used to connecting the prob to the eye and water was used for calibration (1.46x). A lid retractor was used to keep the eye open during measurements and anesthesia was not applied to avoid any

potential protein changes due to the drug's effect. An average of 3 repeats of measurements were done on each eye for analysis. Ocular components including the (A) anterior chamber depth, (B) lens thickness, (C) vitreous chamber depth, (D) retina thickness, and choroid thickness are shown in Figure 2.3 D were analyzed and compared in this study. The refractive error was measured using a streak retinoscope (Beta 200 Streak Retinoscope Set 2.5v, Heine, Germany) with a trial lens bar ($\pm 16.00D$ in $0.5D$ steps) in dim light conditions, shown in Figure 2.3 E. Equivalent sphere measurements were used to define the refractive error in this animal study ($S. E = \text{Spherical power} + \frac{1}{2} \text{cylindrical power}$). The weight of each chick was measured using an electronic balance (200M, Precisa, Switzerland) after A-scan and refractive measurements.

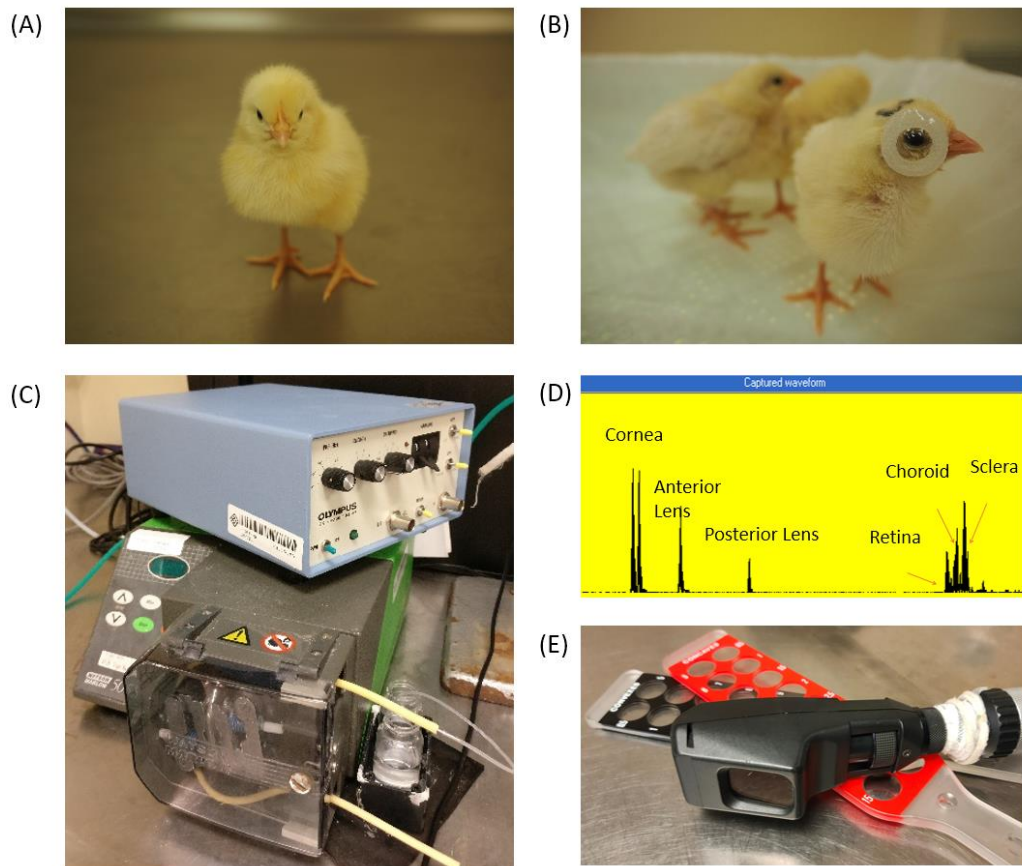


Figure 2.3 Normal and lens-induced myopia (LIM) chickens along with A-Scan and refractive error measurements equipment. (A) Normal growing white leghorn chicks at 3 days post-hatch. (B) -10D PMMA lens attached to one side of the eye of the chick's eye using a velcro ring. (C) A-Scan Ultrasound system setup connected with an adjustable pump system. (D) A-Scan ultrasound peaks for ocular component diameter measurement showing the cornea, lens, retina, choroid, and sclera thickness. (E) Refractive measurements using steak retinoscopy with trial lens bars.

2.2 Vitreous humor (VH) tissue protein and peptide extraction

2.2.1 Vitreous collection

Chicks were sacrificed with CO₂ overdose, and the optic nerve was cut immediately to isolate the eyeball. The eyeball was then kept and washed with ice-cold

phosphate-buffered saline (PBS). Any excess surrounding muscle around the eyeball was carefully removed using a small pair of scissors while on an ice-cold plate shown in Figure 2.4 A. The eyeball was washed again with ice-cold PBS to remove excess blood. The eyeball was then hemisected equatorially using a razor blade, cutting the eyeball into the anterior and posterior parts, exposing the vitreous shown in Figure 2.4 B. The vitreous was then pushed out using a pair of tweezers without damaging the retina layer shown in Figure 2.4 C. The main body of the vitreous will be extracted alongside the pecten oculi inside (Figure 2.4 D). After removing the main vitreous body, remains of the liquid vitreous were also collected using a pipette shown in (Figure 2.4 E) and immediately put into a 1.7 ml tube (Eppendorf, Germany) to be weighed and kept in liquid nitrogen during the dissection period. Collected samples were transferred to -80 °C for storage until further use after the collection period. It was ensured that there was no evidence of blood or tissue contamination in the vitreous at the time of sample harvesting at all the time points shown in Figure 2.4 F.

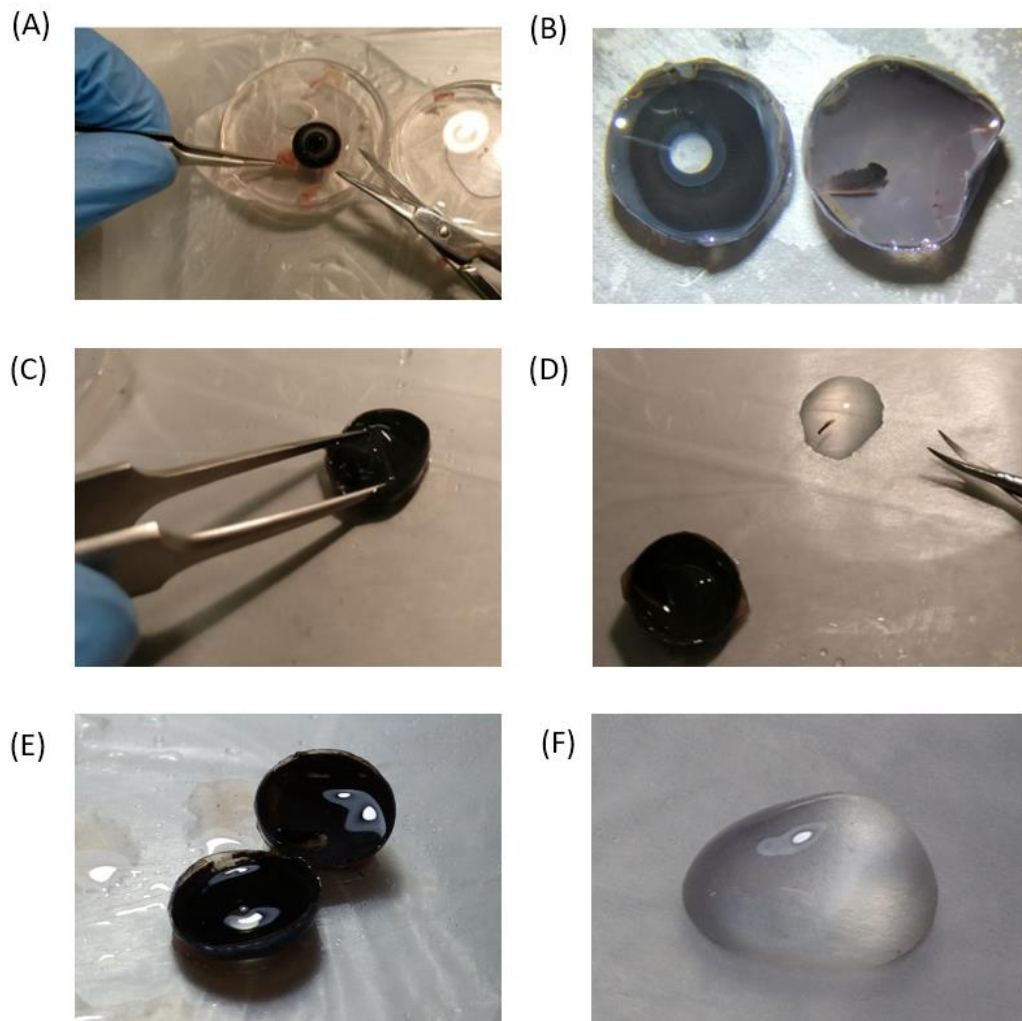


Figure 2.4 (A) The eyeball was transferred to ice-cold PBS and the removal of excess muscles and blood. (B) Hemisecting the eyeball equatorially into the anterior part showing the lens on the left and the posterior part showing the vitreous, pecten oculi, and the retina. (C) Pushing the vitreous out of the posterior eyeball using a pair of tweezers while keeping the retina intact. (D) Removal of the vitreous to the RPE/retina layer, while having the pecten oculi visible inside the vitreous. (E) Remains of liquid vitreous after the collection of the main vitreous body, which were also collected using a pipette. (F) Clean extracted vitreous body, free from blood or extra surrounding tissues such as the retina.

2.2.2 Homogenization of vitreous

Frozen vitreous samples were taken out from $-80\text{ }^{\circ}\text{C}$ and warmed to room temperature (RT) for weight measurement. Then the samples were put back into

liquid nitrogen to snap freeze. A 1:1 w/v (vitreous sample: lysis buffer) ratio of tissue protein extraction reagent (T-PER, Cat# 78510, Thermo Fisher Scientific, USA) with protease inhibitor (Cat# 11836145001, Roche, Switzerland) was added into a 2 ml homogenization tube containing 1.4mm + 2.8mm ceramic (zirconium oxide) beads (Cat# KT03961-1-009.2, Bertin, France). After loading the frozen sample, it was then homogenized with a homogenizer (Precellys evolution homogenizer, Bertin, France) under the following settings: 5000 rpm for 4 x 30sec rounds with a 15-sec break in between. Tubes were then centrifuged at 21380 x g at 4 °C for 5 mins to allow the foams to set, as shown in Figure 2.5. Then, the tissue lysis was transferred into a new 1.5 ml Eppendorf tube and centrifuge for 30 mins at 21380 x g at 4 °C. Next, the lysis was transferred into a new 1.5 ml Eppendorf tube and centrifuge for 15 mins at 21380 x g at 4 °C. Tissue lysis was then transferred into a new 1.5 ml Eppendorf tube for storage for experiments.

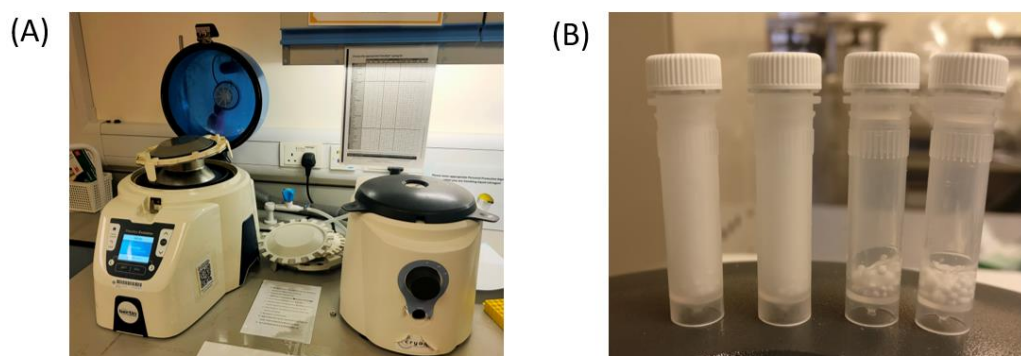


Figure 2.5 (A) Two milliliter homogenization tubes with 1.4mm + 2.8mm ceramic (zirconium oxide) beads used in the vitreous sample homogenization process. (B) Two tubes on the left: after homogenization of vitreous; Two tubes on the right: before homogenization of vitreous (with T-PER lysis buffer).

2.2.3 Protein concentration determination

Rapid gold BCA protein assay kit (Cat# A53225, Thermo Fisher Scientific, USA) was used to determine the protein concentration of the T-PER homogenized vitreous samples. The protocol was performed according to the manufacturer's instructions with slight modifications in preparing for the standard curve. In brief,

6 dilutions (1, 0.5, 0.25, 0.125, 0.025, and 0 $\mu\text{g}/\mu\text{l}$) of the bovine serum albumin solution (BSA, 2 $\mu\text{g}/\mu\text{l}$) were prepared using deionized water. Four microliters of homogenized vitreous samples were diluted with 16 μl of deionized water for protein measurements (a 5x dilution factor). Two hundred microliters of working reagent dye were added to each sample, and the plate was then placed into a microplate reader (AC3000, Azure biosystems, USA) for measurements at 480 nm. After incubation in RT for 5 minutes, the absorbance (ABS) was subtracted with blank (deionized water), and each sample was done in triplicates for the determination of the protein concentration of vitreous samples.

2.2.4 Reduction and alkylation

For reduction and alkylation, 0.1M Dithiothreitol (DTT) ($\text{C}_4\text{H}_{10}\text{O}_2\text{S}_2$, Cat# 43815, Sigma-Aldrich, USA) and 0.4M Iodoacetamide (IAA) ($\text{C}_2\text{H}_4\text{INO}$, Cat# I1149, Sigma-Aldrich, USA) were prepared by dissolving with deionized water. DTT was added to the sample to a final concentration of 10mM and incubated at 37 °C for 1 hour at 300 rpm. IAA was added immediately to the sample at a final concentration of 40mM and incubated at RT for 30 mins in the dark.

2.2.5 Precipitation of proteins

After alkylation, 100% ice-cold acetone was added to samples with a ratio of 1:4 (v/v) and kept at -20 °C overnight for acetone precipitation. Samples were centrifuged at 21380 x g for 30 mins at 4 °C. The supernatant was discarded, and 500 μl of 80% acetone was then added into the tubes and centrifuged again at 21380 x g for 10 mins at 4 °C. Samples were then air-dried in a fume hood until drying of the pellets. Ten microliters of 4M Urea (CON_2H_4 , Cat# 51456, Sigma-Aldrich, USA) in 25mM Ammonium bicarbonate (NH_4HCO_3 , Cat# A6141, Sigma-Aldrich, USA) were added into each tube for dissolving the pellets. Thirty microliters of NH_4HCO_3 were added fold-wise to a final concentration of 1M Urea.

2.2.6 Trypsin digestion

Sequencing grade modified trypsin (Cat# V5111, Promega, USA) was used throughout this study. Vials containing dried trypsin (20 μg) were taken out from -20 °C, and the dried pellet was dissolved with 20 μl dissociation buffer and 20 μl

of deionized water under slow vortex. A trypsin ratio of 1: 25 (trypsin concentration: protein concentration w/w) was added to each sample for digestion for 16 hours at 37 °C in the thermomixer (Eppendorf, Germany). Digestion was stopped by adding an appropriate amount of trifluoroacetic acid (TFA) to a final concentration of 0.1% TFA.

2.2.7 Peptide cleanup

Digested samples were subjected to desalting using 1cc/10 mg C18 columns (Oasis HLB, Waters, USA) combined with a vacuum system (Visiprep, Supelco, USA), shown in Figure 2.6. Acidified samples from the previous step were topped up with 0.1% TFA to 1 ml. The column was firstly conditioned by adding 1 ml of 100% ACN to run through, then washed again with 1 ml of 0.1% TFA. Samples were loaded into the column slowly twice for binding peptides onto the resin bed. Subsequently, 0.1% TFA was added to the column for washing, followed by a solution of 0.1% TFA with 0.5% methanol as a second washing step. Trapped peptides were eluted with 500 µl of 60% ACN with 0.1% TFA, and eluted samples were then finally vacuumed dried (CentriVap, Labconco, USA). Forty microliters of 0.1% FA were added to re-dissolve the dried pellets, and peptide concentration was measured using a peptide quantitation kit (Cat# 23275, Thermo Fisher Scientific, USA) according to the manufacturer's protocol. In brief, digested peptide standard were diluted into 0.5, 0.25, 0.125, 0.063, 0.031, and 0.016 µg/ µl using 0.1% FA for the standard curve measurements using 5 µl of digested vitreous peptides. The absorbance (ABS) was subtracted with blank (0.1% FA), and each sample was done in duplicates.

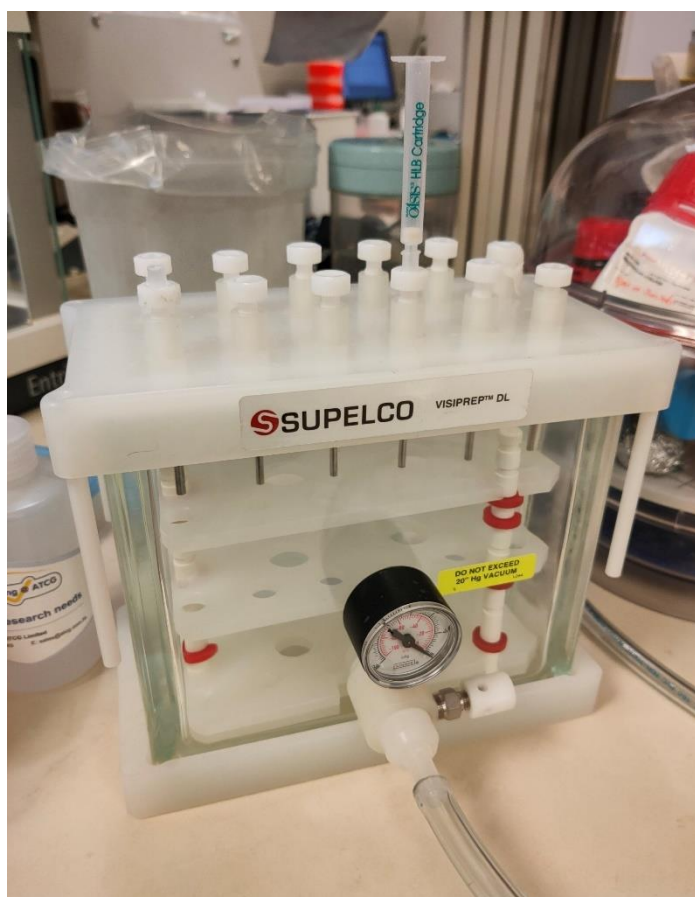


Figure 2.6 Oasis[®] C18 HLB column (1 cc/10 mg) inserted into the Visiprep[™] SPE manifold system (12 ports) for peptide clean-up step.

2.2.8 High-pH peptide fractionation

Desired concentration of digested peptides was subjected to offline fractionation using the high-pH reversed-phase peptide fractionation kit (Cat# 84868, Thermo Fisher Scientific, USA) according to the manufacturer's protocol. In brief, two fractions of high pH solution (Fraction A: 12.5% acetonitrile (ACN) in 0.1% Triethylamine (TEA) and Fraction B: 50% ACN in 0.1% TEA) were prepared and used to elute the peptides for fractionation. After column conditioning using ACN and 0.1% TFA, the digested peptides were then loaded onto the resin bed. Fraction A buffer was then firstly loaded to the column and centrifuged at 3000 x g for 2 mins. The elution was then collected as fraction A elution. Secondly, Fraction B buffer was added to the same column and centrifuged at 3000 x g for 2 mins,

resulting as fraction B elution. Both parts of fraction elution were then dried and resuspended in 0.1% FA. The final peptide concentration after fractionation of Fraction A (12.5% ACN in 0.1% TEA), Fraction B (50% ACN in 0.1% TEA), and unfractionated samples was set as around 0.2 µg/µl for MS injection.

2.3 Identification and quantitation of proteins by SWATH-based label-free proteomics

2.3.1 LC-MS/MS settings

Both information-dependant acquisition (IDA) and data-independent acquisition (SWATH-MS) were performed on a TripleTOF[®] 6600 quadrupole time-of-flight (QTOF) mass spectrometer (Sciex, USA) coupled to an Eksigent 415 nano-LC system (Sciex, USA). Equal amounts of digested peptides (according to each experiment condition settings) were loaded onto a C18 trap column (PepMap100, 5 µm, 100 Å, 100 µm i.d. × 20 mm, Thermo Fisher Scientific, USA) at a flow rate of 2 µL min⁻¹ for 15 mins and was then separated with a C18 nano-LC column (5µm, 100 µm i.d. x 300 mm, Column Scientific, China) at a flow rate of 350 µL min⁻¹. Mobile phase A was a mixture of 0.1% formic acid (v/v) and 5% ACN (v/v) in water, and mobile phase B contains 0.1% FA (v/v) and 98% ACN (v/v) in water. The gradient settings and conditions used are shown in Figure 2.7 A and B. **For 155 mins long gradient:** 0-0.5 min: 5%B, 0.5-90 min:10%B, 90-120 min:20%B, 120-130 min:28%B, 130-135 min:45%B, 135-141 min:80%B, 141-155 min:5%B. **For 90 mins short gradient:** 0-0.25 min: 5%B, 0.25-45 min:10%B, 45-60 min:20%B, 60-65 min:28%B, 65-75 min:80%B, 75-90 min:5%B.

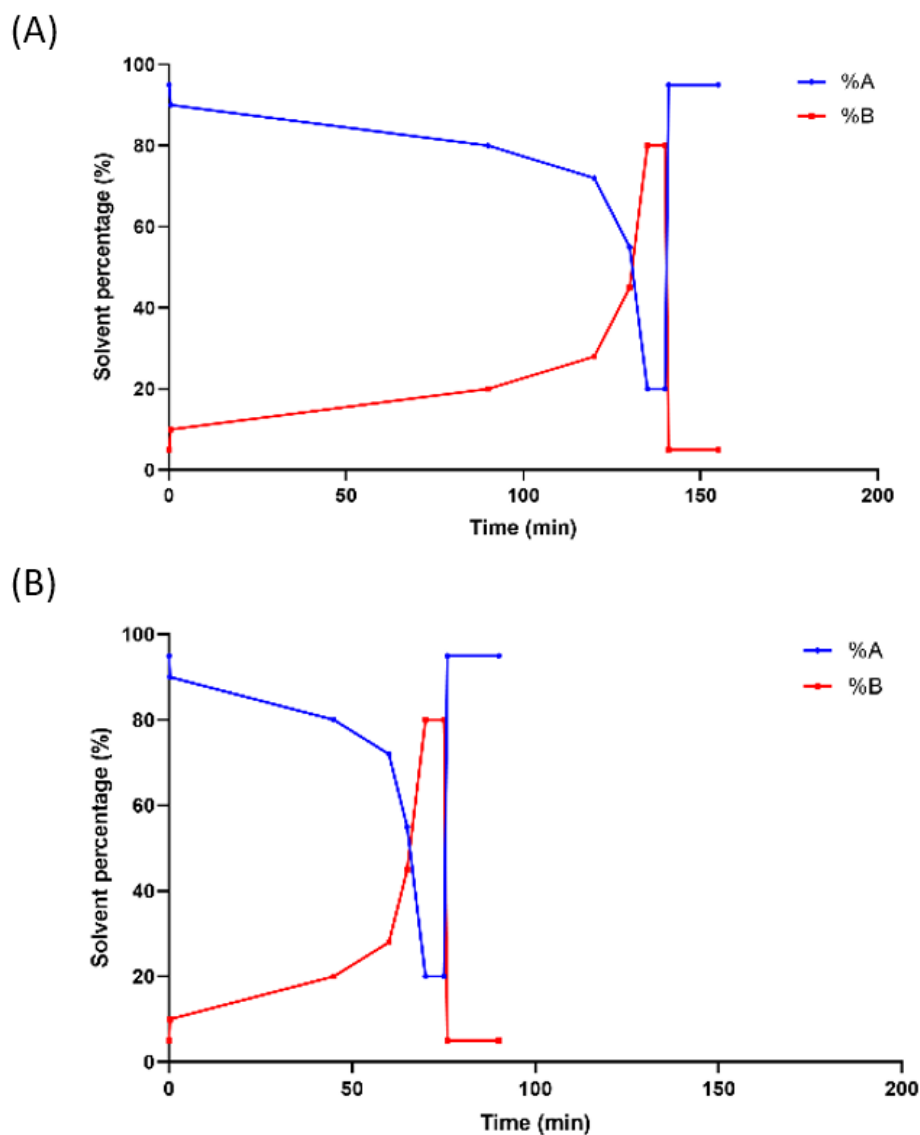


Figure 2.7 Gradient profiles for (A) long (155 minutes total) and (B) short (90 minutes total) LC/MS running time. Mobile phase A was a mixture of 0.1% FA (v/v), 5% ACN (v/v) in water, and mobile phase B contains 0.1% FA (v/v), 98% ACN (v/v) in water.

For Information-dependent acquisition (IDA), the eluent was introduced into the TripleTOF[®] 6600 quadrupole time-of-flight (QTOF) mass spectrometer (Sciex, USA) with a 10 μ m SilicaTip electrospray emitter (FS360-20-10-N-20-C12, New Objective, USA). TOF-MS scan range was set at 350 to 1800 m/z with an accumulation time of 250 ms, followed by an MS/MS scan at 100 to 1800 m/z in high sensitivity mode with an accumulation time of 50 ms to up to 50 ion candidates per cycle. A threshold of 125 cps was set for MS/MS counting with the charge stage

between 2 to 4. For Data-independent acquisition (DIA/ SWATH-MS), a setting of 100 variable isolation windows in a looped mode was set over the mass range of 100 to 1800 m/z with an accumulation time of 30 ms, resulting in a total duty cycle < 3 sec. A general XIC of an IDA, SWATH runs, and the SWATH windows calculation chromatogram is shown in Figure 2.8.

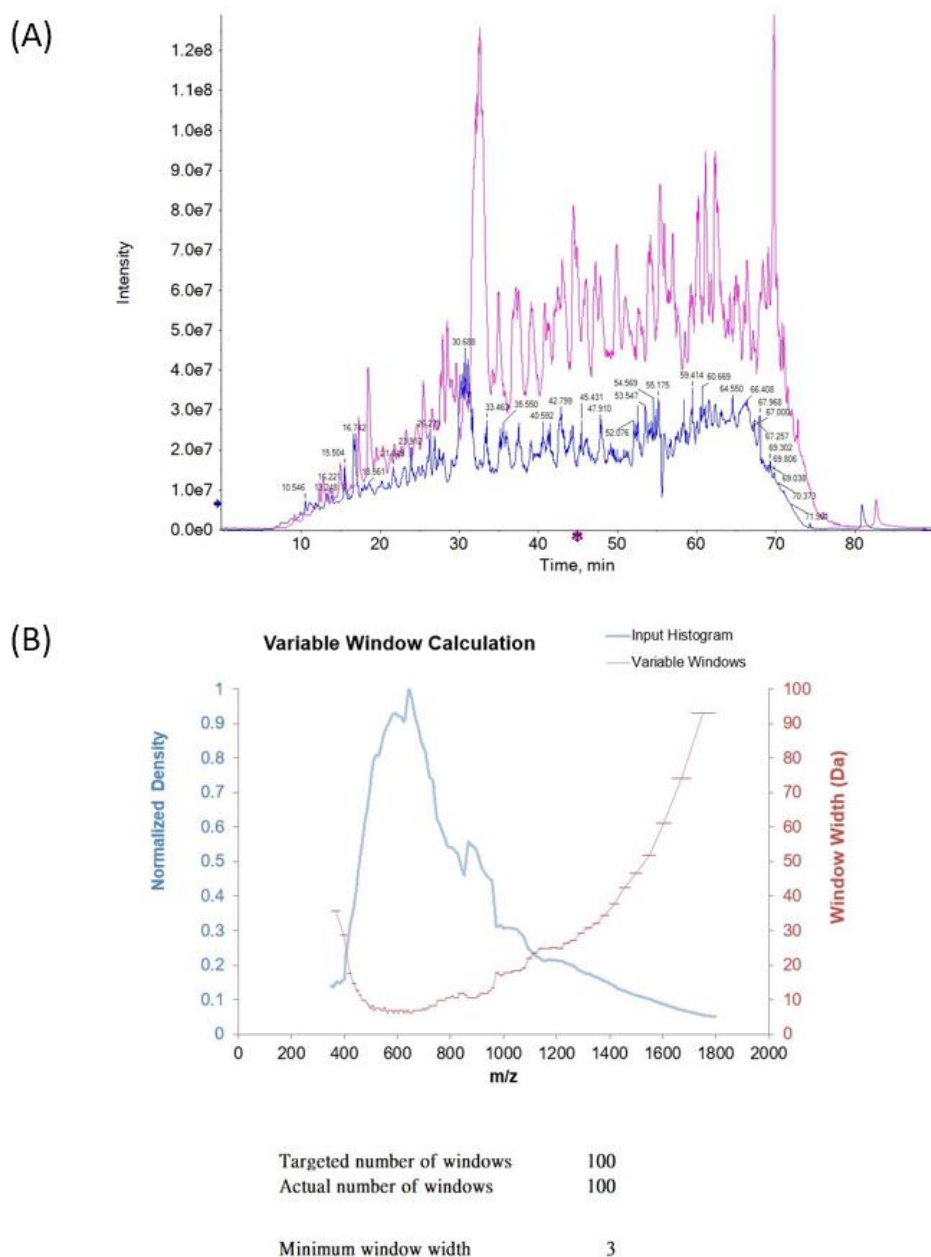


Figure 2.8 (A) A general extracted-ion chromatogram (XIC) of a vitreous IDA (blue), and SWATH (purple) under a 90 mins run. (B) A variable SWATH-MS windows calculation (100 windows) chromatogram of vitreous.

2.3.2 MS data analysis

Raw.wiff files of MS generated Information dependent acquisition (IDA) were searched against the Gallus gallus Uniprot database, and protein identification (ID) was acquired using ProteinPilot (v5.0, Sciex, USA). Trypsin as the enzyme, cysteine alkylation using iodoacetamide (IAA), thorough search effort, and biological modification were selected. A 1% false discovery rate (FDR) was set as the filter for protein identification. For label-free quantification, a combined search of IDA injections was selected as the ion library for SWATH quantification. Both the IDA ion library and the SWATH injection files were loaded onto the SWATH Acquisition MicroApp 2.0 in PeakView (v2.2, Sciex, USA). Up to 10 peptides per protein, 6 transitions per peptide, 90% peptide confidence threshold, 1% FDR, 10 min extracted-ion chromatogram (XIC) extraction window, and 75 ppm width were selected for processing. Processed data were normalized using the Most-Likely ratio (MLR) method (Lambert et al., 2013) and analyzed with MarkerView (v1.3, Sciex, USA), and exported to excel for protein fold change calculation. Proteins that have less than 1 peptide were removed to reduce the chances of false-positive results, and the filter for differential expressed proteins was considered at ≥ 1.50 or ≤ 0.70 fold change.

2.3.3 High-resolution multiple reaction monitoring (MRM^{HR}) confirmation

The transition list of targeted peptides and MRM^{HR} acquisition methods was created with Skyline (v20.2.0.286, MacCoss Lab, USA) (MacLean et al., 2010). MRM^{HR} acquisitions were acquired using a TripleTOF[®] 6600 quadrupole time-of-flight (QTOF) mass spectrometer (Sciex, USA). Digested samples were loaded onto a C18 nano trap column (PepMap100, 5 μm , 100 \AA , 100 μm i.d. \times 20 mm, Thermo Fisher Scientific, USA) by loading buffer (0.1% Formic acid, 2 % Acetonitrile in water) at 2 $\mu\text{l min}^{-1}$ for 15 min. It was then separated on a C18 nano-LC column (100 μm \times 30 cm, C18, Column Scientific, China) using an Eksigent 415 nano-LC system at a flow rate of 350 nl min^{-1} with the following gradient: 0- 0.25 min: 5%B, 0.25- 45 min:10%B, 45- 60 min:20%B, 45- 60 min:28%B, 60- 65 min:45%B, 65- 75 min:80%B, 75- 90 min:5%B. Peptides were injected into the mass spectrometer with a 10 μm SilicaTip electrospray emitter (FS360-20-10-N-20-C12, New

Objective, USA). DIA mode was acquired with the mass range of 100 m/z to 1800 m/z scan. An accumulation time of 29ms was set for each fragment ion resulting in a total duty cycle of 3.0 sec. Raw data of MRM^{HR} results were processed using MultiQuant (v3.0, Sciex, USA), and the MQ4 algorithm was selected for automatic peak integration, resulting in a list of retention time, integrated peak area, peak height, and a signal-to-noise ratio for each transition. Transitions areas were then calculated from the average of three technical replicates of individual biological samples (if possible). Furthermore, only transitions with an S/N ratio cut-off ≥ 20 were selected for calculation. The top 3 transitions with the highest intensity area of ions were selected and averaged into each peptide. Then the top 3 peptides (if possible) were then average again for each protein and normalized with Glyceraldehyde 3-phosphate dehydrogenase (GAPDH) for fold change calculation.

Chapter 3. Optimization of vitreous proteomic protocols

A basic bottom-up proteomics approach workflow contains multiple steps from sample preparation stages for proteins to be digested into peptides for MS analysis. This has always been considered a critical phase for a typical proteomic study, as the availability of the starting material determines the flexibility of downstream experiment designs. As proteins are extracted and prepared for analysis, a degree of proteins will be lost throughout these steps. This is especially important for vitreous experiments as it contains a high volume of water, making it a very diluted material with a low protein concentration. Furthermore, due to the differences in equipment and models, an optimized protocol for vitreous proteomics study has not yet been determined. Therefore, these steps must be optimized to archive the minimum sample loss and variability for protein analysis for a successful SWATH-MS workflow. The following optimization studies aim to comprehensively identify the preferable protocols for vitreous proteomic workflow while providing a balanced and compromised workflow from various limiting factors (time consumption, sample volume, MS settings) to ensure a successful proteomic workflow for subsequent studies.

3.1 Vitreous sample preparation

This part of the optimization section includes the initial part of the proteomic workflow, which covers the area from protein extraction to peptide cleanup before protein analysis by the MS.

3.1.1 Homogenization methods of chick vitreous protein extraction

3.1.1.1 Introduction

Sample preparation in a proteomics study is vital as it will determine the starting sample material and a limiting factor to use for downstream studies (Patel et al., 2008). Protein extraction is the very first stage in a typical bottom-up proteomics workflow. Several methods have been commonly used in this process, including physical disruption methods that employ mechanical forces such as homogenization and sonication to disperse or shear cells and tissues, disrupting the structure (Cañas et al., 2007). These methods often combine the addition of commonly used detergents such as sodium dodecyl sulfate (SDS) (Andersen et al., 2009), Urea (Mandal et al., 2015), sodium deoxycholate (SDC) (Lin et al., 2008) as a lysis buffer to help in facilitating the breakdown of the tissue, so that proteins can then be extracted from the cellular/ tissue components of the sample. Vitreous humor (VH) has a gel-like structure due to its collagen and hyaluronic acid meshwork, giving the tissue a certain degree of shock absorbance. This would pose a potential problem for physical disruption methods as the tissue component can easily slide or compensate for the force. Secondly, having a high-water content (~99%) makes the vitreous a diluted tissue; therefore, the volume of lysis buffer to be used for extraction is also an essential parameter to obtain. Although homogenizer is the current preferred protein extraction method in-lab for our proteomic studies as it offers the best solution in breaking down the tissue completely, the waiting time (only 1 sample per turn) severely hampers the efficiency of data collection. Therefore, a quicker method should also be used to shorten the process to save valuable time. Sonication is an alternative disruption method often used in cell studies, and this method could be used to disrupt and break down the crosslinks of collagen fibers and their cellular components. Hence, this study aims to compare

the protein extraction efficiency between the two protein extraction methods. Furthermore, the volume of lysis buffer used to extract vitreous will also be tested with two methods to determine the optimal volume for protein extraction.

3.1.1.2 Method and materials

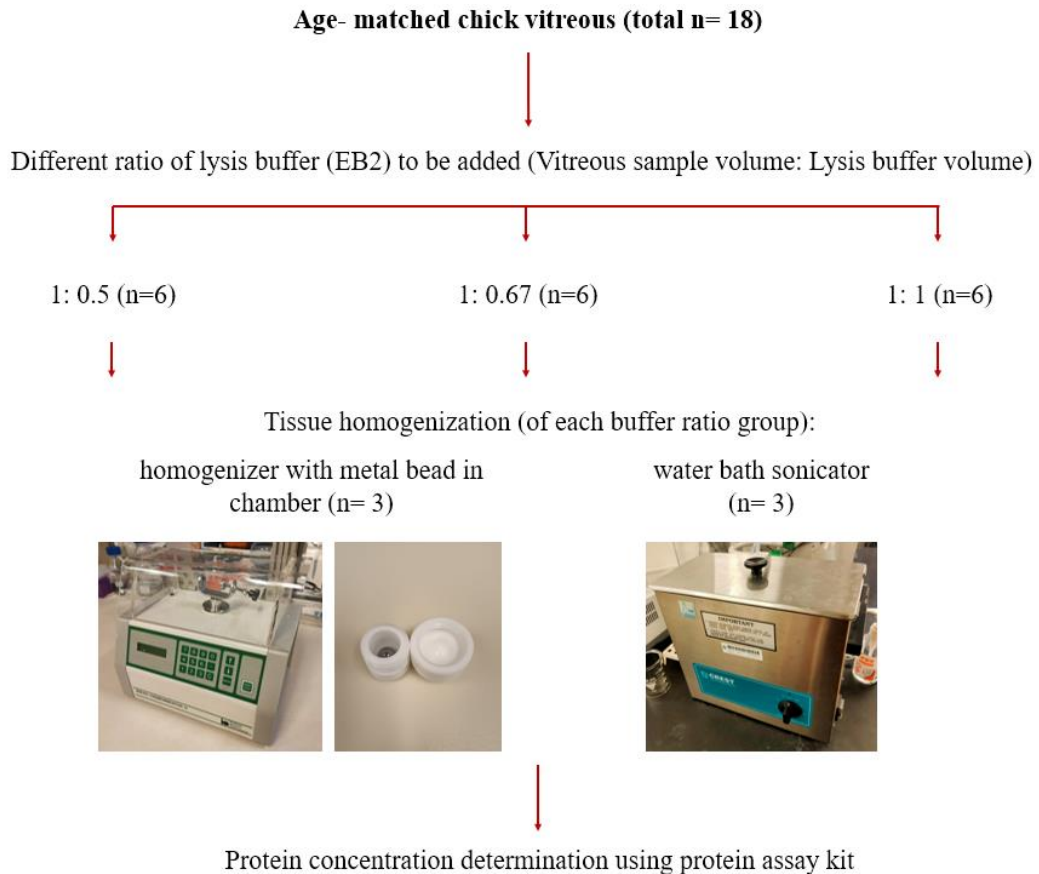


Figure 3.1 Tissue homogenization methods (metallic bead with the homogenizer and water-bath sonicator) with different lysis buffer volume ratios.

Chick vitreous collection and lysis buffer (EB2)

Age-matched chicks vitreous (2 weeks old, total n= 18 eyes) were collected (with similar weight/ volume) and were divided into 3 groups (n=6, from random eyes) in terms of different lysis buffer volume ratios (ratio of 1:1, 1:0.67, and 1:0.5, protein sample volume to lysis buffer volume). EB2 lysis buffer (7M Urea, 2M thiourea, 30mM Tris, 2% CHAPS, 1% ASB14, and protease inhibitor) was used

throughout the experiment. It was then further divided into 2 groups (n=3 in each group) for different homogenization methods: homogenizer with metal beads in chamber (Mikrodismembrator, Braun Biotech, Germany) or water bath sonicator (CREST P2600, Cleansonic, USA) shown in Figure 3.1. The protein concentration of the lysed samples was then determined using the 2D Quant protein assay kit (Cat# 80648356, Cytiva, USA).

Homogenization using water bath sonicator

A layer of aluminum foil was placed inside the sonication bath (CREST P2600, Cleansonic, USA) to determine the position where the sonicator gave the highest energy output. In brief, water was filled to cover most of the aluminum foil under the maximum power settings (132kHz/ 230V), and time measurements and location inside the water bath were taken until the aluminum foil was broken down first. During sonication, the water temperature was measured each minute to ensure the temperature would not change drastically during sonication, which could affect the sample as sonicators are known for generating heat after prolonged usage. Frozen vitreous samples with cold lysis buffer (EB2) were placed in the water bath by a plastic holder (to ensure the positions of sonication were the same) and each tube was sonicated in the bath for 4 minutes with ice added for temperature control. After that, the lysed samples were centrifuged at 4 °C for 30 minutes at 16.1 x 1000 g with only the supernatant collected.

Homogenization using homogenizer with metal bead in chamber

Frozen pallets of vitreous samples were transferred into a liquid nitrogen-cooled Teflon chamber (3 ml) with a tungsten carbide grinding bead (9 mm) and the sample was then homogenized using a tissue homogenizer (Mikrodismembrator; Braun Biotech, Germany) shown in Figure 3.1 for 4 minutes at 16.1 x 1000 g. After that, the closed chamber was incubated at room temperature for 20 minutes before transferring the homogenized sample into a 1.7ml Eppendorf tube. Homogenized samples were then centrifuged at 4 °C for 30 minutes at 16.1 x 1000 g with only the supernatant collected.

Protein concentration determination

The protein concentration of the homogenized samples was determined by the 2D quant protein assay kit (Cat# 80648356, Cytiva, USA) using a standard curve with known BSA concentration according to the manufacturer's protocol. The cuvettes were then placed in a spectrophotometer (Genesys 20, Thermo Fisher Scientific, USA) for measurements.

3.1.1.3 Result

3.1.1.3.1 Initial sample location determination for homogenization using water bath sonicator

As there were multiple nodes of sonicator inside the water bath, a foil was placed inside to determine the strongest point of sonication. Within two minutes of sonication, the area (20 cm from the top and 10 cm from the left) of the foil has been broken down (shown in Figure 3.2 A and B); therefore, this location was set for where the samples will be kept during sonication. The water temperature slightly increased by 1.3 °C after 10 minutes of sonication (Figure 3.2 C). Even with the minor increase in temperature, ice was added into the water bath to reduce the temperature to around 5 °C further to keep the vitreous sample cool during sonication.

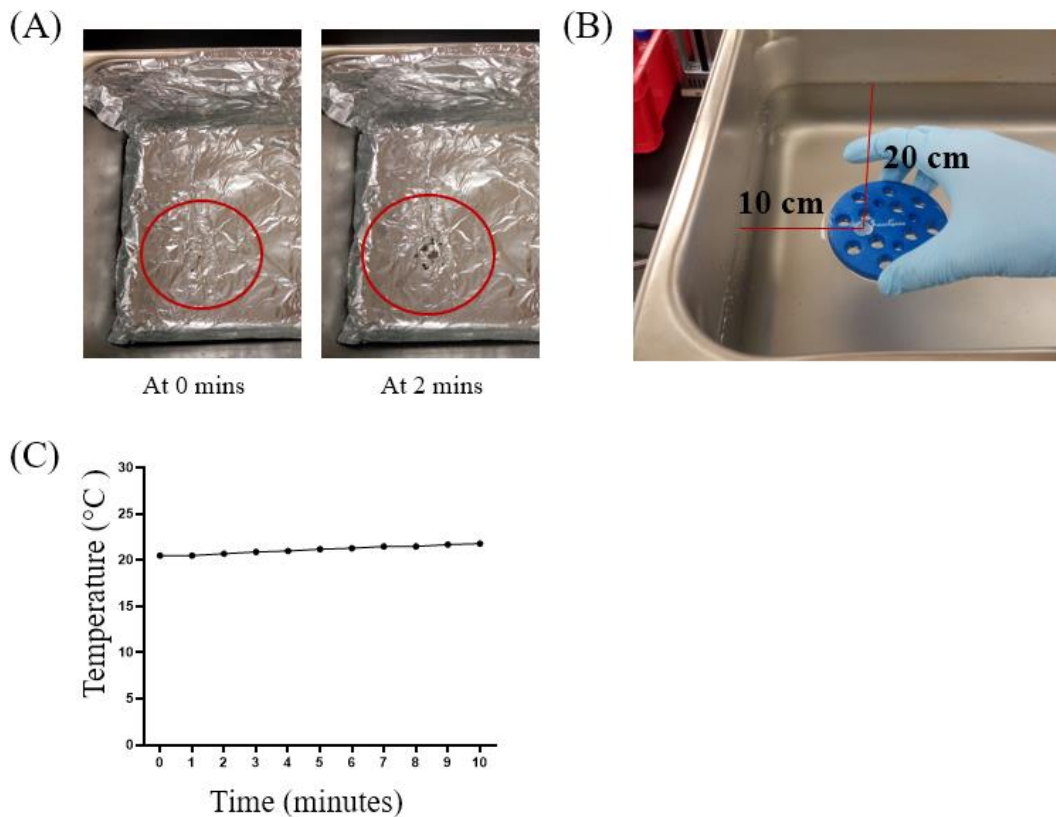


Figure 3.2 (A) The use of foil to determine the location of the sonicator inside the water bath (before and after 2 mins of turning on). (B) The location of where samples were placed for each set of homogenization with sonicator water bath experiments was determined by the foil test. (C) The monitoring of temperature changes with water bath sonicator on for 10 mins.

3.1.1.3.2 Total sample volume after each homogenizing method

Homogenization using water bath sonicator

The total sample volume collected after homogenization was also measured (μl) shown in Figure 3.3 A: Samples underwent homogenization using sonication had an average volume of $123.333 \pm 5.774 \mu\text{l}$, $110.000 \pm 26.458 \mu\text{l}$, and $83.333 \pm 23.094 \mu\text{l}$ from 1:1, 1:0.67, and 1:0.5 (sample: lysis buffer ratio) were measured, respectively. One-way ANOVA testing indicated that there were no significant differences between the three groups and a slight decrease trend in the total sample volume (μl) with the decrease of lysis buffer volume was observed. ANOVA tests can be found in Appendix 1.1.

Homogenization using homogenizer with metal bead in chamber

In terms of total volume collected (shown in Figure 3.3 A), an average volume of $210.000 \pm 36.056 \mu\text{l}$, $130.000 \pm 17.321 \mu\text{l}$, and $123.333 \pm 5.774 \mu\text{l}$ from 1:1, 1:0.67, and 1:0.5 (sample: lysis buffer ratio) were measured, respectively. One-way ANOVA testing indicated that there were significant differences in terms of total sample volume between the 1:1 group with the two other groups: 1:0.67 group ($P=0.013$) and 1:0.5 group ($P=0.009$) as well as a slight decrease trend in the total sample volume (μl) with the decrease in lysis buffer volume.

Comparison of two methods in terms of total sample volume

There were significant differences between the two methods in the 1:1 ($P=0.015$) and 1:0.5 ($P=0.006$) groups, but no significant differences were found in the 1:0.67 group using an unpaired T-test.

3.1.1.3.3 Protein concentration after each homogenizing method

Homogenization using water bath sonicator

In terms of protein concentration (shown in Figure 3.3 B), samples that underwent homogenization with water bath sonicator had an average protein concentration of $0.127 \pm 0.011 \mu\text{g}/\mu\text{l}$, $0.178 \pm 0.049 \mu\text{g}/\mu\text{l}$ and $0.190 \pm 0.710 \mu\text{g}/\mu\text{l}$ from 1:1, 1:0.67, and 1:0.5 (sample: lysis buffer ratio), respectively. One-way ANOVA testing indicated that there were no significant differences between the three groups, and a slight increase trend in the protein concentration ($\mu\text{g}/\mu\text{l}$) with the decrease of lysis buffer volume was observed.

Homogenization using homogenizer with metal bead in chamber

For samples that were homogenized using the homogenizer with a metal bead in a chamber (shown in Figure 3.3 B): an average protein concentration of $0.158 \pm 0.053 \mu\text{g}/\mu\text{l}$, $0.140 \pm 0.012 \mu\text{g}/\mu\text{l}$, and $0.180 \pm 0.039 \mu\text{g}/\mu\text{l}$ from 1:1, 1:0.67, and 1:0.5 (sample: lysis buffer ratio) were determined, respectively. One-way ANOVA testing indicated that there were no significant differences between the three groups.

Comparison of two methods in terms of protein concentration

No significant differences were found comparing both methods at all lysis buffer volume groups using an unpaired T-test.

3.1.1.3.4 Total protein amount after each homogenizing method

Homogenization using water bath sonicator

The total protein amount was calculated by the total volume after homogenization measured multiplied by the protein concentration ($\mu\text{g}/\mu\text{l}$) shown in Figure 3.3 C: For samples that underwent homogenization using sonication, an average total protein amount was $15.707 \pm 2.160 \mu\text{g}$, $20.300 \pm 9.617 \mu\text{g}$, and $16.770 \pm 10.696 \mu\text{g}$ from 1:1, 1:0.67, and 1:0.5 (sample: lysis buffer ratio), respectively. One-way ANOVA testing indicated no significant differences between the three groups.

Homogenization using homogenizer with metal bead in chamber

For samples that were homogenized using the homogenizer with a metal bead in chamber shown in Figure 3.3 C: the average total protein amount was $32.694 \pm 10.117 \mu\text{g}$, $18.380 \pm 4.050 \mu\text{g}$, and $22.038 \pm 4.014 \mu\text{g}$ from 1:1, 1:0.67, and 1:0.5 (sample: lysis buffer ratio) were calculated, respectively. One-way ANOVA testing indicated that there were no significant differences between the three groups.

Comparison of two methods in terms of total protein amount

There were significant differences between the two methods in the 1:1 ($P=0.047$) group in terms of total protein amount, but no significant differences were found in the other two groups using an unpaired T-test.

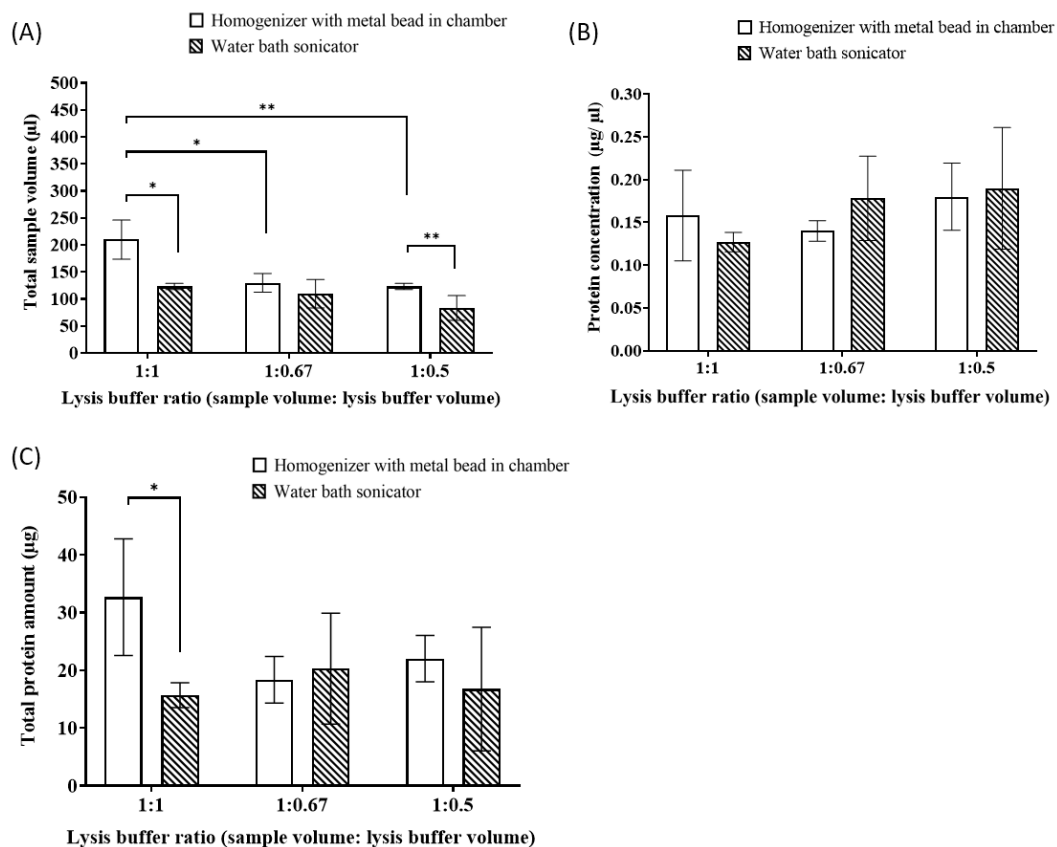


Figure 3.3 (A) The total sample volume after each homogenizing method (Homogenizer with metal bead in chamber and water bath sonicator) for each lysis buffer ratio group. (B) The protein concentration was measured after each homogenizing method for each lysis buffer ratio group. (C) The total protein amount after each homogenizing method for each lysis buffer ratio group. Statistical analysis was analyzed by one-way analysis of variance (ANOVA) with a significance level of 0.05, and an unpaired T-test was applied when comparing individual groups (* $P \leq 0.05$, ** $P \leq 0.01$, and * $P \leq 0.001$, total $n = 18$).**

3.1.1.4 Discussion

Numerous homogenization methods for protein extraction have been employed for proteomics studies (Bodzon-Kulakowska et al., 2007). They can generally be categorized into mechanical, ultrasonic, pressure, freeze-thaw, and osmotic/detergent lysis. For typical softer tissues, methods like thermal-lysis cell rely on the

formation of ice could be used to breakdown the cell membrane from the freeze-thawing process for E.Coli cells (Johnson & Hecht, 1994), and ultrasonic/sonication homogenization was commonly used on bacteria cells by the shear forces of vibration (Racay & Kollarova, 1996). Targeting ocular tissues, Lam et al. used mechanical homogenization by physical contact of the sample to another hard material such as metal/ ceramic to breakdown the chick retina (Lam et al., 2006), In regardless of homogenization methods, lysis buffer is often added to increase the ability of protein solubilization and extraction. These usually contain a high concentration of urea, such as the lysis buffer from our in-house protocol (EB2)-lysis buffer cocktail (7M Urea, 2M thiourea, 30mM Tris, 2% CHAPS, 1% ASB14, and protease inhibitor) which showed its effectiveness for cell lysis ability from previous studies from the lab in various ocular tissues such as the retina (Lam et al., 2006) and vitreous (Yu et al., 2017) proteomic studies.

For this experiment using the chick model, a 1:1 sample volume to lysis buffer volume ratio was applied initially to start the homogenization process as it was to ensure there was enough lysis buffer to break down the sample tissue. A slight trend in the increase of protein concentration ($\mu\text{g}/\mu\text{l}$) with the decrease in volume of lysis buffer used for both homogenization methods was observed, as this might be due to the dilution effect from the lysis buffer where 1:1 ratio was starting to dilute the protein concentration of the sample. Not surprisingly, the 1:1 group also had the highest volume remaining for both homogenization methods, as the volume of lysis buffer used was the highest. After the sonication in the water bath, gel deposits were observed to remain at the bottom of the tubes showing incomplete tissue breakdown, possibly from the lack of power from the sonicator in breaking down the tissue. The second possibility is that being a visco-elastic solid, the collagen-hyaluronic acid meshwork of the vitreous provides a degree of shock absorption, resisting the sonication pattern (Lee et al., 1992). This could explain why the volume of the samples was lower in all three buffer ratio settings in water bath sonication compared to the homogenizer with metal bead in chamber.

This leads to the overall total protein yield (μg) obtained from all three lysis buffer ratios being lower in sonication compared to the homogenizer, making the

homogenizer with metal bead in chamber a better method for protein extraction in vitreous. The lack of power from the sonicator may be unable to break down the rich collagen fibers in the vitreous as a portion of the protein concentration is from collagen (Theocharis et al., 2002). This can be reflected from the sample volume after homogenization, where the remaining volume was higher from the samples that were homogenized using the homogenizer at all the buffer ratio settings.

3.1.1.5 Conclusion

Two homogenization methods (homogenizer with metal bead in chamber and water bath sonicator) were tested and compared for vitreous protein extraction. On top of that, three lysis buffer volume (1:1, 1: 0.67, and 1: 0.5, sample volume: lysis buffer volume) was also used for these two methods to compare the extraction of T-PER lysis buffer on the vitreous.

In terms of total sample volume after homogenization, one-way ANOVA testing indicated that there were significant differences in a homogenizer with metal bead in chamber method between the 1:1 group with the two other groups: 1:0.67 group ($P= 0.013$) and 1:0.5 group ($P= 0.009$) as well as a slight decrease trend in the total sample volume (μl) with the decrease in lysis buffer volume. While there were no significant differences between the three groups, a slight decrease trend in the total sample volume (μl) with the decrease of lysis buffer volume was observed in the water bath sonicator method. When comparing the two homogenization methods, there were significant differences between the two methods in the 1:1 ($P= 0.015$) and 1:0.5 ($P= 0.006$) groups, but no significant differences were found in the 1: 0.67 group using unpaired T-test. In terms of protein concentration after homogenization, no significant differences were found between both methods and the use of different lysis buffer volumes.

Taking the sample volume remained, the total highest protein amount obtained was using a 1:1 sample to lysis buffer ratio using the homogenizer with metal bead in chamber method ($P=0.047$) when compared to sonication with water bath method. Furthermore, a complete breakdown of the vitreous tissue was obtained by snap freezing the vitreous before the homogenization process with the homogenizer.

Therefore, the mechanical homogenization method with bead was chosen for future experiments.

3.1.2 Protein precipitation (Acetone vs. TCA/Acetone/methanol-chloroform)

3.1.2.1 Introduction

After the initial protein extraction, the desired amount of protein samples will undergo reduction with strong reducing agents such as dithiothreitol (DTT) (Konigsberg, 1972) and Tris(2-carboxyethyl)phosphine (TCEP) (Burns et al., 1991) to break down the disulfide bonds and alkylation with iodoacetamide (IAA) to block reduced cysteine residues to prevent disulfide bonds formation (Sechi & Chait, 1998). The next step will often contain a protein purification step, where contaminants such as detergents like SDS and salts that could interfere with downstream applications are removed (Garcia-Rodriguez et al., 2003). Classical purification approaches include the use of dialysis (Reynolds & Tanford, 1970), Solid-phase extraction (Sun et al., 2012), electrophoresis (Kachuk et al., 2016), and precipitation. Precipitation with salts (Chick & Martin, 1913) and organic solvents such as chloroform/methanol (Wessel & Flugge, 1984), acetone (Buxton et al., 1979), and TCA (Arnold & Ulbrich-Hofmann, 1999) can be seen as a common precipitation agent to use for this step. Contaminates will be removed alongside the supernatant, leaving only proteins to precipitate at the bottom. Furthermore, salt precipitation using ammonium sulfate has long been a traditional technique for protein purification and fractionation (Wingfield, 2001), where the addition of salt reduces the protein solubility leading to protein precipitation (Green & Hughes, 1955). It has been demonstrated that adding a low concentration of salts (0.1-100mM) during the acetone step can promote a higher % protein recovery in BSA and yeast samples (Crowell et al., 2013).

While proteins can be precipitated using these methods, the unpredictable recovery of the rate of protein aggregation remains the primary concern at this stage of the sample workflow. Vitreous's low protein amount at the beginning remains a challenge for the downstream application; therefore, three common precipitation methods have been used to determine an optimized protein precipitation method for the analysis of vitreous proteins. On top of that, the effect of adding salts during acetone precipitation on chick vitreous protein extraction process. An increase in

recovery rate is undoubtedly beneficial for vitreous studies as one of the critical limitation factors was the low protein/ peptide concentration.

3.1.2.2 Methods and materials

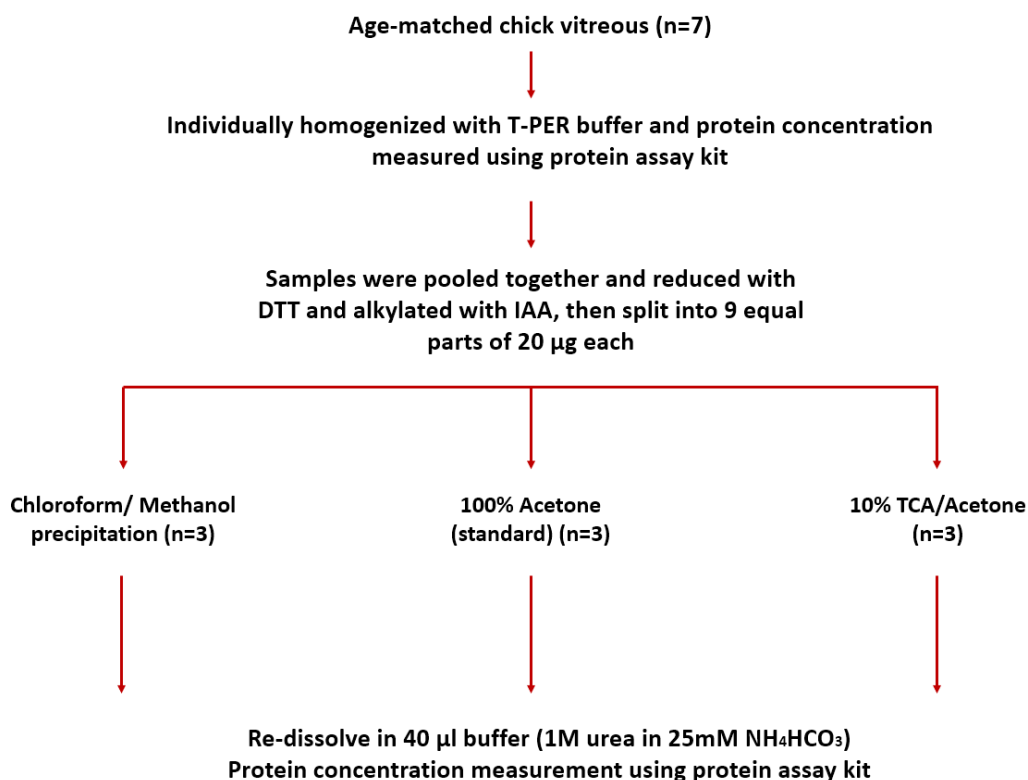


Figure 3.4 Seven individual age-matched chicks vitreous were collected. Samples were individually homogenized using T-PER lysis buffer and reduced and alkylated. These were then pooled together and split into 9 parts of equal amounts of 20 µg. Three precipitation methods (Chloroform/ methanol, 100% Acetone, and 10% TCA/Acetone, n= 3 each) were tested, the protein precipitant was re-dissolved in a buffer, and protein concentration was compared.

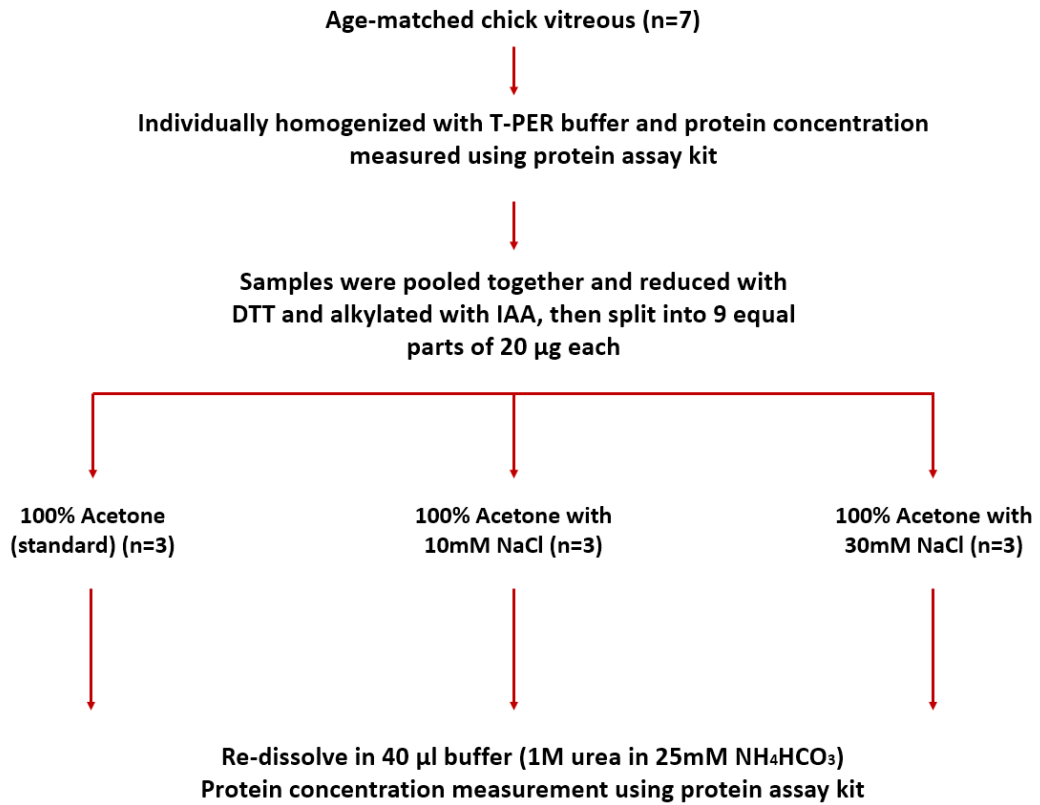


Figure 3.5 Seven age-matched chicks vitreous were pooled together for reduction and alkylation. The protein concentration was determined using protein assay kit, and equal amounts (20 µg) of vitreous proteins (n= 3 in each group) underwent three different precipitation methods: 100% Acetone precipitation, Acetone with the addition of different concentrations of NaCl (10mM and 30mM). The protein concentration was determined again with protein assay for recovery yield calculation after re-dissolving in a buffer consisting of 1M Urea in 25mM NH₄HCO₃.

Vitreous sample collection and preparation

The overall experiment design is shown in Figure 3.4. Age-matched vitreous (n= 7) homogenized with T-PER buffer was pooled together, and the protein concentration was determined. A total of 180 µg of vitreous proteins were reduced with dithiothreitol (DTT) at a final of 10mM for 1 hour at 37 °C and 40mM iodoacetamide (IAA) for 30 mins at RT in the dark. The solution was then aliquoted into 9 equal parts (~20 µg each) for precipitation method testing. This exact

collection and preparation process was repeated using a separate batch of vitreous samples for the addition of sodium chloride (NaCl) experiment set (shown in Figure 3.5).

Acetone precipitation

100% ice-cold acetone was added overnight at -20 °C with a ratio of 1:4 (v/v). Samples were then centrifuged at 21380 x g for 30 mins at 4 °C. The supernatant was discarded, and 500 µl of 80% acetone was added into each tube. The samples were then centrifuged again at 21380 x g for 10 mins at 4 °C. After discarding the supernatant, and the tubes were air-dried in a fume hood.

Chloroform/ methanol precipitation

All the steps were performed at room temperature. 100% methanol was added to the sample with a ratio of 1:4 (v/v) and vortexed for 20 sec. Then 100% chloroform was added to the sample in a 1:1 ratio (v/v) and vortexed for 20 sec. Deionized water was added in a 1:3 ratio (v/v) and vortexed for 20 sec. The mixed solution was then centrifuged at 10000 x g for 5 mins at RT. The aqueous layer (methanol) was removed carefully, leaving only the protein at the boundary between the aqueous methanol layer and the chloroform layer. Four times the volume of methanol was added and vortexed. Finally, samples were centrifuged at 10000 x g for 15 mins at RT, and the supernatant was removed. The pellet was air-dried in a fume hood.

10% TCA/Acetone precipitation

A volume of 20% trichloroacetic acid (TCA) was prepared and added to a volume of a protein sample at 4 °C. The mixture was then vortexed and incubated for 1 hour at -20 °C. The sample was subsequently centrifuged at 15000 x g for 15 mins, and the supernatant was removed. Five hundred microliters of 100% ice-cold acetone were added, and the solution was centrifuged at 13 000 x g for 15 mins at 4 °C. The supernatant was discarded, and the pellets were air-dried.

Addition of sodium chloride with acetone precipitation (NaCl)

Samples were then prepared according to the conditions (n= 3 for each group), shown in Figure 3.5: (A) 100% acetone (n= 3), (B) 10mM NaCl + Acetone (n= 3) and (C) 30mM NaCl + Acetone (n= 3). Samples were kept at -20 °C overnight. Next, the samples were centrifuged at 21380 x g for 30 mins at 4 °C. The supernatant was discarded, and 500 µl of 80% acetone was added into each tube. The samples were centrifuged again at 21380 x g for 10 mins at 4 °C. After discarding the supernatant, and the tubes were air-dried in a fume hood.

Re-dissolve of protein precipitant and protein concentration measurements

After the pellet was dried from various methods, it was then dissolved in 40 ul of 1M Urea in 25mM ammonium bicarbonate, followed by sonication. Protein concentration was measured in duplicates using rapid gold BCA protein assay, and the protein recovery (%) was determined by the ratio of protein quantity (µg) from before and after precipitation.

3.1.2.3 Results

Protein concentration

The protein concentration (µg/µl) from acetone precipitation yielded (shown in Figure 3.6 A) the highest among the three tested methods with 0.203 ± 0.017 µg/µl compared to Chloroform/methanol and TCA/ acetone where 0.136 ± 0.014 and 0.111 ± 0.029 µg/µl were archived, respectively. Significant differences were found comparing acetone to the rest of the groups using one-way ANOVA testing. No significant differences were found from chloroform/ methanol compared to TCA/Acetone. ANOVA tests can be found in Appendix 1.2.

Protein recovery

In terms of protein recovery (%), it was calculated by the protein concentration (µg/µl) x the starting volume (40 µl) divided by the initial starting concentration (20 µg) shown in Figure 3.6 B. The protein recovery (%) from acetone yielded the highest at around $42.241 \pm 3.676\%$ compared to Chloroform/methanol and TCA/ acetone, where $29.039 \pm 2.418\%$ and $20.921 \pm 0.2.146\%$ were calculated. There were significant differences between all comparison groups.

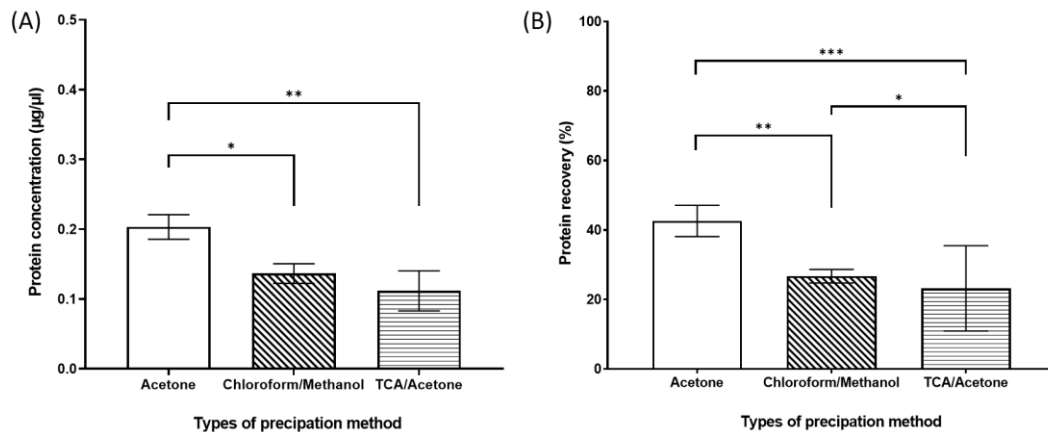


Figure 3.6 (A) The protein concentration ($\mu\text{g}/\mu\text{l}$) after precipitation ($n=3$ from each condition). B) Overall protein recovery (%) for three precipitation methods. One-way ANOVA testing was performed with a significant level set at 0.05, Tukey post hoc test ($P \leq 0.05$, $*=0.05$, $=0.01$, and $***=0.00$, $n=3$ for each condition).**

3.1.2.3.1 Addition of sodium chloride with acetone precipitation (NaCl)

Two concentrations of NaCl (10mM and 30mM) were added to the vitreous samples for an additional step of “salting- out” the proteins within samples. Both the average protein concentration and protein recovery were looked at:

The average protein concentration ($\mu\text{g}/\mu\text{l}$)

Acetone precipitation alone yielded the lowest protein concentration ($\mu\text{g}/\mu\text{l}$), giving 0.137 ± 0.019 compared to 10mM addition of NaCl and 30mM addition of NaCl, giving 0.157 ± 0.014 and 0.142 ± 0.049 , respectively shown in Figure 3.7 A. However, one-way ANOVA testing showed no significant differences between the obtained concentrations.

The protein recovery after precipitation (%)

To estimate the protein recovery (shown in Figure 3.7 B), the protein concentration was multiplied by the dissolved buffer volume added and divided by the initial concentration (20 μg). Similar to the findings of protein concentration ($\mu\text{g}/\mu\text{l}$), precipitation using acetone alone yielded the lowest recovery rate at 33.863 ± 4.04 % compared to 10mM addition of NaCl and 30mM addition of NaCl, giving 38.553

± 5.000 and 35.073 ± 12.030 , respectively. However, one-way ANOVA testing also showed no significant differences between the obtained concentrations.

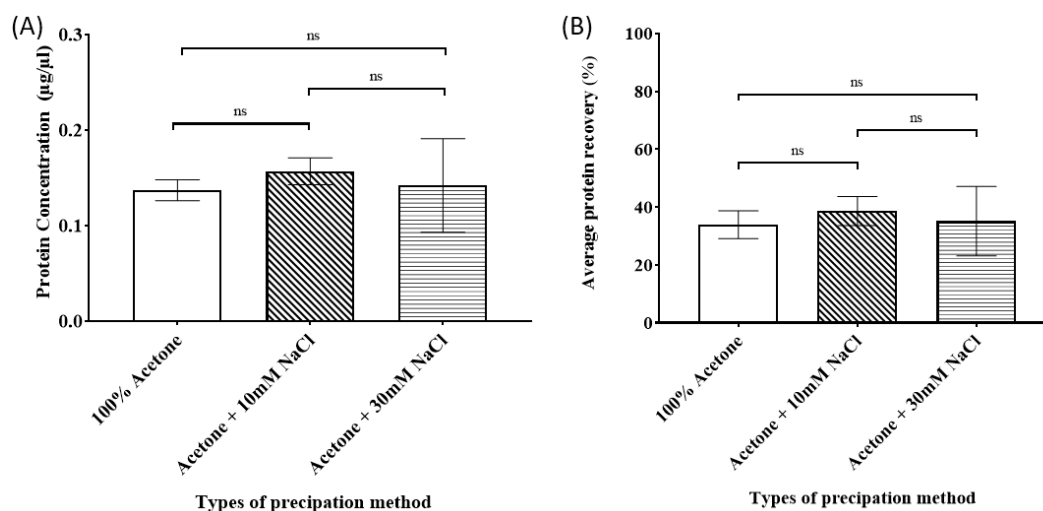


Figure 3.7 (A) The protein concentration ($\mu\text{g}/\mu\text{l}$) after each precipitation method (100% Acetone, Acetone+ 10mM NaCl, and Acetone+ 30mM NaCl). (B) Overall protein recovery (%) for three precipitation methods. One-way ANOVA testing with a significant level set at 0.05, ($n= 3$), Tukey post hoc test ($P \leq 0.05$, $*=0.05$, $=0.01$, and $***=0.00$, $n= 3$ for each condition).**

3.1.2.4 Discussion

Precipitation is a common and essential practice for a proteomic workflow to remove contaminants such as detergents and salts. Not only the type of precipitating agent used would alter the types of protein to be precipitated (Chan et al., 1986), the starting concentration of the protein sample also affects (while small amounts are harder to be precipitated) resulting in a variable and unpredictable protein recovery for different tissue nature. The principle behind precipitation is now suggested to be the aggregation of proteins due to the alteration of protein hydration by hydrogen bonds (Wingfield, 2001). The protein hydration is further reduced by adding organic solvents leading to protein aggregation. The supernatant will carry the proteins to aggregate against the liquid phase. Traditional precipitation involves the use of acetone (Buxton et al., 1979), combinations of organic solvents like TCA (Arnold & Ulbrich-Hofmann, 1999; Peterson, 1977), and chloroform (Mirza

et al., 2007) has also been reported for this purpose. As several steps involve the removal of liquids, samples are prone to a certain degree of sample loss, resulting in unpredictable protein loss during this aggregation step (Griffin & Schnitzer, 2011). The low starting protein concentration (around 10-20 μg) of vitreous is heavily affected during these precipitation steps, resulting in a low protein recovery for all three methods (below 50%).

Using the acetone alone required minor handling/ steps compared to the other two Chloroform/ methanol (challenging to handle and time-consuming) and TCA/ Acetone (similar to acetone, but with the additional step of adding TCA). Chloroform/ methanol required extra steps, including the phase separation and the removal of different layers of solvent, which were more prone to sample loss depending on how well the protein sticks inside the layer and with a low starting concentration. This can be reflected in the SD obtained in protein concentration ($\mu\text{g}/\mu\text{l}$) comparison. Precipitation using only acetone yielded the highest protein concentration ($\mu\text{g}/\mu\text{l}$) and protein recovery (%). However, overall general recovery proteins from all three methods were relatively low (below or around 50%) for all three methods, probably due to the intrinsic limitation of low starting materials after the homogenization step.

Generally, 70-80% of acetone is used in protein precipitation for an acceptable protein recovery (Davidsson et al., 1999). The Addition of salt (NaCl) allowed the “salting-out” event where the protein solubility decreased, leading to protein precipitation. The hydration layer of the protein will be pushed away against the layer of water due to the cosolvent. Therefore, salt should affect the protein precipitation efficiency. A study from Jessica L. Nickerson et al. showed that there was only negligible effect in % recovery in 80% Acetone with the addition of minimal salt (<1mM NaCl), whereas else a higher salt content (>10mM NaCl) can result in a higher recovery rate in BSA (up to 99%) (Nickerson & Doucette, 2020). However, there were no significant differences or drastic improvements in protein recovery with the addition of NaCl (either 10mM or 30mM) observed with the vitreous samples. This could be explained as vitreous tissue mainly containing collagen and hyaluronic acid, and the % of salts within the vitreous is relatively

low. The amount of salt (10mM to 30mM) might not be enough to affect vitreous due to the already diluted nature. These results suggested this method could be tissue oriented. Furthermore, the low starting concentration of vitreous could mean that there are always the chances for uneven precipitation inside the tube. If the evaporation or removal of supernatant is not done completely, precipitants could be removed along the way, affecting the downstream steps such as trypsin digestion. To see the full effect of the addition of NaCl to vitreous proteins, smaller and wide range of the additional concentration steps should be done.

3.1.2.5 Conclusion

This study explored various precipitation methods on the chick vitreous, and the results concluded that acetone precipitation yielded the highest protein recovery rate (with an average of 43%) and 10% TCA/Acetone produced the lowest efficiency. It is clear from the results that the protein recovery from these three methods was below 50%, which makes it challenging for vitreous downstream processing and applications. Although acetone participation requires overnight for proteins to aggregate, it remains the best method out of the three tested and will be used for future vitreous proteomic studies.

The addition of 10mM or 30mM NaCl during acetone precipitation resulted in no significant differences in protein concentration ($\mu\text{g}/\mu\text{l}$) and protein recovery. Although a slight increase in protein concentration ($\mu\text{g}/\mu\text{l}$) and protein recovery was observed, this could just be the variation from the unpredictable protein recovery rate from acetone precipitation. Since the changes in recovery were not drastic and significant, there was no need to add NaCl for additional side effects. Acetone precipitation will be kept as the primary method for precipitation of vitreous proteomic study.

3.1.3 Cleanup method (SPE (HLB) /ZipTip /Spin column)

3.1.3.1 Introduction

Before injecting digested peptides in the MS, cleaning steps such as desalting should be done as these impurities will hamper the performance and the detection of the peptides due to ionization suppression (Annesley, 2003; Hao & March, 2001). Solid-phase extraction (SPE) has been a commonly used technique in the purification and cleaning of samples before being subjected to MS analysis. Various formats of SPE are commercially available in the current market ranging from pipette tips, cartridges, and spin columns (Ötles & Kartal, 2016; Płotka-Wasyłka et al., 2016). The current vitreous proteomics suffers from the low starting protein concentration available for sample preparation. After acetone protein precipitation, the sample is in a large volume of re-dissolving buffer (1M Urea in 25 mM Ammonium bicarbonate). This volume posed a problem in the current clean-up method using ZipTip as the loading volume is restricted to around 10 µl and below. Other column-based kits, such as spin-columns and cartridges, offer a larger loading volume and peptide binding amount, which could be helpful in the preparation of vitreous samples. The main objective of this study was to compare three commercial SPE clean-up kits: ZipTip (C-18), C-18 spin column, and hydrophilic-lipophilic balance (HLB) cartridge in terms of peptide recovery (%), recovery repeatability, and the initial trial of protein analysis of vitreous samples from these methods.

3.1.3.2 Methods and materials

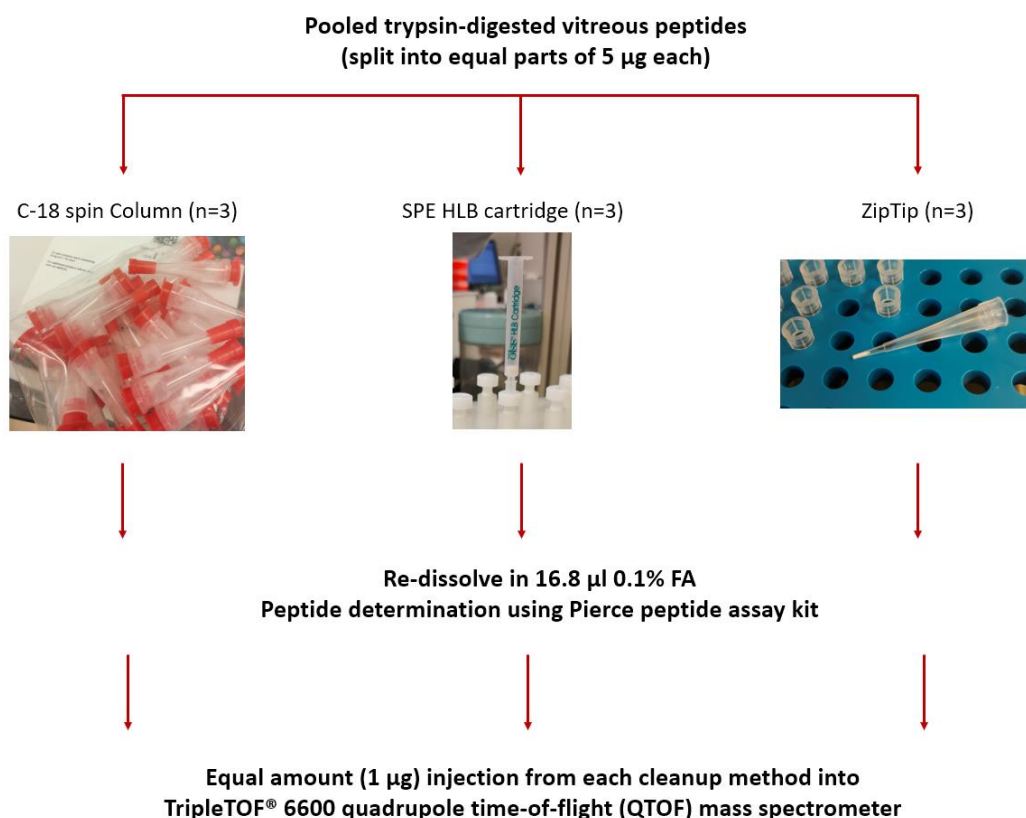


Figure 3.8 Pooled trypsin-digested vitreous was split into 9 equal parts (5 µg each) and went through each type of cleanup method (n= 3 for each method: C-18 spin column, SPE HLB cartridge, and ZipTip). Samples were vacuum dried and re-dissolved in equal amounts of 0.1% FA. The peptide concentration was measured for peptide recovery (%) and was injected into MS for protein analysis.

Trypsin-digested vitreous peptides preparation

Precipitated vitreous proteins were pooled together from the previous experiment, and the protein concentration was determined again using a protein assay kit. A total pool of 54 µg of vitreous proteins was digested in-solution with trypsin (1:25, w/w, protein concentration: trypsin concentration) for 16 hours at 37 °C. After that, the pool of digested peptides was split into 9 equal parts (5 µg each) and was cleaned up using the three cleanup methods (C-18 Spin column, HLB SPE cartridge, and ZipTip, shown in Figure 3.8).

Pierce C18- Spin column

A commercially available spin column containing C-18 resins was purchased (Cat# 89870, Thermo Fisher Scientific, USA), and procedures were done according to the manufacturer's protocol. In brief: samples were adjusted to 0.1% TFA. Twenty microliters of 0.1% TFA in 80% ACN were loaded into the spin tip and centrifuged for 1000 x g for 1 minute. The spin tip was then equilibrated by adding 20 µl of 0.1% TFA and centrifuged at 1000 x g for 1 minute. Samples were loaded and centrifuged at 1000 x g for 1 minute; this step was repeated twice to ensure peptide binding. The tip was washed by adding 20 µl of 0.1% TFA and centrifuged at 1000 x g for 1 min twice. Samples were eluted by adding 20 µl of 0.1% TFA in 80% ACN and centrifuged for 1 minute 2 times. Samples were then vacuumed dried (CentriVap, Labconco, USA) and resuspended in 0.1% FA.

Oasis HLB C-18 cartridge

Commercially available SPE HLB cartridges were purchased, and the protocol was done according to the manufacturer's protocol; in brief: Samples were adjusted to 0.1% TFA and cartridges were placed into a vacuum system (Visiprep SPE system, Supelco, USA) for elution. Columns were conditioned by adding 1 ml of 100% ACN, then 1 ml of 0.1% TFA was added to wash the column. Samples were then loaded into the column slowly, and this step was repeated twice to ensure peptide binding. Then, the column was washed with 1ml of 0.1% TFA, then with 0.1% TFA with 5% methanol. Lastly, the peptides were eluted by adding 500 µl of 60% ACN with 0.1% TFA. Samples were then vacuumed dried (CentriVap, Labconco, USA) and resuspended in 0.1% FA.

ZipTip C-18 column

Commercially available ZipTip tips containing C-18 resins were purchased (Cat# ZTC18S960, Merck Millipore, USA), and the protocol was done according to the manufacturer's protocol, in brief: Samples were adjusted to 0.5% FA. Seven microliters of 100% ACN were carefully pipetted and allowed to pass through the ZipTip at least 7 times for the conditioning of the tip. Then 7 µl of distilled water was pipetted at least 10 times to ensure all the ACN were washed out. Samples were

then pipetted into the ZipTip slowly 10 times to ensure the most peptide binding. Then the tip was washed with 0.5 % FA at least 10 times for desalting peptides. After that, an elution buffer (0.5% FA in 1:1 (v/v) water: Acetonitrile) was used, pipetted into the tip, and was allowed to hold on for 20 sec to ensure extraction. The solution was eluted to a 1.7 ml Eppendorf tube, and the process was repeated for the remaining volumes. Samples were then vacuumed dried (CentriVap, Labconco, USA) and resuspended in 0.1% FA.

Protein identification using Information-dependent acquisition (IDA)

The MS running condition and gradient were the same as stated in the Methods section (Chapter 2.3) unless otherwise specified. In brief, the standard long gradient (155mins) was used with the gradient profile: 0-0.5 min: 5%B, 0.5-90 min:10%B, 90-120 min:20%B, 120-130 min:28%B, 130-135 min:45%B, 135-141 min:80%B, 141-155 min:5%B. The TOF-MS survey scan range was set between 350 m/z-1800 m/z (250ms accumulation time), then MS/MS scans from 100 m/z- 1800 m/z (50ms accumulation time) in high sensitivity mode with rolling collision energy for collision-induced dissociation followed. Equal amounts (1 μg) of peptides were injected into MS for protein identification.

3.1.3.3 Results

Peptide concentration and recovery

To see the effect of cleanup methods on the peptide recovery, a peptide assay kit (Cat# 23275, Thermo Fisher Scientific, USA) was used to measure the peptide concentration ($\mu\text{g}/\mu\text{l}$) and the actual peptide amount (μg). The peptide recovery (%) was calculated by the initial concentration (5 μg) divided by the obtained peptide concentration after cleanup. For peptide concentration ($\mu\text{g}/\mu\text{l}$) measurements (shown in Figure 3.9 A), the SPE HLB cartridge method had the highest concentration with $0.204 \pm 0.036 \mu\text{g}/\mu\text{l}$ and followed up with C-18 spin column and ZipTip having $0.148 \pm 0.042 \mu\text{g}/\mu\text{l}$ and $0.14 \pm 0.012 \mu\text{g}/\mu\text{l}$, respectively. In terms of peptide recovery (%) shown in Figure 3.9 B, the SPE HLB cartridge method had the highest recovery of $42.864 \pm 7.480\%$ and followed up with C-18 spin column

and ZipTip, having $31.081 \pm 8.912\%$ and $29.365 \pm 2.621\%$, respectively. ANOVA tests can be found in Appendix 1.3.

Protein identified from IDA mode

At 1%FDR, 474 proteins (3479 peptides) were identified in the SPE HLB cartridge group, 431 proteins (3056 peptides) were identified in the C-18 spin column group, and 566 proteins (4213 peptides) were identified in the ZipTip group (Figure 3.9 C). A total of 680 distinct proteins were found from all the injections using combined search, where 312 proteins (46%) were found across all the IDA injections shown in Figure 3.9 D. From the 211 proteins that were distinct from each group, 58% belonged to the ZipTip group, 20% to the C-18 spin column group, and the remaining 22% to the SPE group. The full list of distinct proteins found from each cleanup method can be found in appendix 1.4. The Venn diagram was plotted using the interactive shiny app (Khan & Mathelier, 2017), and distinct proteins from each group were analyzed based on their Grand Average of Hydropathy (GRAVY) score. Proteins from ZipTip had an average score of -0.4, HLB SPE cartridge with -0.4, and C-18 spin column with -0.3 (shown in Figure 3.10), indicating that the proteins are primarily hydrophilic.

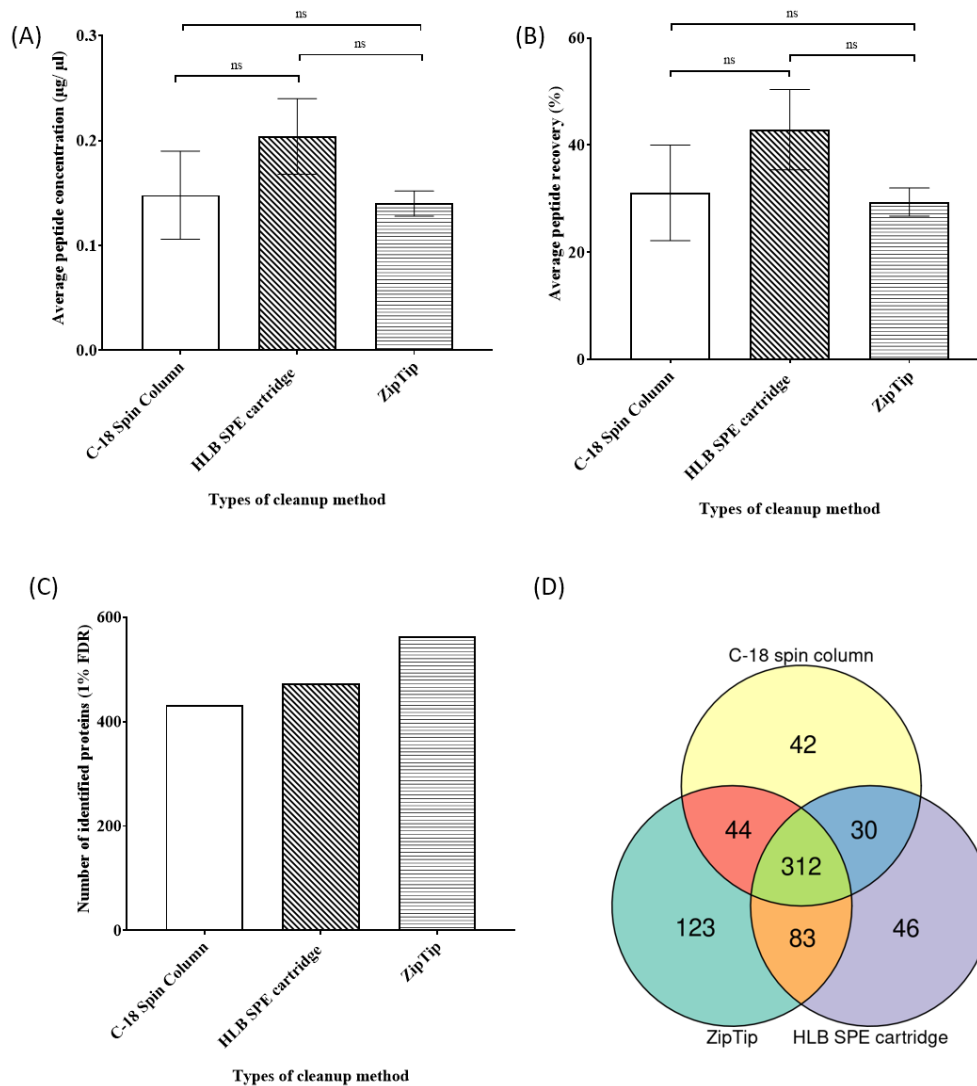


Figure 3.9 (A) The average protein concentration ($\mu\text{g}/\mu\text{l}$) was measured after each cleanup method. One-way ANOVA, significant different setting as 0.05, $n= 3$. (B) The average peptide recovery (%) from the three types of cleanup methods. One-way ANOVA, significantly different setting as 0.05, $n= 3$. (C) The number of proteins identified at 1% FDR for each clean-up method. (D) Venn diagram showing the overlapping and individual proteins obtained from the IDA experiment at 1% FDR.

Table 3.1 Top 10 vitreous proteins found overlapped from all three clean-up methods at 1% FDR.

Uniprot ID	Protein name	Gene name	Length	Mass
A0A1D5NW68	Serum albumin	ALB	565	64004
F1NJT4	Fibronectin	FN1	2526	277189
A0A1D5P4L7	Ovotransferrin	TF	705	77819
F1NII7	Fibrillin 1	FBN1	2861	311028
F1NE63	Reelin	RELN	3462	388525
A0A1D5PU94	C4a anaphylatoxin	C4A	1687	189992
A0A1D5PJN7	Follistatin like 5	FSTL5	846	95678
F1NA61	Retinol-binding protein 3 precursor	RBP3	1235	136345
A0A1D5P380	EGF containing fibulin like extracellular matrix protein 1	EFEMP1	451	50654
A0A1L1RJF5	Apolipoprotein A-I	APOA1	264	30680

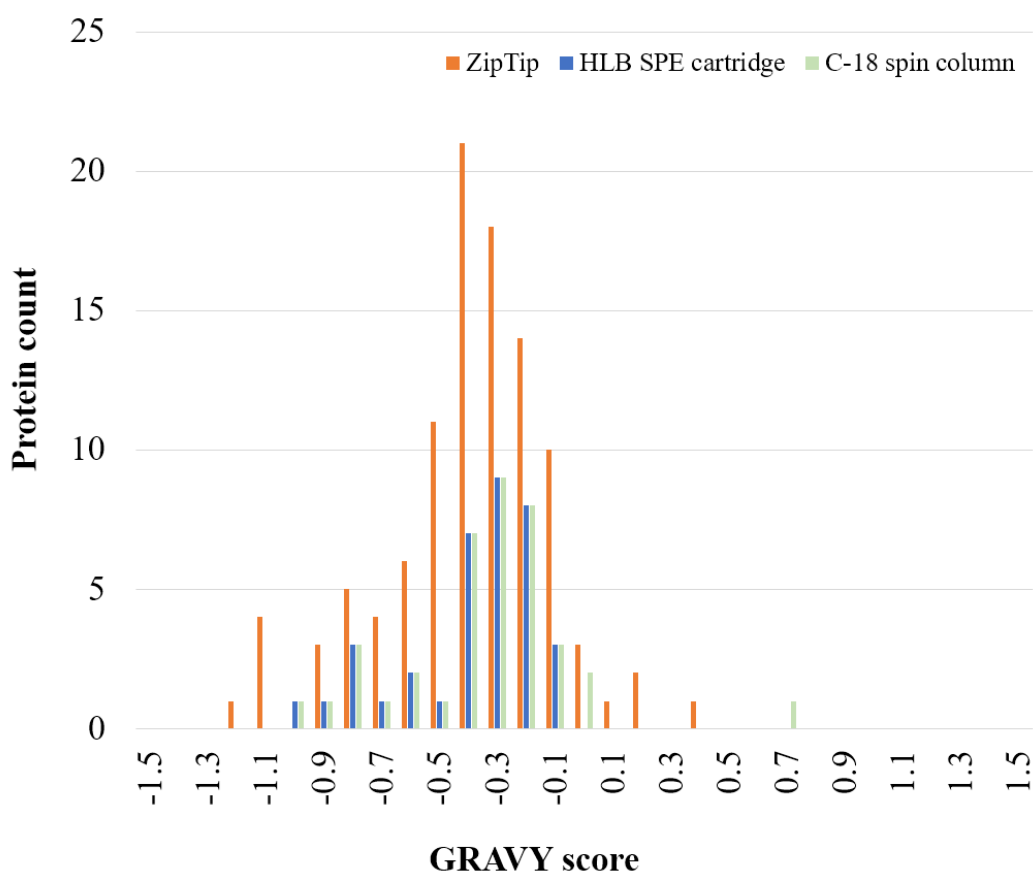


Figure 3.10 Gravy index score (average hydrophobicity and hydrophilicity) of vitreous proteins under three clean-up methods. Hydrophobicity scores below 0 are more likely to be hydrophilic proteins, whereas above 0 are more likely to be hydrophobic proteins. (ZipTip: Orange, HLB SPE cartridge: Blue, and C-18 spin column: Green).

3.1.3.4 Discussion

The main objective for this comparison of cleanup methods was to see the effect of commercially available cleanup columns on the recovery of vitreous peptides. It is essential to determine a workflow with a minimum sample loss for downstream vitreous proteomics study. A cleanup step before MS injections will remove the contaminants, which can affect the performance where extra peaks that might cover peptides of interest are detected and ion suppression of ESI (Annesley, 2003). The peptide recovery (%) and the ease of handling were mainly focused on and compared. The protein data analysis from MS served as a trial for establishing a

vitreous proteome as the sample remained after the cleanup part was only available for one IDA injection each.

The workflow of column-based cleanup mainly involves three steps: column activation, peptide binding, and elution of peptides. ZipTip C18 contains the same material found in a typical C18 reversed-phase column, often used to remove the salts and contaminants of peptide samples. The binding capacity is around 5 μg , but the loading volume is only around 10 μl or less which is undesired for large volumes of peptides. Also, as this is in small tip form, multiple pipetting will be needed for a large volume sample, and therefore a high amount of workload and time consumption will be required for a large sample size.

HLB SPE cartridges can load up to 30 mg of peptides with a load volume of 1 ml. Multiple samples (up to 12) can be done using a vacuum-based system, further shortening the time needed overall. The C-18 spin columns include a C-18 reversed-phase resin for peptide binding. The spin-column relies on the centrifugation forces from a centrifuge for solutions to pass through the resin bed. It allows 10 ng to 30 μg and a bed volume of 10 to 150 μl binding capacity, and multiple samples can be done simultaneously in around 30mins. Although no significant differences were found in peptide concentration ($\mu\text{g}/\mu\text{l}$) as well as the peptide recovery (%), HLB SPE cartridge workflow provided the simplest workflow steps in the compared methods, as well as allowing the largest volume to be loaded in which is an advantage when diluted samples are used. The time consumption was also the shortest in the tested groups. ZipTip resulted in the lowest peptide concentration ($\mu\text{g}/\mu\text{l}$) and recovery yield out of the three methods. It could be due to the sample volume loading limit where repeated pipetting of the sample was needed. This will increase the handling time, as well as be subject to more errors with each time loading the digested samples. One-way ANOVA testing showed that there were no significant differences in protein concentration ($\mu\text{g}/\mu\text{l}$) and protein recovery (%) indicating that all three types of cleanup methods could be used for vitreous peptide cleanup, and the remaining deciding factor is the ease of handling procedures as well as the time consumption. The HLB SPE cartridge method had the advantage of multiple samples while having the highest loading capacity.

Protein analysis

Only one IDA injection was done on the three groups due to the low volume of the samples; therefore, this is just an initial showcase of the current proteomics workflow of vitreous. Despite the low recovery rate from ZipTip, the protein ID from this group was the highest among the three cleanup groups. The 312 proteins that were found across all groups can be seen as “core” vitreous proteins (the top 10 highly abundant proteins are shown in table 3.1) and are expected to be identified in vitreous samples also in human studies (Shitama et al., 2008; Skeie et al., 2015). From the 680 distinct proteins identified in all three groups, 211 proteins were found to be distinct proteins that were only identified from the individual groups. Surprisingly, the lowest protein recovery ZipTip group had the largest portion (58%) of the distinct peptides identified, while the HLB SPE cartridge group had (22%) and the rest (20%) from the C-18 spin column. It is worth noting that these extra proteins acquired might be due to the stochastic nature of IDA; there is just a list of proteins that could potentially be due to the different types of cleanup methods. Guo et al. showed that SPE HLB columns tend to favor hydrophilic peptides with the sacrifice of hydrophobic peptides in human plasma (Guo & Kristal, 2012). However, the distinct proteins had similar GRAVY scores and characteristics from this vitreous study. Due to the low resulting peptide concentration, equal amounts of peptides from each cleanup method were injected into the MS, but it was only enough for one IDA injection run; therefore, variable repeatability should be considered for the identified proteins. This won't reflect the actual differences in these cleanup methods in terms of ID but will give a first impression of the vitreous protein ID and an initial vitreous proteome.

3.1.3.5 Conclusion

Three cleanup methods (ZipTip, SPE, and spin-column) were tested for vitreous peptide clean-up. One-way ANOVA tested no significant differences in terms of the peptide concentration ($\mu\text{g}/\mu\text{l}$) and the peptide recovery (%). Cleanup using SPE was chosen as the main method due to the highest loading/ binding capacity while yielding the results of the peptide concentration ($\mu\text{g}/\mu\text{l}$) and the peptide recovery

(%) in the least amount of time. The ZipTip group had the highest number of distinct proteins and peptides identified (58%), and a vitreous proteome of a total of 680 distinct proteins was established. Initial IDA results showed that 312 “core” vitreous proteins could be identified in all three clean-up methods. Further optimization from MS condition settings will be the next step in optimizing vitreous workflow.

3.2 MS optimization

Throughout the previous sections in Chapter 3, the vitreous sample preparation is now mostly optimized, and an initial proteome was established. This stage will be focused on how vitreous peptides are loaded and bound to the liquid chromatography (LC) and mass spectrometer (MS) system, including the conditions of the running parameters for a better optimized vitreous proteomic workflow.

3.2.1 Vitreous sample loading quantity in information-dependent acquisition (IDA) mode

3.2.1.1 Introduction

With the limited sample quantity (μg) obtained from sample preparation, there is a need to find an optimal injection concentration for vitreous proteomic studies that can provide quantifiable results without sacrificing the number of proteins identified. Ideally, the number of proteins should increase as the loading high amount (μg) increases, but this will level off slowly at a certain level as the number of proteins in the sample should be limited. Too much sample injection load may also over-load high abundant peptides, which will adversely impact quantification. The low number of proteins from the initial steps limits the flexibility for downstream applications; therefore, it is best to use the least amount at each stage to preserve peptides for later studies. The number of proteins identified from various loading amounts will allow us to decide how many biological samples can be used for downstream applications such as quantification with SWATH and validation (MRM). To determine the effect of loading quantity on protein identification, 3 concentrations of digested peptides (low- 0.5 μg , normal- 1 μg , and high- 2 μg) were injected into the TripleTOF MS system for protein identification.

3.2.1.2 Method and materials

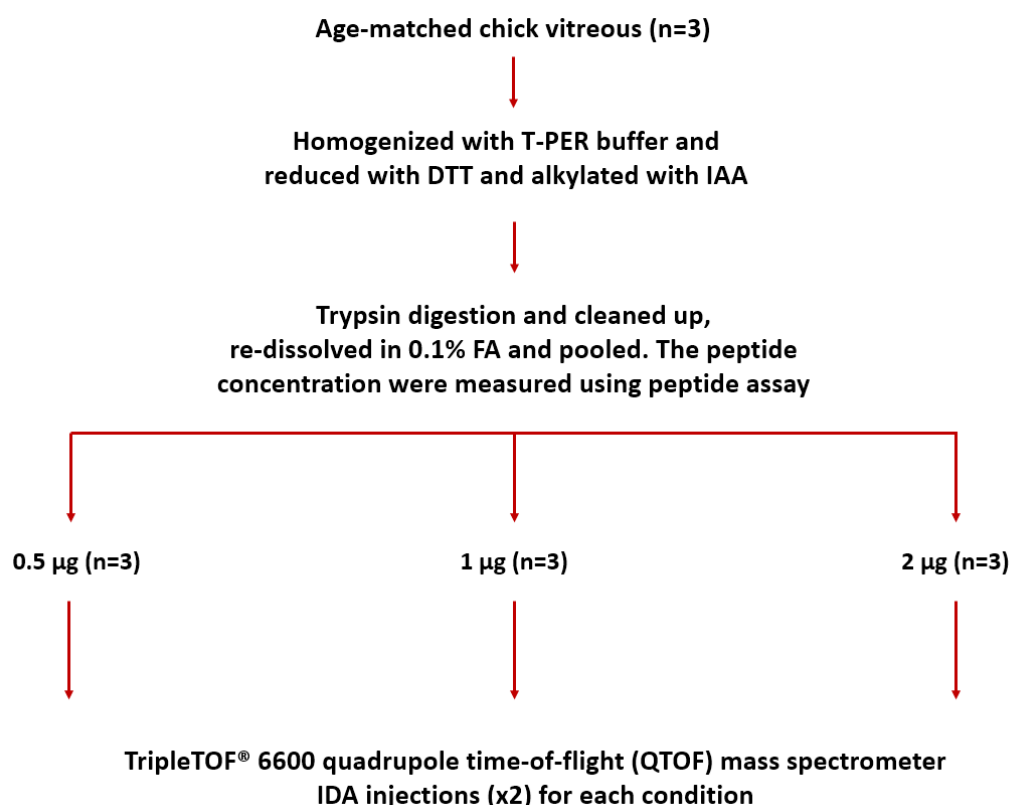


Figure 3.11 Age-matched vitreous samples were collected (n= 3) and digested. These were then pooled together, and the peptide concentration was measured using a peptide assay kit. Digested peptides were then diluted into 3 groups: 0.5 µg, 1 µg, and 2 µg (n= 3) for quantity injection determination into the MS in IDA mode (2 injections for each condition).

The experiment design is shown in Figure 3.11, and the vitreous sample preparation method is shown in Chapter 2 unless otherwise stated. In brief: Age-matched chick vitreous (n= 3) was homogenized with T-PER buffer, reduced with DTT, and alkylated with IAA. Samples underwent acetone precipitation overnight and were digested overnight with trypsin (1:25, w/w). Digested samples were then cleaned up using the HLB SPE cartridges, and peptide concentration was measured. Digested vitreous samples were pooled together, and the peptide concentration was set as three different concentrations (0.5 µg, 1 µg, and 2 µg) injections by dilution using 0.1% FA. Samples were injected in duplicates in IDA mode, running a standard 155 mins gradient.

Data analysis

Technical replicates (n= 2) of IDA injections were searched using ProteinPilot (v5.0, Sciex, USA) against a Uniprot gallus gallus database (39805) for protein identification. The settings are the same as in Chapter 2.3 unless otherwise specified. Venn diagram was plotted using the interactive shiny app (Khan & Mathelier, 2017).

3.2.1.3 Results and discussion

Protein and Peptides identification

Three different concentrations of vitreous peptides (0.5 µg, 1 µg, and 2 µg) injections were prepared and run through the Triple TOF MS system. A combined search was performed on the technical replicates (x2) of each condition using the ProteinPilot software. A total of 695 proteins (8161 peptides), 859 proteins (9898 peptides), and 923 proteins (10637 peptides) were identified for 0.5 µg, 1 µg, and 2 µg, respectively shown in Figure 3.12 A and B. There was a 24% increase in protein numbers in 1 µg injections from 0.5 µg injections and a 7% increase in 2 µg from 1 µg (Figure 3.12 A). Distinct proteins from each loading quantity are listed in Appendix 1.5. In terms of identified peptides (Figure 3.12 B), the increase was similar, with a 21% increase from 0.5 µg to 1 µg and an 8% increase from 1 µg to 2 µg. There were 593 proteins identified across all three groups, while 37, 91, and 150 distinct proteins were found from 0.5 µg, 1 µg, and 2 µg groups, respectively.

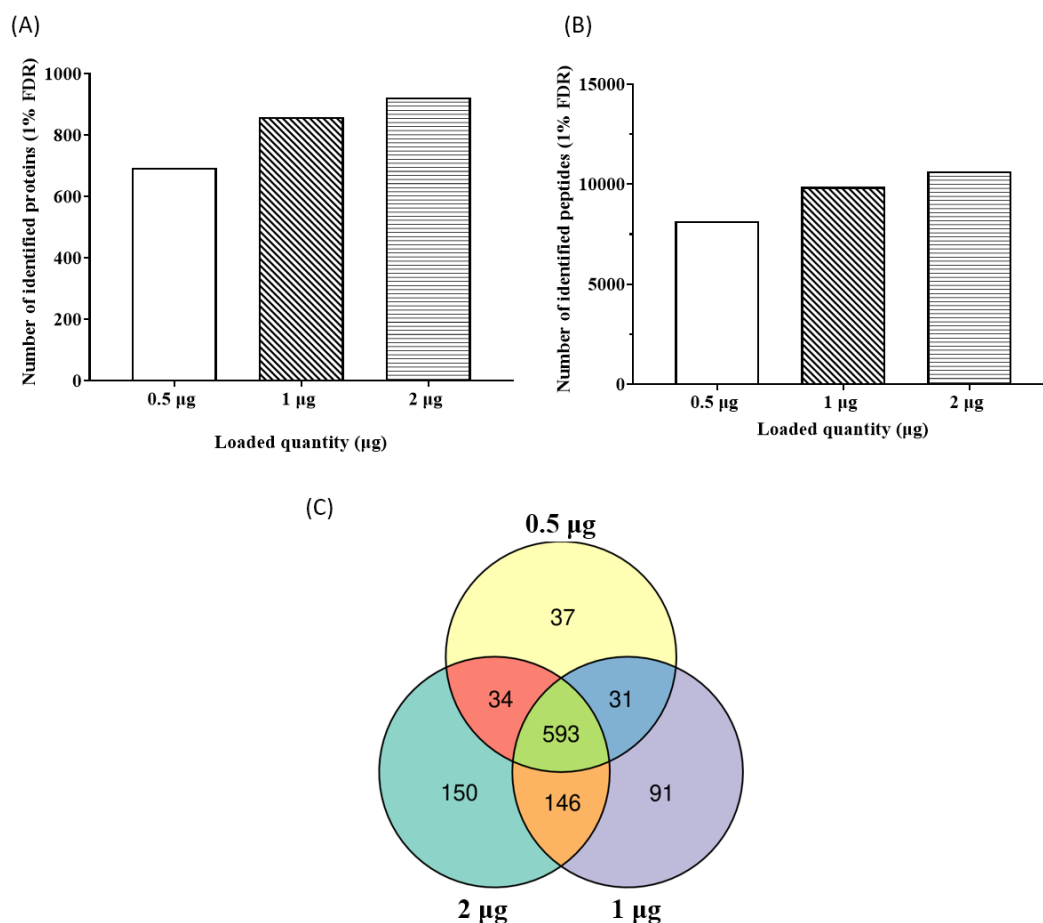


Figure 3.12 (A) Proteins and (B) peptides identified from three injections quantity (0.5 µg, 1 µg, and 2 µg) at 1 % FDR (2 technical replicates for each injection amount group). (C) Venn diagram showing the number of proteins identified (from combined search) overlapped from each group.

To see the effect of the sample loading amount on the number of proteins identified, we have set three sample loading amounts (0.5 µg, 1 µg, 2 µg) of vitreous peptides. Two micrograms were set as it was the highest possible concentration we could get at the moment after sample cleanup. One microgram has been used in previous studies, and 0.5 µg was the lowest for the ideal column condition. As expected, the highest amount (2 µg) injection yielded the highest amount of identified proteins among the three groups, and 0.5 µg had the least proteins to be identified. There was a mere increase of 7% in proteins (8% in peptides) from having 2 µg compared to 1 µg injection, while the increasing gap was drastic from 0.5 to 1, which is 3 times more in comparison. The change in distinct peptides is also similar, with 2 µg injection having the highest extra distinct proteins (14%). Around 55% of all the

distinct proteins can be seen as “core vitreous proteins”, which are all highly abundant. These proteins are well-known components identified in the vitreous across species and are often found in vitreous proteomic studies. The top 5 are serum albumin, Reelin, agrin, Ovotransferrin, and apolipoprotein A-1. Although a 2- μg injection yielded the highest amount of proteins to be identified, it was not without problems. The tradeoff with a small jump only in terms of protein and peptide amounts is not feasible when the input material needed is doubled.

Furthermore, the nano separate column and emitter were more prone to blockage with a higher amount of loading peptides. These sampling problems (using a double amount of peptides) and technical problems that can affect the performance outweighs the benefit of having a slight increase in protein amount; hence the 1 μg injection load was set as the preferred quantity for upcoming vitreous proteomics studies. This study has several limitations: ideally, having a wider range of injection concentration dilution should result in a slope to demonstrate the effect of quantity loading. A higher amount of loading (μg) might result in more protein identification; however, this was not archivable with our current proteomics workflow.

3.2.1.4 Conclusion

Three injection quantity loading of vitreous peptides (0.5 μg , 1 μg , 2 μg) was tested on the effect of protein identification. One μg was chosen as the optimized injection quantity for future vitreous experiments as it is a balanced option in terms of sample usage. Loading a higher amount of sample will only lead to an addition of 7% of proteins to be identified but using much more samples in return. Although it makes sense that loading more μg from each sample yields a higher protein amount to be identified, this limits the number of runs that can be done for downstream applications such as SWATH (DIA) and MRM/ MRM^{HR} validations. Taking this result, the benefits of having 1 μg as the optimal injection quantity outweighed the slight increase in protein/ peptides number in 2 μg .

3.2.2 Vitreous protein repeatability under information-dependent acquisition (IDA) mode

3.2.2.1 Introduction

Tandem mass spectrometry acquires data from the MS/MS threshold of specific spectra that pass the ionization threshold. It is beneficial with abundant proteins where the signal is usually much higher than the threshold. However, it would be a problem for lower abundant proteins that might be covered by nearby peptide fragments and fail to reach the threshold. This resulted in problems such as the lack of repeatability and reproducibility when acquiring the ion library using the traditional IDA method (Tabb et al., 2010). Although there are ways to protein quantitation, such as spectra counting (Choi et al., 2008), there is a need for a more precise method for protein quantitation as the number of samples injection increases.

Furthermore, other variations can also be introduced, such as the variation from sample drawing from the autosampler to the LC (van Midwoud et al., 2007) and protein identification differences from using different algorithms in database searching (Kapp et al., 2005). Since no published data is available now to see the variation in IDA using the TripleTOF 6600 system in vitreous samples, this study serves as the first to see the IDA injection repeatability of the chick vitreous and the % of overlapping proteins as the injection increases. Those overlapping proteins can then be seen as a “core” proteins of interest that could be essential for quantitation purposes such as using label-free (DIA-SWATH). The variation in the proteome will also be useful for guiding the number of IDA injections needed for later experiments.

3.2.2.2 Method and materials

Digested vitreous peptides were obtained following the standard protocol mentioned in the methods Chapter. The peptide concentration was set as 0.2 $\mu\text{g}/\mu\text{l}$, and the injection amount was at 1 μg injection load setting from the previous experiment. The gradient was set as a 155 mins gradient. The pooled vitreous peptide sample (1 μg injection) was injected into the MS 5 times. Then the data

acquired were searched individually against a gallus gallus Uniprot database using the ProteinPilot software with settings shown in Chapter 2.3.

3.2.2.3 Results

Five repeated injections of the same sample were acquired to identify the repeatability of the IDA injections with our vitreous proteomic workflow. The number of proteins identified in each injection is shown in Table 3.2. A total of 967 distinct proteins were identified at 1% FDR in (1-2), with 696 overlapping (72%) proteins found between the two injections. For 3 injection searches (1-3), 1064 distinct proteins were identified at 1% FDR, with 648 overlapped (61%). For 4 injection searches (1-4), 1064 distinct proteins were identified at 1% FDR with 605 overlapped (54%). For 5 injections searching (1-5), a total of 1148 distinct proteins were identified at 1% FDR with 567 overlapped (49%), shown in Figure 3.13 A. The number of distinct proteins increased by 9% from 2 injections searched compared to 5 injections searched, while the % of proteins identified across all injections was reduced by 9%. There was a 16% increase in distinct proteins identified from 1 injection to 2 injections combined, while a 10%, 5%, and 3% increase were found from 2-3, 3-4, and 4-5 injections, shown in Figure 3.13 B. The overlapped proteins decreased remained a constant 7% from 2-3, 3-4, and 4-5 injections, shown in Figure 3.13 C.

Table 3.2 Number of proteins and distinct peptides identified at 1% FDR for 5 repeated injections (T1 -T5) of the vitreous digest.

	Injection				
	T1	T2	T3	T4	T5
Number of proteins identified (at 1%FDR)	847	826	882	823	794
Number of distinct peptides identified (at 1%FDR)	8350	8464	8663	8183	8009

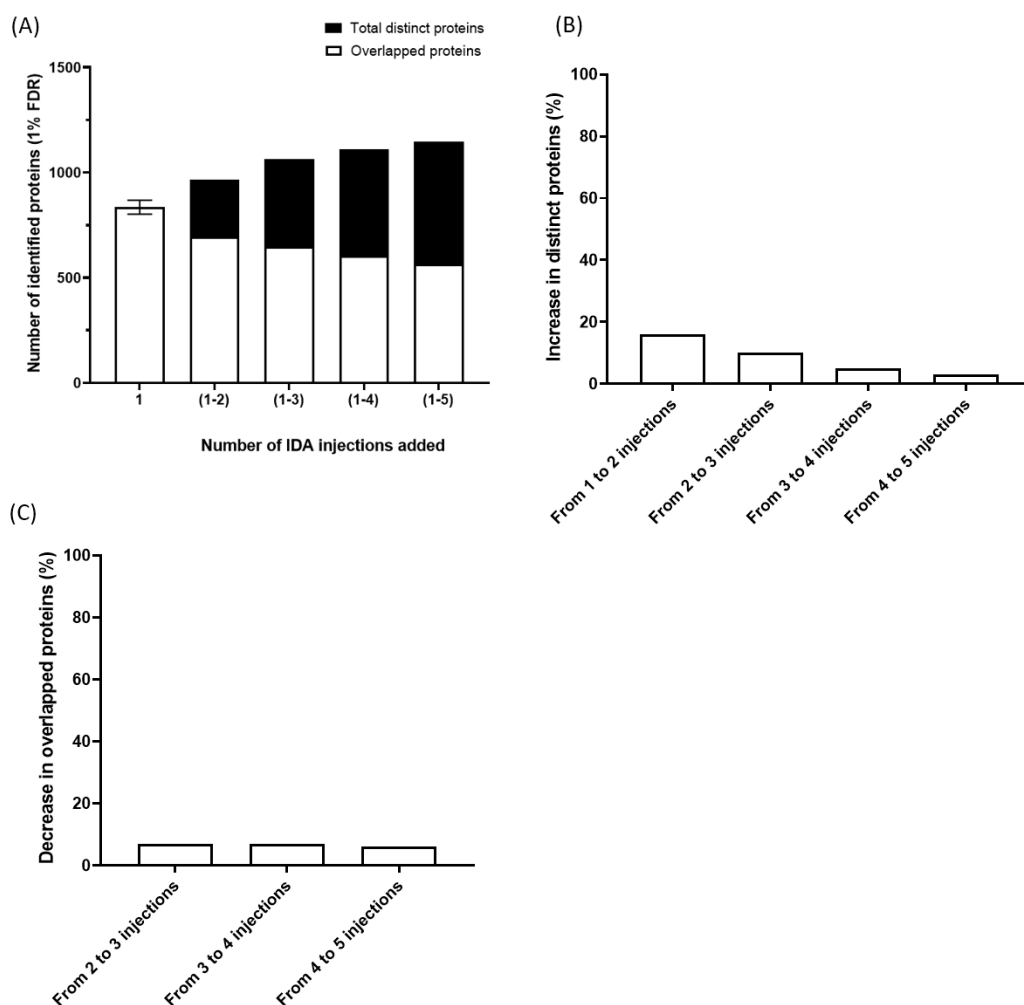


Figure 3.13 (A) The number of proteins identified at 1% FDR from all technical replicates. The black bar indicates the total distinct proteins found from injections; the white bar indicates the number of overlapped proteins. (1) shows the number of proteins identified from only 1 injection, while (1-2) indicates 2 injections were added together, (1-3) indicates 3 injections, (1-4) indicates 4 injections, and (1-5) indicated all 5 injections. **(B)** The increase in distinct proteins from when each technical replicate was added together (%). **(C)** The decrease in overlapping proteins from searching when each technical replicate was added together (%).

3.2.2.4 Discussion

Proteomics studies often employ the typical tandem mass spectrometry with an LC systems approach based on information-dependent acquisition (IDA), where the

most abundant precursor ions from an MS1 scan that passes the threshold will trigger the MS/MS for fragmentation and acquisition of the MS2 spectra (Domon & Aebersold, 2010; McDonald & Yates, 2002; Sajic et al., 2015). As a result, only partial precursors were selected due to the stochastic nature of the IDA method (Liu et al., 2004). This is where problems will start to arise during the quantification phase as proteins lower abundant proteins were not found across the samples. This study aims to look at the degree to which the vitreous samples are affected by the DIA method for the generation of ion library as well as the % of overlapping proteins that could be used for quantification purposes. As expected, the number of distinct proteins increased when replicate injections were introduced. The highest % gap (a 20% increase) was observed from 1 injection to 2 injections combined. However, the gap was reduced to 10% and below compared to 2 to 3 injections and more. This indicates that having more than 3 injections is not that beneficial based on the time needed vs the protein gain. The overlapping of proteins between each injection declined as the number of technical replicates increased. The steady decrease of 7% in overlapping proteins indicated that the % overlapped proteins would be further reduced as the injections increase. A total of 567 proteins (~50%) of these proteins can be seen as core vitreous proteins as these are found even after many technical replicates. These proteins include common vitreous proteins, which were also identified from the previous experiment in earlier Chapters. To quantify a protein, the specific protein should be monitored across all the samples. This is challenging if the pool of overlapped proteins is reduced when there are multiple samples and injections. This variation in proteins identified in IDA mode makes it more challenging to quantify low-abundance proteins precisely. Therefore, other methods, such as data-independent acquisition (DIA) or SWATH, would provide a more precise and accurate quantification method of vitreous proteins (B. C. Collins et al., 2013; Huang et al., 2015).

3.2.2.5 Conclusion

As expected, the % of overlapping proteins declines as the IDA repeat injections of the sample increase. Although there is a slight increase in total distinct proteins identified (~16%), proteins found across all the samples declined drastically from

70% with only 2 repeats to only 50% with 5 repeats in total. Regarding creating an ion library using IDA mode, 2- 3 technical repeats are enough to archive a high % of distinct proteins coverage of vitreous proteome.

3.2.3 HPLC fractionation

3.2.3.1 Introduction

The size of the ion library of a sample is crucial in a successful SWATH proteomics study as the number of proteins within will be the limiting factor of protein to be identified and quantified. For the expansion of the library, apart from repeated IDA measurements of the same sample, we have tested the use of peptide fractionation before MS as an alternative to improve the resolving power for further differentiating the protein isoforms, allowing the coverage for the detection of low abundant proteins. It works by separating the peptides into different compartments based on the nature of the stationary phase, where each fraction can be analyzed to gain deeper learning of the total proteome. There are two commonly used fractionation methods such as charge- (ion exchange) (Choudhary & Horvath, 1996) and size (size exclusion)(Lathe & Ruthven, 1955). Vitreous has many highly abundant proteins, such as albumin and ovotransferrin, which can cover up lower abundant proteins. Fractionation could separate these low-abundant proteins, further expanding the vitreous proteome. This experiment aims to see if fractionation can significantly improve the protein to be identified from the vitreous so that an extensive ion library can be a generation that would greatly help in the quantitation of proteins of interest, especially low abundant proteins that are normally “covered” by high abundant proteins.

3.2.3.2 Methods and materials

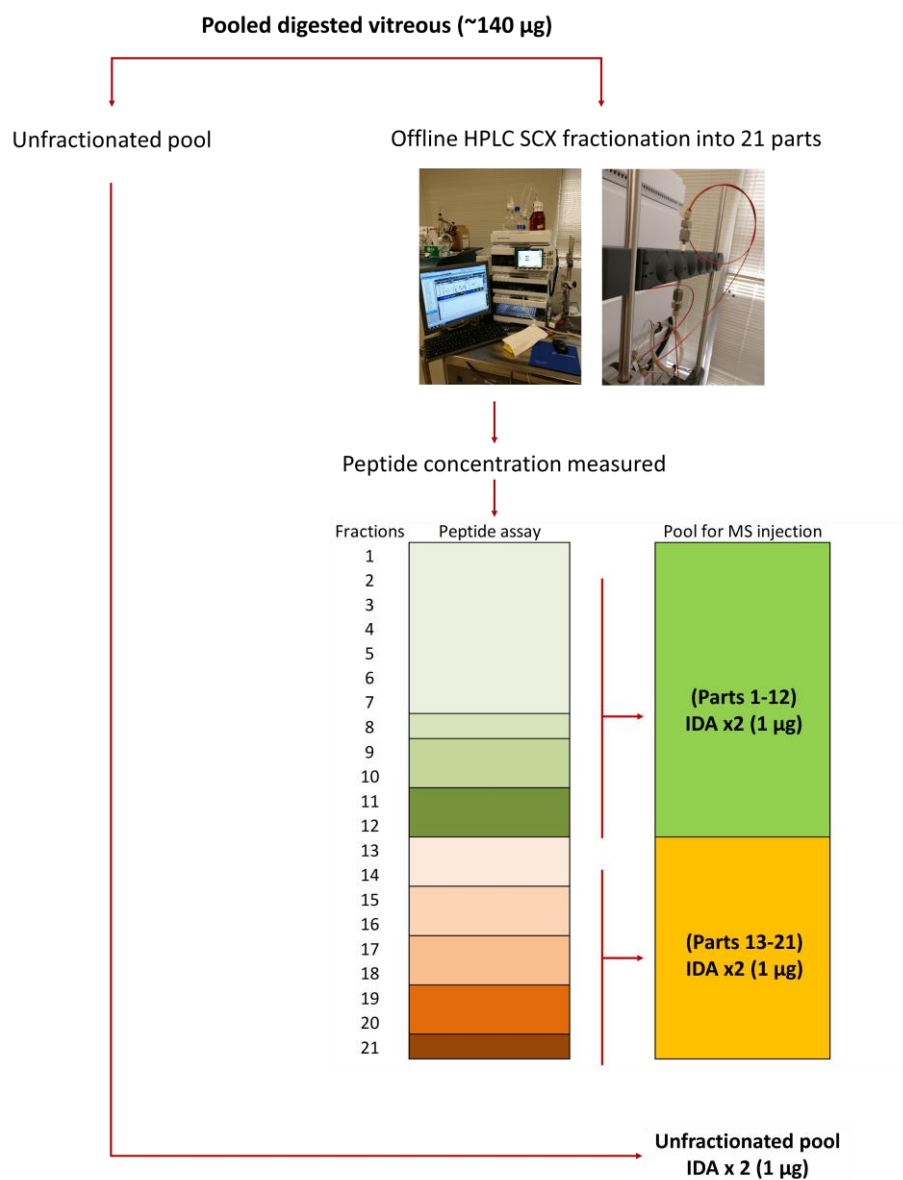


Figure 3.14 A pooled sample of ~140 µg digested vitreous for the unfractionated sample and the fractionation workflow using HPLC fractionation with a reversed-phase (RP) strong cation-exchange SCX column. The sample was separated into 21 parts, and the peptide concentration for each part was measured using a peptide assay kit. These parts (Parts 1-12 and Parts 13-21) were then further combined based on the peptide concentration for loading into the MS under IDA mode.

Vitreous sample preparation

Age-matched vitreous (n= 7) were collected and homogenized with T-PER buffer and prepared the same as described in Chapter 2.2. Around 140 µg of digested vitreous were pooled, and 10 µg of the sample was kept as unfractionated vitreous. The rest were subjected to HPLC fractionation using a strong cation exchange (SCX) column, shown in Figure 3.14.

Strong Cation Exchange (SCX) HPLC fractionation

Vitreous peptides were desalted using an HLB SPE cartridge, the same as described in Chapter 2.2. One milliliter of Buffer A (10mM Ammonium formate in 25% ACN, pH 3) was added to the dried peptides for separation using an SCX column (5 µm, 200 Å, 100 x 4.6mm, PolyLC, USA) using a 1200 infinity series 1260 infinity LC system (Agilent technologies, USA). The fractionation system was composed of buffer A (10 mM Ammonium formate, 25% ACN, pH 3) and buffer B (500 mM Ammonium formate, 25% ACN, pH 6.8). The elution gradient was as follows: 0- 9 mins/ 0% B, 9- 24 mins/ 50% B, 24- 49 mins/ 100% B, 49- 65 mins/ 0% B at a flow rate of 0.8 ml/min at a 65 mins gradient and the sample was separated into 21 fractions. Fractionated parts were then vacuumed dried (CentriVap, Labconco, USA). After that, 10 µl of 0.1% FA was used to redissolve the pellet and the peptide assay was used to determine the peptide concentration of each part. After peptide concentration measurement using a peptide assay kit (Cat# 23275, Thermo Fisher Scientific, USA), fractions were then pooled into 2 parts (1-12) and (13-21), with a 1 µg injection (2 IDA technical replicates) into LC-MS for protein analysis shown in Figure 3.14.

MS settings

The MS settings used in this experiment were the same as shown in Chapter 2.3 (using the 155 mins gradient) unless otherwise specified. In brief, IDA injections were performed on a TripleTOF[®] 6600 quadrupole time-of-flight (QTOF) mass spectrometer (Sciex, USA) coupled to an Eksigent 415 nano-LC system (Sciex, USA). Equal amounts of digested samples (1 µg) from each fraction (1-12, 13-21, and unfractionated) in duplicates were loaded onto the trap column (350 µm x 0.5 mm, C18) at a flow rate of 2 µL min⁻¹ for 15 mins and was then separated with a

nano-LC column (100 μm x 30 cm, C18) at a flow rate of 350 $\mu\text{L min}^{-1}$. Mobile phase A was a mixture of 0.1% formic acid (v/v), 5% acetonitrile (v/v) in water, and mobile phase B contains 0.1% formic acid(v/v), 98% acetonitrile (v/v) in water with the following gradient: 0-0.5 min: 5%B, 0.5-90 min:10%B, 90-120 min:20%B, 120-130 min:28%B, 130-135 min:45%B, 135-141 min:80%B, 141-155 min:5%B. The eluent was introduced into the TripleTOF[®] 6600 quadrupole time-of-flight (QTOF) mass spectrometer (Sciex, USA) with a 10 μm SilicaTip electrospray emitter (FS360-20-10-N-20-C12, New Objective, USA). The TOF-MS survey scan range was set between 350 m/z-1800 m/z (250ms accumulation time), then MS/MS scans from 100 m/z- 1800 m/z (50ms accumulation time) in high sensitivity mode with rolling collision energy for collision-induced dissociation followed.

3.2.3.3 Results

Peptide concentration after fractionation

As equal amounts of peptides should be injected into the MS for comparison, the peptide concentration was determined from each part (21 parts). Multiple parts (8-10, 17-20) were found to have very low peptide content (below detection); therefore, parts were pooled together, and the peptide concentration was measured again. Fractions (1-7) had 2.570 μg , Fractions 11-12 had 9.485 μg , Fractions 13-14 had 3.633 μg , Fraction 15-16 had 0.678 μg , and Fraction 21 with 1.3 μg . As the concentration was still low, parts were pooled together into 2 pooled fractions (1-12 and 13-21), and the peptide assay was done again for IDA (1 μg) injection, shown in Figure 3.15.

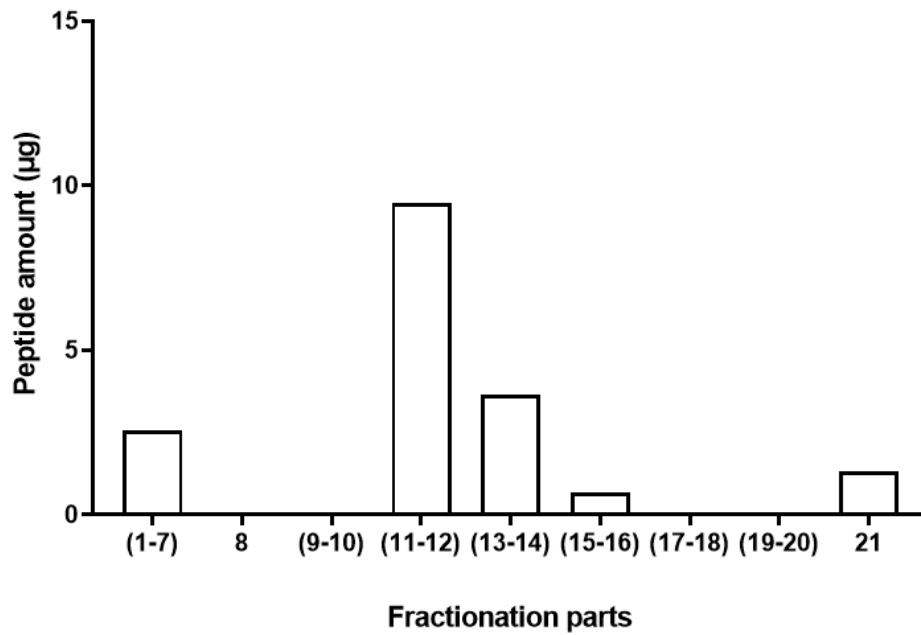


Figure 3.15 The total peptide amount (μg) of each fraction (1- 21). Fractions without bars indicated the concentration was too low for detection.

Protein identification

An equal amount (1 μg) of each fraction: Fraction (1-12), (13-21), and unfractionated vitreous peptide groups were injected into the MS in duplicates. For fractionation parts, 923 proteins and 7496 distinct peptides were identified at 1% FDR for fraction (1-12), whereas 707 proteins and 4837 distinct peptides were identified at 1% FDR for fraction (13-21). For unfractionated samples, a total of 862 proteins and 9767 distinct peptides were identified at 1% FDR from a combined search. When all the fractions were combined and searched, a total of 1097 proteins and 11175 distinct peptides were identified at 1% FDR, showing a 27% increase in terms of proteins from fractionated samples compared to unfractionated, where the increase in peptides was around 31% (shown in Figure 3.16 A and B).

Regarding fractionation efficiency, 62% of proteins were found in only 1 fraction from the SCX fractionation (shown in Figure 3.17 A), indicating that vitreous proteins can be effectively separated using this fractionation. When comparing the two fractions, Fraction (1-12) had more distinct proteins (~39%) compared to Fraction (13-21), which had 23%, while around 482 (40%) of the proteins were found across both fractions shown in Figure 3.17 B. About 55% of proteins were

found in both fractionated and unfractionated groups, while 399 proteins were found distinctly in fractionated groups compared to 168 proteins found only in the unfractionated group.

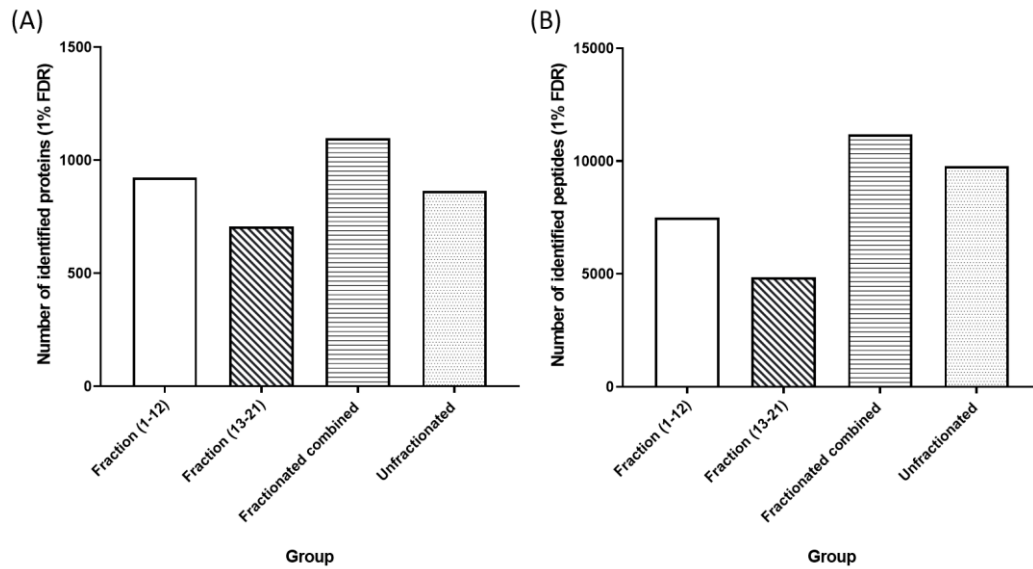


Figure 3.16 The number of (A) proteins and (B) distinct peptides identified at 1% FDR for fraction (1-12), (13-21), fractionated combined (combined search of 1-12 and 13-21 parts) and unfractionated groups.

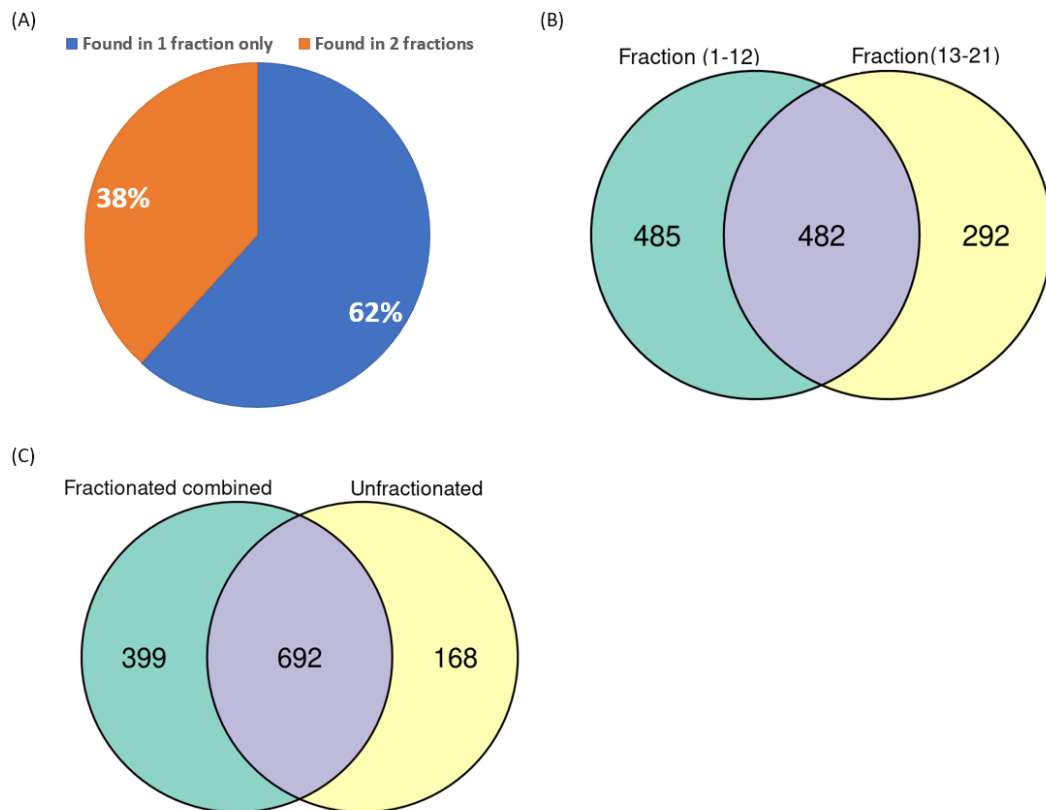


Figure 3.17 (A) The % of proteins identified (1% FDR) in the number of fractions (either only found in 1 or found in 2 fractions). Blue indicates the % proteins that were found in only one fraction [Either in Fraction (1-12 or 13-21)]. Orange indicates % of proteins that were found in both fractions. (B) The number of proteins identified in Fraction (1-12) and Fraction (13-21). (C) The number of proteins identified in fractionated combined (combine search of fraction 1-12 and 13-21) and unfractionated group.

3.2.3.4 Discussion

Fractionation is a helpful technique in proteomics in further extending the ion library, which is often the limiting factor in MS studies (Manadas et al., 2010). Many fractionation methods have been used extensively for the separation of peptides, such as ion-exchange chromatography reversed-phase liquid chromatography (RPLC), strong cation exchange (SCX), and isoelectric focusing (IEF) charge such as ion-exchange chromatography (Brod et al., 2016). This allowed the peptides to be eluted into the MS at different times, separating further

away from each other and reducing the overlapping, allowing the MS to have more time to identify different proteins. Published vitreous proteomic studies have employed the use of fractionation; Gao et al. employed sodium dodecyl sulfate-polyacrylamide gel electrophoresis (SDS-PAGE) to identify 252 proteins in vitreous (Gao et al., 2008) and 1111 distinct proteins were successfully identified by a combination of liquid-phase isoelectric focusing and 1D SDS gel electrophoresis by Aretz et al. (Aretz et al., 2013). A total of 1205 proteins were identified from a combination of SCX, SDS-PAGE, and OFFGEL fractionation by Murthy et al. (Murthy, Goel, Subbannayya, Jacob, Murthy, Manda, Patil, Sharma, Sahasrabuddhe, Parashar, Nair, Krishna, Prasad, et al., 2014). These showed that there are possibilities for further expanding the vitreous proteome by creating an extensive ion library to understand the vitreous better. Peptide concentration after HPLC SCX fractionation in this study was very low in some of the parts, and others had essential no peptides detected by peptide assay. Therefore, they were largely pooled together into 2 parts. The time needed for fractionation via this method was greatly increased by drying and reconstituting the pellet; multiple peptide assay was done on the sample due to the low peptide concentration.

While a large portion of the proteins was found in both fractions, more proteins were found in the earlier fraction (1-12) compared to fraction (13-21) which was in line with the peptide measurements as the earlier part had a higher peptide amount after the fractionation process. With a combined search with all the fraction parts (1-12 and 13-21), there was a 27% increase in terms of protein ID from fractionation compared to its unfractionated counterpart. While this is a welcome addition to the protein number, the extra time consumption needed for the relatively low increase in protein content using fractionation might not be suitable for our vitreous proteomic workflow and the possible errors introduced during the pooling steps. More complex tissue might benefit this type of fractionation, while a high concentration is needed at the start for better separation.

3.2.3.5 Conclusion

There is a 27% increase in the number of proteins using HPLC SCX fractionation compared to unfractionated samples. However, the initial 21 fractions had to be pooled into 2 parts as the peptide concentration was very low in some parts. The time needed for fractionation was very long compared to its unfractionated counterpart due to the drying and reconstitution of fraction parts. At the same time, there was no drastic increase in the number of proteins acquired. Therefore, it was thus not justifiable to adopt peptide fraction for all the subsequent analyses.

3.2.4 Gradient time (90 vs. 155 mins)

3.2.4.1 Introduction

Numerous studies on the effect of the LC separation parameters as the column material, stationary phase, and gradient times/ lengths could easier affect the LC-MS/MS performance (Xu et al., 2009). Typically, a longer length of the separation gradient would yield a higher number of proteins to be identified compared to a shorter gradient (Köcher et al., 2012). Furthermore, more complex samples should use a longer gradient to separate the peptides better. One hundred fifty-five minutes total gradient time has been used in our lab for successful proteomics studies in our previous studies in guinea pig retina (S. W. Shan et al., 2018) and our vitreous study from the last Chapter. As the vitreous is a relatively simpler tissue and more diluted than its neighboring parts such as the retina, there is a chance for shortening the gradient profile while maintaining a similar protein identification profile. It will also reduce the chances of blockage of LC columns, as well as the maintenance of emitters. This experiment aims to see how the change in gradient times affects protein identification.

3.2.4.2 Materials and method

MS gradient

Sample preparation was the same as shown in the Chapter 2.2 section unless otherwise specified. A Pool of digested vitreous peptides was used in this experiment with equal amounts (1 µg) of samples to be injected into the MS in IDA mode in duplicates. Two gradients were used in this experiment: For 155 mins long gradient: 0-0.5 min: 5%B, 0.5-90 min:10%B, 90-120 min:20%B, 120-130 min:28%B, 130-135 min:45%B, 135-141 min:80%B, 141-155 min:5%B (shown in Figure 3.18 A) and a shorter 90mins gradient: 0-0.25 min: 5%B, 0.25-45 min:10%B, 45-60 min:20%B, 60-65 min:28%B, 65-75 min:80%B, 75-90 min:5%B (shown in Figure 3.18 B). Solvent A contained 2% ACN, 0.1% FA, and Solvent B contained 98% ACN, 0.1% FA.

Protein analysis

Two IDA injections were done for each of the gradient settings. The two replicates of IDA were then combined searched against a Gallus gallus Uniprot database using the settings mentioned in Chapter 2.3. The protein ID from the two sets was then compared in terms of protein and peptide amount.

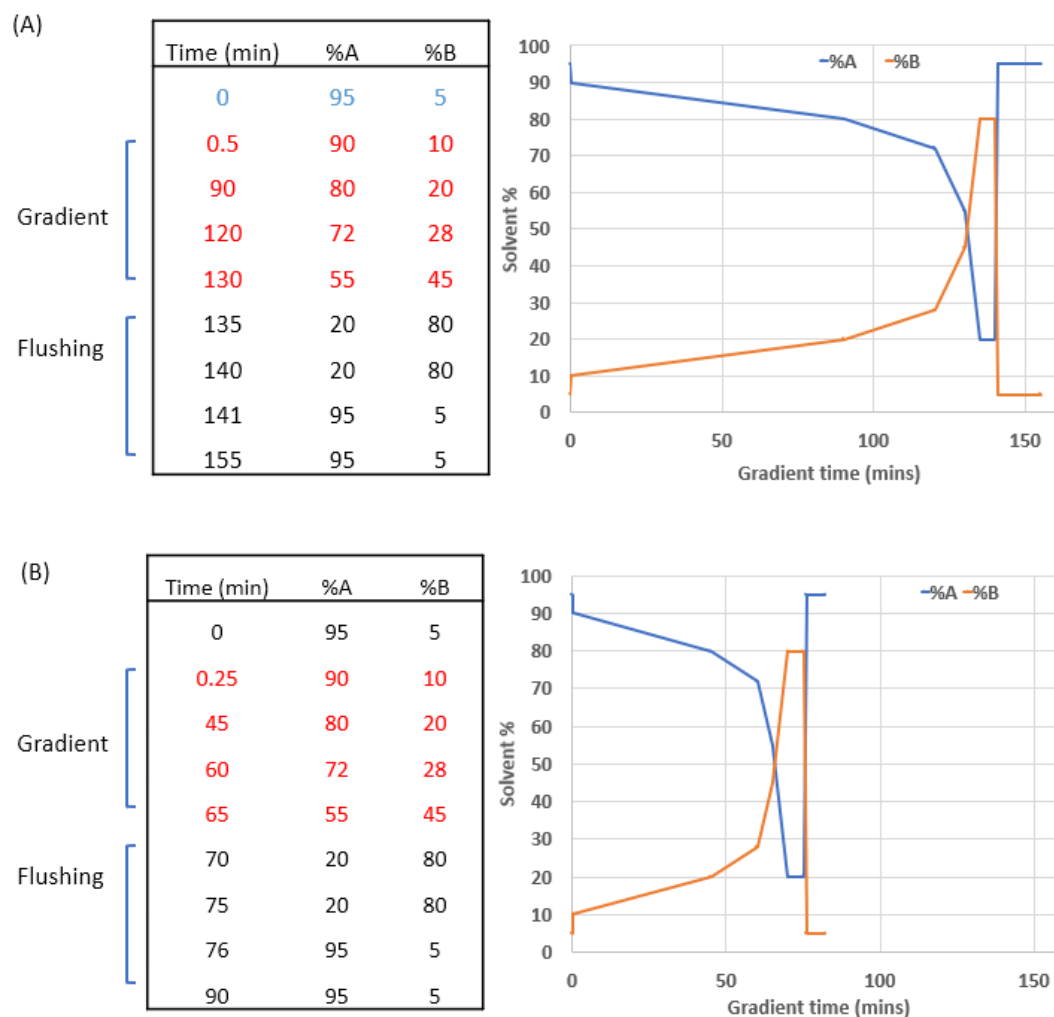


Figure 3.18 Running settings of two MS gradients. (A) standard long (155mins) gradient (B) A shorter (90mins) gradient. Solvent A contained 2% ACN, 0.1% FA, and Solvent B contained 98% ACN, 0.1% FA.

3.2.4.3 Results

Protein identified

A total of 850 proteins (7197 distinct peptides) and 899 proteins (8019 distinct peptides) were identified from the short 90 mins gradient and long 155 mins

gradient, respectively (shown in Figure 3.19 A and B). There was a 5.8% increase in proteins and 11% in peptides from using a long gradient compared to the shorter gradient. While 64% of the proteins were found across the two gradients, 155 mins had more distinct proteins (21%) than 90 mins (16%). The list of distinct proteins found in each gradient can be found in Appendix 1.6.

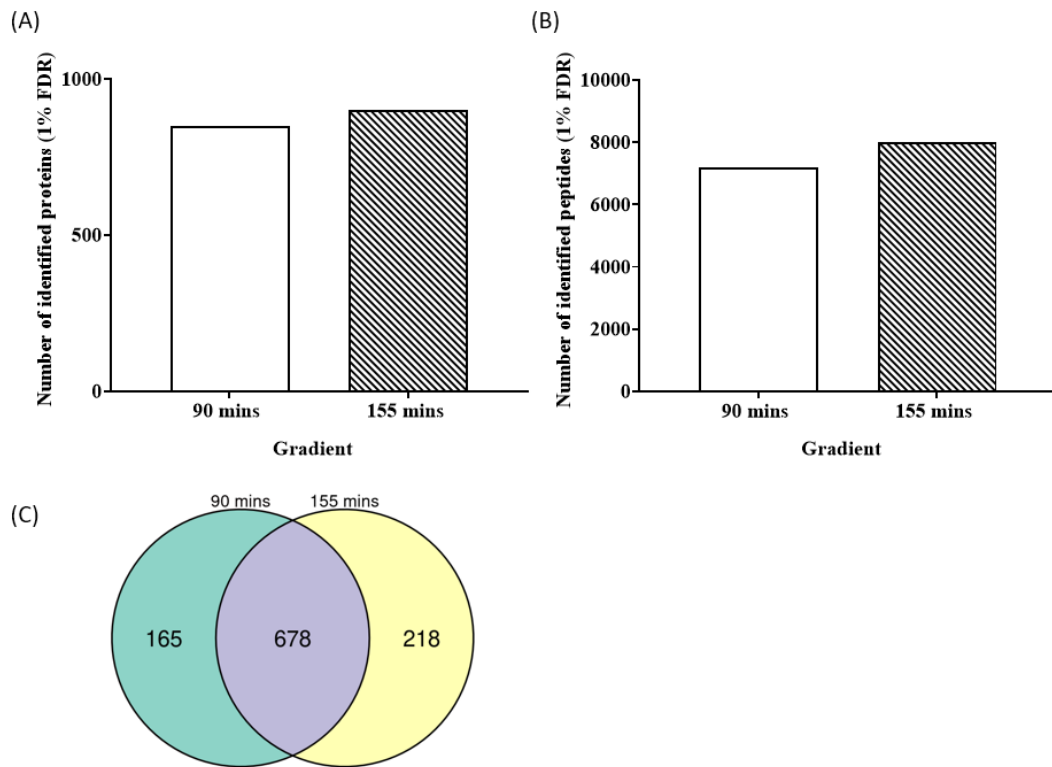


Figure 3.19 The number of (A) proteins and (B) distinct peptides identified in vitreous from 90 mins and 155 mins gradient at 1% FDR (C) The number of proteins found in each and overlapped from two gradient settings.

3.2.4.4 Discussion

Various methods can be introduced to increase the proteins to be identified, including fractionation (Govaert et al., 2017) and changing the column conditions [e.g., length (Wöhlbrand et al., 2017)]. Although these methods can be beneficial, they are often time-consuming and somewhat expensive as chemicals and products have to be purchased. Another method is to change the effecting gradient running time as this will allow the peptides to be separated at different times, effectively

allowing peptides to run longer/ shorter on the reversed-phased column before MS injection. However, this gradient time can be tissue-specific and depends on the way of sample preparation and the machine (Wöhlbrand et al., 2017). Here we have explored the effect of having a different gradient on the amount of protein identified in vitreous samples. The vitreous proteome seems to be less complicated than other tissues within the eye such as the retina, which would benefit from a long separation time. For vitreous, around 800- 1000 proteins can be identified in our previous settings (155mins gradient). Having a shorter gradient might have its benefit on the overall experiment as the time can be shortened by half. By changing the gradient to a shorter 90 mins while having the same elution profile, there was only a 5.8% increase (from short to long gradient) in total protein identified. Furthermore, the machine's stability will be reduced with a longer gradient time, making it harder to obtain repeatable results if a large number of runs are conducted in an experiment. While the overall protein number is larger when a longer gradient was used, the shorter gradient also covered most of the vitreous proteins, as over 64% of the proteins were found in all the injections.

3.2.4.5 Conclusion

A long standard gradient of 155 mins was compared to a short gradient of 90mins on the effect of protein ID in the vitreous sample. With the same elution profile, there was only a mere 5.8% increase in protein amount using the long gradient compared to the short gradient. 64% of proteins were found from both gradients, while 155 mins offered more distinct proteins (20% compared to 16% in short gradient). Despite a slight drop in protein amount identified using the short (90 mins) gradient, the overall experiment running time can be reduced by half for each run. This could save a considerable amount of time in a whole set of experiments; therefore, a shorter gradient was implied for future vitreous studies.

3.2.5 High-pH fractionation

3.2.5.1 Introduction

Identifying low-abundant proteins remained a crucial obstacle in vitreous-related proteomic studies due to its diluted nature and highly abundant proteins such as albumin (Skeie et al., 2015), which could mask the expressions of lower abundant proteins. While various fractionation techniques have been applied in vitreous studies, including 1D/ 2D SDS PAGE and protein depletion (Aretz et al., 2013; Murthy, Goel, Subbannayya, Jacob, Murthy, Manda, Patil, Sharma, Sahasrabuddhe, Parashar, Nair, Krishna, Prasad Ts, et al., 2014) to separate into different fractions for MS analysis, the large sample volume needed. Lengthy procedures remained an obstacle for applying it to the chick vitreous samples. In Chapter 3.2.3, a high-performance liquid chromatography (HPLC) method using strong cation exchange chromatography (SCX) column to fractionate chick vitreous increased ~27 % proteins. Despite the increase in protein amount, the increased time consumption for preparation and handling, the high initial peptide amount needed, and the poor peptide recovery indicated that this method was somewhat unfavorable for chick vitreous. High-pH fractionation is an alternative popular fractionation method that utilizes the peptides' pH nature, offering good performance in identifying proteins with high separation efficiency (Kong et al., 2011; Wang et al., 2011). Its mechanism works by getting sample peptides to be “trapped” onto the hydrophobic resin bed, where a gradient consisting of different steps of ACN concentration in a high-pH elution solution will be added to separate the peptides into several fractions. This reduces the complexity of the sample and hence lower abundant proteins then can be identified (Batth et al., 2014; Yang et al., 2012). As the protein concentrate extracted from chick vitreous was low, the low minimum requirement (10 µg) of peptide concentration of the Thermo pH-fractionation kit could be beneficial for chick vitreous proteomic studies in terms of sample preparation time consumption as well as the protein amount. Here in this experiment, an offline prefractionation strategy (high-pH reversed-phase fractionation kit, name, country) was used with the short 90 mins gradient setting in an attempt to for the improvement compared to its non-fractionated counterparts.

3.2.5.2 Method and materials

Three separate batches (sets 1, 2, and 3) of chick vitreous samples (total n= 32 chick vitreous, n= 14 for each set) were collected and digested according to the sample preparation methods mentioned in Chapter 2. For each respective set (1,2 and 3), a total of 10 µg of digested peptides were kept as unfractionated samples, whereas the rest of the samples (20 µg) were subjected to an offline high-pH reversed-phase peptide fractionation kit (Thermo) according to the manufacturer's protocol. In brief, two fractions of high pH solution (Fraction A: 12.5% acetonitrile (ACN) in 0.1% Triethylamine (TEA) and Fraction B: 50% ACN in 0.1% TEA) were prepared and used to elute the peptides for fractionation. After column conditioning using ACN and 0.1% TFA, the digested peptides were then loaded onto the resin bed. Fraction A buffer was first loaded to the column and centrifuged at 3000 x g for 2 mins. The elution was then collected as Fraction A elution. Secondly, Fraction B buffer was added to the same column and centrifuged at 3000 x g for 2 mins, resulting in Fraction B elution. Both parts of fraction elution were then dried and resuspended in 0.1% FA. The final peptide concentration after fractionation of Fraction A (12.5% ACN in 0.1% TEA), Fraction B (50% ACN in 0.1% TEA), and unfractionated samples was set as 0.2 µg/µl for MS injection, and a total of 1 µg of peptides were injected into the MS. Two technical IDA injections were done for each sample (unfractionated, Fraction A, and B). MS running conditions can be found in Chapter 2.3 with the short (90mins) gradient. Both injections were combined searched using ProteinPilot against the Gallus gallus Uniprot database using the mentioned settings shown in Chapter 2.3. The overall experiment design is shown in Figure 3.20.

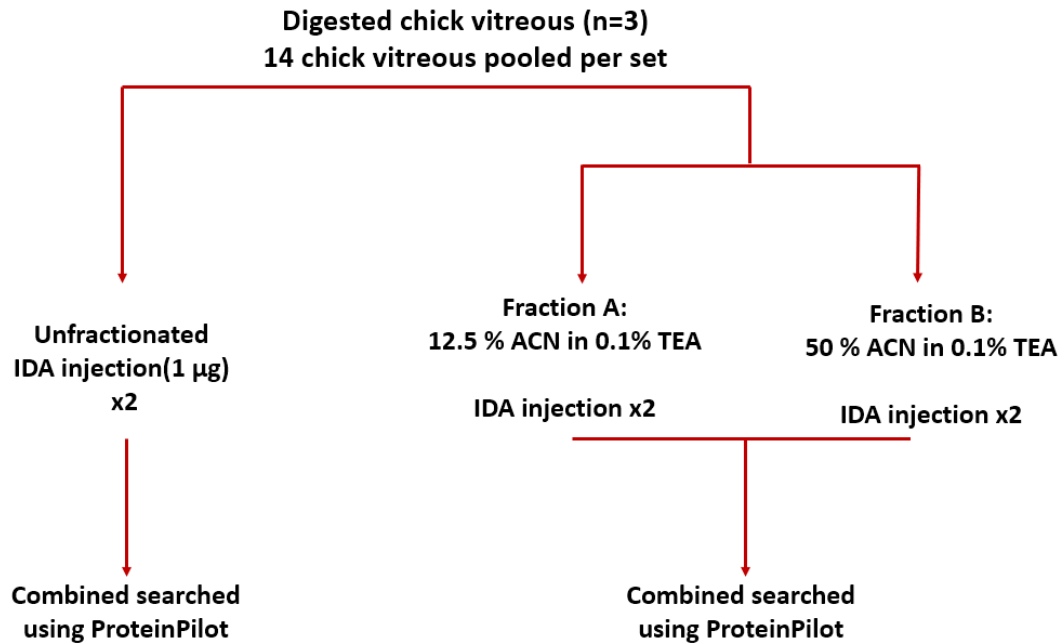


Figure 3.20 Three separate batches of chicks (n= 14 vitreous pooled for each set, total n= 42) were homogenized and digested. Unfractionated and high-pH fractionated (Fraction A: 12.5% ACN in 0.1% TEA and Fraction B: 50% ACN in 0.1% TEA) samples were injected with two technical IDA injections each.

3.2.5.3 Results

In terms of protein numbers identified for 3 different batches (set 1, 2, and 3): 728, 845, and 842 proteins were found from the 3 unfractionated samples, respectively, compared to their fractionated counterparts): 886, 965, and 940 proteins, respectively, having a 22%, 14%, and 12% increase in raw protein amount observed from set A, B, and C, respectively (shown in Figure 3.21). When comparing the samples' proteins, around 62-66% of proteins were found commonly in both fractionated and unfractionated portions. Around 22- 27% of proteins were only found in fractionated samples (combined of Fraction A and B only), whereas 11-12% of proteins were only found in unfractionated samples in all three sets (shown in Figure 3.22). To see the efficiency of high-pH reversed-phase fractionation has on vitreous peptides, the proteins obtained from the two fractionated parts (Fraction

A: 12.5% ACN in 0.1% TEA and Fraction B: 50% ACN in 0.1% TEA) were compared. More than half (56-61%) of proteins were only found in one fraction (either 12.5% or 50%), whereas the rest of the proteins were found in both fractions (Figure 3.23).

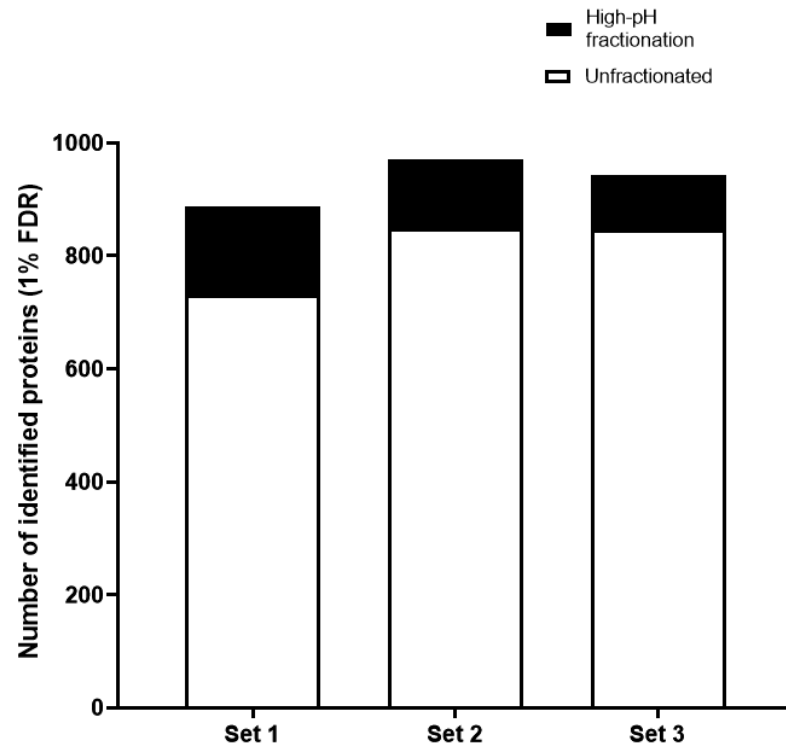


Figure 3.21 The number of proteins identified at 1% FDR in three sets (1, 2, and 3) of vitreous digest (n= 14 chick vitreous for each set). Solid black bars resemble proteins that were identified from a combined search of two fractions (Fraction A: 12.5% ACN in 0.1% TEA and Fraction B: 50% ACN in 0.1% TEA), and white bars resemble the proteins that were from the unfractionated group.

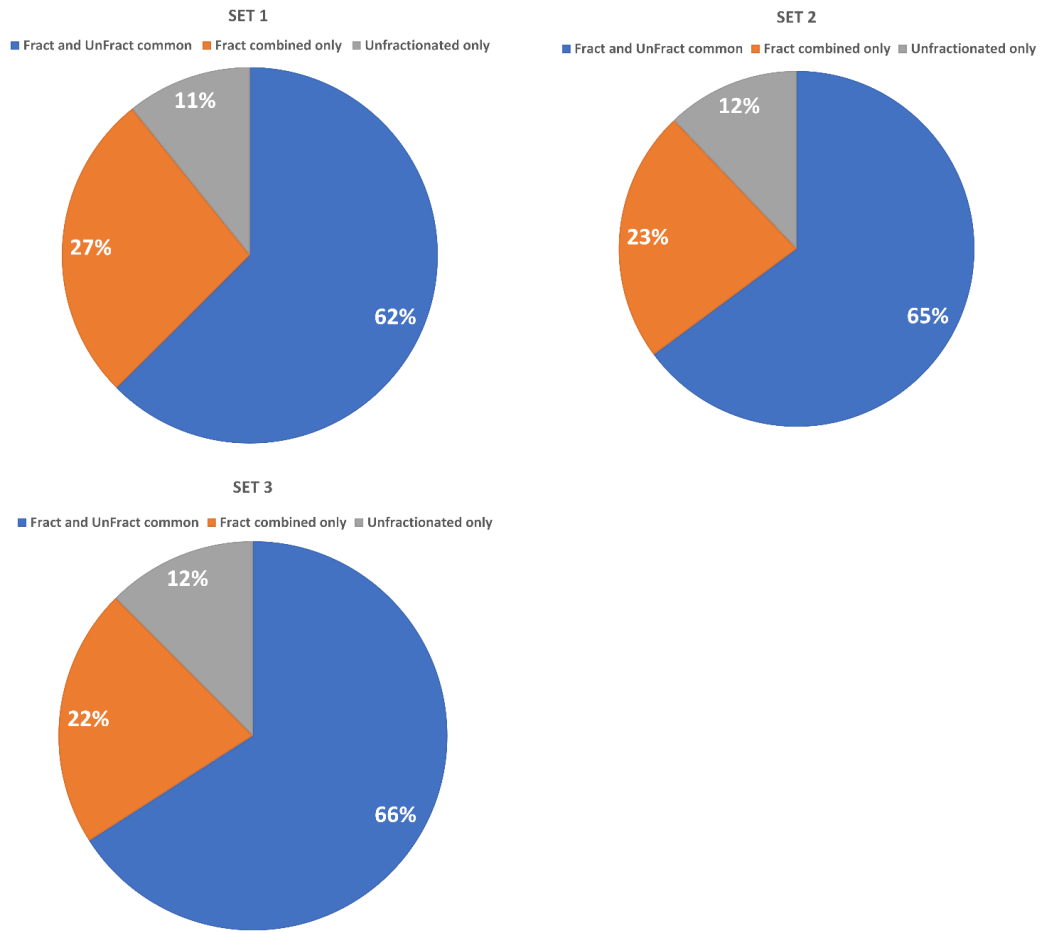


Figure 3.22 The % of proteins that were identified at 1% FDR in fractionated, unfractionated and common overlaps in three sets (1,2 and3). Blue indicates the proteins that were found overlapped from high-pH fractionated and unfractionated samples. Orange indicates % of proteins that were only found in fractionated samples. Grey indicates % of proteins that were only found in unfractionated samples.

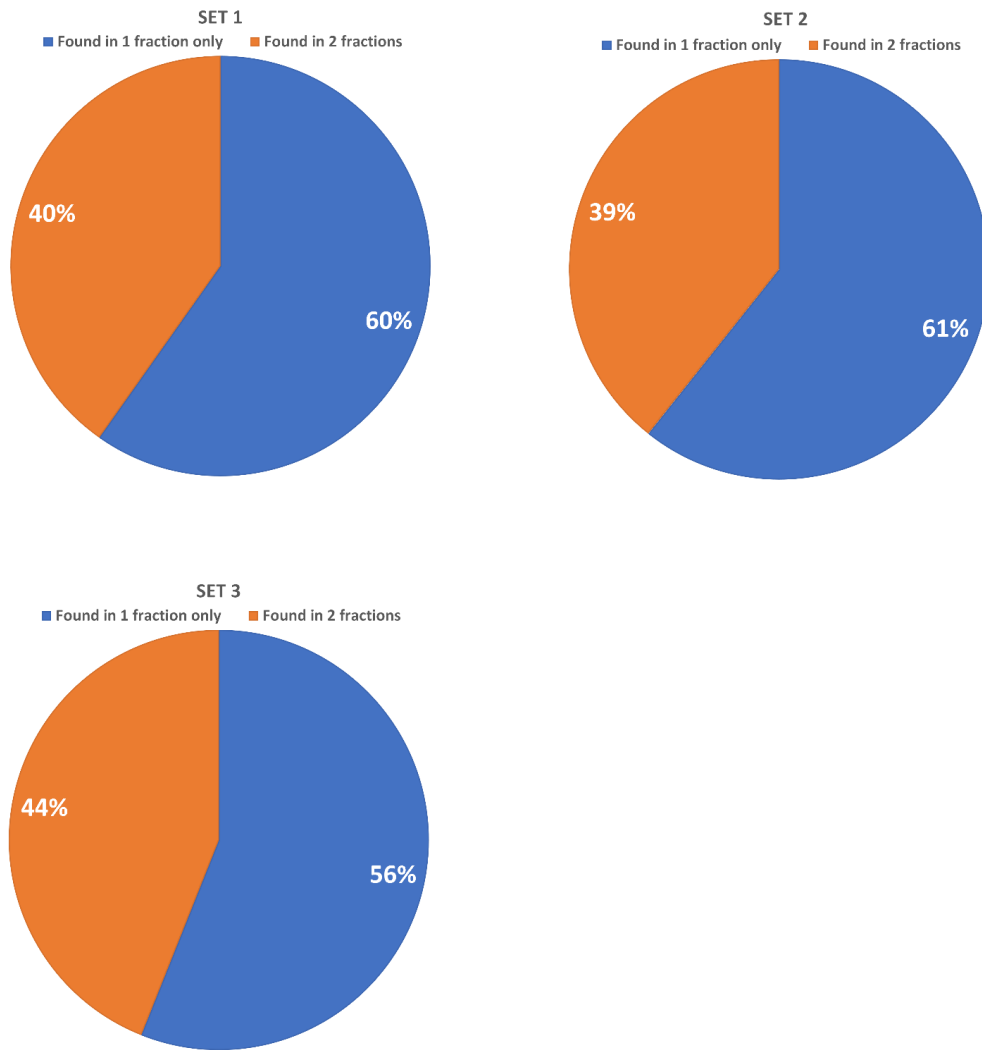


Figure 3.23 The % of proteins identified (1% FDR) in the number of fractions (either only found in 1 or found in 2 fractions) in three sets (1,2 and 3). Blue indicates the % proteins that were found in only one fraction (Either in Fraction A or B). Orange indicates % of proteins that were found in both fractions.

3.2.5.4 Discussion

The low initial peptide requirement (10 µg of peptides) of the high-pH fractionation kit provided an alternative pre-fractionation method to apply to our sample and its effect has also been demonstrated by Kang et al in increasing the number of proteins to be identified in chick cornea (Kang et al., 2019). Using the shorter gradient in

mind, combined with the high-pH fractionation method, the acquired protein amount was further increased to have an average of 16 ± 0.05 % increase from those 3 sets in terms of proteins identified. Although this was not as high as the 27% increase using the traditional HPLC method, the time consumption and the ease of use during the steps were much preferable. With unique proteins identified from both fractionated and unfractionated samples, around 24 ± 2.65 % of unique proteins were found only from fractionated samples. This increase in proteins can compensate for the reduction in proteins using the shorter gradient while having a more extensive ion library for quantitative such as SWATH. Given the less complicated nature of vitreous proteins, over 60% of proteins were found within fractionated and unfractionated samples, demonstrating the efficiency of our sample preparation workflow for the vitreous. Around 12% of proteins were only found in unfractionated samples, which could be due to the nature of how shotgun proteomic acquires fragments(Liu et al., 2004; Tabb et al., 2010), with fewer overlapped proteins with the increase in injections. The number of proteins increased, and found comparing fractionation to unfractionated samples was similar in the three groups. Here we have applied 2 levels of pH ranges to fractionate vitreous peptides, as a higher number of fractions could be damaging for vitreous due to its low amount of protein concentration to begin with, which could result in a total loss for peptide recovery. The 2 levels were set in the middle of the range from the kit instruction protocol. The peptide fractionation efficiency was also looked at by checking the number of fractions the protein belongs to. Around 60% of proteins were found only in 1 fraction (either 12.5% or 50%), indicating that vitreous proteins can benefit from this fractionation method. Since the samples were only subjected to two-step pH range fractions, the time needed for fractionation was shorter than the previous HPLC SCX fractionation, making this a preferable fractionation technic to use on vitreous peptides.

3.2.5.5 Conclusion

Using a high-pH reversed phased fractionation kit in combination with a shorter gradient (90 mins) showed that the protein number can be increased by $\sim 16 \pm 0.05$ % compared to unfractionated samples. Over 60% of proteins were only found in 1

fraction, indicating the beneficial effects on vitreous peptides using this kit. Furthermore, due to the steps' simplicity during the high-pH fractionation kit, time consumption for the overall experiment was kept shorter compared to the other forms of offline fractionation (e.g., on-column HPLC SCX fractionation). The high-pH reversed-phase fractionation kit will be used along the optimized short gradient in future vitreous experiments.

3.3 SWATH-MS optimization

3.3.1 Sequential Windowed Acquisition of All Theoretical Fragment Ion Mass Spectra (SWATH-MS) windows size comparison

3.3.1.1 Introduction

A successful generation of an optimized vitreous protein library generation was archived throughout Chapters 3.1 and 3.2, which was crucial for label-free quantification methods such as Sequential Windowed Acquisition of All Theoretical Fragment Ion Mass Spectra (SWATH) as the number of quantifiable proteins in SWATH is determined by the size of the proteome. SWATH is a data-independent acquisition (DIA) technique that utilizes a number of windows ranging from 20- 30 m/z in the fragmentation of all precursor ions. It has been shown that SWATH windows with 25Da fixed windows are standard (Gillet et al., 2012) for a typical DIA run in the TripleTOF system. Having a set window throughout the whole m/z range might not utilize the full use of the given gradient time. Therefore, other time frame options should be explored. With the new TripleTOF 6600 system's upgraded scanning speed, up to 100 windows can be set up to scan across the whole mass range. Ideally, a smaller window size should yield a better acquisition as the resolution will be higher, but this is limited by the acumination time, which should be enough for it to have an optimal scanning peak for acquisition. Here in the experiment, several window sizes were explored to see the effect on vitreous proteome acquisitions with the retention time (RT) windows size was also determined for the best fit of the chosen SWATH window size.

3.3.1.2 Method and materials

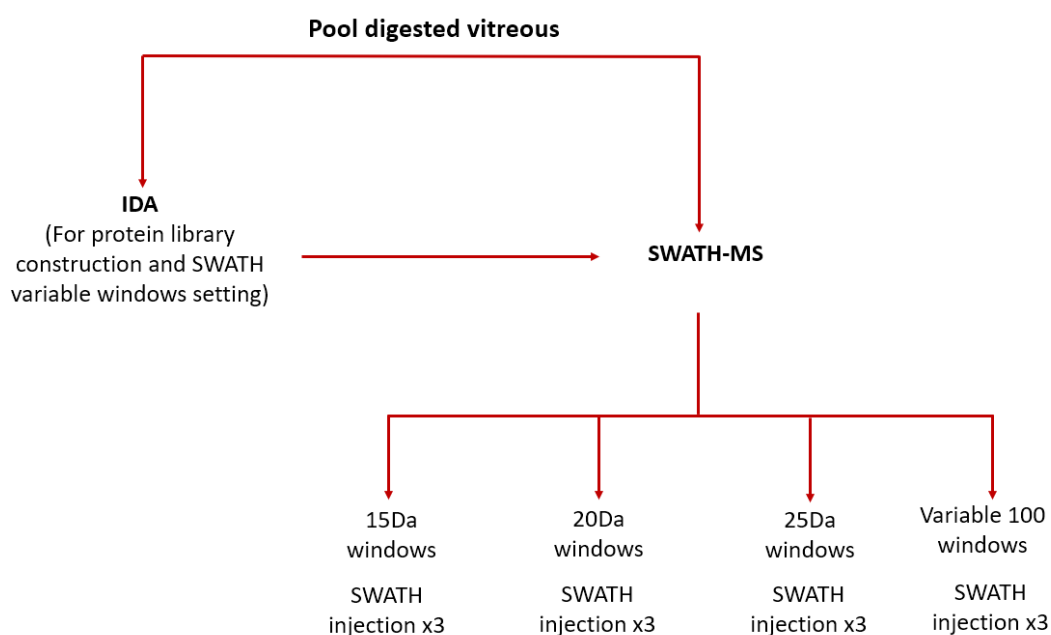


Figure 3.24 A proteome was firstly generated under IDA mode, and four SWATH window settings were used for comparison (15Da, 20Da, 25Da, and variable windows 100).

Vitreous peptides were prepared the same as in Chapter 2.2, and the experiment design is shown in Figure 3.24. Equal amounts of vitreous peptides (1 μ g) were loaded onto the MS with 3 technical replicates and were combined search using ProteinPilot (v5.0, Sciex, USA). Three fixed window sizes (15Da, 20Da, 25Da) were set using the analyst software (v1.7.1, Sciex, USA), and the variable window (vw100) was generated by SCIEX SWATH variable window calculator v.1.1 based on a previous vitreous IDA run. The calculation method was based on the number of precursors and their intensities section (Zhang et al., 2015). The cycle time was set to be near 3 seconds for all settings and the number of cycles to be around 3000. The accumulation time was kept constant at 50 ms for the TOFMS scan (Detailed settings can be found in Appendix 2). The coefficient of variance (CV) was checked to measure the reproducibility and variability of those matched proteins, peptides, and transitions among the various SWATH-MS windows sizes (Govaert et al., 2017)

SWATH processing

Three technical repeats of SWATH injections (1 μ g) were performed for each window setting and were loaded onto PeakView (v2.2, Sciex, USA) for data processing. SWATH injections from each group were processed using 3 different extraction windows settings (5 mins, 10 mins, and 15 mins) with an extracted ion chromatogram (XIC) width of 75 ppm. Retention time (RT) was calibrated using high-intensity peptides and exported to excel for comparison. Processed data was then exported to MarkerView (v1.3, Sciex, USA) for statical analysis.

3.3.1.3 Results

Data of SWATH windows sizes were compared on the number of quantifiable proteins and peptides (shown in Figure 3.25 A and B) under different retention time settings (5, 10, and 15) using PeakView software. For VW100, 1071 proteins (7308 distinct peptides), 1075 proteins (7387 distinct peptides), and 1069 (7272 distinct peptides) were quantified using the three windows of 15mins, 10min, and 5 mins, respectively. For the 25 Da window, 1015 proteins (6776 distinct peptides), 1012 proteins (6817 distinct peptides), and 1025 (6864 distinct peptides) were quantified using the three windows of 15mins, 10min, and 5 mins, respectively. For the 20 Da window, 1046 proteins (6981 distinct peptides), 1044 proteins (6991 distinct peptides), and 1047 (6998 distinct peptides) were quantified using the three windows of 15mins, 10min, and 5 mins, respectively. For the 15 Da window, 1024 proteins (6951 distinct peptides), 1027 proteins (7000 distinct peptides), and 1029 (6943 distinct peptides) were quantified using the three windows of 15mins, 10min, and 5 mins, respectively. The % cumulative frequency of the sample injection using various SWATH window size settings (25Da, 20Da, 15Da, and variable windows 100) along with different retention time window sizes (5, 10, and 15 mins) at 20% coefficient of variance (CV) is shown in Figure 3.25 C. The highest cumulative frequency was obtained using the 15Da setting (83.155%), while a cumulative frequency of 79.310%, 79.941%, and 80.615% was obtained for the 20Da, 25Da, and vw100 window.

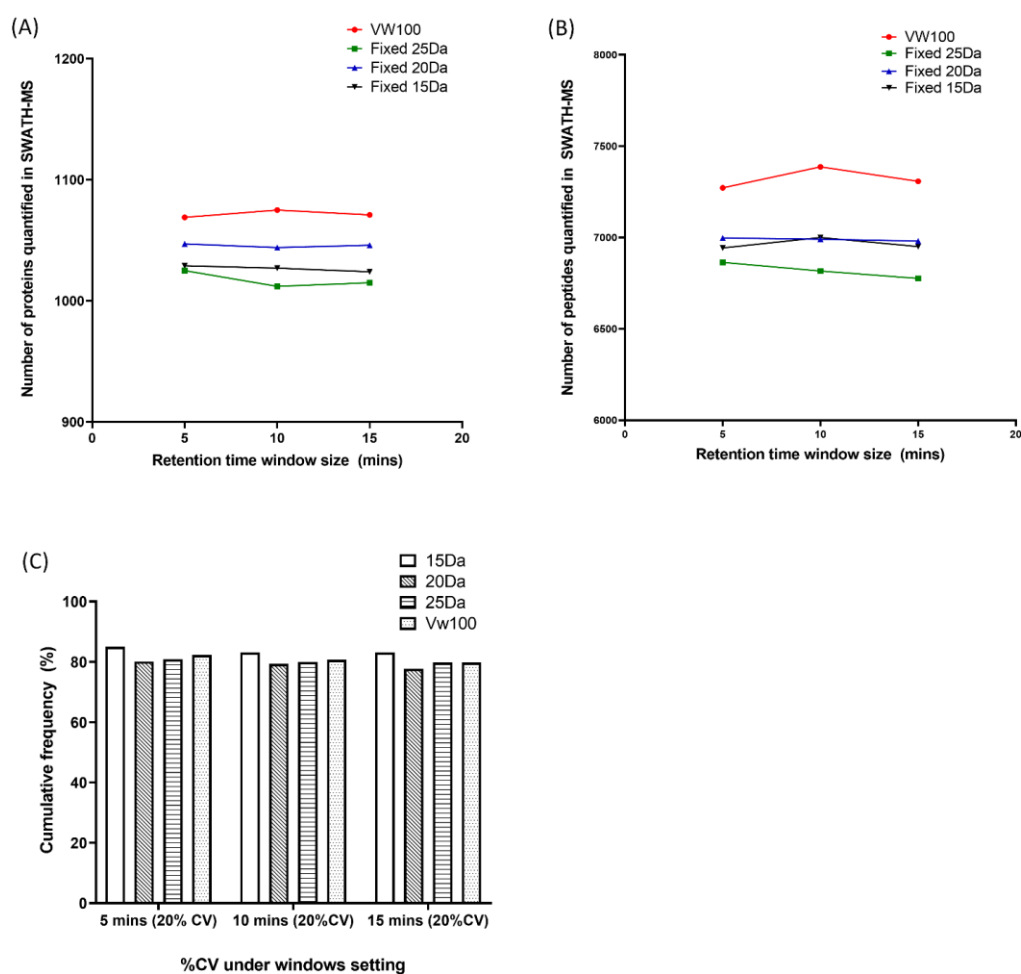


Figure 3.25 (A) The proteins and (B) peptides quantified (at 1%FDR) using various SWATH window size settings (25Da, 20Da, 15Da, and variable windows 100). Three retention time window settings (5, 10, and 15 mins) were compared during PeakView processing. (C) The cumulative frequency (%) at 20%CV under 3 PeakView retention time settings (5, 10, and 15 mins) for various SWATH window size settings (15Da, 20Da, 25Da, and variable windows 100).

3.3.1.4 Discussion

The standard isolation width of 26 Da (25 Da with 1 Da overlapping window) was optimized by Gillet et al in providing a standard DIA quantitation workflow (SWATH) for general proteomic study (Ben C Collins et al., 2013; Liu et al., 2013) as this emulates SRM window width in the TripleTOF system (Gillet et al., 2012).

While this setting is optimized for the mass range across 400 – 1200 m/z (with 100 ms accumulation per swath window resulting in a 3.3s total cycle time), several parameters such as the width of the LC peak, accumulation time, and the precursor is also playing key roles in the efficiency of proteins to be quantified affecting the SWATH windows size. With these parameters in mind, the Q1 window width was then altered by changing parameters to meet the needs (Raetz et al., 2019; Zhang et al., 2015). As the 6600 TripleTOF system was capable of a faster scanning rate, the window size was further reduced to fixed 15, 20, and 25Da and a variable 100 window setting while keeping the total cycle time within 3.3 sec. Ideally, the reduced number in size should be beneficial as the windows were smaller and could separate the mass range into finer segments.

Furthermore, smaller windows increase the selectivity in fragmentation hence improving protein quantification. With the standard MS setup in our lab, the 25 Da step window provided a “baseline” and starting point setting parameter for our vitreous study. As expected, the lowest amount of protein and peptide were quantified across all the retention time window size using the standard 25Da setting, while acquisitions using a smaller window size, such as 15 and 20 Da, offered a similar number of protein identification. The variable window settings were calculated based on an existing IDA spectrum to determine the width of the window size which can be demonstrated by Schlotterbeck et al (Schlotterbeck et al., 2019) (26 variable windows), where smaller window sizes will be offered to more complicated parts while else the wider windows will be associated with less complex parts.

In this experiment, VW100 showed the best overall performance in terms of having the highest number of proteins (1075 proteins at 1% FDR and quantified in SWATH) and peptides (7308 distinct peptides) throughout all retention window size settings while having a cumulative frequency above 80% at 20%CV setting.

3.3.1.5 Conclusion

Four SWATH window sizes have been tested in this experiment (15Da, 20Da, 25Da, and VW100). For all the retention time settings during data processing (5, 10, and 15mins), VW100 had the highest number of proteins to be quantified compared to all the other groups and a low %CV compared to the other settings. Therefore, the setting of 10 mins retention time window in PeakView processing and a VW100 SWATH setting will be employed for future vitreous proteomic studies.

3.3.2 IDA and SWATH-MS comparison in protein quantitation

3.3.2.1 Introduction

Shotgun proteomics remains the main way of protein identification (Domon & Aebersold, 2010; McDonald & Yates, 2002; Sajic et al., 2015), where tandem mass spectrometry acquires data by MS/MS threshold of spectra that pass a pre-defined threshold. As seen from the previous experiment, the overlapping of proteins will decrease as the number of injections increases, resulting in problems such as the lack of repeatability and reproducibility when acquiring the ion library using the traditional IDA method (Tabb et al., 2010). Sequential Windowed Acquisition of All Theoretical Fragment Ion Mass Spectra (SWATH) as a data-independent acquisition (DIA) technique that utilizes selection windows in the fragmentation of all precursor ions allowed proteins to be quantified without the need for previous information for triggering the MS/MS threshold (Gillet et al., 2012). This experiment is to compare the traditional label-free IDA method with the DIA mode (SWATH-MS) in the ability of protein quantification.

3.3.2.2 Method and materials

Vitreous peptide digest was prepared as mentioned in Chapter 2. For protein analysis, 3 injections of IDA and 3 injections of SWATH were done using the 155 mins long gradient. IDA was searched individually against the Uniprot database resulting in 3 files shown in Chapter 2.3. SWATH ion library was acquired by combining the 3 IDA files as a spectral library and processing using PeakView (v2.2, Sciex, USA) for peak integration. Results were then exported to MarkerView (v1.3, Sciex, USA) and excel for statistical analysis. Proteins that have <2 peptides identified were removed for more stringent filter criteria for false-positive results.

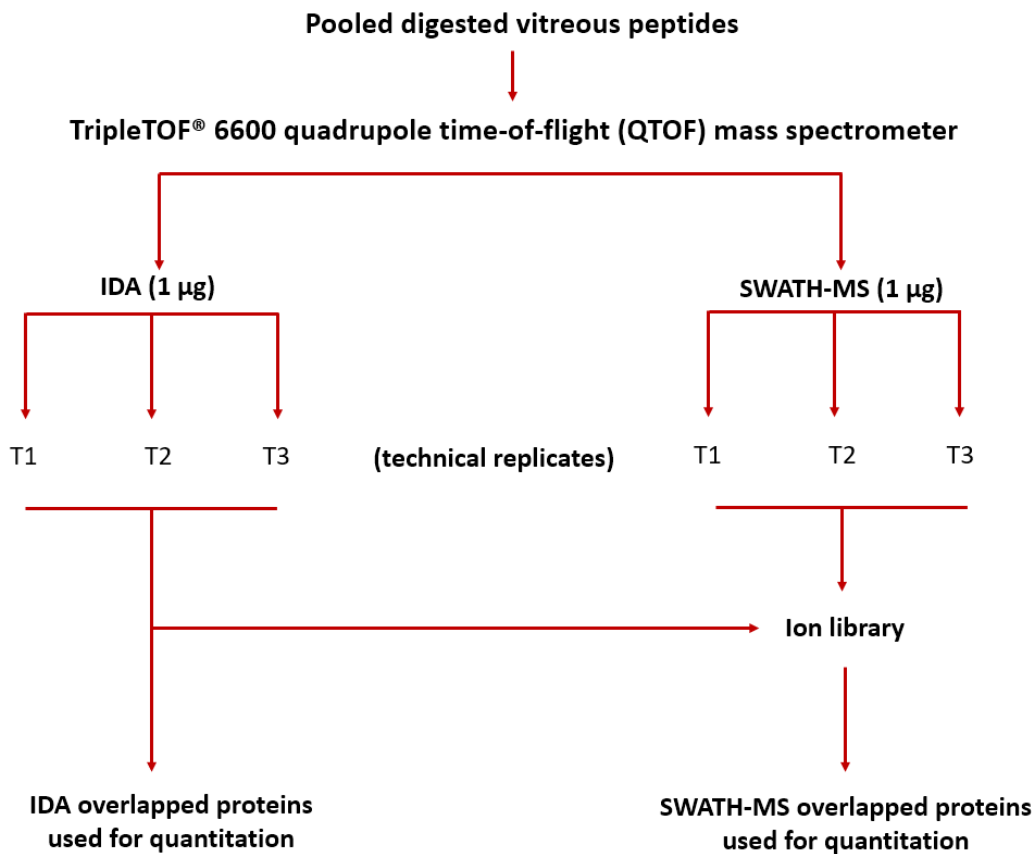


Figure 3.26 Same amount (1 µg) of digested vitreous was loaded into the MS under IDA and SWATH-MS mode with three technical replicates for each mode. Three injections of IDA were combined searched for the generation of a protein ion library. SWATH-MS data were then loaded onto the library for protein quantitation.

3.3.2.3 Results

Protein identification and total quantifiable protein

Three technical replicates of the pooled vitreous digest were loaded in the MS under IDA mode. Each injection was searched individually, and 1049 proteins (11644 distinct peptides), 1130 proteins (12265 distinct peptides), and 1089 proteins (12077 distinct peptides) were identified at 1% FDR for IDA T1, T2, and T3, respectively. A total of 1418 distinct proteins were found, and 782 proteins (55%) were found across all 3 IDA technical replicates shown in Figure 3.27 A. For SWATH-MS quantitation, a combined protein ion library generated (1284 proteins, 15265 distinct peptides) from the 3 IDA injections was created. A total of 1123

proteins (98%) were found across all three technical replicates under SWATH-MS mode (shown in Figure 3.27 B). With those proteins that have less than 2 peptides removed, 905 proteins (>70%) remained quantifiable with higher confidence.

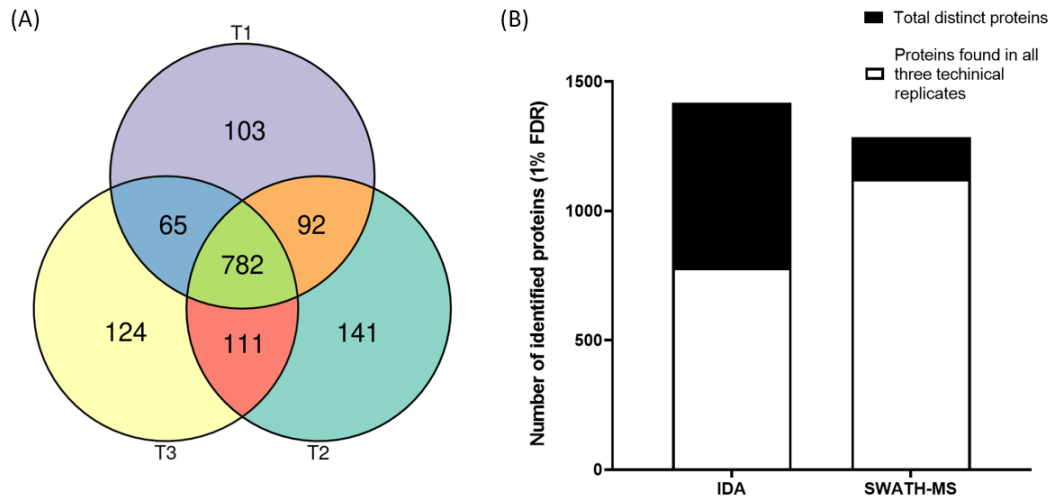


Figure 3.27 (A) The number of identified proteins in each IDA technical replicate (T1, 2, and 3) (B) The number of overlapped proteins (white bars) found from all three technical replicates (under IDA or SWATH-MS mode). Black bars indicate the total distinct proteins in each mode.

3.3.2.4 Discussion

Continuous injection of IDA can result in a greater number of proteins due to the stochastic nature of the IDA method. However, IDA lacks the ability to detect less abundant proteins, and the intensity-based filtering of peptide precursors leads to inconsistent peptide selection between replicate runs (Liu et al., 2004; Tabb et al., 2010). The disadvantage of this is the repeatability which hampers the rate of proteins overlaps. This will become a problem for protein quantitation with a low overlapping rate of proteins (55%) found in this experiment. With the introduction of SWATH, the trigger of MS/MS will not be based on the specific threshold, lifting the restriction on selected fragmentation. Therefore, repeatability can be maintained, resulting in much higher repeatability for quantifying proteins across multiple injections. Using this acquisition, SWATH was able to pick up a large portion of the proteins identified (~98%) from the ion library across all the SWATH

injections acquired. This is much higher than the 55% overlapping from the IDA mode. SWATH was also able to pick up lower abundance proteins in vitreous compared to IDA mode (due to inconsistency), greatly enhancing the possibility of protein quantitation.

3.3.2.5 Conclusion

The repeatability for IDA injections of vitreous is around 55% protein overlapped compared to SWATH (nearly 98%) of the proteins from the ion library can be quantitated across all the sample injections. This enables a greater possibility for quantifying vitreous proteins (including lower abundant proteins, which were not detectable from many individual IDA runs). SWATH proved to be a superior technique in protein quantitation which will be beneficial, especially in quantifying low-abundant proteins in the vitreous.

3.3.3 Fold change cut-off determination for SWATH

3.3.3.1 Introduction

Having a cut-off level sets a filter for minimizing false-positive IDs that could potentially arise from sample preparation and machine technical variance. Although a fold change of 1.5 is typically used in many proteomics publications, there is no gold standard to fix cut-off values used in proteomics studies. All the factors, including sample types, sample preparation procedure, acquisition mode, machine stability, and so on, could cause variations that should be considered. As we have determined our optimized vitreous proteomics setup from previous experiments, it is critical to determine the lowest cut-off value to increase the number of detectable changes in future studies. After acquiring the data, the normalization method also matters as this will affect how the intensity of the sample, masking some of those potential fold change that is supposed to be there. There are several common normalization methods used in proteomics studies (Välikangas et al., 2016), including total area sum (TAS) and most-likely ratio (MLR) (Lambert et al., 2013). TAS is unitized by adding up all the intensity areas from each sample, then a ratio is determined for each sample to the largest sum. This ratio is then used for the normalization of each individual sample.

On the other hand, MLR normalization considers the technical replicates of each sample. Then, the intensity of each sample will be normalized, minimizing the variance with samples with low-intensity responses. This chapter will calculate variations (including technical and biological) to determine a usable fold-change for future proteomics studies with the vitreous using SWATH-MS.

3.3.3.2 Method and materials

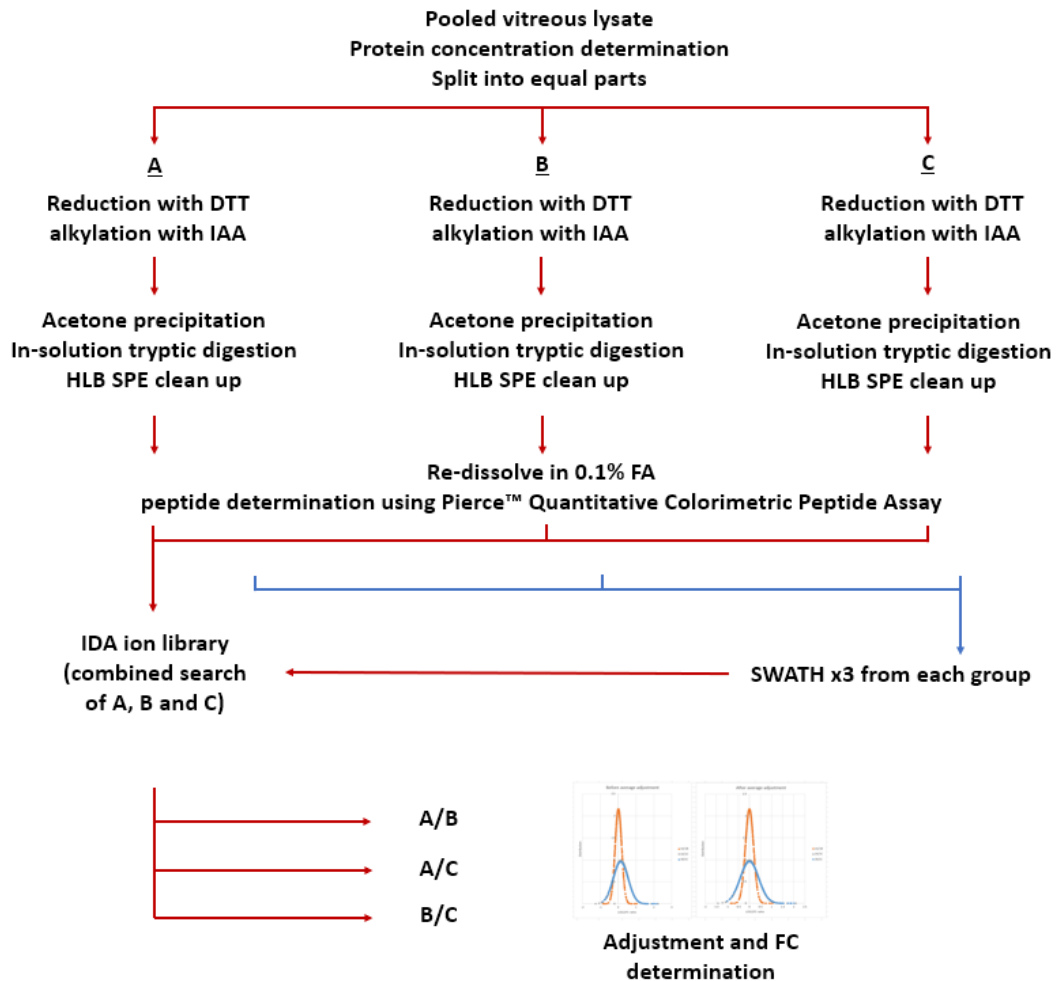


Figure 3.28 The pooled vitreous lysate was split into 3 equal parts: A, B, and C for sample preparation and digestion. An ion library was generated from a combined search of the 3 IDA injections. Then the SWATH injections from the 3 groups were loaded onto the ion library and quantified. Ratios from each group were calculated to determine the Fold Change cutoff.

Sample preparation

T-PER lysis buffer homogenized vitreous samples were pooled together and split into 3 equal parts for individual sample preparation (A, B, and C), shown in Figure 3.28. The sample preparation methods were the same as in Chapter 2.2 unless otherwise specified. Two μg of samples were injected in IDA mode to generate an ion library and 1 μg of SWATH injections with 3 technical replicates of SWATH

injections from each group (A, B, and C). The MS solvent loading conditions and running gradient settings were the long gradient (155mins) in Chapter 2.3.

Data analysis

Three IDA injections were combined searched using ProteinPilot (v5.0, Sciex, USA) against the Uniprot database (unreviewed 39805). Data acquired under SWATH-MS mode were loaded to PeakView (v2.2, Sciex, USA) and were processed with the following process settings: 10 peptides per protein, 6 transitions per peptide, 95% peptide confidence threshold, and 1% false discovery rate (FDR) threshold, modified peptides excluded and a 10 min XIC extraction window. Data were exported to MarkerView (v1.3, Sciex, USA) and excel for statistical analysis.

Fold change calculation

Protein intensities from each set (A, B, and C) were compared. Two sets of Fold changes (FC) were done: Raw data without any normalization method, where technical replicates were averaged and compared with each other (A/B, A/C, and B/C). The other set was normalized using the most-likely-ratio (MLR) normalization method (Lambert et al., 2013), then compared with each other (A/B, A/C, and B/C). The average intensity of the compared proteins was adjusted by LOG2FC- AVERAGE LOG2FC intensity, then the adjusted LOG2FC was calculated with $(\text{LOG2FC} + \text{AVE} + \text{or} - (1.96 * \text{SD}))$, with 95% confidence resulting in an up (+) and down (-) FC for each comparison. Finally, the average from the three comparison groups was calculated for up and down as the FC cut-off value for our vitreous SWATH study.

3.3.3.3 Results

Generation of the Ion library

A total of 1211 proteins (18457 peptides) were identified from a combined search from IDA injections of A, B, and C. A total of 1082 proteins (95%) were quantified in SWATH across 9 injections after spectra processing. To reduce false-positive results, those proteins that have <2 peptides were removed were a total of 834 proteins remained after.

FC adjustment with MLR normalization

The A/B group had an average LOG2FC of 0.0140 ± 0.185 from raw data and $8.720 \text{ E-}18 \pm 0.185$ after adjustment. The normal distribution curve before and after adjustment can be seen in Figure 3.29 A. A/C group had an average LOG2FC of 0.153 ± 0.403 from raw data and $-2.130 \text{ E-}18 \pm 0.403$ after adjustment. The normal distribution curve before and after adjustment can be seen in Figure 3.29 B. B/C group had an average LOG2FC of 0.139 ± 0.416 from raw data and $-7.535 \text{ E-}18 \pm 0.416$ after adjustment. The normal distribution curve before and after adjustment can be seen in Figure 3.29 C

FC adjustment without MLR normalization

The A/B group had an average LOG2FC of -0.2116 ± 0.186 from raw data and $-1.664 \text{ E-}16 \pm 0.186$ after adjustment. The normal distribution curve before and after adjustment can be seen in Figure 3.29 A. A/C group had an average LOG2FC of -0.226 ± 0.405 from raw data and $-1.267 \text{ E-}16 \pm 0.405$ after adjustment. The normal distribution curve before and after adjustment can be seen in Figure 3.29 B. B/C group had an average LOG2FC of -0.0146 ± 0.417 from raw data and $-4.233 \text{ E-}17 \pm 0.417$ after adjustment. The normal distribution curve before and after adjustment can be seen in Figure 3.29 C.

The fold change (FC) is calculated by the average of the 3 FC cut-offs obtained from the three comparison groups (A/B, A/C, and B/C), shown in Table 3.3. MLR normalization did not affect the values of FC in all three comparison groups. The FC was calculated as above 1.5 for up-regulation and below 0.7 for down-regulation to be a statistical difference with 95% confidence.

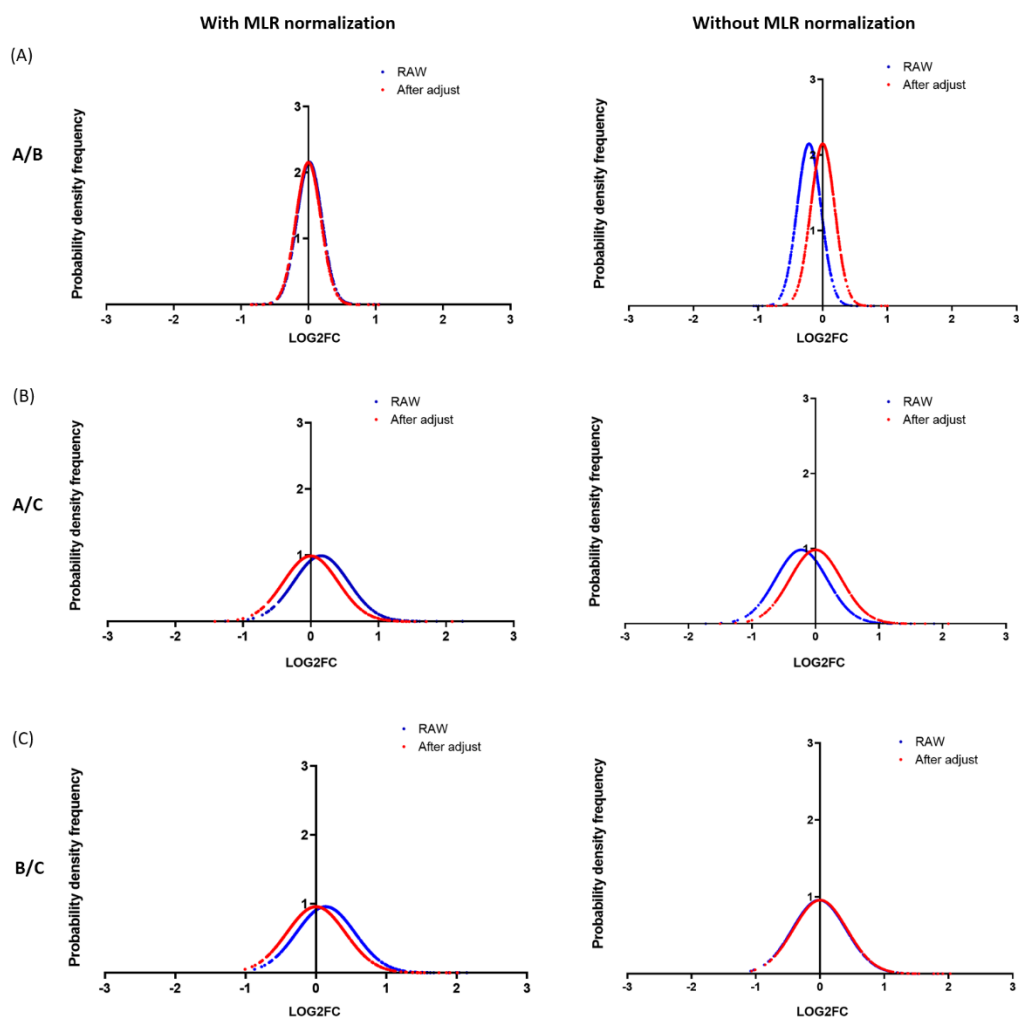


Figure 3.29 The normal distribution curve of raw values and adjusted values for the three SWATH comparison groups, with and without Most-likely-ratio (MLR) method for normalization.

Table 3.3 Average adjusted fold change (FC) calculated from all SWATH-MS injections (with and without MLR normalization)

Average Overall (with MLR)	LOG2FC	FC	Average overall (without MLR)	LOG2FC	FC
(+)	0.6	1.5	(+)	0.6	1.5
(-)	-0.6	0.7	(-)	-0.6	0.7

3.3.3.4 Discussion

Quantitative proteomics studies rely on monitoring the changes in protein expression to mark out proteins of interest. A specific threshold or cut-off is often used to filter out which proteins are differentially expressed, but this “mark” is hard to define and will be different for different tissues. Technical errors such as sample handling and machine performances can also introduce variation that will also affect the results even if the workflow is the same. Therefore, determining the FC cut-off for our vitreous proteomics workflow allowed us to see the variation in protein expression and will further refine the filter criteria of whether the proteins are to be classified as differentially expressed in vitreous studies. By doing this, the false positive can be reduced, and shorten the time consumption for selecting proteins of interest for further confirmation. Often data normality is first checked for statistical analysis. The data obtained in this study for vitreous SWATH-MS studies were all normally distributed. A 95% confidence interval indicates that there are less than 1.96 standard errors away from the sample value (average in this case), so all the values within this interval will be $p > 0.05$, making sure that we have 95% confident in where the mean values will be within $p < 0.05$. Since the data obtained is normally distributed, we can safely take 2.5% from each side and adjust based on the variation. MLR normalization considers the technical replicates of each sample then the intensity of each sample will be normalized, hence minimizing the variance with samples with low-intensity responses. In this study, normalization using the MLR method did not affect the fold change indicating that variance from technical replicates was consistent. As a limitation, this study only considers the technical errors which were introduced during sample preparation, such as sample handling, precipitation, and digestion, as well as the machine running variations as only one biological “pool” sample, was used from the beginning.

3.3.3.5 Conclusion

Pool vitreous samples were separated into 3 groups with its individual sample preparation and were injected into the MS with technical replicates (which will introduce technical variation due to multiple steps). Most-likely ratio (MLR) normalization method was employed as it incorporates technical replicates into

account, and a fold change of ≥ 1.5 and ≤ 0.7 was determined from its 95% confidence for false positives. This FC will be used for future SWATH-MS workflows with chick vitreous samples.

Chapter 4. In-depth proteomic analysis of inter-and Intra-ocular differences in normal growing chick vitreous using SWATH quantitation

4.1 Introduction

Unlike most organs in the human body, eyes are found in pairs, and it is usually assumed that both eyes have similar functions and construction. In most ocular-related studies, both eyes are treated the same as they are assumed symmetric. In most myopia studies using the chick model, one eye was selected as the treatment eye, while the paired eye was selected as the control (Muralidharan et al., 2022; Stone et al., 2016; Thomson et al., 2020). Using a gel-based 2-DE proteomic technique on the retina, it has been previously reported that there were good similarities in intra-animal comparison but poor inter-animal comparison. However, no study has been conducted on comparing vitreous proteins between the two eyes using a liquid chromatography-based proteomic technique workflow. With the successful setup of optimization of vitreous proteomics workflow from previous Chapters, this Chapter aims to investigate the differences in vitreous of the left (OS) and right eye (OD) by intra-ocular (paired eyes of the same chicks) and inter-ocular (eyes from different chicks) comparison. Although this experiment does not tackle all the physical property aspects of the eyeball, the characterization of vitreous protein changes between two eyes is essential as the starting baseline for future vitreous studies (e.g., LIM models), where protein changes should be specific to the introduction of the lens.

4.2 Methods and materials

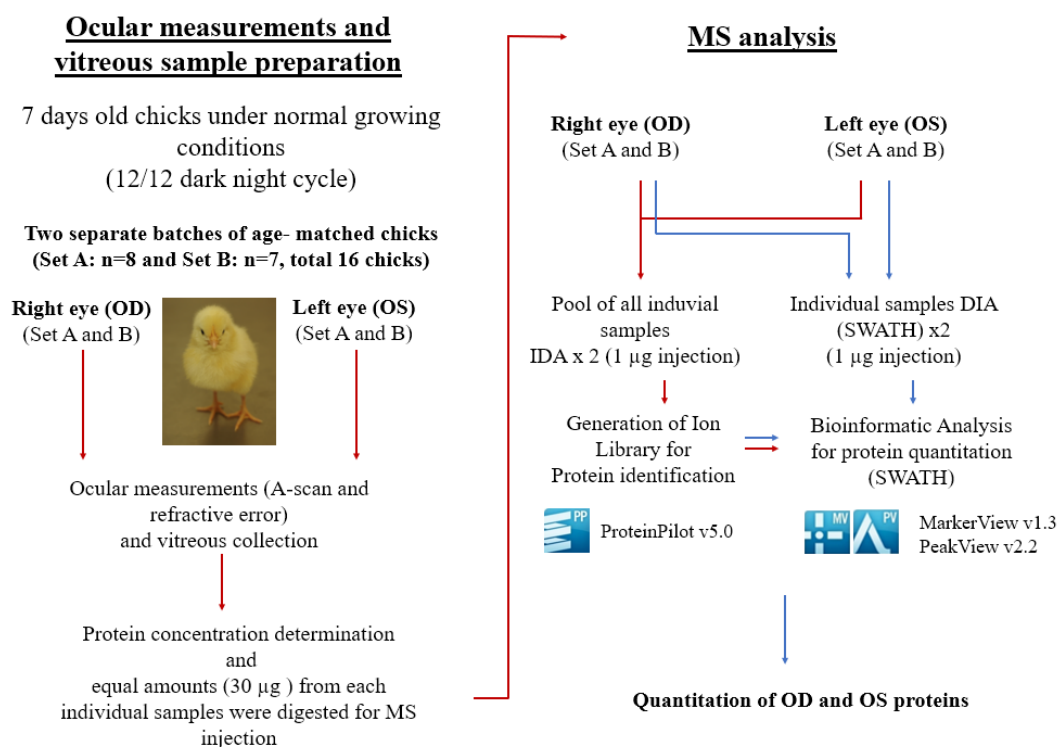


Figure 4.1 The workflow for quantification of proteins between the Right (OD) and the Left (OS) eyes in two separate batches of chicks (Set A: n= 8 and Set B: n= 7) using SWATH quantification workflow. Individual samples from both sets were pooled into their respective group, and 2 technical injections under IDA mode were done and were combined searched as their respective ion library. DIA (SWATH) injections were done in duplicates on each individual sample from OD and OS groups in both sets. Obtained spectra were processed in PeakView and exported using MarkerView for statistical analysis.

The animal raising condition and sample collection methods are the same as shown in the Methods section (Chapter 2.1). In brief, two separate batches (age-matched) of chicks (set A: n= 8 and set B: n= 7, a total of 15 chicks) were raised under normal lighting conditions with a 12/12 dark-light cycle. To ensure the eyes are growing normally, ocular parameter measurements (A-scan and refractive error) were measured on Day 7 (treatment time) where both eyes were collected on Day 7. After digestion, equal amounts (2 µg) of digested vitreous peptides from each sample

(right and left eye) were pooled to form a pooled sample in each set (A and B), shown in Figure 4.1. The Peptide concentration was determined for each sample, and the concentration was equalized to 0.2 µg/µl for MS injections. Two replicates of IDA injections were done on the Pool sample (for sets A and B) and were combined searched in ProteinPilot against a Uniprot database (201119_56937) for protein identification. Two replicates of DIA (SWATH-MS) injections were done on each sample for SWATH quantitation with 100 variable windows calculated based on the IDA injections (running gradient and MS settings can be found in Chapter 2.3).

Data processing and statistical analysis

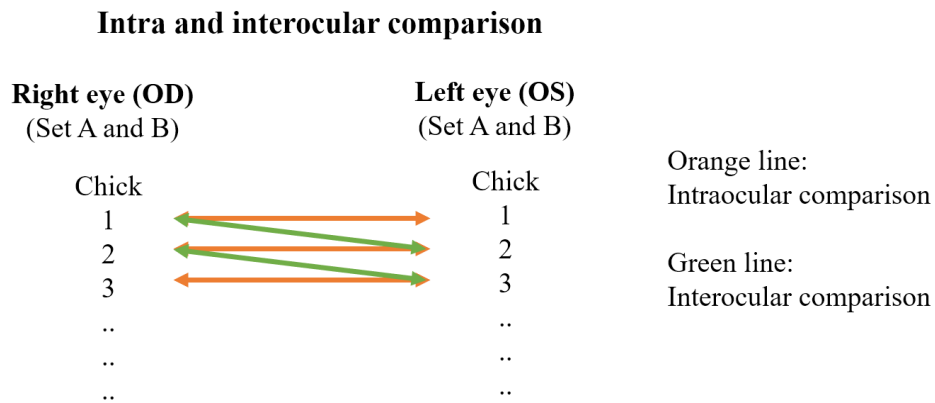


Figure 4.2 The intra and interocular comparison method. Obtained data for OD and OS were compared within each animal (Intra, shown in orange lines). For interocular comparison, the OD was compared to the OS from a different animal (Inter, shown in green lines) for each animal in each set.

For intraocular difference analysis, the left (OS) and right (OD) eyes were compared within each individual chick (shown in Figure 4.2, orange lines). The difference was calculated from the obtained measurement values of OD – OS for ocular parameter measurements and protein concentration analysis. And for protein analysis (from SWATH quantification), the protein intensity of each protein of OS and OD were averaged and compared against each other (in terms of FC, OS/OD ratio).

For interocular difference analysis, the OS and OD eyes of each chick were compared against different chicks (shown in Figure 4.2, green lines). The difference was calculated from the obtained measurement value of one chick's OD takeaway from another chick's OS measurement value for ocular parameter measurements and protein concentration analysis. And for protein analysis (from SWATH quantification), the protein intensity of each protein of one chick's OD was compared to the another chick's OS (e.g., chick1's OD vs. chick2's OS, chick2's OD vs. chick3's OS, chick3's OD vs. chick4's OS...etc.).

Using the ion library generated from the combined IDA injections, SWATH files were loaded using PeakView with the setting mentioned in the methods sections. Data were then grouped and normalized using the MLR method in MarkerView and exported to excel for statistical calculation. Proteins were considered to be statistically different with the following filter criteria: >1 peptide, fold change (average of OD/OS ratio) (FC) ≥ 1.5 or ≤ 0.67 .

4.3 Results

Refractive error

Regarding intraocular comparison, the difference in refractive error between each eye of the same animal was measured. An average difference of 0.031 ± 0.784 D and 0 ± 0.736 D (Mean \pm SD, n= 8 for set A and n= 7 for set B) were measured for sets A and B, respectively (shown in Figure 4.3). In terms of interocular comparison, the difference in refractive error between each eye of different animals was measured, and an average difference of 0.031 ± 1.145 D and 0 ± 1.216 D (Mean \pm SD, n= 8 for set A and n= 7 for set B) were measured for set A and B, respectively.

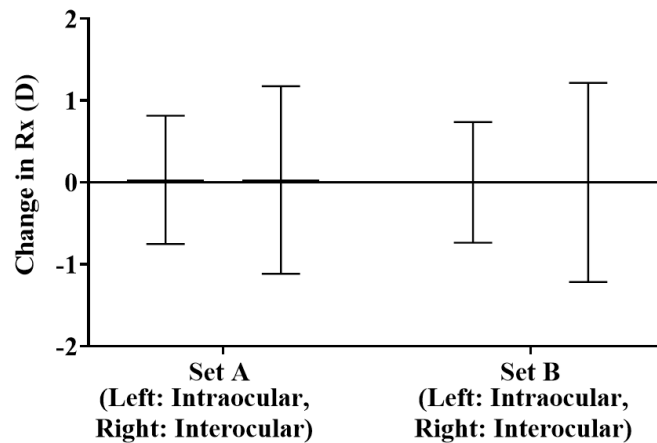


Figure 4.3 The change in refractive error (D) in OD and OS for Intra (left bar) and inter (right bar) ocular comparison for both sets (n= 8 for set A and n= 7 for set B, Error bars = Mean \pm SD).

Ocular parameter

For intraocular comparison of set A, four ocular parameters (ACD, LT, VCD, and AXL) were measured and compared between each eye of the same animal, and an average difference of 0.008 ± 0.015 mm, -0.002 ± 0.040 mm, 0.041 ± 0.071 and 0.047 ± 0.047 mm (Mean \pm SD, n= 8) ACD, LT, VCD, and AXL, respectively. The SD was slightly larger for interocular comparison, having an SD of 0.065, 0.080, 0.191, and 0.248 for ACD, LT, VCD, and AXL, respectively, while having the same average (Figure 4.4 A). The results were also similar for set B: An average difference of 0.013 ± 0.02 mm, 0.012 ± 0.023 mm, 0.021 ± 0.070 , and 0.046 ± 0.084 mm (Mean \pm SD, n= 7) ACD, LT, VCD, and AXL, respectively for intraocular comparison. The SD was slightly larger for interocular comparison, having an SD of 0.044, 0.048, 0.206, and 0.220 for ACD, LT, VCD, and AXL, respectively, while having the same average results as an intraocular comparison (Figure 4.4 B).

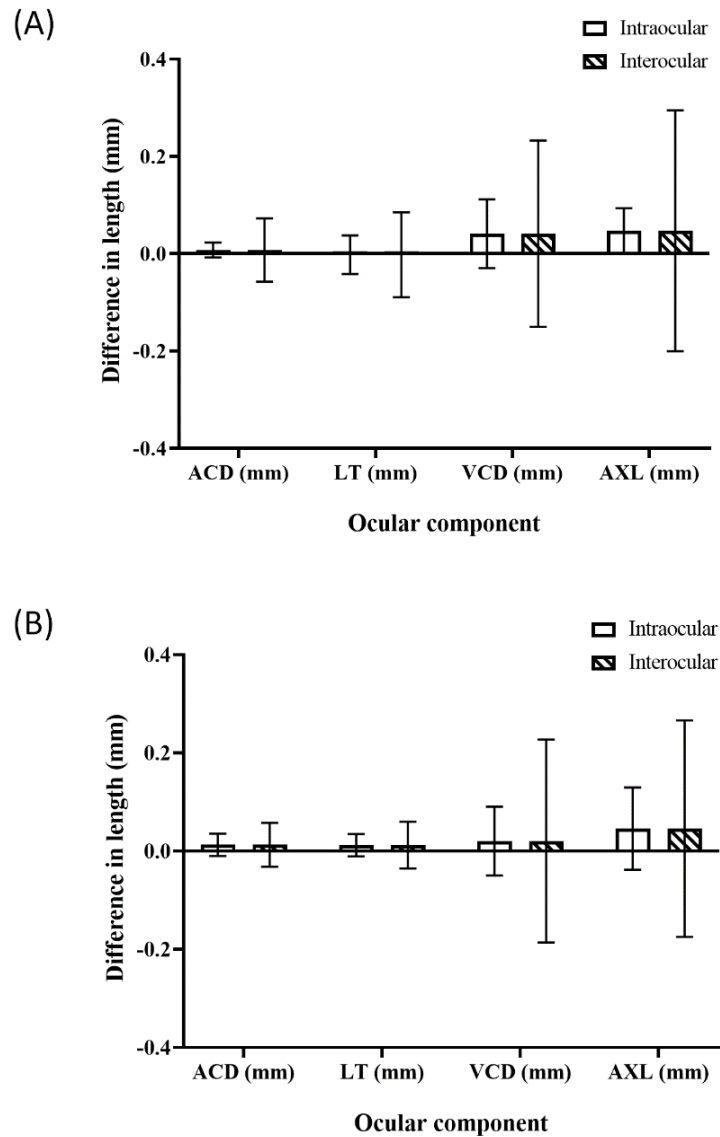


Figure 4.4 The change in ocular components in length (mm) in OD and OS for intra and interocular comparison for both sets (n= 8 for set A and n= 7 for set B, Error bars = Mean ± SD) from A-scan for (A) set A and (B) set B. ACD: anterior chamber depth, LT: lens thickness. VCD: vitreous chamber depth, AXL: axial length from the front of the cornea to the front of the retina

Protein concentration

In terms of intraocular comparison, the difference in protein concentration between each eye of the same animal after homogenization was measured and an average difference of $0.001 \pm 0.056 \mu\text{g}/\mu\text{l}$ and $-0.001 \pm 0.020 \mu\text{g}/\mu\text{l}$ (Mean ± SD, n= 8 for

set A and n= 7 for set B) were measured for set A and B, respectively (shown in Figure 4.5). The SD was slightly larger for interocular comparison for both sets, where an SD of 0.067 and 0.043 was observed for sets A and B, respectively, while having the same average results as an intraocular comparison (Figure 4.5).

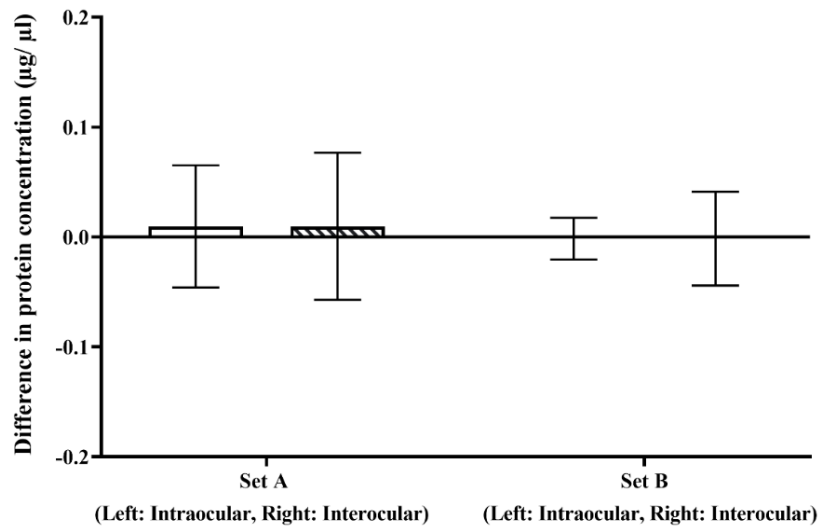


Figure 4.5 The average difference in protein concentration ($\mu\text{g}/\mu\text{l}$) of lysed vitreous (T-PER, 1:1 w/v ratio) from the right eye (OD) and the left (OS) for intra and interocular comparison (set A, n= 8 and set B, n= 7, Error bars = Mean \pm SD).

Proteomic analysis

The intraocular difference was measured in terms of an overall fold change (FC, OD/OS ratio) of each protein (in SWATH quantification) between the left (OS) and right eye (OD) of the same animal (n= 8 for set A and n= 7 for set B). An overall average protein (OD/OS) FC of 0.973 ± 0.153 and 1.033 ± 0.261 were calculated for sets A and B. In terms of interocular difference, an eye from each animal was compared to the fellow eye from another animal (n= 8 for set A and n= 7 for set B). An overall average protein (OD/OS of an eye from different animals) FC of 1.003 ± 0.212 and 1.063 ± 0.360 were calculated for sets A and B. Significant differences (P= 0.020) were found in comparing Intra and interocular differences in set A only (Shown in Figure 4.6 A and B).

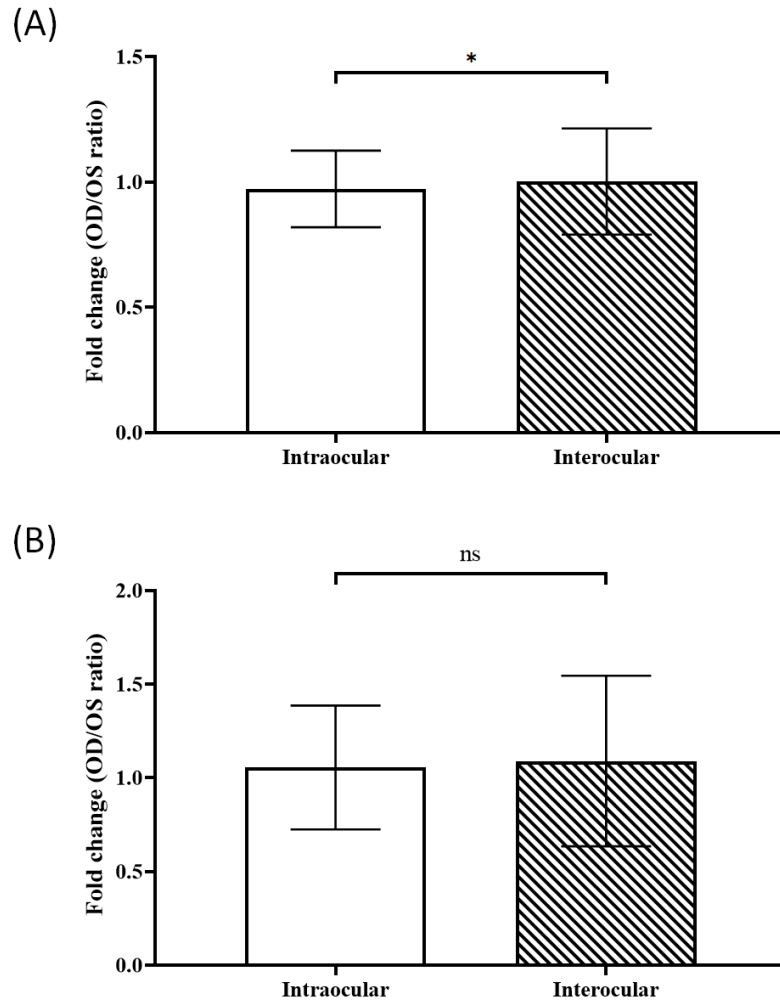


Figure 4.6 Intra (OD/OS FC of the same animal) and interocular (OD/OS FC of different animals) comparison of (A) set A and (B) set B in terms of protein fold change acquired from SWATH quantitation. * $p \leq 0.05$, ns: not significant, unpaired T-test (set A, $n = 8$ and set B, $n = 7$, Error bars = Mean \pm SD).

The protein intensity obtained for each protein within the vitreous from SWATH quantitation in OD was also compared to OS within each animal having a very high R-squared (R^2) value ranging from 0.968 to 0.999 from both sets (set A, $n = 8$ and set B, $n = 7$) for intraocular comparison (Figure 4.7 A and C shows a typical intraocular comparison of a chick). For interocular comparison, although a high R^2 value ranging from 0.960 to 0.999 from both sets (set A, $n = 8$ and set B, $n = 7$), the average intercept was much further away from 0 compared to intraocular

comparison (Figure 4.7 B and D). The full list of graphs for both intra and interocular comparisons can be found in Appendix 3.

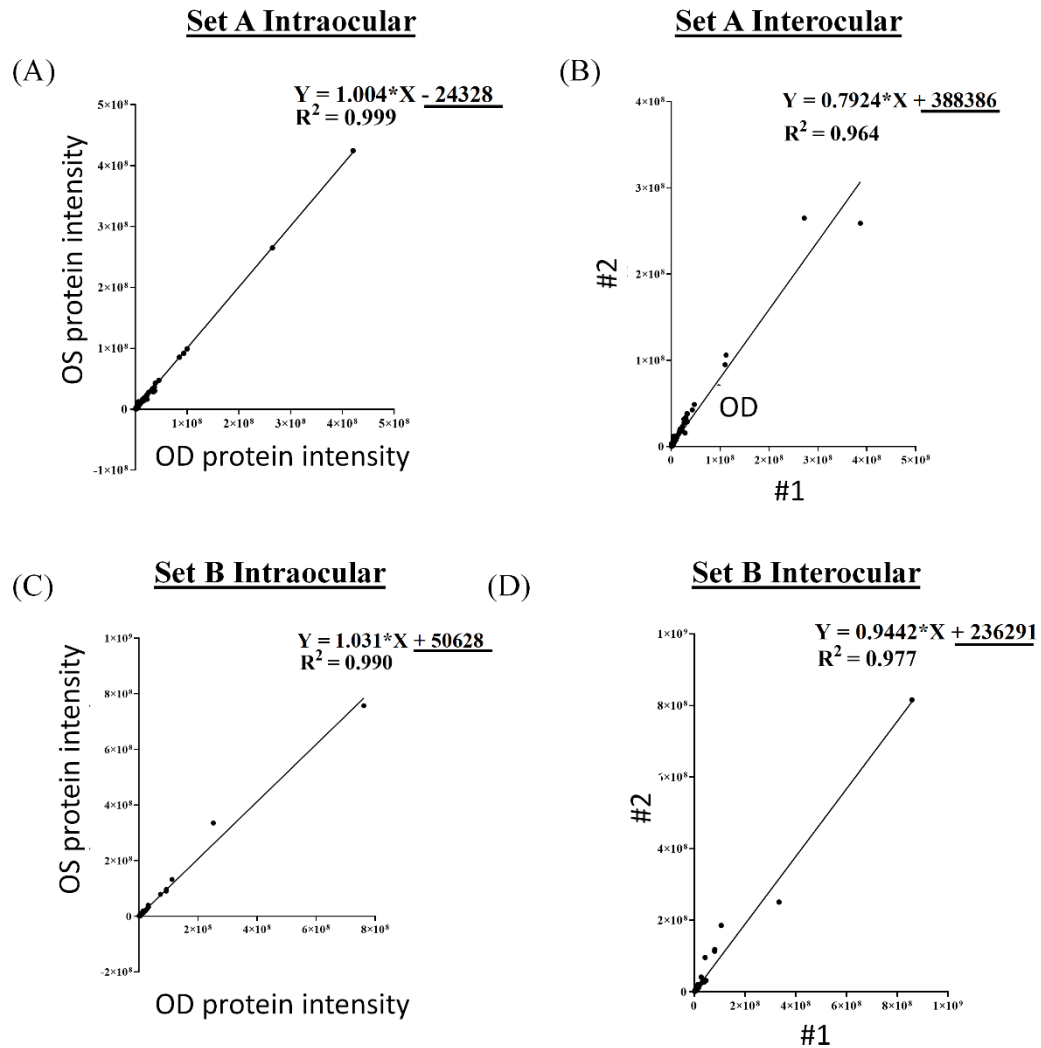


Figure 4.7 Scatter plots of protein intensities acquired from SWATH quantitation. Typical intraocular protein intensities comparison between the OD and OS vitreous of the same animal for (A) set A and (B) set B. Typical interocular protein intensities comparison between the OD and OS vitreous of different animals for (C) set A and (D) set B. (A much higher + C intercept indicating a higher rate of false up-regulation).

Using filter criteria mentioned (>1 peptides, $FC \geq 1.5$ or ≤ 0.67) on the results from SWATH quantitation, a total of 25 (5 up and 18 down-regulated) and 32 (30 up and 2 down-regulated) proteins were found between OD and OS of the same animal in

set A and B, respectively for intraocular comparison. In contrast, the total DEPs number for interocular comparison had a total of 22 (12 up and 10 down-regulated) and 39 (39 up and 0 down-regulated) proteins found between OD and OS of a different animal from set A and B, respectively (shown in Table 4.1).

Table 4.1 The number of DEPs found intra and interocular comparisons using SWATH quantitation (set A, n= 8 and set B, n= 7). An FC cutoff filter (FC ≥ 1.5 or ≤ 0.70) was applied to reduce false-positive results.

	Set A	
(OD/OS)	Intraocular	Interocular
No. of up-regulated proteins	5	12
No. of down-regulated proteins	18	10
	Set B	
(OD/OS)	Intraocular	Interocular
No. of up-regulated proteins	30	39
No. of down-regulated proteins	2	0

4.4 Discussion

Unlike other body parts, eyes are found in pairs across multiple species, including humans. Although the physical aspect may be symmetrical, each eye could react to the environment slightly differently (intraocular). Moreover, this difference is further amplified among different compared to individuals due to biological differences (interocular). When designing a typical experiment using the proteomic approach, a treatment (e.g., myopic treated) and a control group are usually defined. The protein expression from these groups is then identified and compared. The expression changes are therefore affected by the variations (e.g., biological) from the sample where it should be consistent. The comparison of vitreous between the left (OS) and right (OD) eye in terms of physical aspects (ocular parameters using a chick model), as well as protein profiles using SWATH quantitation (protein expression profile), will pave a foundation for future vitreous proteomics study experimental designs.

In terms of physical aspect studies (refractive error, ocular parameters from A-scan), variation within each animal can be seen in intraocular difference, but the differences (shown in SD) are much larger for interocular comparisons as expected (repeated from two separate batches of age-matched animals) indicating a much larger difference from biological variation (SD were more than doubled comparing intra to interocular results). These results are similar to Schaeffer and Howland et al. demonstrated, where the refraction between both eyes in FDM was highly correlated. At the same time, a much higher variation was found between different animals (Schaeffel & Howland, 1991). This biological variation was found to be higher at earlier time points and will gradually reduce as the eye matures.

The protein concentration measurement after vitreous homogenization gives similar findings as the SD is much larger in interocular comparisons ($SD \pm 0.043$, set B, $n=7$) compared to intraocular comparisons ($SD \pm 0.019$, set B, $n=7$) for both sets. Since the VCD was similar from all the animals, similar weight/ size of the vitreous were collected for homogenization, and it showed no significant differences between the two eyes reflecting the stable nature of the vitreous in a normal condition, as one of the main features of vitreous was to remain structurally and

chemically stable for molecule compartmentation (Pounder et al., 1998). In cases where possible leakage of blood was present, such as in specific ocular diseases like diabetic macular edema (DME) (Ouchi et al., 2005) and proliferative diabetic retinopathy (PDR) (Kim et al., 2007), the protein concentration could be ten times higher than control vitreous samples due to the addition of transferrin proteins from the blood. However, with complications without the involvement of blood, such as myopia, Pickett-Seltner et al. have concluded that there was no difference in vitreous protein concentration between myopic and nonmyopic eyes on day 14 of post-hatched chicks (Pickett-Seltner et al., 1992). A study by Amith Mulla et al. concluded that vitreous electrolytes and potassium concentrations had a very linear relationship between the same pair of eyes at identical postmortem intervals (PMI) (Mulla et al., 2005). The stable protein concentration between both eyes indicates that any foreign stimulation introduction will require a high impact to be seen in the vitreous.

To further minimize variations introduced, digested vitreous samples were equalized into equal amounts before the injection into the MS. The same amount of samples were then injected into the MS using the same running conditions for a fair comparison. The average protein fold change (OD/OS, from SWATH quantitation) of both sets was close to 1 as expected, and the SD (FC of each protein) was higher for interocular comparisons ($SD \pm 0.456$, set B, $n= 7$) compared to intraocular comparisons ($SD \pm 0.331$, set B, $n= 7$) for both sets. Taking the intensity from each protein for comparison, the high correlation value (R^2) was obtained between OD and OS of individual animals and a C intercept value ($R^2 = 0.990$ and $C= 50628$, set B, chick #1) closer to 0 was found. In contrast, a lower R^2 value and a much larger C intercept value ($R^2 = 0.977$ and $C= 236291$, set B, chick #1 and #2) indicated a high chance of detecting false up-regulated proteins. Indeed, the number of up-regulated proteins was higher in interocular comparison than intraocular using this method (a cutoff filter of $FC \geq 1.5$ or ≤ 0.67 was applied), indicating a slight bias towards the up-regulated part.

The results obtained in this study indicated eyes should be compared intraocularly when designing an animal experiment using the nanoLC-MS workflow of the

vitreous, as the protein intensities acquired were similar between individual animals. Future treatment groups (e.g., LIM treated with – 10D lens) should be compared to its fellow up, and applying the lens on a random eye (either left or right eye in the group) on the animal could further reduce the chances of obtaining false-positive results. In addition, the impact on potential protein changes caused by individual genetic variations, independently from optical defocus from different animals, could be neglected in the proteomic ocular analysis.

4.5 Conclusion

Two separate batches of normal growing age-matched chicks (n= 8 for set A and n= 7 for set B) were raised under the same lighting condition where the left (OS) and right (OD) of individual animals (intraocular) and across different animals (interocular) were compared. There were very good similarities found in the intraocular comparison between individual animals' eyes, while a higher SD was found for inter-animal comparison in terms of physical aspects such as refractive error and ocular measurements and vitreous protein concentration. Vitreous protein analysis (from SWATH quantitation) was measured using the nanoLC-MS workflow and while the average FC (OD/OS) of proteins was close to 1 for both intra and interocular comparisons, the SD was higher for the interocular comparison group. Furthermore, inter-animal protein analysis also indicated a higher chance of obtaining up-regulated proteins (which increases the chance of false-positive results) than intraocular comparison. The results obtained showed that the vitreous proteomic profiles from both eyes are more similar between individual animals (intraocular) compared to across different animals (interocular) and future studies (e.g., myopia model) should be carried out on the same animal in typical eye research with the in-solution nanoLC-MS setup between a treatment and control group.

Chapter 5. Changes in chick vitreous proteomes during normal eye growth

5.1 Introduction

As the optimized vitreous proteomics workflow has been established in Chapter 3, vitreous samples were collected during the emmetropization period (from D7 to D28) to investigate the dynamic vitreous proteome changes. This study serves as the first attempt to identify and quantify vitreous protein regulation in normal eye development during the initial stage of emmetropization using a high-resolution label-free approach (SWATH-MS).

The emmetropization period (normal growth) describes the stage where the eye elongates from a shorter stage (hyperopic) towards the normal refraction stage where the image aligns to the retina under normal growing conditions. This is a critical period common in humans (Ehrlich et al., 1995) and across various animal species such as monkeys (Bradley et al., 1999), tree shrews (Norton & McBrien, 1992), chicks (Wallman et al., 1981), and guinea pigs (Howlett & McFadden, 2007).

Myopia is considered a failure of emmetropization where the eyeball further elongates, passing the emmetropization state with an indefinite stop sign as it progresses. From this accelerated normal growth pattern, proteins responsible for this elongation might bring us more insight into the potential factors related to myopia progression. Chick has long been used as the animal model for ocular research (Kisilak et al., 2006; Wallman & Adams, 1987; Wallman et al., 1981; Wallman et al., 1978) due to the ability of their eyes to compensate for the surrounding environment. Just like humans, the eye will be hyperopic at early stages and slowly elongate towards emmetropia. Using the white leghorn chick model, the results showed that the refractive error has shifted from a hyperopic state towards under the conditions of normal lighting 12/12 hours showing the normal growth of the eyeball similar to previous reports using the same animal model (Wallman et al., 1981).

Vitreous humor (VH) is a transparent gelatin-like substance composed of networks of collagen fibrils and hyaluronic acid that takes up to 80% of the eyeball at the posterior part of the eye cavity. During myopia progression, vitreous chamber depth (VCD) is the main factor contributing to the eyeball's elongation. As it is located adjacently to the retina, it has been well documented the biochemical changes in the vitreous could be due to the changes from the retina, allowing the vitreous to act as an indirect indicator of the changes occurring in the retina. VH allows the transportation of chemicals and proteins within itself via diffusion to maintain homeostasis within the eyeball (Murthy, Goel, Subbannayya, Jacob, Murthy, Manda, Patil, Sharma, Sahasrabuddhe, Parashar, Nair, Krishna, Prasad Ts, et al., 2014). The collagen/ hyaluronic acid meshwork (gel-like substance) is also ideal for protein storage reservoirs within its close space, allowing soluble proteins within the vitreous metabolic nutrient movements to other parts of the eyeball including the retina and lens from the retina and ciliary body (Halfter et al., 2008; Mahajan & Skeie, 2014; Theocharis et al., 2002).

However, published proteomic research on vitreous is still scarce due to the limitation of the traditional gel-based proteomic approach on identifying low abundant proteins within the diluted nature of the vitreous. The demanding sample volume and concentration used in traditional gel-based proteomics greatly limits the detection of proteins in the vitreous, hampering its potential use and scientific research values. Quantitative proteomics offers an additional method to understand protein dynamics by comparing the levels of proteins under different conditions.. Sequential Window Acquisition of all Theoretical Mass Spectra (SWATH) is a data-independent acquisition (DIA) method that adjusts the stochastic nature of IDA problems by essentially taking everything in from the MS/MS without being dependent on the previous ionization threshold of MSTOF (Gillet et al., 2012). This allows all the transition ions in a set of sequential windows, enabling a deeper acquisition and quantification of proteins.

This study aims to build up the first and most comprehensive proteome of vitreous covering the normal growth period of the chick in the first month of hatching. Identification of these differentially expressed proteins (DEPs), including their

functions and roles involving the biological pathways, will provide a better understanding of the proteomic changes during emmetropization. Also, the findings may provide insights into the myopia mechanism from a range of time points (D7, 14, 21, 28) with proteins that are actively responsive to rapid ocular elongation during different time frames.

5.2 Methods and materials

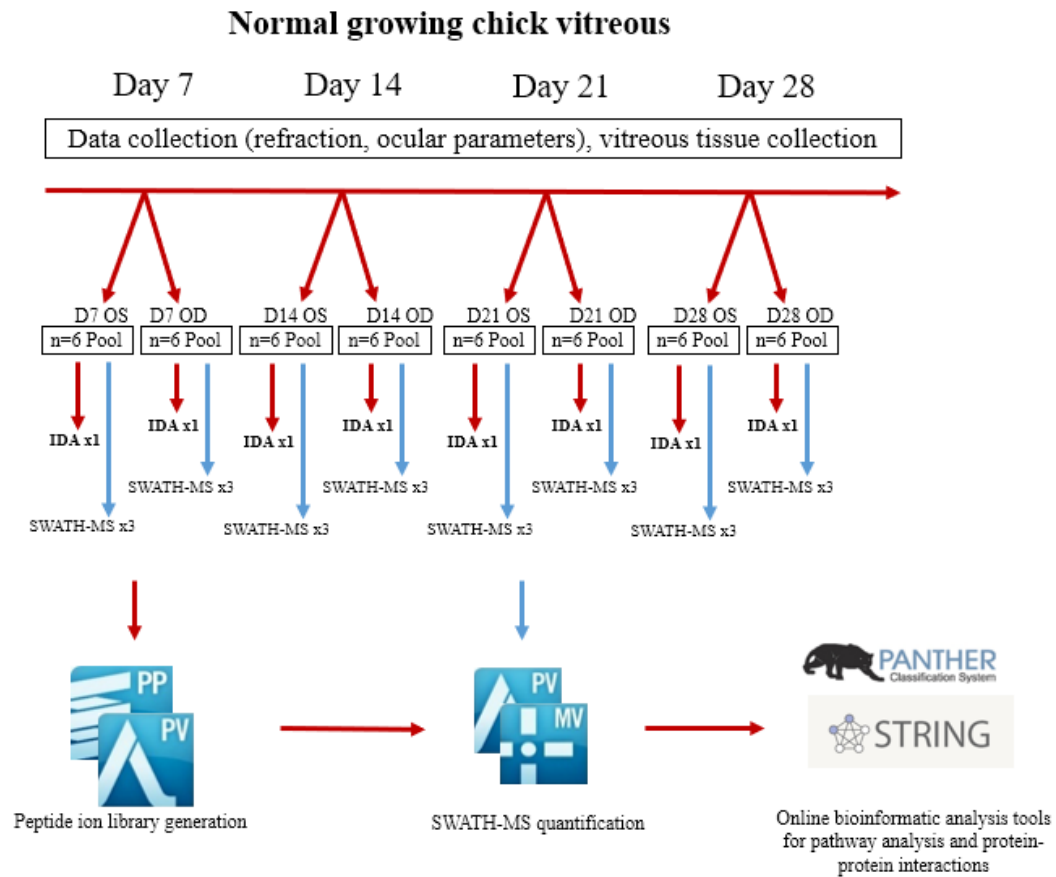


Figure 5.1 The SWATH-MS experimental workflow of normal growth (emmetropization) period. Chick vitreous samples were collected at Day 7, 14, 21, and 28 (a total of 24, n= 6 at each time point). These were then pooled into the right eye (OD) and left eye (OS) for sample preparation. IDA injections were performed on each of the samples with 3 SWATH injections for quantification. The ion library was generated from the combined search of all the IDA injections. Acquired data were then exported for data analysis software.

Housing of chickens

The experimental design is shown in Figure 5.1. A total of 24 (6 for each time point). White Leghorn chicks (*Gallus gallus domesticus*) hatched from specific pathogen-free (SPF) eggs were housed in stainless steel brooders under a 12/12 dark/ light cycle.

Ocular parameter measurements and vitreous sample collection

Measurements of ocular growth and weight were taken at set time points: Day 4 (Baseline data), 7, 14, 21, and 28 to cover the normal emmetropization process. The refractive error was measured using a streak retinoscope (Beta 200 Streak Retinoscope Set 2.5v, Heine, Germany) with a trial lens bar ($\pm 16.00D$ in 0.5D steps) in dim light conditions. Equivalent sphere measurements were used to define the refractive error in this animal study ($S. E = \text{Spherical power} + \frac{1}{2} \text{cylindrical power}$). An A-Scan Ultrasound (5073PR, Olympus, Japan) coupled with a 30MHz probe (PZ25-025-R1.00, Panametrics, USA) was used to measure ocular components for ocular growth measurements. A lid retractor was used to keep the eye open during measurements, and anesthesia was not applied to avoid any potential protein changes induced. An average of 3 repeats of measurements were done on each eye for analysis. Ocular components, including the anterior chamber depth (ACD), lens thickness (LT), vitreous chamber depth (VCD), and axial length (AXL), were analyzed and compared in this study. Vitreous samples from each eye at each time point were then extracted and collected according to the methods section in Chapter 2.2.

Vitreous sample preparation for LC-MS

Collected vitreous were then prepared according to the methods section in Chapter 2.2. without the use of high-pH fractionation. In brief, A 1:1 w/v ratio of T-PER buffer (T-PER, Cat# 78510, Thermo Fisher Scientific, USA) was added to each collected vitreous sample. The individual sample was homogenized using the homogenizer (Precellys evolution homogenizer, Bertin, France) with the following settings: 5000rpm, 4x 30sec, 15-sec breaks under liquid nitrogen cooled environment. Samples were then centrifuged, and the protein concentration was measured using Bradford protein assay (Cat# 5000006, Bio-Rad, USA). Equal protein amounts of samples were then reduced by 10mM dithiothreitol (DTT) (Cat# 43815, Sigma-Aldrich, USA) to a final concentration of 10mM at 37 °C for 1 hour and alkylated at a final concentration of 40mM iodoacetamide (IAA) (Cat# I1149, Sigma-Aldrich, USA) in the dark at room temperature for 30 mins. Acetone precipitation was done by adding 4x volume of ice-cold acetone overnight at -20 °C, then centrifuge at 21380 x g for 30 mins at 4 °C. The pellet was then washed

with 500 µl of 80% acetone and centrifuged at 21380 x g for 10 mins at 4 °C. The protein pellet was then dissolved in 1M Urea in 25mM ammonium bicarbonate. Samples were redissolved in 1M Urea and 25mM ammonium bicarbonate were subjected to in-solution digestion with trypsin (Cat# V5111, Promega, USA) at 1:25 (enzyme: protein) ratio w/w for 16 hours at 37 °C. Digestion was stopped with TFA and was desalted and cleaned up with C-18 SPE HLB column (Cat# WAT094225, Waters, USA). Cleaned-up tryptic peptides were dried by vacuum centrifugation (CentriVap, Labconco, USA) and were reconstituted in 0.1% formic acid. The peptide concentration was estimated using peptide Assay (Cat# 23275, Thermo Fisher Scientific, USA), and equal amounts of peptides from 5 samples were pooled together as OD and OS groups, resulting in an OD pool and OS pool for each time point. The peptide concentration was then measured again, and 1 µg of digested vitreous peptides were loaded for MS injection.

LC-MS data acquisition

The MS loading condition according to the methods section in Chapter 2.3.1 using the long gradient (155 mins). One IDA injection was done on each sample, and 3 injections (technical repeats) were done under SWATH-MS mode.

Data processing for protein identification and quantification

All the raw files (.wiff) of Information dependent acquisition (IDA) were combinedly searched against the Gallus gallus Uniprot database (Unreview + isoform), and protein identification (ID) was acquired using ProteinPilot (v5.0, Sciex, USA). Trypsin as the enzyme, cysteine alkylation using iodoacetamide (IAA), thorough search effort, and biological modification was selected. A 1% false discovery rate (FDR) was set as the filter. For label-free quantification, a combined search of 8 IDA injections was selected as the ion library for SWATH quantification. Both the IDA ion library and the SWATH injection files were loaded onto the SWATH Acquisition MicroApp 2.0 in PeakView (v2.2, Sciex, USA). Up to 10 peptides per protein, 6 transitions per peptide, 90% peptide confidence threshold, 1% FDR, 10 min XIC extraction window, and 75 ppm width were selected for processing. Processed data were normalized with the MLR method, analyzed with MarkerView (v1.3, Sciex, USA), and exported to excel for protein fold change calculation.

Bioinformatic analysis and statistical analysis

Proteins that have less than 1 peptide were removed to reduce the chances of false-positive results, and the filter for differential expressed proteins was considered at ≥ 1.5 -fold change, which must be the same direction for both eyes. All values were presented as means \pm standard deviation. The list of identified proteins was converted into gene names using the Uniprot batch gene name tool online ([http://www. Uniprot.org/](http://www.Uniprot.org/))(UniProt, 2019). Gene ontology (GO) analysis for functional classification biological processes, molecular functions, and Cellular components was performed using the online analysis tool PANTHER (www.pantherdb.org) database version 14 (Mi et al., 2019). The protein-protein interactions network analysis of significant differential expressed proteins was identified using STRING v10.0 (Search Tool for the Retrieval of Interacting Genes/Proteins) online database (<http://www.string-db.org>) (Szklarczyk et al., 2015). The search engine was set as multiple proteins, and the list input was accession numbers of the proteins; Gallus gallus was set as the organism.

5.3 Results

Chick biometric parameters

For biometric measurements at the 4 experimental time points (Day 7, 14, 21, and 28), 6 normal growing chicks were used at each time point (a total of 24 chicks throughout this study), and the raw data can be found in Appendix 4. The baseline measurements were measured on day 4 to ensure the eyes grew normally. No significant differences in ocular parameters were found between the left (OS) and right (OD) eyes using unpaired T-tests at all time points.

In terms of refraction (shown in Figure 5.2), all eyes measured on baseline (Day 4) were hyperopic (5.27 ± 0.60 D for OS and 5.36 ± 0.56 D for the OD). The most significant differences in refractive error were found only between D14 and D21 for both the right and left eyes.

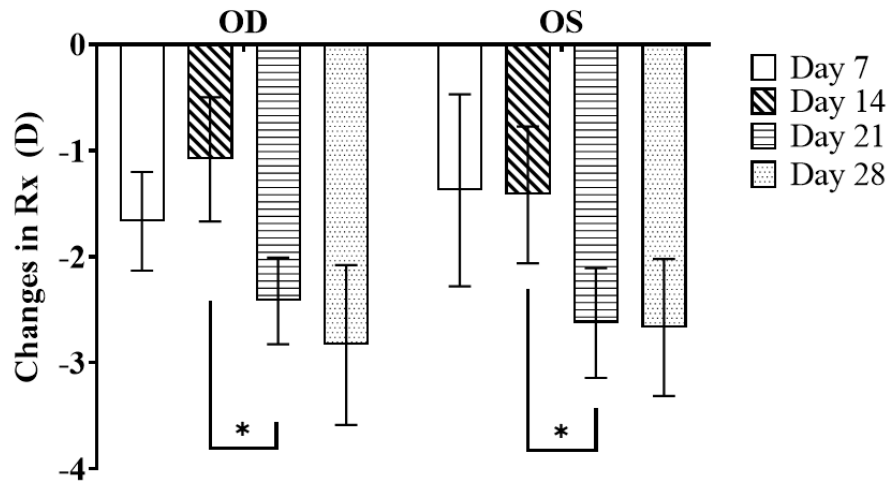


Figure 5.2 Average changes of refractive error of the right eye (OD) and left eye (OS) as compared to the baseline (D4) during different time points of normal growth: n= 6 at each time point. *P ≤ 0.05 and **P ≤ 0.01, one-way ANOVA. No significant differences were found between OD and OS at all time points for Rx.

In accordance with this, there was an increase in length (mm) of all ocular parameter measurements, including anterior chamber depth (ACD), lens thickness (LT), vitreous chamber depth (VCD), and the axial length (AXL) during this period, where significant differences were found between each time points ($p < 0.05$, one-way ANOVA). The average changes of various ocular parameters measured from A-Scan are shown in Figure 5.3 (A - D).

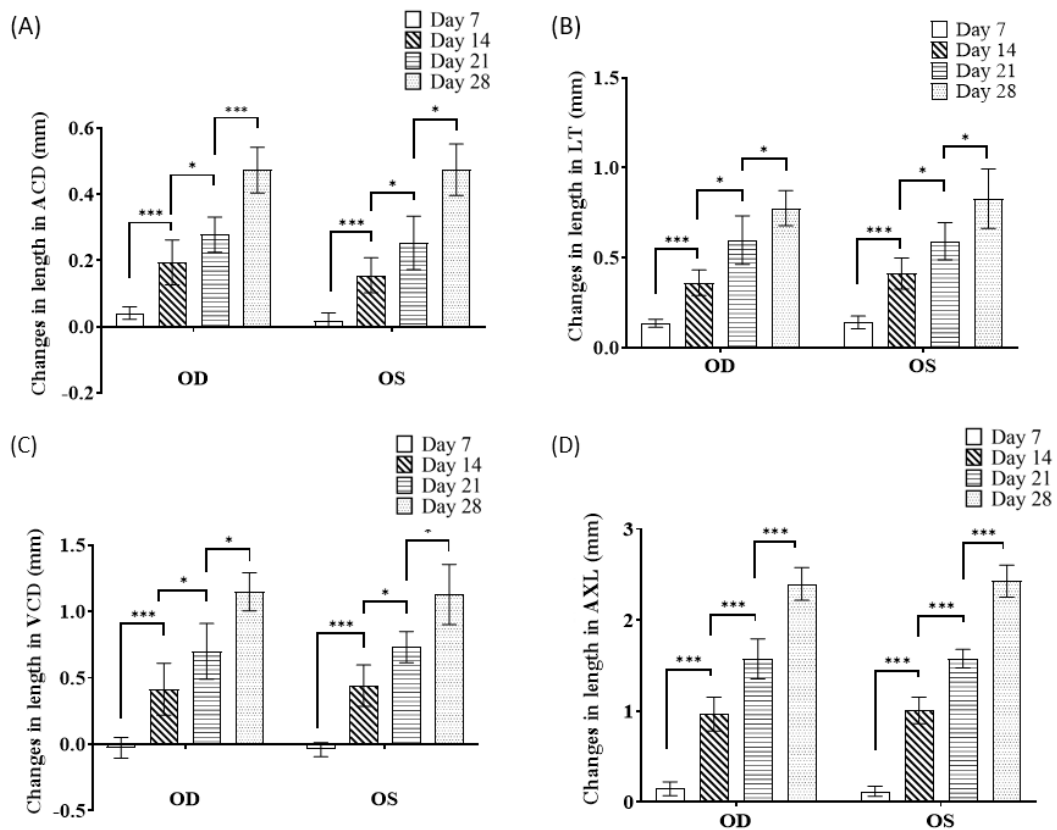


Figure 5.3 Average changes of ocular components of the right eye (OD) and left eye (OS) during different time points of normal growth: (A) ACD: anterior chamber depth, (B) LT: lens thickness. (C) VCD: vitreous chamber depth, (D) AXL: from the front of the cornea to the front of the retina), n= 6 at each time point. *p ≤ 0.05, **P ≤ 0.01 *p ≤ 0.001, one-way ANOVA. No significant differences were found between OD and OS at all time points for ACD, LT, VCD, and AXL.**

In terms of protein concentration after homogenization with T-PER buffer (1:1, vitreous volume: lysis buffer ratio) shown in Figure 5.4, an average of 0.187 ± 0.023 $\mu\text{g}/\mu\text{l}$ and 0.205 ± 0.020 $\mu\text{g}/\mu\text{l}$ for OS and OD on day 7, respectively. For day 14, an average of 0.189 ± 0.026 $\mu\text{g}/\mu\text{l}$ and 0.179 ± 0.033 $\mu\text{g}/\mu\text{l}$ for OS and OD were observed, respectively. For day 21, an average of 0.186 ± 0.026 $\mu\text{g}/\mu\text{l}$ and 0.187 ± 0.022 $\mu\text{g}/\mu\text{l}$ for OS and OD were observed, respectively. Lastly, for day 28, an average of 0.179 ± 0.022 $\mu\text{g}/\mu\text{l}$ and 0.190 ± 0.011 $\mu\text{g}/\mu\text{l}$ for OS and OD was observed, respectively.

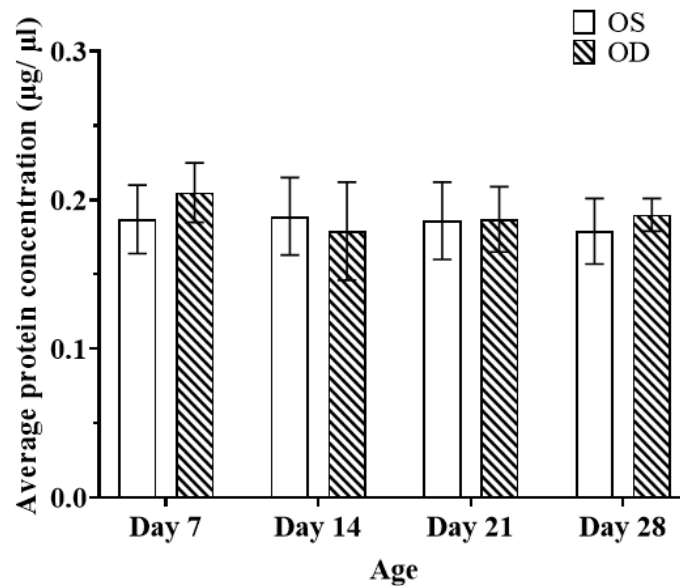


Figure 5.4 Average protein concentration of homogenized vitreous, n= 6 at each time point. * $p \leq 0.05$, ** $P \leq 0.01$ * $p \leq 0.001$, paired T-test between eyes and one-way ANOVA for multiple time points.**

Chick vitreous proteome - Ion library

A total of 1576 non-redundant proteins (22987 distinct peptides) were identified from the information-dependent acquisitions (IDA) consisting of all the eyes (OD and OS) at the 4-time points at 1% FDR. These identified proteins at 1% FDR were loaded onto the PATHER™ online gene ontology system (Mi et al., 2019) for the global overview of the gene ontology (GO) functions on the chick vitreous normal proteome. A total of 935 ID proteins (60% of all the identified proteins) were successfully mapped, and their classification (Biological process, molecular functions, and cellular components) is shown in Figure 5.5. In terms of biological process (Figure 5.5 A), the top 3 processes were found to be cellular process (GO:0009987) 34%, metabolic process (GO:0008152) 18%, and biological regulation (GO:0065007) 11%. For molecular functions (Figure 5.5 B), the top 3 functions were catalytic activity (GO:0003824) 40%, binding (GO:0005488) 34%, molecular function regulator (GO:0098772) 9%; in terms of cellular component (Figure 5.5 C), top 3 leading portions were Cell (GO:0005623) 41%, extracellular region (GO:0005576) 23.6%, organelle (GO:0043226) 15%.

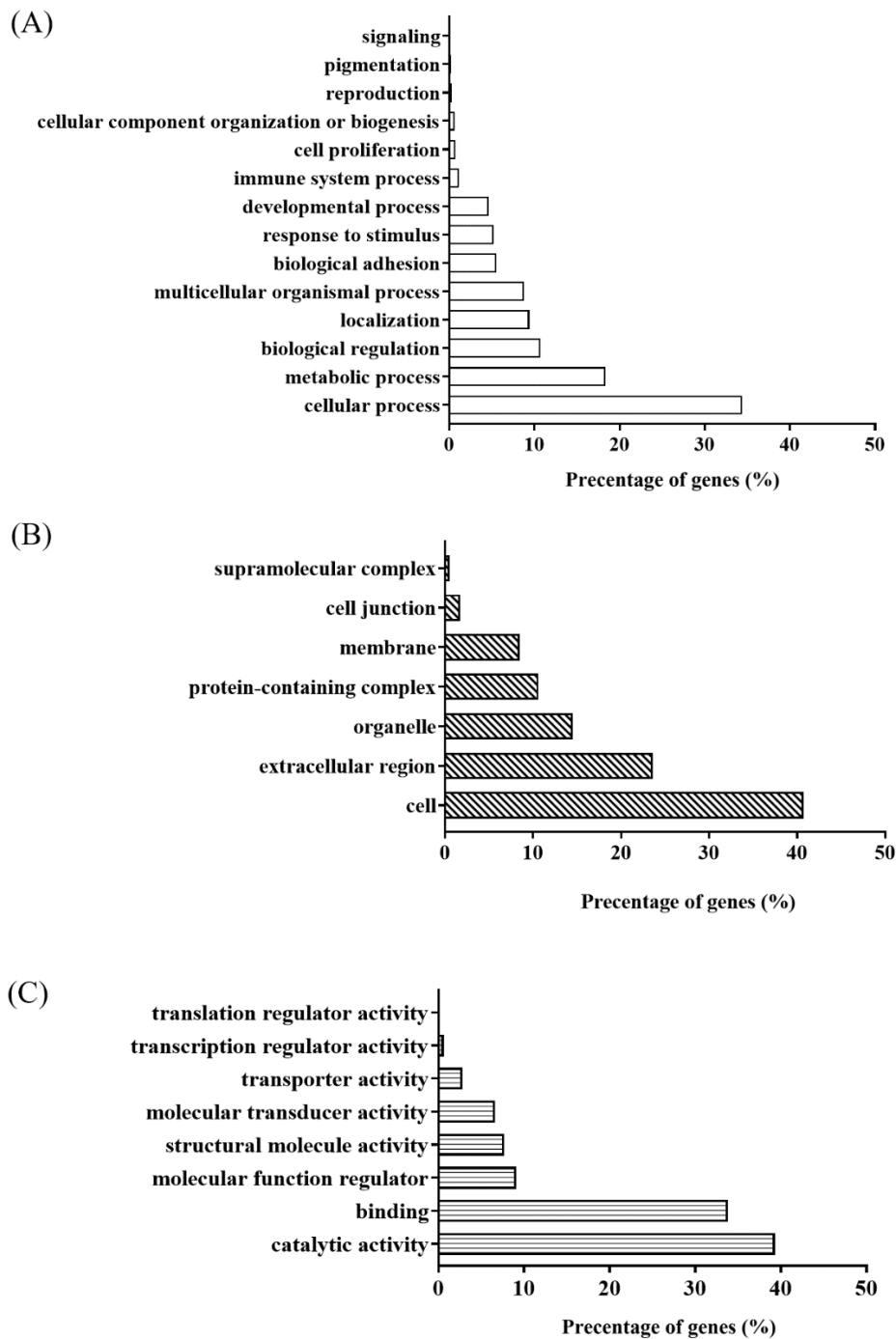


Figure 5.5 Gene ontology (GO) classifications of proteins from combined search proteins of normal growing chick vitreous. (A) Biological process (B) Molecular function (C) Cellular components using PANTHER.

Ion library generation for comparing common proteins under IDA and DIA approaches

The number of protein identification (at 1%FDR) from each time point was listed in Figure 5.6 A. A merged ion library consisting of unique proteins from these 8 IDAs from all experimental groups (OD and OS groups at each time point) was generated (shown in Figure 5.6 B). Although a total of 1988 unique proteins were identified, only 542 (27%) proteins were commonly found across all the samples to allow quantitation under IDA mode. However, 1456 (92%) common proteins could still be acquired across all the samples using this method from the 1576 total proteins found from the combined generated ion library for SWATH-MS.

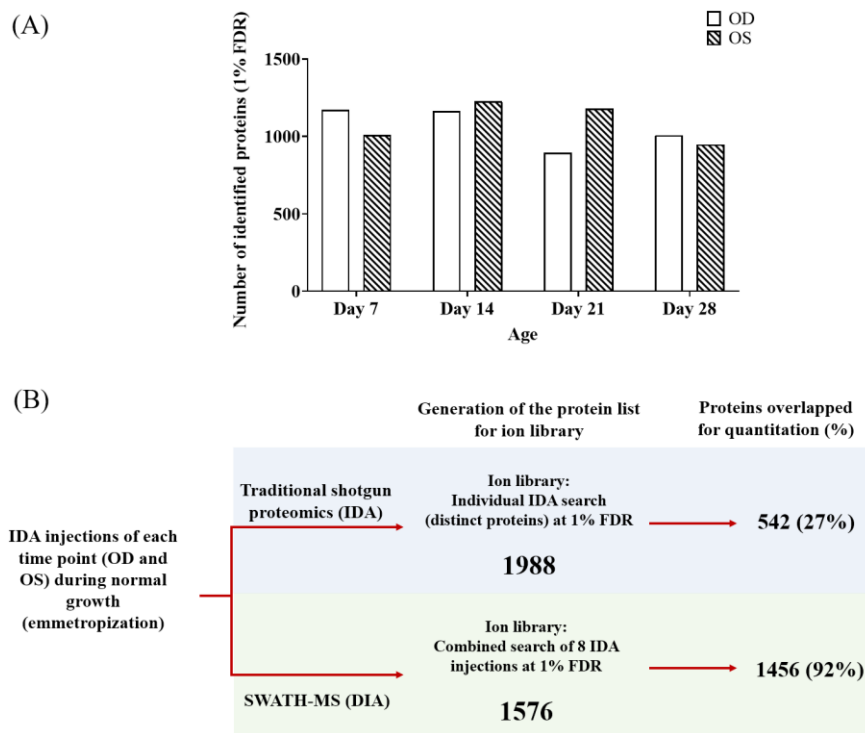


Figure 5.6 (A) The number of proteins identified at 1% FDR at each time point (individually searched of the pooled sample). (B) The Comparison between the combined library and 8 individual libraries; Traditional shotgun proteomics (8 individual injections, individually searched) and combined searched library (8 injections combinedly searched). The total unique proteins (peptides) identified from all 8 individual injections, and a combined search were 1988 and 1576, respectively. The total overlapping unique proteins found across all 8 injections in IDA and DIA mode were 542 and 1456, respectively.

Protein quantitation of chick vitreous proteins using SWATH-MS

As more common proteins could be detected using the SWATH-MS approach, we aimed to investigate the aging effect on protein profiles during the normal growth period in the chick vitreous using this DIA quantification (Figure 5.6 B). A total of 28 SWATH injections (OD and OS at each time point, with 3 technical replicates) were integrated and processed using PeakView software, and the results were exported for statistical calculation.

Using a filter criterion listed in the method section FC (≥ 1.5 -fold change, at least 2 peptides per protein, and FC must be the same direction for both eyes), compared to the baseline at Day 7 (Figure 5.7): 58 up-regulated and 71 down-regulated proteins were found in the D14 group. A total of 60 up-regulated and 54 down-regulated proteins were found in the D21 group. A table of all the DEPs identified can be found in Appendix 5. Moreover, a total of 120 up-regulated and 117 down-regulated proteins were found in the D21 group. All raw data generated from Information-dependent acquisition (IDA) and SWATH acquisitions (DIA) were accepted and published in the Peptide Atlas public repository (<http://www.peptideatlas.org/PASS/PASS01258>) for public open access (Cheung et al., 2020).

Among these differentially expressed proteins, a total of 64 proteins were found commonly identified across these time points: 27 up-regulated and 37 down-regulated proteins (D14/7, D21/7, and D28/7). These were submitted to draw clustered heatmaps using the HeatmapMaker in R program (Juan Pablo Carreón Hidalgo), shown in Figure 5.8. The expression level for each protein was calculated using the formula: [(total area of each protein) – mean/ SD]. Dark red indicates a more positive value (i.e., up-regulated proteins), and yellow indicates a more negative value (i.e., down-regulated proteins). Among these, potential normal growth-related DEPs are listed in Table 5.1.

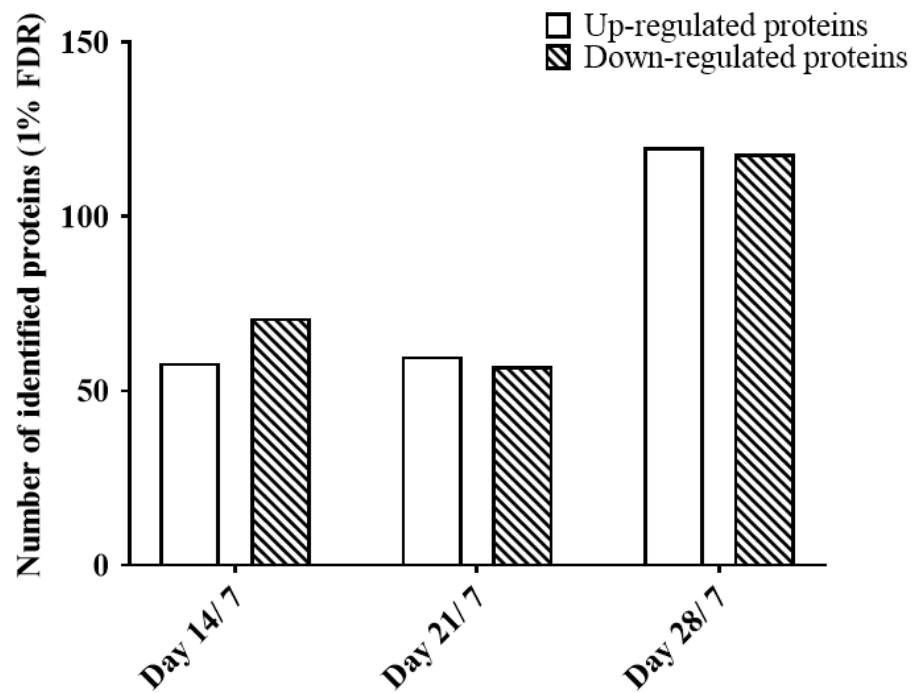


Figure 5.7 The number of proteins found differentially expressed from each time point using the combined ion library. The FC ratio was calculated by comparing it to the baseline (D7). The fold change calculation filter was set as ≥ 1.5 or ≤ 0.7 FC, same direction for both eyes.

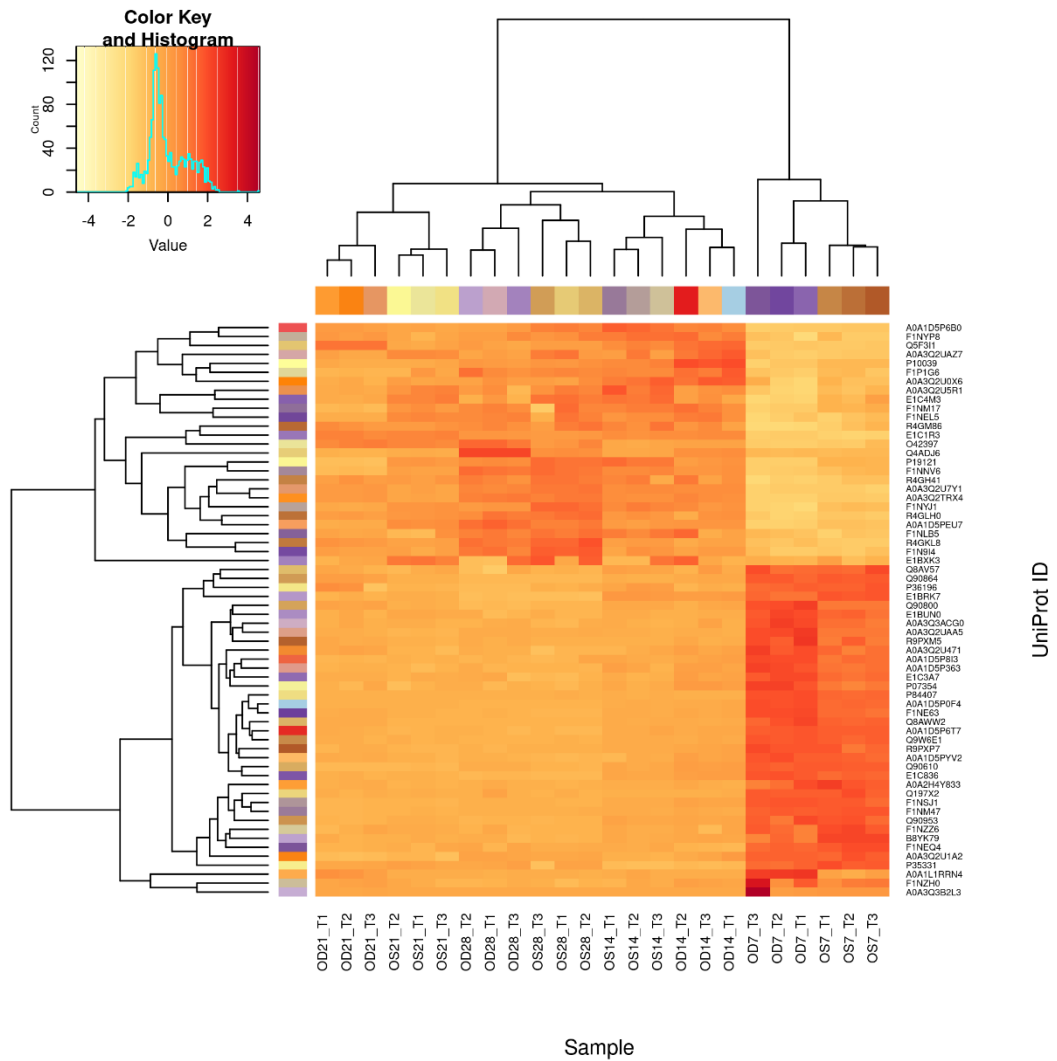


Figure 5.8 Heatmap showing DEPs in normal eye growth period (Day 7, 14, 21, and 28). Dark red indicates a more positive value (i.e., up-regulated proteins), and yellow indicates a more negative value (i.e., down-regulated proteins).

Table 5.1 Growth-related differentially expressed proteins (DEPs) found across all time points (14, 21, and 28). The fold change (FC) was calculated against the baseline (Day 7), FC cut off ≥ 1.5 or ≤ 0.7 , and both eyes have to be in the same FC direction. **Red: up-regulated proteins, **Blue**: down-regulated proteins.**

Uniprot ID	Protein name	Gene name	(Day 14/7) SWATH-MS FC			(Day 21/7) SWATH-MS FC			(Day 28/7) SWATH-MS FC		
			OD14/OD7	OS14/OS7	AVE FC	OD21/OD7	OS21/OS7	AVE FC	OD28/OD7	OS28/OS7	AVE FC
A0A3Q2U0X6	Sema domain-containing protein	LOC112530215	2.47	1.98	2.23±0.35	1.68	1.62	1.65±0.04	2.22	1.89	2.06±0.23
P19121	Serum albumin	ALB	9.2	2.71	5.96±4.59	3.96	2.17	3.07±1.27	13.58	3.45	8.52±7.16
Q4ADJ6	Ovotransferrin	TF	4.09	2.3	3.20±1.27	1.81	2.26	2.04±0.32	9.39	5.11	7.25±3.03
R4GLH0	IGFBP N-terminal domain-containing protein	ESM1	4.08	3.02	3.55±0.75	4.53	3.51	4.02±0.72	6.73	5.09	5.91±1.16
R4GM86	EGF-like domain-containing protein	CCBE1	3.12	2.14	2.63±0.69	3.74	2.1	2.92±1.16	4.33	2.62	3.48±1.21
FETA	Alpha-fetoprotein	AFP	0.01	0.02	0.02±0.01	0.01	0.01	0.01±0.00	0.01	0.02	0.02±0.01
A0A1D5PYV2	Cadherin-10	CDH10	0.46	0.35	0.41±0.08	0.43	0.39	0.41±0.03	0.40	0.35	0.38±0.04
A0A1D5P6T7	Cadherin-11	CDH11	0.39	0.4	0.40±0.01	0.4	0.34	0.37±0.04	0.35	0.33	0.34±0.01
R9PXP7	Cadherin-20	CDH20	0.47	0.48	0.48±0.01	0.44	0.44	0.44±0	0.45	0.53	0.49±0.06
A0A3Q3ACG0	Cadherin-4	CDH4	0.31	0.38	0.35±0.05	0.34	0.43	0.39±0.06	0.37	0.4	0.39±0.02
Q8AWW2	Cadherin-7	N/A	0.33	0.36	0.35±0.02	0.39	0.32	0.36±0.05	0.32	0.34	0.33±0.01
F1NSJ1	Contactin-2	CNTN2	0.51	0.48	0.50±0.02	0.44	0.46	0.45±0.01	0.52	0.52	0.52±0.00

Q9W6E1	Neurocan core protein	N/A	0.23	0.25	0.24±0.01	0.21	0.2	0.21±0.01	0.17	0.19	0.18±0.01
F1NE63	Reelin	RELN	0.41	0.47	0.44±0.04	0.45	0.48	0.47±0.02	0.42	0.47	0.45±0.04
CSPG2	Versican core protein	VCAN CSPG2	0.33	0.32	0.33±0.01	0.2	0.25	0.23±0.04	0.19	0.19	0.19±0.00

Data analysis using bioinformatics software and confirmation using targeted proteomics

As we intended to screen for proteins with temporal changes during emmetropization, commonly found differentially expressed proteins were loaded on the STRING database for protein-protein interaction network analysis (Figure 5.9). Several proteins were grouped and found responsible for cell adhesion: VCAN, HAPLN1, TNC, NEO1, NRCAM, and SDK2, while VCAN had multiple interactions with NRCAM and NEO1 in the cell adhesion molecules pathway. AFP and ALB belong to the serum albumin family, while CTSZ, ASAH1, and ATP6AP1 were involved in the lysosome pathway.

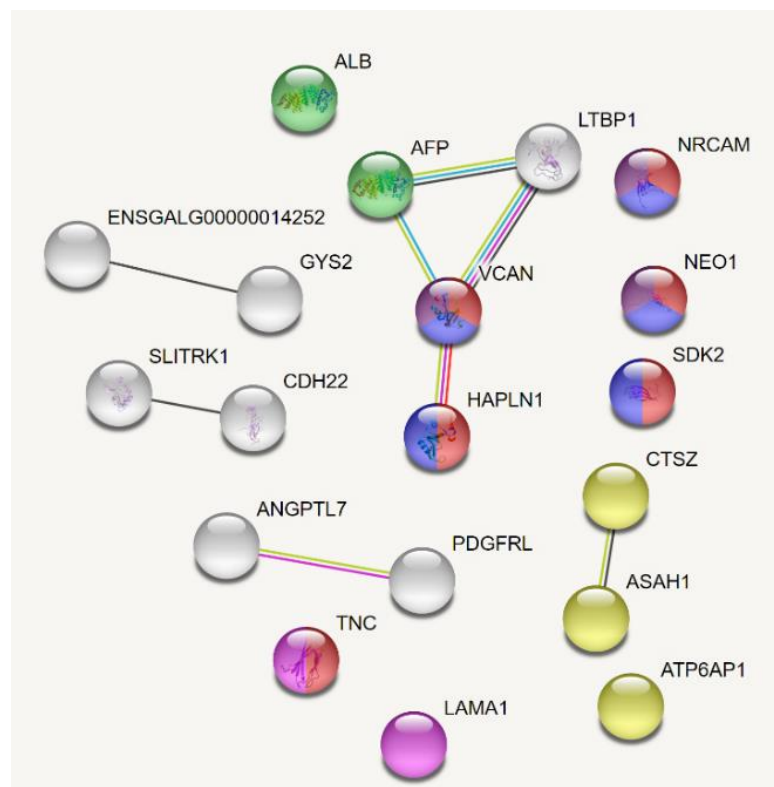


Figure 5.9 STRING analysis on commonly differential expressed proteins (DEPs) across all the time point. The color represents Red- cell adhesion; Blue- nervous system development; Purple: Cell adhesion molecules pathway; Yellow: Lysosome pathway; Pink- ECM-receptor interaction pathway; Green Serum albumin family. Grey: co-expressed proteins.

To further validate the expressions of these key proteins, a separate batch of chicks (n= 4) at the time points on Day 7 and 14, where the most significant changes were observed, was raised with the same conditions for confirmation of protein expressions using a High-resolution Multiple-reaction monitoring (MRM^{HR}) targeted proteomics strategy (Technical details were presented in Chapter 7).

5.4 Discussion

As the change in vitreous chamber depth (VCD) is a crucial indicator during the axial elongation (during myopia progression as well as emmetropization), this is the first study applying a next-generation proteomics approach (SWATH-MS) in tackling the regulated proteomes in the normal growing vitreous. Early gel-based vitreous proteomics studies mainly were hampered by the inability to detect low-abundance proteins due to the high concentration of serum proteins such as albumin and transferrin. Even with fractionation techniques like immune depletion, the identification rate was low in the low-abundance protein gel (Kim et al., 2007). With the advancement in MS technologies, such as improved sensitivity and resolution, the study of vitreous is benefited as the low protein content can now be further identified. Recent studies of various vitreous-related ocular diseases such as age-related macular degeneration (AMD) (Koss et al., 2014), diabetic retinopathy (DR) (Loukovaara et al., 2015), and myopia (Yu et al., 2017) using proteomic approach allowed the acquisition and identification of more proteins within the vitreous, widening the applications of vitreous, especially in ocular diagnostics. In terms of growth studies, Yee et al. identified 1217 proteins, and 43 proteins were differentially expressed in a study comparing the embryonic and young adult vitreous in humans (Yee et al., 2015), and Liu et al. compared the vitreous proteins in young and mature rabbits where 466 proteins were identified (Liu et al., 2016). To overcome the limitations of gel techniques, such as low sensitivity, Isotope-coded protein label (ICPL) LCMS labeling quantitation was recently used by our group to quantify vitreous proteins in the lens-induced myopic chicks (Yu et al., 2017) where APOA-1 and purpurin were successfully quantified and validated as novel findings.

In this study, the overall changes in refraction and ocular parameters (AXL) showed normal eye growth, which is in line with early findings in chicks study (Wallman et al., 1981) with a reduction in diopters (D) after hatching and confirming the emmetropization period. The average changes in the refraction showed a reduction in diopter (D) from a hyperopic state on Day 7 to near normal on Day 28, where both eyes at each time point remained the same (≥ 0.05 , paired T-test). Due to limited vitreous volume acquired from chicks, lysed vitreous samples from 6

individual chicks of the same age were combined (equal amount of protein from each eye) as a pool of vitreous samples (The left and right eyes were pooled at each time point), as a similar strategy adopted in our previous vitreous proteomics study design (Yu et al., 2017). More stringent filters were applied to minimize the chances of false-positive findings, where separate injections were acquired on the left and right eye samples. The proteins quantified needed the same FC direction on both eyes with an $FC \geq 1.5$ fold.

Using a highly sensitive nanoLC-ESI-MS/MS system, this study was able to identify a total of 1576 non-redundant proteins (22987 distinct peptides) at 1% FDR without the need for fractionation or protein depletion, making it the most comprehensive chick vitreous protein library covering the emmetropization period (from day 7 across today 28) to date, further expanding from our previous study (Yu et al., 2017), while 159 proteins were considered as “core proteins”. The top abundance proteins identified were namely Serum albumin, reelin, fibronectin, tenascin, and ovotransferrin and GO analysis of this data set indicated similarities in molecular functions, biological process, and cellular components compared to human studies of the vitreous proteome (Murthy, Goel, Subbannayya, Jacob, Murthy, Manda, Patil, Sharma, Sahasrabuddhe, Parashar, Nair, Krishna, Prasad Ts, et al., 2014).

The use of SWATH-MS in the quantification of vitreous proteins greatly enhanced the capabilities of detection and repeatability of protein detection, including those lower abundant proteins, enhancing the ability the search for differentially expressed proteins (S. W. Shan et al., 2018). SWATH-MS was able to acquire more than 92% of the proteins across all the sample injections compared to traditional DIA-based proteomics, where only 29% of proteins were found across all the samples. SWATH-MS was not only able to acquire the overlapped proteins found from IDA, but also an addition of an extra 70% of proteins were quantifiable across all time points, or else would be missed in the conventional data-dependent acquisition. This illustrated that it is more favorable to use SWATH-MS in chick vitreous compared to the traditional IDA method as it provided a larger pool of vitreous protein ID candidates to be quantified. In addition to the proteins acquired

from IDA, SWATH-MS was able to pick up x2.5 more (77% extra) proteins within the vitreous proteome. This greatly enhanced the chances for the detection of desired proteins as the available proteins to be compared will be much larger. Using the strict filter criteria mentioned, the number of DEPs was similar in the first two time points (D14 and D21), but the number increased by 2 folds in the last time point (D28/7). This was expected as the changes physically were also the greatest at the near end of the holding period. This, however, the degree of FC was the greatest at the first time point (D14/ D7) to further narrow down the proteins for normal growth/ emmetropization specific proteins.

Alpha-fetoprotein protein (AFP) is one of the earliest serum glycoproteins which is synthesized by the liver, and it is found in the fetal yolk sac, cerebrospinal fluid, amniotic fluid, vitreous body (Adinolfi et al., 1975) during embryo and fetal development and rapidly declines as it reaches adulthood at around (<10ng/mL) in human (Ball et al., 1992). It was found to be the early form of albumin (Taketa, 1990) as it has a similar molecular weight and structure to albumin and α 1-globulin and slowly diminishes as it matures. It carries multiple functions, such as binding to fatty acids and bilirubin for a transportation role during early development phases (Gillespie & Uversky, 2000). It has been identified in human fetal vitreous peaking at week 17 and slowly declines towards 24 weeks of age (Panova et al., 2011). Also, AFP levels rise rapidly during fetal life and drop shortly after birth across species such as rats (Nayak & Mital, 1977; Sell & Becker, 1978).

Cadherin superfamily group CDH4, CDH7, CDH8, CDH10, CDH11, CDH20, and CDH22 were all downregulated from SWATH-MS in all the time points and two (**CDH7 and CDH10**) were successfully confirmed using MRM^{HR} (which will be discussed in Chapter 7). Cadherins are cell surface adhesion glycoproteins that play a major role in the development of tissue and organs (Niessen et al., 2011). They are Ca⁺ dependent trans-membrane structural proteins with the main function of cell-cell adhesion during cellular growth, cell polarization, and differentiation (Halbleib & Nelson, 2006). As a structural protein, cadherin is vital in maintaining cells' integrity. In the vitreous, it localizes to focal adhesions and promotes adhesion to fibronectin which is presented all over the vitreous to provide structural support. CDH10 and CDH7 are type II classical cadherin of the cadherin superfamily which

are usually found in specific brain regions or circuits such as cerebellar, retinal, and hippocampal circuits. Cadherin-10 was discovered in restricted brain regions and neural retinas (Liu et al., 2006). CDH10 expression level was found to be increased in the embryonic nervous system of embryonic zebrafish (Liu et al., 2006) and chicken brain (Fushimi et al., 1997), whereas Cadherin-7 is encoded from the CDH7 gene found in the development of the vertebrate nervous system and expressed in the early phase of cranial motoneuron development (during axon extension)(Barnes et al., 2010).

Contactin-2 (TAG-1/ CNTN2) is a neural cell adhesion molecule that belongs to the immunoglobulin superfamily (IgSF), having six immunoglobulin-like domains and four fibronectin repeats (Furley et al., 1990; Karagogeos et al., 1991). It plays a key role in axon extension, growth cone guidance, and myelination during development (Baeriswyl & Stoeckli, 2008; Wolman et al., 2008). It helps to form axon connections in developing nervous systems by guiding development on the axon surface during the fetal period (Furley et al., 1990). It has a high affinity to neural cell adhesion molecule (NCAM), acting as a neural cell adhesion molecule ligand for binding to neurocan for cell-cell interactions during nervous tissue histogenesis in chicken (Milev et al., 1996).

Neurocan core protein (NCAM) is a brain chondroitin sulfate proteoglycan (CSPG) that is synthesized by neurons (Engel et al., 1996). Other members include aggrecan, versican, and brevican (Rauch et al., 1992) have a function on cell-cell interactions and nervous tissue histogenesis. Being a member of the lectican family, it bears the ability of hyaluronan binding. Neurocan is one of the most abundant CSPGs during brain development, with its structural and function mainly in the role of neuron guidance and modulation of cell adhesion/ migration during normal development (Margolis et al., 1996; Oohira et al., 2000; Rauch et al., 1991). It has been reported that neurocan detection can be found in the retinal layers of the embryonic rat retina but not in later stages (Aquino et al., 1984; Inatani et al., 1999). Neurocan was also detected in rat brains peaking at late embryogenesis but was found slowly decreases after the first month of birth (Meyer-Puttlitz et al., 1996) as the possible proteolytic processing of neurocan might occur, reducing its level.

Reelin (RELN) is a bulky extracellular glycoprotein expressed highly in the brain for neural cell positioning, neuronal migration (D'Arcangelo, 2014), growth cone

guidance (Leemhuis et al., 2010), and synaptic plasticity (Weeber et al., 2002). It can regulate microtubule functions and neuronal migration during the development of the brain by binding to the ApoER2 receptor (Hiesberger et al., 1999). Reelin is essential for the normal development of cortical, hippocampal, and cerebellar neuronal lamination (Frotscher, 2010). It binds to its receptors apolipoprotein E receptor 2 (ApoER2) and very-low-density lipoprotein receptor (VLDLR), resulting in the Src family tyrosine kinase (SFK)-mediated tyrosine phosphorylation of disabled-1 (Dab 1) in the reelin signaling pathway (Hiesberger et al., 1999). It has been shown in hepatocellular carcinoma (HCC) that reelin and TGF- β 1 had an opposite expression pattern of each other, where TGF- β 1 may function upstream of reelin (Luo et al., 2019).

Ovotransferrin (TF) is part of the transferrin family which are iron-binding glycoproteins (Williams, 1968) mainly for iron metabolism in tissues by transferring ferric ions. It has been suggested that it has an anti-oxidative (Moon et al., 2015) effect. Up-regulation of ovotransferrin could suggest that there might be oxidative stress during the elongation of the eyeball. The ovotransferrin gene and protein from choroid could be a regulator of myopic eye growth (Rada et al., 2001), where an increase in mRNA level in recovering retina/PRE/choroid FDM model. The up-regulation of Ovotransferrin was also found in chick vitreous after LIM treatment (Yu et al., 2017), further suggesting that this could be an early biomarker during axial elongation in emmetropization and myopia progression.

Although the changes of these proteins were not previously reported in the developmental process in the vitreous, similar changes in the expressions of these proteins during tissue development from other studies have suggested potential roles of these MS-confirmed molecules involved in emmetropization eye growth. Apart from proteins responsible for structural properties, the identified proteins also included several neuronal-specific proteins, further suggesting that the vitreous could serve as a compartment for biofluid leakages from surrounding locations such as the retina and brain. Our results supported the hypothesis that the vitreous is a potential collecting or diagnostic site for neuron-related proteins. As the vitreous are easily extracted in routine vitrectomy, it might offer an alternative substance to brain-related diseases diagnostic. The downregulation of these cell-cell adhesion

proteins might suggest an elongation and stretching of the vitreous gel structure, or once the axon growth is finished, these structural proteins are no longer needed. Reelin functions downstream of TGF- β 1, an opposite expression might indicate the increased level of TGF- β 1 where TGF- β 1 is associated with myopia in the remodeling of sclera during myopia development (Jobling et al., 2009; McBrien, 2013; Schippert et al., 2006). All these changes in proteins further showed that the vitreous is not just a clear, transparent gel tissue just offering structure stability, but it is also shown to have a dynamic exchange of proteins within this material, expanding its potential as a tissue for reporting the ocular condition. One of the potential weaknesses of this study is the pooling of chick vitreous, as this study will be most likely to underestimate the actual changes found during the conditions. However, this issue was adjusted by using a strict filter applied in this study where the fold change must be in the same direction and pass the cut-off.

5.5 Conclusion

This is the first study investigating the proteomic changes in chick vitreous during normal growth using next-generation mass spectrometry techniques (SWATH-MS). This study provided a comprehensive spectral library of chick vitreous during normal growth, serving as the foundation for future proteomic studies on the chick SWATH-MS allowing a more in-depth identification and quantification of vitreous proteins, greatly enhancing the chances of detection of differentially expressed proteins. The comprehensive proteome acquired from this study further refines the knowledge of the small portion of proteins within the vitreous, even though it is known to be mainly composed of water. This allowed a better understanding of the mechanism of myopia formation or progression. Quantitative proteomics of the vitreous during various time points in the immortalization period unraveled growth-related structural proteins such as cadherins and contactins that could contribute to the elongation of the eyeball, which warrants further study.

Chapter 6. Vitreous: Myopia study – Lens Induced Myopia (LIM)

6.1 Introduction

Published proteomics research explicitly looking into myopia using the vitreous is still scarce as the diluted nature of the vitreous (99% water) made it more difficult for low-abundance proteins to be detected. Early vitreous proteomics studies were hampered by the low detection of proteins and technical limitations such as silver-staining as well as overexposure of highly abundant proteins such as albumin (García-Ramírez et al., 2007; Kim et al., 2007; Yamane et al., 2003). While our group was among the first to study myopia progressing within the chick vitreous (Yu et al., 2017), the slower rate and sensitivity of the machines in the gel-based approach hampered the number of proteins that could be identified (358 proteins in Day 3 and 339 proteins in Day 7) and quantified (4 proteins were found DEPs in LIM vitreous). A different experimental design using bi-directional -10D and +10D lens on the same chick was adopted to exaggerate the difference as the magnitude of DEPs in response to defocus signals has shown to be relatively small (Lam et al., 2007; Wu et al., 2014).

With the help of a more robust and sensitive DIA- based method (SWATH-MS), DEPs were identified and quantified in this study, with a study design with individual samples comparing LIM and its controlled eye, which can reflect the actual dynamic protein expressions under myopia condition. With SWATH-MS data acquisition, a LIM-specific vitreous proteome will be established for detecting specific proteins involved in the myopic compensated eye growth. Previous studies in this thesis have demonstrated a feasible vitreous proteomic workflow and the identification of regulated protein biomarkers from a comprehensive proteome during emmetropization with SWATH quantitation. Lens-induced myopia (LIM) chick vitreous proteome reference database can then be constructed with further technological advances using high-pH fractionation and a shorter MS gradient. This study aims to compare the differential protein expressions during LIM at two different time points, the early stage (LIM3: 3 days LIM) and the later stage (LIM7:

7 days LIM), using this newly established reference proteome for a better understanding of the mechanism for myopia in the vitreous.

6.2 Methods and materials

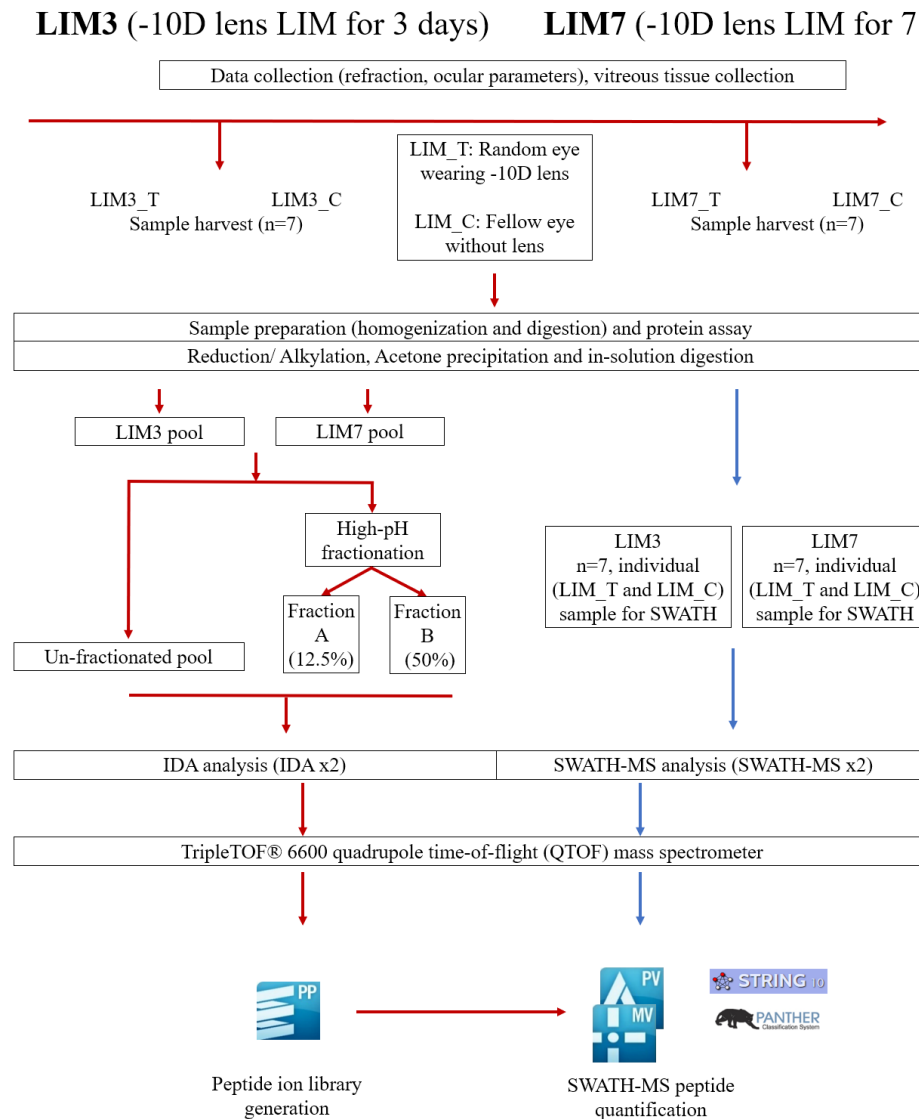


Figure 6.1 Schematic workflow of quantitative discovery proteomics in myopic lens-induced (LIM_T) eyes vs control eyes (LIM_C). Seven vitreous lysates from 7 chicks (7 treated and 7 control eyes) were included. Three micrograms of sample digest from individual samples from both groups (LIM3 and LIM7) were subjected to high-pH fractionation, and 5 µg remained as the unfractionated pool. The three pools (LIM3, LIM7, and unfractionated pool) were injected into the MS with two technical replicates

to establish the proteome library under IDA. One microgram of digested proteins from each individual sample in two technical replicates was analyzed under SWATH-MS mode. Protein identification was performed using ProteinPilot, and quantification with PeakView and MarkerView software. Identified proteins were then analyzed further with online bioinformatic analysis tools.

Housing of chickens

White Leghorn chicks (n= 7) at each time point (LIM3: LIM for 3 days and LIM7: LIM for 7 days) were raised in-house under the conditions shown in Chapter 2.1.2, and the workflow of this chapter is shown in Figure 6.1. Baseline ocular measurements such as refractive and ocular parameters by A-scan were done on day 7 after hatching. Straight after the measurements, a -10D lens was attached to a random eye of the chick while the other eye was left untouched (shown in Chapter 2.1.3). Vitreous samples were then collected and prepared according to the procedures established in Chapters 2.1.4 and 2.2.

High-pH fractionation for generating an ion library

Three micrograms of sample digest (from individual treatment and control samples) were pooled and underwent high-pH fractionation using the same method stated in the methods section (Chapter 2.2.8) for each LIM3 and LIM7 group. Of the pooled peptides, five micrograms remained as an unfractionated pool while 20 µg (for each LIM group) were subjected to an offline fractionation using the high-pH reversed-phase peptide fractionation kit (Cat# 84868, Thermo Fisher Scientific, USA) according to the manufacturer's protocol. In brief, two high-pH solution fractions, Fraction A (FRACT A): 12.5% ACN in 0.1% TEA and fraction B (FRACT B): 50% ACN in 0.1% TEA, were prepared and used to elute the peptides. After column conditioning using ACN and 0.1% TFA, the digested peptides were then loaded onto the resin bed. Fraction A buffer was loaded to the column and centrifuged at 3000 x g for 2 mins. The elution was then collected as Fraction A elution. Secondly, Fraction B buffer was added to the same column and centrifuged at 3000 x g for 2 mins, resulting in FRACT B elution. Fraction A and B elutions (of respective LIM3 and LIM7 groups) were then dried and resuspended in 0.1% FA to 0.2 µg/µl for

MS injection. One microgram of digested (in duplicate runs) was injected under IDA mode for the generation of a combined vitreous protein library.

LC-MS/MS setting

The LC-MS running conditions (IDA and SWATH) used in this study are shown in Chapter 2.3.1 with the short 90 mins gradient settings. One microgram of each vitreous digest sample was loaded onto the MS under SWATH-MS mode (in duplicates), and the MS Data analysis used can be found in Chapter 2.3.2. For ion library generation, two technical replicates of all fractionated parts (Fraction A and B) and Pool samples for the two time points (LIM3 and LIM7) were loaded onto ProteinPilot and searched against Uniprot database (Gallys_240419_UN+rev+ISO (42584).fasta).

6.3 Results

Changes in ocular parameters for lens-induced 3 days (LIM3) and 7 days (LIM7)

The relative changes in refractive errors at the two treatment time points are shown in Figure 6.2, and the raw data can be found in Appendix 6. Compared to the baseline (post hatched 7 days), after 3 days -10D LIM treatment, the change in refraction was -7.92 ± 2.2 D on the LIM-treated eyes (LIM3_T) and -0.61 ± 0.92 D on the control eyes (LIM3_C) respectively at LIM3. For LIM7, higher myopia was found in the treated eyes (LIM7_T) (-11.61 ± 0.90 D) than in the control eyes (LIM7_C) (-0.46 ± 0.96 D). The changes were highly significant at both time points ($P < 0.01$, unpaired T-test).

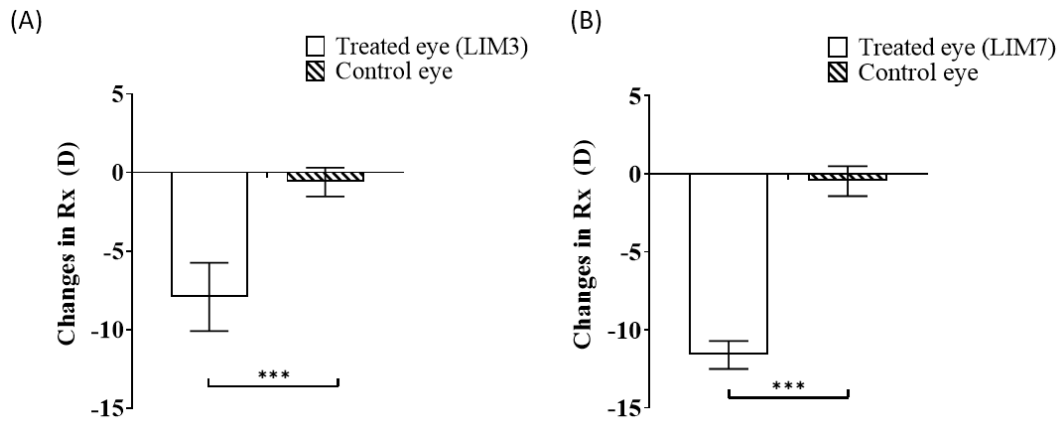


Figure 6.2 Average changes of refractive error during (A) -10D LIM for 3 days and (B) -10D LIM for 7 days compared to the control eyes (n= 7 at each time points, *p ≤ 0.05, **P ≤ =0.01 *p ≤ =0.001, unpaired T-test. Error bars= Mean ±SD).**

For LIM3, there were significant differences in all the ocular parameters, with the VCD (LIM3_T: 0.303 ± 0.106 mm; LIM3_C: -0.065 ± 0.069 mm) being the main contributor to the overall elongation in AXL (LIM3_T: 0.424 ± 0.109 mm; LIM3_C: 0.053 ± 0.07 mm) ($P < 0.01$, unpaired T-test) (Figure 6.3 A). Also, there was significant thinning in the retina thickness (LIM3_T: -31.633 ± 18.060 μ m, LIM3_C: -5.606 ± 10.068 μ m) and choroidal thickness (LIM3_T: -46.845 ± 55.075 μ m, LIM3_C: 28.869 ± 24.145 μ m), where else the sclera thickness remained similar (Figure 6.3 B). In terms of LIM7, significant changes were observed in ACD, VCD, and AXL only, with the VCD (LIM7_T: 0.751 ± 0.135 mm, LIM7_C: 0.245 ± 0.066 mm) being the main contributor to the overall changes in AXL (LIM7_T: 1.205 ± 0.116 mm, LIM7_C: 0.621 ± 0.083 mm) ($P < 0.01$, unpaired T-test) (Figure 6.3 C). However, the overall magnitude of change was larger in LIM7 than in LIM3. None of the posterior tissues showed a significant difference in thickness between the treated and control eyes (Figure 6.3 D).

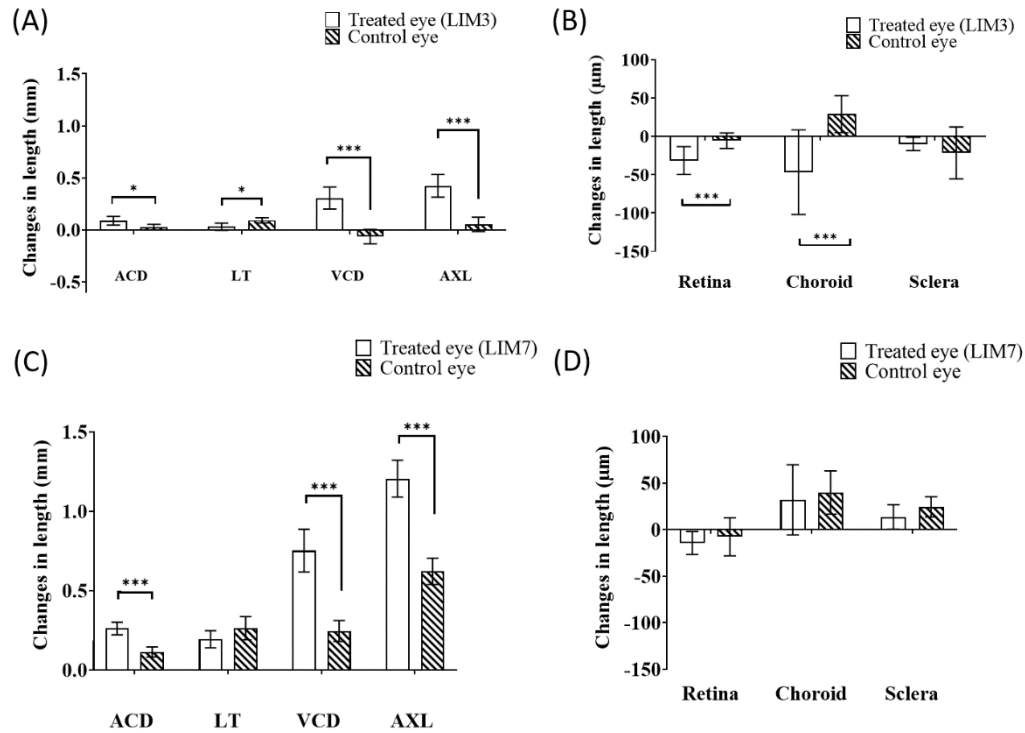


Figure 6.3 Average changes of ocular components during (A & B) -10D LIM for 3 days and (C & D) -10D for 7 days compared to the control eyes. ACD: anterior chamber depth, LT: lens thickness, VCD: vitreous chamber depth, AXL: from the front of the cornea to the front of the retina (n= 7 at each time point. *p ≤ 0.05, **P ≤ 0.01 *p ≤ 0.001, unpaired T-test, Error bars= Mean ±SD).**

Protein concentration

The protein concentration was determined using the rapid gold BCA protein assay (Figure 6.4). There was no significant difference in protein concentration between the treated eye (both LIM3 and LIM7) compared to its respective control group for both LIM3 and LIM7. The average protein concentrations for LIM3_T and LIM3_C were $0.172 \pm 0.021 \mu\text{g}/\mu\text{l}$ and $0.199 \pm 0.067 \mu\text{g}/\mu\text{l}$, respectively. For LIM7, the average protein concentrations for the LIM7_T group and LIM7_C were $0.165 \pm 0.024 \mu\text{g}/\mu\text{l}$ and $0.178 \pm 0.0156 \mu\text{g}/\mu\text{l}$, respectively.

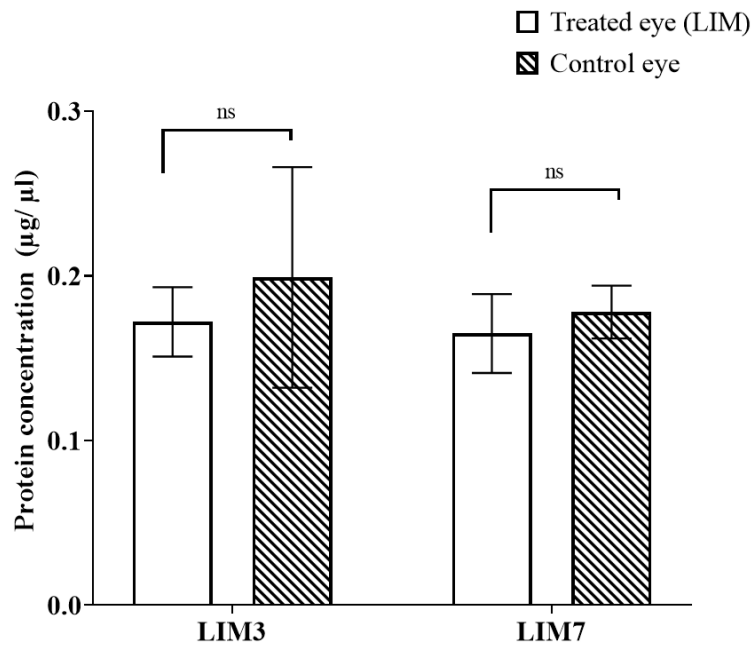


Figure 6.4 Protein concentration of chick vitreous in 1:1 T-PER buffer ratio for (A) -10D LIM 3 days and (B) -10D 7 days between the treated and control eyes. (n= 7 at each time points, ns= not significant, unpaired T-test, Error bars= Mean \pm SD).

Generation of LIM vitreous protein ion library

A global proteome profiling of LIM chick vitreous samples from a total of 28 eyes (n= 7 from LIM3 and LIM7) using label-free SWATH-MS quantitative proteomics was analyzed. The SWATH-MS workflow relies on a reference protein library consisting of sample-specific proteins within the desired condition for extensive peptide detection. Fractionated samples from both groups (LIM3 and LIM7) were loaded into the MS to generate a LIM chick vitreous specific spectral library under IDA mode. A spectra library of 15181 peptides from 28 samples, corresponding to 1333453 identified spectra, were matched into 1242 proteins at 1% FDR. All raw data generated from Information-dependent acquisition (IDA) and SWATH acquisitions (DIA) were accepted and published in the Peptide Atlas public repository (<http://www.peptideatlas.org/PASS/PASS01366>).

SWATH-MS based quantitative analysis of LIM studies

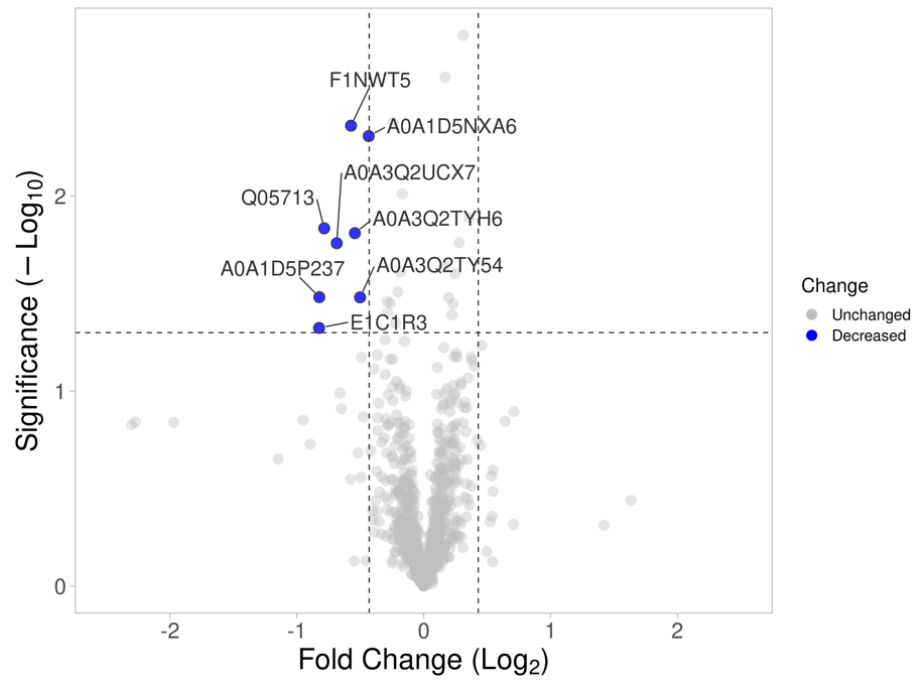
Out of the 1242 proteins, 1046 proteins (84% of the library) and 1051 proteins (85% of the library) were successfully mapped and quantified in the LIM3 group and

LIM7 group at 1% FDR using SWATH-MS, respectively. Proteins that have less than 1 peptide were removed to reduce the chances of false-positive results, and the filter for differential expressed proteins was considered at fold change (FC) cut off ≥ 1.5 or ≤ 0.7 and $p \leq 0.05$, unpaired T-test. After three days (LIM3) of -10D lens wear, 8 down-regulated proteins were found (shown in table 6.1) compared to the LIM3_C group. Figure 6.5 A and B show the volcano plot and heatmap illustrating the distribution and the high level of similarity between replicates within each group of the 1242 proteins in our LIM3 dataset. Volcano plots were drawn using VolcanoR using the R program (Goedhart & Luijsterburg, 2020). All DEPs were submitted to draw clustered heatmaps using the HeatmapMaker in R program (Juan Pablo Carreón Hidalgo). The expression level for each protein was calculated using the formula: [(total area of each protein) – mean/ SD]. Dark red indicates a more positive value (i.e., up-regulated proteins), and yellow indicates a more negative value (i.e., down-regulated proteins).

Table 6.1 DEPs found in LIM3 using SWATH-MS, n= 7, unpaired T-test, FC cut off ≥ 1.5 or ≤ 0.7 and $p \leq 0.05$. Blue: down-regulated proteins.

Uniprot ID	Protein name	Gene name	SWATH-MS Fold change (FC, LIM3_T/ LIM3_C)	P-Value
A0A1D5NXA6	Inter-alpha-trypsin inhibitor heavy chain 3	ITIH3	0.74	0.005
A0A1D5P237	Secreted frizzled related protein 4	SFRP4	0.57	0.033
A0A3Q2TY54	PLD phosphodiesterase domain-containing protein	N/A	0.71	0.033
A0A3Q2TYH6	Ig-like domain-containing protein	N/A	0.69	0.015
A0A3Q2UCX7	Otospiralin	OTOS	0.62	0.017
E1C1R3	Corticotropin-releasing factor-binding protein	CRHBP	0.56	0.047
F1NWT5	Vasoactive intestinal peptide	VIP	0.67	0.004
Q05713	Alpha-crystallin B chain	CRYAB	0.58	0.015

(A)



(B)

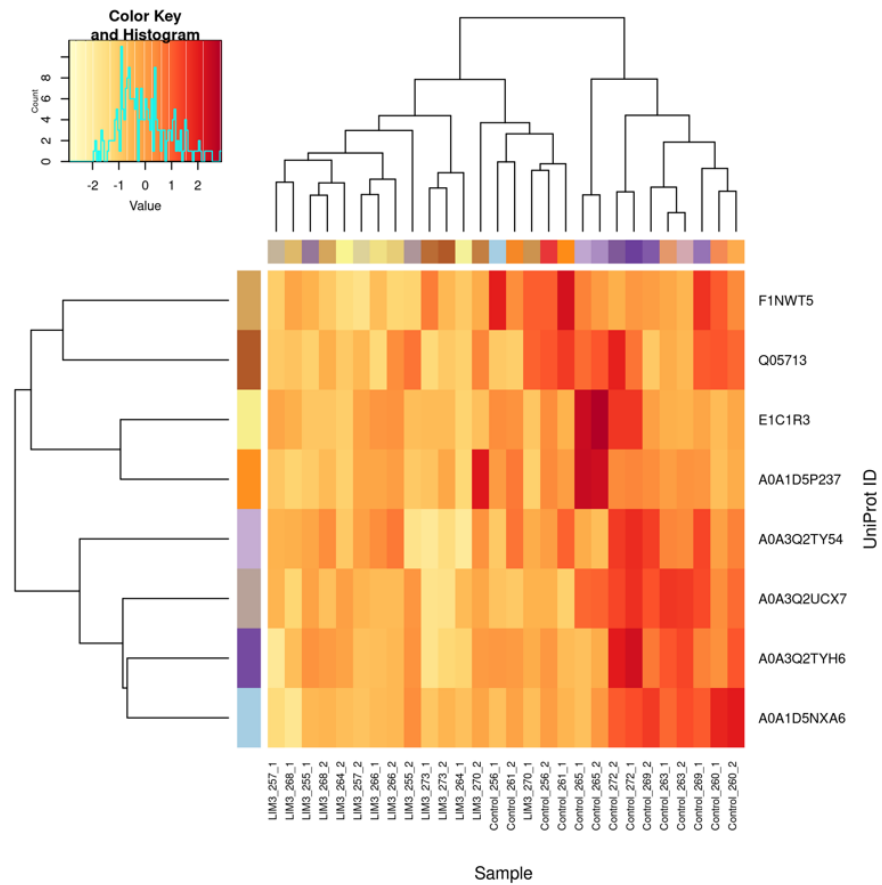


Figure 6.5 (A) Volcano plot displaying the statistical p-value with the magnitude of fold change between lens-induced myopia for 3 days (LIM3) vs.

fellow eye control. The non-axial vertical dashed lines denote a fold change, of $\pm 0.58 \text{ Log}_2$ unit (i.e., ± 1.5 fold change) whereas the non-axial horizontal dashed line denotes $1.30 -\text{Log}_{10}$ p-value (i.e., $p = 0.05$), which is the significance threshold prior to logarithmic transformation. A total of 8 DEPs out of 1242 proteins were found to be differentially expressed (Blue: down-regulated). (B) Heatmap showing DEPs in LIM3 study. Dark red indicates a more positive value (i.e., up-regulated proteins), and yellow indicates a more negative value (i.e., down-regulated proteins).

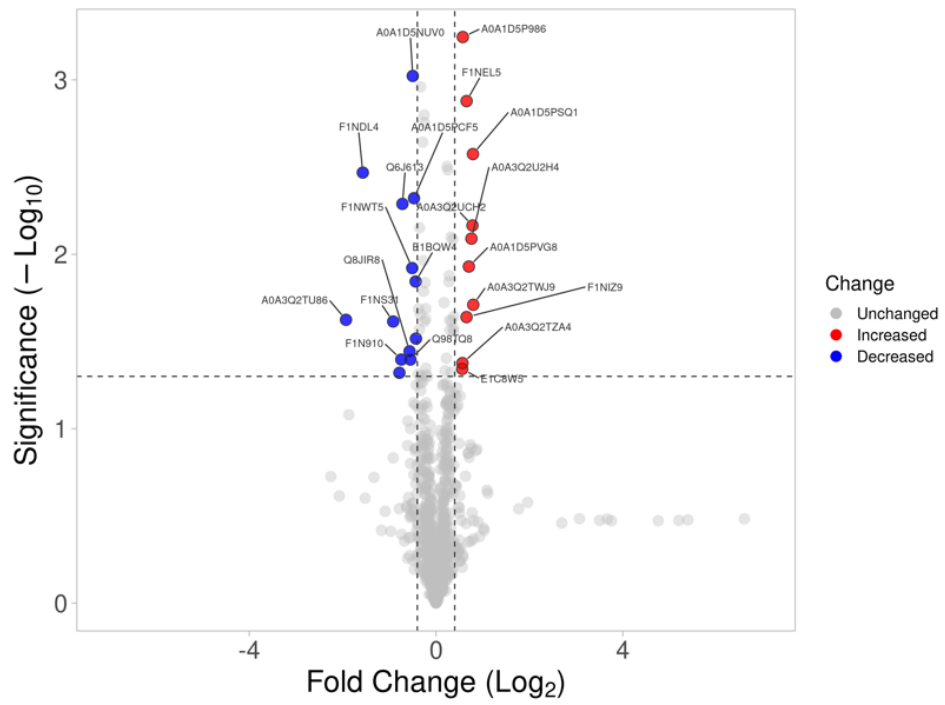
For LIM7, 10 up-regulated and 13 down-regulated proteins were found (shown in table 6.2) compared to LIM7_C. Figure 6.6 A and B show the volcano plot and heatmap illustrating the distribution and the high level of similarity between replicates within each group of the 1242 proteins in our LIM7 dataset. Only 1 protein (vasoactive intestinal peptide, VIP) was found in both time points: LIM3 (FC= 0.67, P= 0.017) and LIM7 (FC= 0.70, P= 0.012) compared to its control counter group, with the same down-regulation direction where a lesser extent of FC was found in LIM7.

Table 6.2 DEPs found in LIM7 using SWATH-MS, n= 7, unpaired T-test, FC cut off ≥ 1.5 or ≤ 0.7 and $p \leq 0.05$. Red: up-regulated proteins, Blue: down-regulated proteins.

Uniprot ID	Protein name	Gene name	Fold change (FC: LIM7_T/ LIM7_C)	P-Value
A0A1D5P986	Lipase G, endothelial type	LIPG	1.49	0.001
A0A1D5PSQ1	Alpha-2-macroglobulin	N/A	1.73	0.003
A0A1D5PVG8	Lysosomal Pro-X carboxypeptidase	PRCP	1.63	0.012
A0A3Q2TWJ9	MG2 domain-containing protein	N/A	1.74	0.019
A0A3Q2TZA4	A2M_recep domain-containing protein	N/A	1.48	0.042
A0A3Q2U2H4	Alpha-2-macroglobulin	N/A	1.69	0.008

A0A3Q2UCH2	A2M domain-containing protein	N/A	1.72	0.007
E1C8W5	Carbohydrate sulfotransferase 15	CHST15	1.48	0.045
F1NEL5	Alpha-1,6-mannosylglycoprotein 6-beta-N-acetylglucosaminyltransferase A	MGAT5	1.57	0.001
F1NIZ9	Sema domain-containing protein	SEMA7A	1.57	0.023
A0A1D5NUV0	Secretogranin-2	SCG2	0.71	0.001
A0A1D5PCF5	Insulin-like growth factor-binding protein 7	IGFBP7	0.72	0.005
A0A1D5PLR0	Seizure 6-like protein	SEZ6L	0.74	0.030
A0A3Q2TU86	Trans-golgi network protein 2	TGOLN2	0.26	0.024
E1BQW4	EGF like, fibronectin type III and laminin G domains	EGFLAM	0.74	0.014
E1BTQ4	Avidin	AVDL	0.58	0.048
F1N910	Nucleoside diphosphate kinase	NME1	0.60	0.040
F1NDL4	Nidogen-2	NID2	0.34	0.003
F1NS31	Low-density lipoprotein receptor-related protein 8	LRP8	0.53	0.024
F1NWT5	VIP peptides	VIP	0.70	0.012
Q6J613	Invariant chain isoform p41	Ii CD74	0.61	0.005
Q8JIR8	Interphotoreceptor matrix proteoglycan 1	IMPG1 SPACR	0.68	0.036
Q98TQ8	Connective tissue growth factor	CTGF	0.68	0.040

(A)



(B)

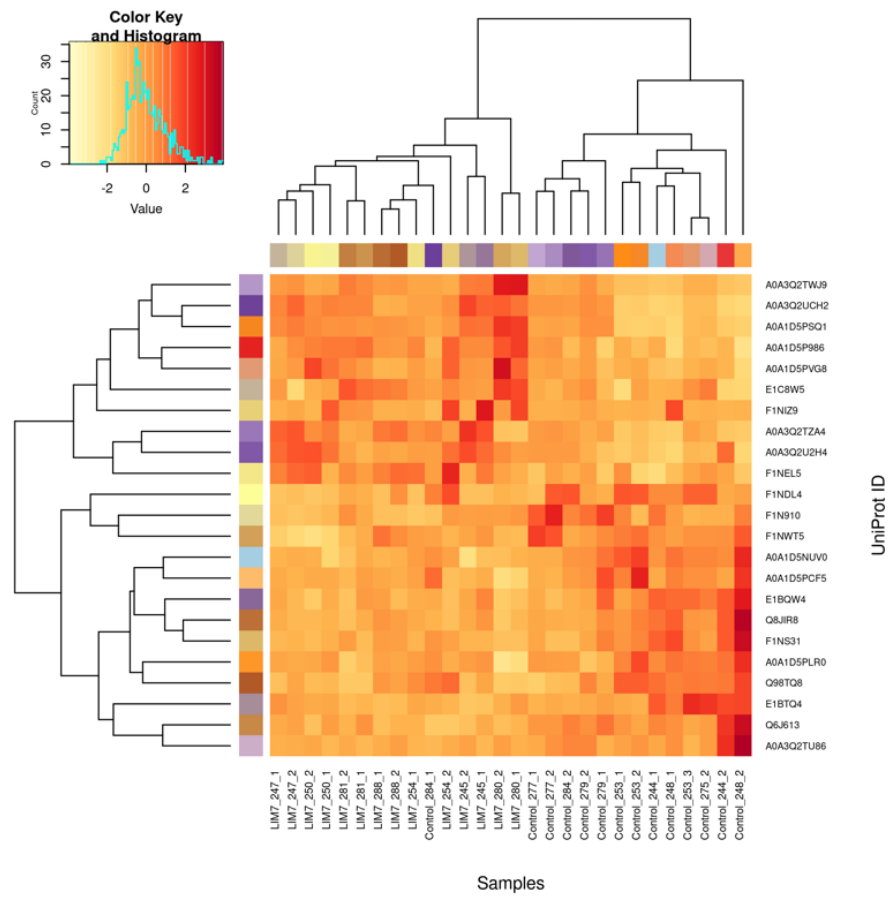


Figure 6.6 (A) Volcano plot displaying the statistical p-value with the magnitude of fold change between lens-induced myopia for 7 days (LIM7) vs. fellow eye control. The non-axial vertical dashed lines denote a fold change of $\pm 0.58 \text{ Log}_2$ unit (i.e., ± 1.5 fold change), whereas the non-axial horizontal dashed line denotes $1.30 -\text{Log}_{10}$ p-value (i.e., $p = 0.05$), which is the significance threshold prior to logarithmic transformation. A total of 23 DEPs out of 1242 proteins were found to be differentially expressed (Blue: down-regulated). (B) Heatmap showing DEPs in LIM7 study. Dark red indicates a more positive value (i.e., up-regulated proteins) and yellow indicates a more negative value (i.e., down-regulated proteins).

6.4 Discussion

The chick model was one of the earliest and the most mature myopia animal models as the eye growth and refractive development can be easily modulated (Schaeffel & Howland, 1991; Wallman et al., 1981). Attributes like the rapid growth rate, ease of breeding, and relatively large eyeball size made it a popular and extensively used model in ocular research (Troilo et al., 2019; Waldvogel, 1990). In the LIM model, the eyes of chicks wearing -10D lenses could adapt to the lens power and elongate to compensate for the induced power (Irving et al., 1992; Schaeffel et al., 1988). In this study, the overall refractive error measured and ocular components elongation in terms of overall axial length (mainly contributed by the VCD) were similar to previously published studies (Irving et al., 1992; Yu et al., 2017) using the chick LIM animal model, where 7 days of -10D lens introduced a much more significant difference compared to controlled eyes showing compensation to the lens power.

The change in choroidal thickness is one of the indications of the myopia model as studies have shown that choroidal thickness becomes thinner in myopic eyes compared to normal eyes cross-species such as marmosets (Troilo et al., 2000), chick (Wallman et al., 1995) and guinea pig (Howlett & McFadden, 2009). This change was also observed in this study with the changes in LIM3 being more noticeable than in LIM7 as it is a rapid process where the difference in choroidal

thickness feedback mechanism can be as fast as 1 hour (Hammond et al., 2013; Kee et al., 2001) with the rate slowing down the longer the treatment time and its effect wearing off after lens wear for 2 days (Hammond et al., 2013).

Since the VCD elongation is the main contributor to LIM eyes (Pickett-Seltner et al., 1988; Wallman & Adams, 1987), the vitreous volume also increased slightly (Seltner & Sivak, 1987). Although there were no significant differences found in the total protein concentration (μg) in both groups (LIM3 and LIM7), using the 1:1 sample volume to lysis buffer ratio, the protein concentration after homogenization had a slight trend to be lower in LIM eyes in comparison to controlled eyes in both groups (although not significant). This observation was also reported by Pickett-Seltner's group using the chick model comparing myopic and non-myopic eyes of vitreous proteins on day 14 (Pickett-Seltner et al., 1992), indicating that the total amount of proteins inside the vitreous did not change significantly under myopia progression.

While the change in VCD is the primary indicator of LIM progression in many species, the protein changes within this tissue are rarely studied during this process. Mainly due to the highly hydrated nature of the tissue, which made it more difficult for sample preparation and protein analysis. This study provided a workflow for identifying 1242 proteins in the vitreous, which was not possible in previous studies as the vitreous is a highly hydrated tissue where 99% of it is water. The more robust and sensitive label-free approach (SWATH-MS) also allowed a more repeatable result across all the individual samples, LIM3: 1046 (84%) and LIM7: 1051 (85%), which was not possible before. The detection of DEPs from individual samples compared to the previous study's pooling approach better reflected more confident protein candidates involving myopia progression.

Protein quantitation in LIM3

Although no direct protein-protein interaction was found between the 8 DEPs in the LIM3 group using STRING analysis, most of these proteins are expressed in the extracellular matrix (ECM) apart from PLD phosphodiesterase domain-containing protein (FC: 0.71, $P= 0.005$) which can be found in the endomembrane system.

Proteins from the ECM have been shown to play a fundamental role in cell migration, metastasis, and differentiation, as well as providing physical effects on the support and structural protection and support of a tissue (Bissell et al., 1982). The change in expression of these ECM proteins might take a potential role in myopia progression since common complications such as liquefaction and posterior detachment of the vitreous from the extra elongation of the eyeball are common attributes in myopia progression.

Inter-Alpha-Trypsin Inhibitor Heavy Chain 3 (ITIH3, FC: 0.74, P= 0.005) is a protease inhibitor and a proteoglycan that interacts with hyaluronic acid (HA) by covalently binding to it and stabilizes the ECM (Bost et al., 1998; Lord et al., 2020). As the vitreous is mainly composed of HA, the down-regulation of this protein could result from dysfunction in the vitreous's structural integrity during myopia progression as the eyeball elongates abnormally. These ITI proteins have been reported in the central nervous system in human (Kim et al., 2020) and ovine (Spasova et al., 2014) as well as in the nerve fibers in mouse brain (Chan et al., 1995) further indicated that the possible movements of these proteins from the brain into the vitreous similar to results obtained from the emmetropization study (Chapter 5). Two other neuropeptides found differentiated in LIM3 were **Vasoactive intestinal peptide (VIP, FC: 0.67, P= 0.004)** and **Corticotropin-releasing factor-binding protein (CRHBP, FC: 0.56, P= 0.047)** which are both from the glucagon/ secretin family receptors which are involved in the G alpha (s) signaling events (Iwasaki et al., 2019). VIP is the only protein found differentially expressed in both time points (LIM3 and LIM7) and will be discussed further in this Chapter. CRHBP is a unique binding protein of corticotropin-releasing factor (CRH) which was first identified in human plasma (Orth & Mount, 1987). CRHBP is a secreted glycoprotein that binds to CRH, which is expressed in the liver, brain, and placenta (Westphal & Seasholtz, 2006). It is related to stress pathways that have a role in inhibiting CRF activation in stress response. As it has been demonstrated that CRF has the potential protective effect from oxidative stress via intracellular signal transduction network in human cells study (Lezoualc'h et al., 2000), the down-regulation of this protein could indicate that the level of CRF is

reduced hence limiting the ability to prevent damages such as cell apoptosis caused by the increase in oxidative stress during eye growth in myopia.

Protein quantitation in LIM7

Similar to the findings in the LIM3 study, most of the total 23 DEPs found in the LIM7 study were also ECM proteins. Since a number of these proteins were listed as uncharacterized proteins (generated from computer predicted-annotated database) due to limited studies in ocular proteins, the blast function from Uniprot ([https://www. Uniprot.org/blast/](https://www.Uniprot.org/blast/)) was further employed to in-silico breakdown the sequence and computerized to those proteins that are closely matched in sequence for homological protein prediction and characterization.

A number of these up-regulated proteins (LIM/ Control) were found to be related to inflammatory and immune responses, which will be discussed below: A family of five proteins showed to be the **α 2-macroglobulin (FC: 1.73 and 1.69, P= 0.003 and 0.008)** or its isoforms and structures, such as **α 2-macroglobulin domain-containing proteins (FC: 1.72, P= 0.007)**, **α 2-macroglobulin receptor domain-containing protein (FC: 1.48, P= 0.042)** and **MG2 domain-containing protein (FC: 1.74, P=0.019)**. α -macroglobulin (α M) family includes several protease inhibitors, and α 2-macroglobulin (A2M) is an acute-phase protein that is a significant component of the innate immune system, which is presented in plasma serum and cerebrospinal fluid (Armstrong & Quigley, 1999; Borth, 1992). The listed proteins within this family act as the inhibitor in fibrinolysis (Belch et al., 1984) and coagulation (Ignjatovic et al., 2011), preventing blood clotting in inflammation response. One possible reason for these proteins might be the extra elongation of the eyeball remodeling, triggering some degree of immune response.

Semaphorin 7A (SEMA7A, FC: 1.57, P= 0.023) is a protein with a family of neuronal guidance proteins (NGPs) that are responsible for neuronal growth and migration (Mirakaj et al., 2011; Wu et al., 2001). SEMA7A was to be involved in the initial phase of inflammation where it can induce cytokines production, such as in macrophages and monocytes, which are major components during the effector

phase of inflammatory immune response (Holmes et al., 2002; Suzuki et al., 2007). A recent study on human vitreous in rhegmatogenous retinal detachment and choroidal detachment using the proteomics approach (Luo et al., 2022) showed that SEMA7A was found up-regulated in diseased conditions compared to control subjects further supporting the role of this protein under myopia progression since retinal and choroidal detachment is a common clinical symptom of high myopia (Akiba, 1993; Williams & Hammond, 2019).

Furthermore, a study by Morote-Garcia et al. demonstrated the overexpression of hypoxia up-regulated protein-1 α (HIF-1 α) is associated with the induction of SEMA7A, terminating its regulation during hypoxia (Morote-Garcia et al., 2012). This is interesting as there is evidence that shows the possible role of HIF-1 α in sclera ECM remodeling during FDM myopia development in the murine model via the activation of eIF2- signaling and mTOR-signaling pathways (Wu et al., 2018). Further suggesting that is a possibility of a feedback mechanism with the exchange of proteins from different ocular tissues, such as the retina and sclera, leaking into the vitreous.

For down-regulated proteins, a number of these were shown to have a role in the insulin pathway and basal lamina-related structure functions, which will be discussed below:

It has been demonstrated that the insulin signaling pathway could be active during increased ocular growth in chickens where intravitreal insulin will stimulate axial growth under defocus retinal image conditions (Feldkaemper et al., 2009; Zhu & Wallman, 2009). It was also demonstrated that the elongation of the eyeball in humans under hyperinsulinemia (high peak of insulin) was a result of the increase in insulin-like growth factor-1 (IGF-1) (Galvis et al., 2016).

In this study, the down-regulation **Insulin-like growth factor-binding protein 7 (IGFBP7, FC: 0.72, P=0.005)** in vitreous could again reflect the possible protein changes from nearby tissues of the eyeball in response to the axial elongation in an

opposite manner. **Connective tissue growth factor (CTGF, FC: 0.68, P= 0.040)** is a protein that regulates ECM remodeling (Grotendorst, 1997), and it is presented in various ocular tissues, including cornea, choroid, and sclera (van Setten et al., 2016). A study by Ding et al. showed that the CTGF level was increased in high myopes with macular holes in the vitreous of human eyes (Ding et al., 2019), which was in the opposite direction compared to this study. One possible explanation could be that the control group used in their study was from patients with vitreomacular interface diseases (VID) as normal healthy vitreous were not obtainable in humans due to ethical reasons, where this study employs the fellow healthy eye as control subjects. Therefore, its role in myopia progression is still yet to be studied further.

EGF like, fibronectin type III and laminin G domains (EGFLAM, FC: 0.74, P= 0.014) and **nidogen-2 (NID2, FC: 0.34, P= 0.003)** are basal membrane proteins that are responsible for the structural remodeling including basal lamina proteins, fibronectin and laminin which are present in the human vitreous (Wei et al., 2017) and the brain (Kohfeldt et al., 1998; Thomsen et al., 2017). Similar to the results from LIM3, the down-regulation of these structural proteins could indicate a breakdown in the structure matrix of the vitreous due to the over elongation of the eyeball during myopia progression.

Vasoactive intestinal peptide (VIP) was found to be downregulated in both studies (LIM3-FC: 0.67, P= 0.004 and LIM7: FC: 0.70, P= 0.012) and it didn't have changes during normal growth in Chapter 5 indicates that it might be more specific to the involvement in myopia progression. This protein was also further confirmed using a more target-specific approach (MRM^{HR}) in the vitreous and qPCR in the retina using separate batches of animals which will be discussed in detail in the next Chapter.

VIP is a neuropeptide/ peptide hormone in the large glucagon/ secretin superfamily. It was originally isolated as a vasodilator peptide from the intestine playing a role in the gastrointestinal system. It can be found widely around the body, including the heart, small intestine, brain, kidneys, and lungs (Vaudry et al., 2009). It also acts as a neuromodulator/ neurotransmitter in the brain and eyes, showing its

neuroprotective effect in various neurological diseases such as Parkinson's disease, acute brain trauma, neuroinflammation, and cerebral ischemia (Passemar et al., 2011; Troger et al., 2007). Within the eye, VIP has been found localized in the ciliary body and retina of chickens rabbits (Larsson et al., 1976; Unger et al., 1981) as well as the ciliary muscle in the posterior of the uvea in cats (Uddman et al., 1980).

Secretin/ glucagon (ZENK, EGR-1) has been shown to be a STOP signal in the retina using mouse and chick models during myopia progression (Mathis & Schaeffel, 2007; Vessey et al., 2005). Early VIP- related myopia studies mostly employ the use of FDM in animal studies, where VIP level has been shown to have a positive relationship with the elongation of the vitreous chamber depth in lid fusion Juvenile primates (Stone et al., 1988; Tkatchenko et al., 2006). However, several studies showed that VIP in the gene level was downregulated in the retina of FDM chicks (McGlenn et al., 2007), LIM chicks (Shan et al., 2022), and the injection of VIP reduced the FDM progression in chicks (Basmak et al., 1997; Cakmak et al., 2017; Seltner & Stell, 1995), suggested there could be a species differ in how VIP reacts or express.

From our proteomics results, the down-regulation of VIP was greater in LIM3 compared to LIM7 could indicate an initial influx of VIP consumption at earlier stages of myopia progression, possibly from the retina as the eyeball is compensating for the -10D lens. The VIP level could slowly return as the eyeball elongation is adopted, although the FC difference was not great. Furthermore, our results from the VIP gene level in the retina expression using qPCR (detail methods shown in the next Chapter) showed that the VIP gene expression was not detected in the vitreous. At the same time, it was significantly reduced in LIM3 and LIM7 compared to its respective controlled groups, similar to our recently published study in LIM chicks (Shan et al., 2022). This indicated that VIP production might be halted in the retina under hyperopic defocus. VIP was kept at a low level during myopia progression. This reduced VIP expression at the gene level could reduce the production of VIP proteins, further resulting in the decrease of VIP proteins found in the vitreous. Since most of the studies involving the injection of VIP are

done on the FDM model, LIM models should be further explored in various species of myopia progression.

These DEPs found in both time points (LIM3 and LIM7) in the vitreous are mostly structurally related, and neuropeptides suggested that there might be a protein flux, either actively or passively. During the myopia progression, the vitreous could act as a temporary storage place for protein exchange towards neighboring ocular tissues. The lower number of DEPs in LIM3 could indicate there might be a delay in the molecule transfer process from expression changes from the retina or sclera remodeling, and the protein expression changes will start to arise in later time points (LIM7) as protein-protein interaction is a very dynamic process in biological tissues. The next chapter will attempt to validate these DEPs as potential myopia biomarkers in the vitreous.

6.5 Conclusion

This study demonstrated the feasibility of quantitative proteomics using a label-free proteomics approach (SWATH-MS) in the chick vitreous during myopia progression and the study of potential myopia-related DEPs during this period. In combination with high-pH fractionation, a total of 1242 proteins were identified at 1% FDR using the more robust and sensitive label-free DIA approach (SWATH-MS), which resulted in more than 3 times the amount we have identified from the previous study. A total of 32 DEPs from two time points (LIM3 and LIM7) compared to its fellow controlled eye using individual samples with -10D lens attached to one eye. A high % of proteins were quantified using SWATH-MS, LIM3: 1046 (84%), and LIM7: 1051 (85%), which greatly enhanced the chances of identifying DEPs compared to the previous study using the traditional gel-based proteomics approach.

A total of 8 proteins were found downregulated in LIM3 eyes compared to the paired control eyes, including ITIH3, VIP, and CRHBP, which corresponded to maintaining ECM structural integrity as well as in response to oxidative stress. For

the LIM7 group, 23 DEPs were found, and the A2M protein group and SEMA7A were up-regulated in inflammatory immune responses and their possible role in hypoxia via association with HIF-1 α . Like LIM3, structural remodeling proteins such as EGFLAM and NID2 could indicate a breakdown in the vitreous's structure matrix due to the eyeball's over-elongation during myopia progression. These DEPs suggested that the vitreous could be a compartment for temporal protein exchange. VIP was the only protein found down-regulated in both time points (LIM3 and LIM7) compared to its control group. The down-regulation of this protein could result from protein influx from neighboring ocular tissues from the myopia progress since the level of VIP in gene level was found to be increased in the retina (in the next Chapter).

Multiple earlier studies have shown that VIP has a role in myopia progression, but contradictory results, as well as the use of the FDM animal model, made it difficult for a more evident conclusion on its function. Therefore, further studies are required to confirm this protein and its role in the LIM model.

Chapter 7. Protein validation using High-resolution Multiple-reaction monitoring (MRM^{HR}) and quantitative PCR approach

7.1 Introduction

Label-free SWATH-MS quantitation technique allows us to identify and quantify potential protein candidates that were differentially expressed during biological events. Improving from the first-generation shotgun proteomics, such as spectra-based data processing for quantification (spectra counting), the DIA strategy in SWATH-MS offers extensive mapping and comparison of proteins across multiple biological samples from the built ion library. However, while having a more extensive list of identified proteins will be good for protein pathway data mining, the chance of false-positive during data processing can not be ignored whenever a fixed false discovery rate is defined in a large-scale MS profiling approach.

Typically, specific proteins of interest and their expression levels should be confirmed by an orthogonal technique to further increase the confidence or shortlist for future studies. Traditionally, standard techniques such as polymerase chain reaction (PCR), quantitative polymerase chain reaction (QPCR), and northern blot have been used extensively for validating the expression of the corresponding genes. In contrast, Western blot and enzyme-linked immunosorbent assay (ELISA) are used to validate the expression levels of targeted proteins. However, these approaches have different drawbacks, such as a large sample volume required, a slow throughput, and a high variation that could require a large sample size to archive a presentable result. Furthermore, the lack of suitable antibodies for different species (e.g., chicken) and the high cost prevented an effective quantification and confirmation of interested proteins using these approaches. The sample consumption is another factor that needs to be noticed as these techniques usually require a large amount of samples during each step for validation due to the sensitivity level, which is essential to vitreous-related studies due to its highly hydrated nature as well as its lower protein content.

Single/multiple-reaction monitoring (MRM) has been an emerging MS targeted proteomic quantitation approach for the validation of specific peptides while offering results with high sensitivity and specificity (Leigh Anderson & Christie L Hunter, 2006; Elliott et al., 2009; Gerber et al., 2003). Differ from traditional shotgun proteomics for profiling; the MRM approach targets specific peptides only by selecting the specific precursor mass of the known peptide for tandem MS/MS fragmentation allowing a list of specific peptides to be identified and quantified as long as suitable peptides of a protein are isolated (proteins of interest). While this system usually runs under microflow (with a larger sample amount required) as the size of the columns is usually larger with a higher flow rate, the relatively new high-resolution MRM (MRM^{HR}) with the Triple-TOF MS running under nanoflow (Which is similar to the SRM/MRM approach) was adopted in this study to further solidify our findings of SWATH results of differential expressed proteins found across the time points for the benefit of low peptide amount consumption (Peti et al., 2018). It is essential for vitreous sample studies while maintaining sensitivity (Schilling et al., 2015) since the peptide from an individual sample is very limited. Furthermore, qPCR studies on the vitreous and retina were also attempted to further solidify the findings from Chapter 6.

7.2 Methods and materials

Chick housing and sample collection

Separate batches of chicks were raised under the same condition mentioned in Chapter 2.1.2 for each group. Refractive error and ocular measurements were done to ensure the growth was similar to the results obtained from each study. For the normal growth study in Chapter 5, 4 animals were collected at each time point on day 7 and day 14. For the LIM study in Chapter 6, LIM3: Separate batches of chicks were raised for 7 days and LIM for 3 days (n= 5 for MRM^{HR} and n= 4 for qPCR) and LIM for 7 days (n= 6 for MRM^{HR} and n= 4 for qPCR) with -10D lens placed on a random eye while its fellow eye remained untouched.

The vitreous was collected following the same protocol mentioned in Chapter 3.1.2. And for the qPCR study, after the collection of the vitreous, the dissected eyeball

was placed into PBS and the retina optic nerve was removed using a cutter. The retina was then slowly separated away from the Retinal pigment epithelium (PRE) and was snap-frozen in liquid nitrogen for RNA extraction (which will be shown further down this section).

Workflow for MRM^{HR} validation

All groups of vitreous peptides were injected into a TripleTOF[®] 6600 quadrupole time-of-flight (QTOF) mass spectrometer (Sciex, USA) instrument fitted with an electrospray ionization operating in a positive-ion mode for validation. The MRM^{HR} running condition and calculation can be found in Chapter 2.3, and Glyceraldehyde 3-phosphate dehydrogenase (GAPDH) was used as the internal control for all the validation studies. In brief: Proteins of interest (DEPs from each study) were selected based on the results from SWATH-MS in each study. Then the whole sequence of these DEPs was in FASTA format acquired from Uniprot ([https://www. Uniprot.org/](https://www.Uniprot.org/)) and imported into the Skyline software Skyline (v20.2.0.286, MacCoss Lab, USA). Targeted peptides were then checked and extracted from an IDA database previously acquired just before each MRM^{HR} run by ProteinPilot (v5.0, Sciex, USA). Top-intensity product ions were selected with both b and y ions included, and the MRM^{HR} target list was then exported and loaded onto PeakView (v2.2, Sciex, USA). Equal amounts of peptides in treatment and control groups were injected into the TripleTOF[®] 6600 quadrupole time-of-flight (QTOF) mass spectrometer (Sciex, USA) for each experiment, with each individual sample running in duplicates. Lastly, the area of each transition was integrated and analyzed using MultiQuant (v3.0, Sciex, USA) for algorithm analysis.

For normalization, the three most abundant peptides (if possible) of GAPDH were selected in each experimental group and were used as the internal standard for MRM^{HR} validation experiments (Shown in Table 7.1). The FC of GAPDH was first calculated, and if no change was found between the treatment and control groups, the FC would be used to normalize all the samples within that experimental group.

Table 7.1 The peptides and transition identified and selected in GAPDH as the internal standard for the MRM^{HR} experiments (A) Normal growth study, (B) Myopia study (LIM3), and (C) Myopia study (LIM7).

(A)

Uniprot ID	Protein name	Gene name	Peptide sequence	Transitions
G3P	Glyceraldehyde 3-phosphate dehydrogenase	GAPDH	GAAQNIIPASTGAAK	+2y11, +2y10, +2b6
			VTPNVSVDLTC[CAM]R	+2y11, +2y8, +3y5
			LVSWYDNEFGYSNR	+2y12, +2y10, +2y9

(B)

Uniprot ID	Protein name	Gene name	Peptide sequence	Transitions
G3P	Glyceraldehyde 3-phosphate dehydrogenase	GAPDH	GAAQNIIPASTGAAK	+2y11, +2y10, +2b6
			LVSWYDNEFGYSNR	+2y12, +2y10, +2y9
			VVDLMVHMASK	+2y8, +2y11, +3y5

(C)

Uniprot ID	Protein name	Gene name	Peptide sequence	Transitions
G3P	Glyceraldehyde 3-phosphate dehydrogenase	GAPDH	GAAQNIIPASTGAAK	+2y10, +2y9, +2y8
			LTGMAFR	+2y6, +2y5, +2y3
			LVSWYDNEFGYSNR	+2y12, +2y10, +2y8

RNA isolation

Total RNA of chick vitreous and retina was extracted with TRIzol (Cat# 15596026, Thermo Fisher Scientific, USA). The quantity and quality of RNA were analyzed by NanoDrop ND 2000 (Thermo Fisher Scientific, USA). The purity of RNA was ensured to be within the range of 1.8 to 2.1 for the optical density ratio (OD 260/ OD 280).

Quantitative Real-Time PCR (RT- qPCR)

Equal amounts of cDNA were reversed-transcribed to cDNA using a High-Capacity cDNA reverse transcription kit (Cat# 4368814, Applied Biosystems,

USA). Sequences of qPCR primers (both forward and reverse) used are shown as follows: VIP (forward primer: ACGAGTTAGCTCCCAGGACA; reverse primer: CCTCGAAGTTTGGCTGGA) GAPDH (forward primer: GGGTGGTGTGCTAAGCGTGTTA; reverse primer: ACGCTGGGATGATGTTCTGG). Primers sequences used in this study were designed using Primer3 (v.0.4.0). A Total reaction of 10 μ l which consisted of 8.5 μ l of RT mix with 1.5 μ l of RNA (0.5 μ g/ μ l). Quantitative Polymerase chain reaction (qPCR) study was performed using LightCycler 480 SYBR green kit (Cat# 04707516001, Roche, Switzerland) with LightCycler 480 instrument (Roche, Switzerland). The thermal cycling settings were: 95 °C for 5 minutes, then amplification step, which included 95 °C for 30 sec, 61 °C for 30 sec, and 72 degrees for 30 sec for 45 cycles. Samples were run in replicates. Gene expression was calculated using the $\Delta\Delta$ Ct (Delta Delta Ct = cycle number at threshold) method, which normalized against the housekeeping gene GAPDH in all the samples. Data were analyzed using the LC480 software (v 1.5.1.62 SP3, Roche, Switzerland). Differential expression of the target gene was calculated and analyzed using an unpaired T-test.

7.3 Results

Internal standard

No significant difference in GAPDH expression was found using both SWATH and MRM^{HR} approaches (Table 7.2); therefore, GAPDH was used as the internal standard to normalize all the samples for each experiment for calculation.

Table 7.2 FC of GAPDH acquired from SWATH-MS compared to MRM^{HR} in their respective experiment study.

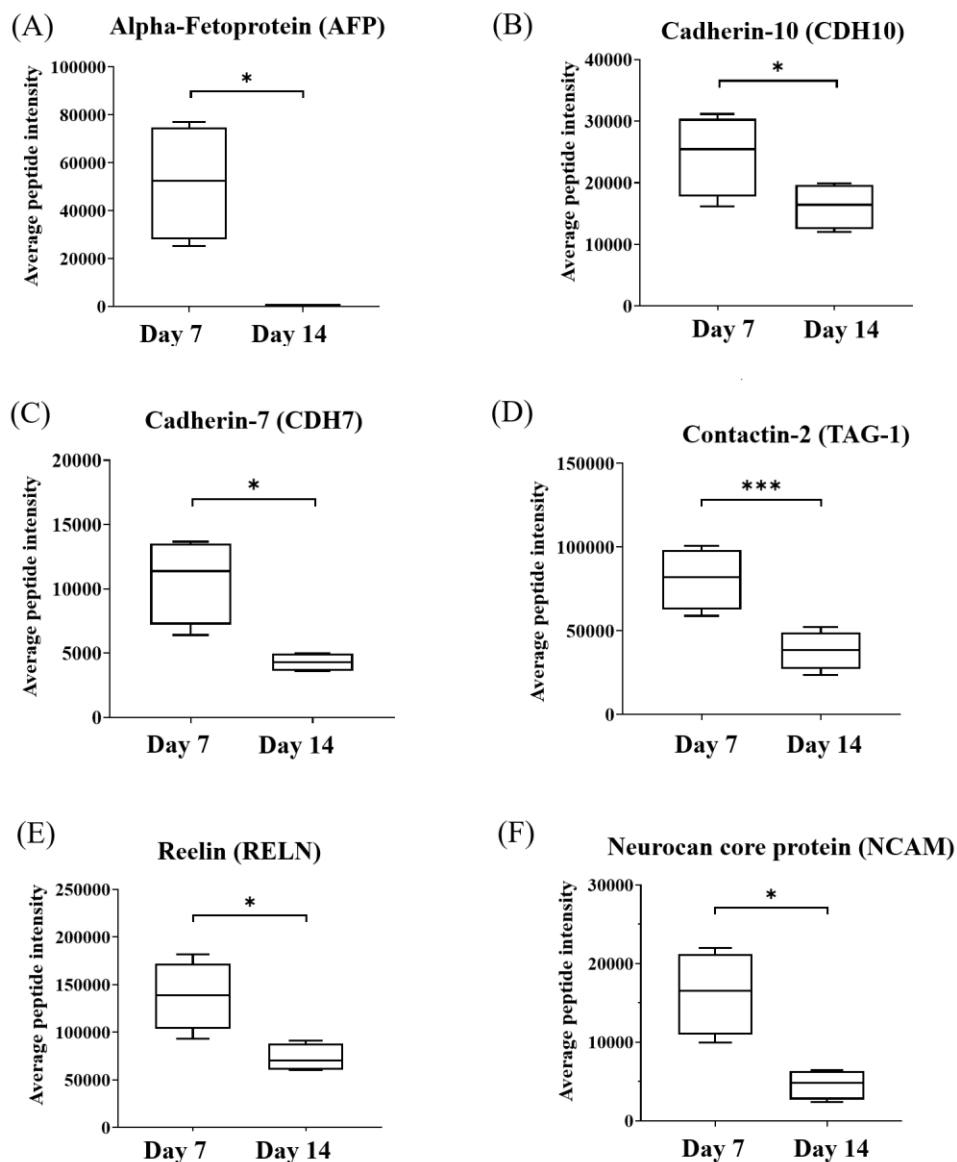
Uniprot ID	Protein name	Gene name	Normal growth study (pooled from 5 eyes into OD and OS)		Normal growth study (n= 4)	
			SWATH		MRM ^{HR}	
			Protein FC	P-Value	Protein FC	P-Value
G3P	Glyceraldehyde 3-phosphate dehydrogenase	GAPDH	1.20	N/A	0.90	0.748

Uniprot ID	Protein name	Gene name	Myopia study LIM3 (n= 7)		Myopia study LIM3 (n= 5)	
			SWATH		MRM ^{HR}	
			Protein FC	P-Value	Protein FC	P-Value
G3P	Glyceraldehyde 3-phosphate dehydrogenase	GAPDH	1.00	0.995	1.05	0.833

Uniprot ID	Protein name	Gene name	Myopia study LIM7 (n= 7)		Myopia study LIM7 (n= 6)	
			SWATH		MRM ^{HR}	
			Protein FC	P-Value	Protein FC	P-Value
G3P	Glyceraldehyde 3-phosphate dehydrogenase	GAPDH	1.00	0.994	0.90	0.689

Data analysis using bioinformatics software and confirmation using targeted proteomics

For the normal growth study (Between Day 7 and 14) from Chapter 5, a total of 8 differentially expressed proteins were selected, and 7 proteins (Ovotransferrin, Reelin, Contactin-2, Alpha-fetoprotein, Cadherin-7, Cadherin-10, and Neurocan core protein) were successfully confirmed using MRM^{HR} with similar FC (D14/D7) ($P \leq 0.05$, shown in Figure 7.1). The average peptide ratio was calculated from the top 3 transitions from 3 peptides of the protein and normalized with GAPDH. A full transition list of the peptides of each protein can be found in Appendix 7.1. Unlisted proteins were not detectable in MRM^{HR} validation study ion library, therefore, were excluded.



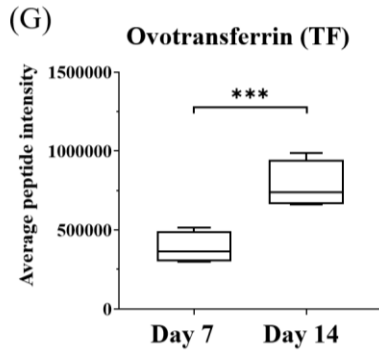


Figure 7.1 The fold change of proteins validated in MRM^{HR} experiments in normal growth study (D7 and D14), n= 4, *p <0.05; *p <0.01, T-test. Error bars= Mean ± SD. Normalized with GADPH.**

Most of the growth-related proteins selected from the DEPs on D14 and D7 in the normal growth study (Chapter 5) were validated using the MRM^{HR} approach, except for Cadherin-4 (CDH4), where the intensity was too low from transitions of the peptides and integration was not possible. The validated proteins using the MRM^{HR} approach had the same directional change in expression compared to the SWATH-MS results in both up and down directions.

For the myopia study (LIM3) from Chapter 6, a total of 3 differentially expressed proteins were selected, and 1 protein (Vasoactive intestinal peptide) was successfully confirmed using MRM^{HR} with similar FC and significantly different from the previous myopia study (LIM3) in Chapter 6 (shown in Figure 7.2). A complete transition list of the peptides of each protein can be found in Appendix 7.2.

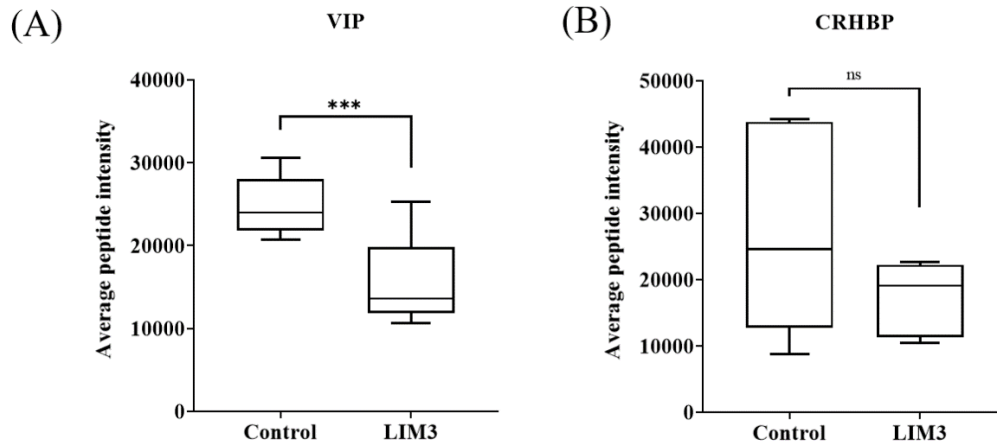


Figure 7.2 The fold change of proteins validated in MRM^{HR} experiments in myopia study (LIM3), n= 4, ns= not significant, ***p <0.01, T-test. Error bars= Mean ± SD.

Both VIP and CRHBP had the same directional FC in MRM^{HR} (VIP FC: 0.62 and CRHBP FC: 0.63) compared to SWATH-MS results (VIP FC: 0.67 and CRHBP FC: 0.56), but only VIP was found significantly different (P= 0.002) and was confirmed in MRM^{HR} experiment. ITIH3 had an FC of 1.15 in MRM^{HR} with a P-value of 0.239, which did not agree with the down-regulation SWATH-MS result (FC: 0.74 in SWATH-MS). The average peptide ratio was calculated from the top 1 transition from peptides (top 3 for VIP and 1 for CRHBP due to low intensity and the lack of peptides and transitions obtained) of the protein and normalized with GAPDH (Shown in Table 7.3).

Table 7.3 The fold change of DEPs in SWATH-MS and MRM^{HR} experiments in myopia study (LIM3), n= 5.

Uniprot ID	Protein name	Gene name	Myopia LIM3 study (n= 7)	Myopia LIM3 study (n= 5)	
			SWATH	MRM ^{HR}	
			Protein FC (LIM/control)	Protein FC (LIM/control)	P-value
A0A1D5NXA 6	Inter-alpha-trypsin inhibitor heavy chain 3	ITIH3	0.74	1.09	0.552

E1C1R3	Corticotropin-releasing factor-binding protein	CRH BP	0.56	0.63	0.237
F1NWT5	Vasoactive intestinal polypeptide	VIP	0.67	0.62	0.028

For the myopia study (LIM7) from Chapter 6, a total of 14 differentially expressed proteins were selected, and 1 protein was successfully confirmed using MRM^{HR} with significant FC and p-value (shown in Figure 7.3), while other proteins either had no significant FC difference or had too low intensity for quantitation, therefore excluded. A full transition list of the peptides of each protein can be found in Appendix 7.3.

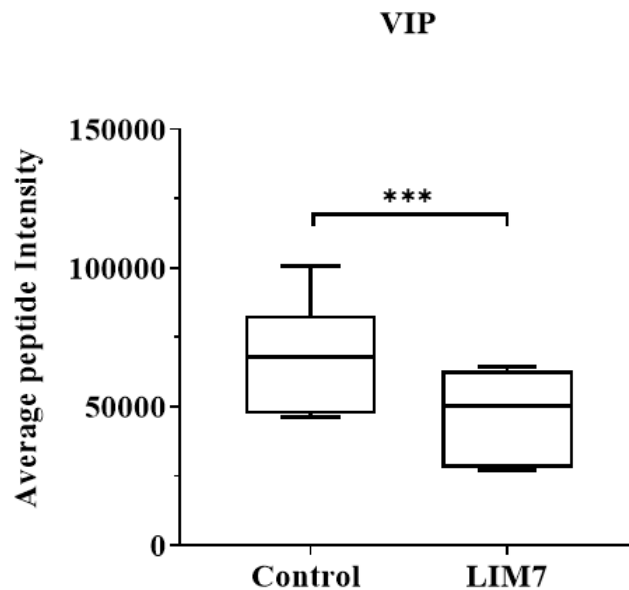


Figure 7.3 The fold change of protein validated in MRM^{HR} experiments in myopia study (LIM7), (*p <0.05, unpaired T-test. Error bars= Mean \pm SD, n= 6).

Only VIP was confirmed to have the same FC direction in MRM^{HR} (VIP FC: 0.69) with the result obtained in SWATH-MS (VIP FC: 0.70) from the previous Chapter and were found to have a significant difference between LIM7 and control (P= 0.01) in MRM^{HR} experiment. The average peptide ratio was calculated from the top 1

transition from peptides (less was used due to the low lack of peptides and transitions obtained) of the protein and normalized with GAPDH (Shown in Table 7.4).

Table 7.4 The fold change of DEPs in SWATH-MS and MRM^{HR} experiments in myopia study (LIM7), n= 6.

Uniprot ID	Protein name	Gene name	Myopia LIM7 study (n= 7)	Myopia LIM7 study (n= 6)	
			SWATH	MRM ^{HR}	
			Protein FC (LIM/control)	Protein FC (LIM/control)	P-value
A0A1D5NUV0	Secretogranin II	SCG2	0.71	0.924	0.636
A0A1D5PCF5	Insulin like growth factor binding protein 7	IGFBP7	0.72	0.96	0.623
A0A1D5PSQ1	A2M_N_2 domain-containing protein	N/A	1.73	1.12	0.240
A0A3Q2TWJ9	MG2 domain-containing protein	N/A	1.74	1.15	0.131
A0A3Q2TZA4	A2M_recep domain-containing protein	N/A	1.48	1.17	0.037
A0A3Q2UCH2	A2M domain-containing protein	N/A	1.72	1.18	0.156
E1BQW4	EGF like, fibronectin type III and laminin G domains	EGFLAM	0.74	1.05	0.631
F1NIZ9	Sema domain-containing protein	SEMA7A	1.57	0.89	0.111
F1NWT5	Vasoactive intestinal polypeptide	VIP	0.7	0.69	0.01

VIP gene expression in the retina using qPCR during myopia progression

VIP gene expression was too low for detection from the collected vitreous (at LIM3 and LIM7); therefore, the results were not shown here. And using the retina at LIM3 and LIM7, according to the real-time quantitative PCR (RT-qPCR) confirmation result, the gene expression of VIP in the retina was significantly down-regulated in both the LIM3 (FC: 0.665 ± 0.267 , $P= 0.046$, Figure 7.1 A) and LIM7 group (FC: 0.696 ± 0.117 , $P= 0.02$, Figure 7.1 B) in the treated eyes, compared to the fellow control eyes.

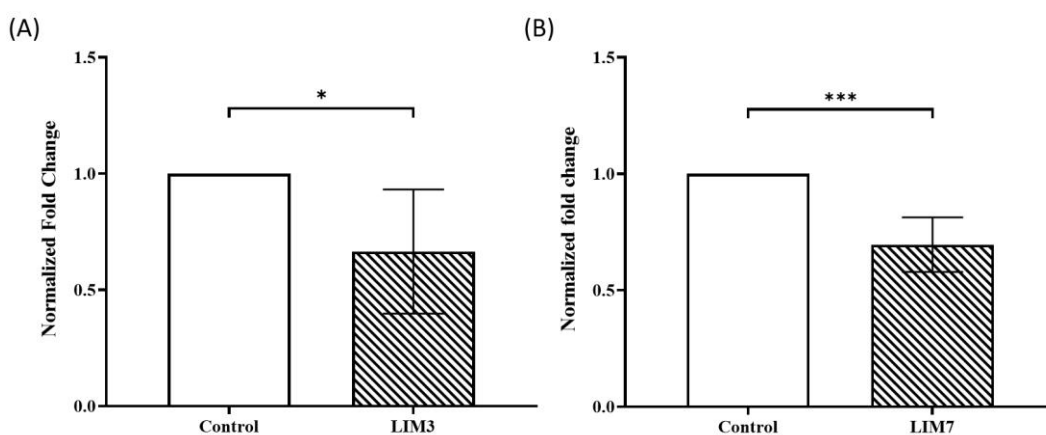


Figure 7.4 Chick retina VIP expression normalized to GAPDH at Lens-induced myopia (LIM) for (A) 3 and (B) 7 days, n= 4 at each time point (*p <0.05; *p <0.01, unpaired T-test. Error bars= Mean ±SD).**

7.4 Discussion

Quantification using SWATH-MS from previous studies allowed numerous potential biomarkers to be identified in a high throughput manner. After acquiring the data by the mass spectrometer, data processing (RT alignment, normalization, peptides QC requirements, and %CV between injections), statistics analysis, and the FC, cut-off offered additional filtering power for the reduction of false-positive candidates. However, due to the intrinsic limitations of the high throughput quantitative MS profiling approach, further validation of selected protein expressions was planned to shortlist highly confident candidates for data mining in considering potential biological variation (sample-specific) and technical errors (from sample preparation to machines).

Western blot and enzyme-linked immunosorbent assay (ELISA) have long been used to pinpoint the expression of specific proteins throughout research history. Western blot (immunoblotting) requires antibodies that can bind against those proteins of interest (Burnette, 1981). This offered the possibility of estimating the protein molecular mass, protein post-translational modifications, and quantifying the amount of protein within the samples. Where else, ELISA uses antigen to detect the antibody offering a high sensitivity and rapid (96 well plates) assay to detect/quantify peptides/ proteins (Engvall & Perlmann, 1971). It relies on the power of antibody conjugation, binding to the reporter enzyme (Biotin), where an enzymatic reaction will occur and change color when the required reactions are completed, offering extremely sensitive detection of proteins even at the picogram level.

Western blot offers cheaper material cost (for gel preparation and required solutions), whereas ELISA assay must be pre-set in plates directly. On the other hand, one of the main drawbacks of Western blotting is the low throughput as multiple gels are required for a single antibody and running limited samples. Multiple processing steps (denaturation, gel transfer to the membrane, blocking and imaging) added potential complications, and therefore time consumption will also be increased.

Furthermore, these techniques are technically challenging for deep vitreous proteome research due to the very dilute nature of this tissue, making lower abundant proteins very hard to detect. Furthermore, the low sensitivity and repeatability of these hampered the use of vitreous as a target. Also, the vitreous is comprised almost entirely of water. The remainder consists of highly abundant albumin (60-70%) with many low-abundant proteins that remain difficult to quantify (Angi et al., 2012). Therefore studies involving the vitreous mainly focused on higher abundant proteins in the human vitreous such as quantitation of basic fibroblast growth factor (bFDG) and platelet-derived growth factor (PDFG) in vitreoretinal disorders (Cassidy et al., 1998), vascular endothelial growth factor (VEGF) and pigment epithelium-derived factor (PEDF) and insulin-like growth factor 1 (IGF-1) in proliferative diabetic retinopathy (PDR) human patients compared to its controlled subjects (Hernández et al., 2002; Simo et al., 2002).

Even though Western blot (protein immunoblotting) and ELISA remains to be the two conventional protein quantification methods as they are the standard technique in almost every laboratory, one of the main disadvantages is still the lack of ability to do multiple biomarkers in one go. These can be extremely time-consuming, especially when advanced mass spectrometry techniques can detect up to thousands of proteins in a single injection. Single reaction monitoring or multiple reaction monitoring (SRM/MRM) eliminates this problem as multiple transitions can be monitored given that the scanning speed was enough and gained popularity in the research field (L. Anderson & C. L. Hunter, 2006; Wolf-Yadlin et al., 2007).

SRM/MRM is a technique where the precursor ions are known, targeting them with the exact window of fragmentation to be recorded and analyzed ions using a triple quadrupole (QqQ) mass analyzer (A. Hu et al., 2016; Kiyonami & Domon, 2010; Peterson et al., 2012). This has the benefit of having a higher sensitivity and selectivity than the traditional identification method (Peterson et al., 2012) where specific transitions of the peptide will be monitored and compared to its control using relative quant. Compared to the widely used immune-based assays mentioned earlier, the MRM approach does not require an antibody, which significantly

reduces the time for antibody development and the ability to quantify multiple peptides simultaneously with high accuracy and sensitivity (Kuzyk et al., 2009).

Similar to the SRM/MRM approach, the relatively new high-resolution MRM (MRM^{HR}) approach was employed with the Triple-TOF MS under nanoLC flow to solidify further our findings of SWATH results of differentially expressed proteins found across the time points. The low peptide amount consumption (Peti et al., 2018) was essential for vitreous studies while maintaining sensitivity (Schilling et al., 2015) since the peptide from an individual sample is very limited. Our group has adopted the MRM^{HR} approach for validation in several ocular-related studies (Shan et al., 2017; S. W. Shan et al., 2018), where consistent results were shown between SWATH-MS, which the workflow would be beneficial to our current study for the first time.

For the normal growth study (in Chapter 5), 9 DEPs from the SWATH-MS study were selected based on their related functions to normal growth, such as structural and neurological properties. Since their FC was at the greatest when comparing D14 to D7 (baseline), the validation experiment was based on these two time points. Almost 80% of the selected DEPs were confirmed using the MRM^{HR} approach with 3 transitions and 3 peptides for calculation. This is not surprising as some of the DEPs were highly abundant in the vitreous such as reelin and ovotransferrin, which gives very confident results since there were multiple peptides to select from. Since the intensity of these transitions was very high, small fluctuations in various lower-intensity transitions were outweighed in the overall calculation. Only one protein (CDH4) could not be validated due to the very low transition intensity obtained in this experiment, with only 1 transition detected for this protein. This might be because of the shorter gradient (shown in Chapter 2.3) used for the validation experiment when this protein sequence could not be detected fully since a shorter gradient will result in a lower number of proteins being identified (Köcher et al., 2012).

An attempt was made to validate the VIP protein level using ELISA but was unsuccessful due to the low protein content even in pooled samples (data not shown).

here). However, using the MS approach, VIP was detected again in validation studies showing its sensitivity compared to more traditional validation methods. For the myopia study (LIM3 and LIM7 in Chapter 6), VIP was the only protein validated with the highest confidence: having the same direction of FC as SWATH and showing a statistical difference in LIM compared to control. Although 3 peptides were used in most of the other proteins, the large variation in transitions resulted in the inconsistency in MRM^{HR} results compared to its results from SWATH-MS. This might be because the filtering applied in the skyline software deemed that some peptides were not at the correct RT and will be hard to match with individual samples, where the addition of synthetic peptides such as iRT (Escher et al., 2012) for retention calibration can adjust the retention time of the LC.

Furthermore, as mentioned in earlier Chapters, one of the main challenges for vitreous proteomics is due to the coverage of high abundant proteins over-masking lower abundant proteins where the range can be up to 4-5 folds: VIP (average intensity around $1.32E+04$ in control sample) compared to APOA1 (average intensity around $1.3E+07$) in the control sample. This remained a challenge in protein validation using the MS approach where lower abundance proteins were hard to detect if more high abundant proteins were present. Their peptide intensity values will fluctuate greatly, making them harder to integrate and calculate. Although modern QqOrbi MS and QqTOF MS achieved sensitivity that is comparable to or even better than that provided by WB /ELISA, the technical procedures and analysis are still not standardized and evolving. For instance, published data on using MRM as a validation method for proteins with the use of a customized weighing system (Peterson et al., 2012), where the calculation is more weighted to higher confidence transitions and less to lesser abundant transitions for a higher confidence result. With further advances in new MS design and bioinformatics tools, targeted proteomics quantification will become a more mature tool for enabling cost-effective and rapid protein validation for biomarker research. This study was the first to adopt MRM^{HR} in successfully validating DEPs in normal growth and myopia study in the vitreous proteomes.

qPCR is a widely accepted method for looking at the specific gene expression of a single/ target gene, allowing us to quantify at the gene level (Gibson et al., 1996). To our understanding, no research was done on the expression of VIP (in the natural environment) in the vitreous at the gene level, which may partly explain our qPCR results where the VIP gene was not detected in the vitreous. qPCR results from the vitreous were shown to be too low for detection even after an extensive increase in the number of cycles which indicated that VIP might not be produced locally in the vitreous and must be transferred from its surrounding tissues. However, we could successfully identify and quantify the VIP gene's relative change in the same eyes' retina, where the vitreous samples were collected. From our result, the VIP gene expression was found to be down-regulated significantly ($P < 0.05$, unpaired T-test) in the retina treated eyes of both of the time points (LIM 3 and 7 days) indicating that the production of VIP may be halted under hyperopic defocus similar to our other study (Shan et al., 2022). This reduction in VIP expression at the gene level could reduce the production of VIP proteins, further reducing the VIP proteins found in the vitreous. This was matched in line with our previous data on the vitreous VIP expression using SWATH-MS quantitation and MRM^{HR} validation at the protein level.

7.5 Conclusion

DEPs acquired from previous SWATH studies (normal growth, LIM3, and LIM7) were validated using the MRM^{HR} system using a shorter gradient (90mins, and without fractionation). Separate batches of chicks were raised, and individual samples were used to reduce the chances of false-positive results. A total of 7 differentially expressed proteins (Ovotransferrin, Reelin, Contactin-2, Alpha-fetoprotein, Cadherin-7, Cadherin-10, and Neurocan core protein) were successfully confirmed using MRM^{HR} with similar FC (D14/D7) found from the previous Normal growth SWATH study ($P \leq 0.05$). VIP was the only protein validated with the highest confidence in both LIM3 and LIM7 studies. Although MRM^{HR} was successfully applied in protein validation, its application is still obstructed by the machine's

sensitivity where lower abundant proteins (transitions) were hard to accurately detect and quantify.

Chapter 8. Summary and conclusion

This thesis has successfully established the first comprehensive vitreous proteomic workflow using the more robust and sensitive next-generation nanoLC SWATH-MS platform. As myopia can be seen as a dysregulation of normal eye growth, studying the emmetropization period (normal growth) allowed us to examine the protein changes during this critical natural growing process.

Firstly, using our optimized protocols from sample preparation to mass spectrometry, 1576 unique proteins (22987 distinct peptides) were identified, representing the most comprehensive chick vitreous proteome reported to date, covering the first month of the normal growth period. Several isoforms of structurally-related and growth-related proteins, such as the cadherin groups and alpha-fetoprotein, were significantly down-regulated in the older vitreous samples for the first time using SWATH quantification. A number of these DEPs were then successfully confirmed using targeted MRM^{HR} under separate batches of samples.

Next, the -10D LIM chick model was employed to study the differential protein changes in response to the induced VCD elongation at 3-day (LIM3) and 7-day (LIM7) treatments. Using a high-pH fractionation technique, 1242 proteins (15181 distinct peptides) were identified with similar Gene Ontology (GO) terms found compared to the normal vitreous proteome in emmetropization. The induced biometric changes in terms of refraction and axial length were greater at the longer treatment time point. Similarly, more DEPs were found significantly changed at LIM7 (23 proteins) than at LIM3 (8 proteins) with a cut-off at ≥ 1.5 or ≤ 0.7 , $p \leq 0.05$, and 95% confidence. The majority of these proteins were down-regulated neuroproteins for both groups. Using the MRM^{HR} approach, VIP was confirmed to be a critical down-regulated vitreous protein in the LIM eyes at the two-time points, which has been mentioned in earlier reports for its role in FDM models. Using the LIM chick myopia model, we provided proteomic evidence of the relative reduction of vitreous VIP in the compensated myopic eyes compared to the paired control eyes based on the SWATH-MS profiling and the validation using the MRM^{HR} approach. Although increasing VIP level has shown its associated effect on inhibiting ocular elongation in FDM chick models, its impact in LIM models has

not yet been fully explored. Hence, the protective effects of VIP in LIM using animal models should be re-visited using functional tests.

VIP comes in powder form and can readily dissolve in water at 0.1% in 1% acetic acid and saline. VIP solution can then be introduced into the LIM eye via topical eye drops or IV injection to study its effect on eye growth and associated protein regulations. Furthermore, different formulations of drug delivery systems such as emulsions (Vandamme, 2002), liposomes (Natarajan et al., 2011), HA-coated nanoparticles (Ibrahim et al., 2010), Chitosan-coated nanoparticles (Nagarwal et al., 2012) should be formulated to maintain the maximum dosage of VIP drug offload when they are introduced into the eye via topical eyedrops or IV once the protective effects have been established. While VIP should be looked at closely with delivery options, further studies of other potential proteins obtained from SWATH studies should also be monitored.

In conclusion, proteomics studies using the next-generation nano-LC-ESI-MS/MS allowed us to study the protein changes in the vitreous in-depth, including those proteins that might not originate from the vitreous (could be from surrounding tissues). In the hope of providing a better understanding of more potential players involved in myopia progression that could have been missed from previous literature.

Reference

- Adinolfi, A., Adinolfi, M., & Lessof. (1975). Alpha-feto-protein during development and in disease. *J Med Genet*, *12*(2), 138-151. <https://doi.org/10.1136/jmg.12.2.138>
- Ahmad, M. T., Zhang, P., Dufresne, C., Ferrucci, L., & Semba, R. D. (2018). The Human Eye Proteome Project: Updates on an Emerging Proteome. *Proteomics*, *18*(5-6), e1700394. <https://doi.org/10.1002/pmic.201700394>
- Akiba, J. (1993). Prevalence of posterior vitreous detachment in high myopia. *Ophthalmology*, *100*(9), 1384-1388. [https://doi.org/10.1016/s0161-6420\(93\)31471-5](https://doi.org/10.1016/s0161-6420(93)31471-5)
- Aldebasi, Y. H. (2013). A descriptive study on compliance of spectacle-wear in children of primary schools at Qassim Province, Saudi Arabia. *Int J Health Sci (Qassim)*, *7*(3), 291-299. <https://doi.org/10.12816/0006057>
- Ali, S., & Bettelheim, F. A. (1984). Distribution of freezable and non-freezable water in bovine vitreous. *Current Eye Research*, *3*(10), 1233-1239. <https://doi.org/10.3109/02713688409000827>
- Alimanović-Halilović, E. (2008). Correlation between refraction level and retinal breaks in myopic eye. *Bosn J Basic Med Sci*, *8*(4), 346-349. <https://doi.org/10.17305/bjbms.2008.2895>
- Amiri-Dashatan, N., Koushki, M., Abbaszadeh, H. A., Rostami-Nejad, M., & Rezaei-Tavirani, M. (2018). Proteomics Applications in Health: Biomarker and Drug Discovery and Food Industry. *Iran J Pharm Res*, *17*(4), 1523-1536.
- Andersen, K. K., Oliveira, C. L., Larsen, K. L., Poulsen, F. M., Callisen, T. H., Westh, P., Pedersen, J. S., & Otzen, D. (2009). The role of decorated SDS micelles in sub-CMC protein denaturation and association. *J Mol Biol*, *391*(1), 207-226. <https://doi.org/10.1016/j.jmb.2009.06.019>
- Anderson, L., & Hunter, C. L. (2006). Quantitative mass spectrometric multiple reaction monitoring assays for major plasma proteins. *Mol Cell Proteomics*, *5*(4), 573-588. <https://doi.org/10.1074/mcp.M500331-MCP200>
- Anderson, L., & Hunter, C. L. (2006). Quantitative mass spectrometric multiple reaction monitoring assays for major plasma proteins. *Molecular & Cellular Proteomics*, *5*(4), 573-588.
- Angi, M., Kalirai, H., Coupland, S. E., Damato, B. E., Semeraro, F., & Romano, M. R. (2012). Proteomic analyses of the vitreous humour. *Mediators Inflamm*, *2012*, 148039. <https://doi.org/10.1155/2012/148039>
- Annesley, T. M. (2003). Ion suppression in mass spectrometry. *Clin Chem*, *49*(7), 1041-1044. <https://doi.org/10.1373/49.7.1041>
- Aquino, D. A., Margolis, R. U., & Margolis, R. K. (1984). Immunocytochemical localization of a chondroitin sulfate proteoglycan in nervous tissue. I. Adult brain, retina, and peripheral nerve. *J Cell Biol*, *99*(3), 1117-1129. <https://doi.org/10.1083/jcb.99.3.1117>
- Aretz, S., Krohne, T. U., Kammerer, K., Warnken, U., Hotz-Wagenblatt, A., Bergmann, M., Stanzel, B. V., Kempf, T., Holz, F. G., Schnolzer, M., & Kopitz, J. (2013). In-depth mass spectrometric mapping of the human vitreous proteome. *Proteome Sci*, *11*(1), 22. <https://doi.org/10.1186/1477-5956-11-22>

- Armstrong, P. B., & Quigley, J. P. (1999). α 2-macroglobulin: an evolutionarily conserved arm of the innate immune system. *Developmental & Comparative Immunology*, 23(4), 375-390.
[https://doi.org/https://doi.org/10.1016/S0145-305X\(99\)00018-X](https://doi.org/https://doi.org/10.1016/S0145-305X(99)00018-X)
- Arnold, U., & Ulbrich-Hofmann, R. (1999). Quantitative protein precipitation from guanidine hydrochloride-containing solutions by sodium deoxycholate/trichloroacetic acid. *Anal Biochem*, 271(2), 197-199.
<https://doi.org/10.1006/abio.1999.4149>
- Ashby, R., Ohlendorf, A., & Schaeffel, F. (2009). The effect of ambient illuminance on the development of deprivation myopia in chicks. *Invest Ophthalmol Vis Sci*, 50(11), 5348-5354. <https://doi.org/10.1167/iovs.09-3419>
- Baeriswyl, T., & Stoeckli, E. T. (2008). Axonin-1/TAG-1 is required for pathfinding of granule cell axons in the developing cerebellum. *Neural Dev*, 3, 7. <https://doi.org/10.1186/1749-8104-3-7>
- Balazs, E. A. (1993). Functional anatomy of the vitreous. *Duane's Foundation of Clinical Ophthalmology*, 1, 1-16. <https://ci.nii.ac.jp/naid/10019301540/en/>
- Balazs EA, D. J. (1972). The vitreous. *The Eye*, 1A(New York, Academic Press), 32-42.
- Ball, D., Rose, E., & Alpert, E. (1992). Alpha-fetoprotein levels in normal adults. *Am J Med Sci*, 303(3), 157-159. <https://doi.org/10.1097/00000441-199203000-00004>
- Barathi, V. A., Boopathi, V. G., Yap, E. P., & Beuerman, R. W. (2008). Two models of experimental myopia in the mouse. *Vision Res*, 48(7), 904-916. <https://doi.org/10.1016/j.visres.2008.01.004>
- Barnes, S. H., Price, S. R., Wentzel, C., & Guthrie, S. C. (2010). Cadherin-7 and cadherin-6B differentially regulate the growth, branching and guidance of cranial motor axons. *Development*, 137(5), 805-814.
<https://doi.org/10.1242/dev.042457>
- Basmak, H., Ozer, A., Yildirim, N., & Tuncel, N. (1997). The effect of vasoactive intestinal peptide on development of form deprivation myopia in the chick.
- Bath, T. S., Francavilla, C., & Olsen, J. V. (2014). Off-line high-pH reversed-phase fractionation for in-depth phosphoproteomics. *J Proteome Res*, 13(12), 6176-6186. <https://doi.org/10.1021/pr500893m>
- Beach, C. A., Mays, D. C., Sterman, B. M., & Gerber, N. (1985). Metabolism, distribution, seminal excretion and pharmacokinetics of caffeine in the rabbit. *Journal of Pharmacology and Experimental Therapeutics*, 233(1), 18-23.
- Bedrossian, R. H. (1979). The effect of atropine on myopia. *Ophthalmology*, 86(5), 713-717.
- Belch, J. J., McArdle, B., Madhok, R., McLaughlin, K., Capell, H. A., Forbes, C. D., & Sturrock, R. D. (1984). Decreased plasma fibrinolysis in patients with rheumatoid arthritis. *Ann Rheum Dis*, 43(6), 774-777.
<https://doi.org/10.1136/ard.43.6.774>
- Bertrand, E., Fritsch, C., Diether, S., Lambrou, G., Muller, D., Schaeffel, F., Schindler, P., Schmid, K. L., van Oostrum, J., & Voshol, H. (2006). Identification of apolipoprotein A-I as a "STOP" signal for myopia. *Mol Cell Proteomics*, 5(11), 2158-2166.
<https://doi.org/10.1074/mcp.M600073-MCP200>

- Bishop, P. N. (2000). Structural macromolecules and supramolecular organisation of the vitreous gel. *Prog Retin Eye Res*, 19(3), 323-344.
<http://www.ncbi.nlm.nih.gov/pubmed/10749380>
- Bishop, P. N., Reardon, A. J., McLeod, D., & Ayad, S. (1994). Identification of alternatively spliced variants of type II procollagen in vitreous. *Biochem Biophys Res Commun*, 203(1), 289-295.
<https://doi.org/10.1006/bbrc.1994.2180>
- Bissell, M. J., Hall, H. G., & Parry, G. (1982). How does the extracellular matrix direct gene expression? *Journal of Theoretical Biology*, 99(1), 31-68.
[https://doi.org/https://doi.org/10.1016/0022-5193\(82\)90388-5](https://doi.org/https://doi.org/10.1016/0022-5193(82)90388-5)
- Bitzer, M., & Schaeffel, F. (2002). Defocus-Induced Changes in ZENK Expression in the Chicken Retina. *Investigative Ophthalmology & Visual Science*, 43(1), 246-252.
- Bodzon-Kulakowska, A., Bierczynska-Krzysik, A., Dylag, T., Drabik, A., Suder, P., Noga, M., Jarzebinska, J., & Silberring, J. (2007). Methods for samples preparation in proteomic research. *J Chromatogr B Analyt Technol Biomed Life Sci*, 849(1-2), 1-31.
<https://doi.org/10.1016/j.jchromb.2006.10.040>
- Borth, W. (1992). $\alpha 2$ “Macroglobulin, a multifunctional binding protein with targeting characteristics. *The FASEB Journal*, 6(15), 3345-3353.
<https://doi.org/https://doi.org/10.1096/fasebj.6.15.1281457>
- Bos, K. J., Holmes, D. F., Kadler, K. E., McLeod, D., Morris, N. P., & Bishop, P. N. (2001). Axial structure of the heterotypic collagen fibrils of vitreous humour and cartilage. *J Mol Biol*, 306(5), 1011-1022.
<https://doi.org/10.1006/jmbi.2000.4429>
- Bost, F., Diarra-Mehrpour, M., & Martin, J. P. (1998). Inter-alpha-trypsin inhibitor proteoglycan family--a group of proteins binding and stabilizing the extracellular matrix. *Eur J Biochem*, 252(3), 339-346.
<https://doi.org/10.1046/j.1432-1327.1998.2520339.x>
- BP, G. (1981). The vitreous. *Physiology of the Eye: Clinical Application*, 255-276.
- Bradley, D. V., Fernandes, A., Lynn, M., Tigges, M., & Boothe, R. G. (1999). Emmetropization in the rhesus monkey (*Macaca mulatta*): birth to young adulthood. *Invest Ophthalmol Vis Sci*, 40(1), 214-229.
<https://www.ncbi.nlm.nih.gov/pubmed/9888446>
- Brand, C., Burkhardt, E., Schaeffel, F., Choi, J. W., & Feldkaemper, M. P. (2005). Regulation of Egr-1, VIP, and Shh mRNA and Egr-1 protein in the mouse retina by light and image quality. *Mol Vis*, 11, 309-320.
<https://www.ncbi.nlm.nih.gov/pubmed/15889015>
- Brod, E., S. Ben-Yosef, V., Bandhakavi, S., & Sivan, U. (2016). Charge-based separation of proteins and peptides by electrically induced dynamic pH profiles. *Journal of Chromatography A*, 1431, 166-175.
<https://doi.org/https://doi.org/10.1016/j.chroma.2015.12.070>
- Buck, C., Schaeffel, F., Simon, P., & Feldkaemper, M. (2004). Effects of positive and negative lens treatment on retinal and choroidal glucagon and glucagon receptor mRNA levels in the chicken. *Invest Ophthalmol Vis Sci*, 45(2), 402-409. <https://doi.org/10.1167/iovs.03-0789>
- Burnette, W. N. (1981). "Western blotting": electrophoretic transfer of proteins from sodium dodecyl sulfate--polyacrylamide gels to unmodified nitrocellulose and radiographic detection with antibody and radioiodinated

- protein A. *Anal Biochem*, 112(2), 195-203. [https://doi.org/10.1016/0003-2697\(81\)90281-5](https://doi.org/10.1016/0003-2697(81)90281-5)
- Burns, J. A., Butler, J. C., Moran, J., & Whitesides, G. M. (1991). Selective reduction of disulfides by tris(2-carboxyethyl)phosphine. *The Journal of Organic Chemistry*, 56(8), 2648-2650. <https://doi.org/10.1021/jo00008a014>
- Buxton, T. B., Crockett, J. K., Moore, W. L., 3rd, Moore, W. L., Jr., & Rissing, J. P. (1979). Protein precipitation by acetone for the analysis of polyethylene glycol in intestinal perfusion fluid. *Gastroenterology*, 76(4), 820-824. <https://www.ncbi.nlm.nih.gov/pubmed/422010>
- Cagianut, B., & Wunderly, C. (1953). Protein studies on the human vitreous body. *Br J Ophthalmol*, 37(4), 229-233. <https://doi.org/10.1136/bjo.37.4.229>
- Cakmak, A. I., Basmak, H., Gursoy, H., Ozkurt, M., Yildirim, N., Erkasap, N., Bilgec, M. D., Tuncel, N., & Colak, E. (2017). Vasoactive intestinal peptide, a promising agent for myopia? *Int J Ophthalmol*, 10(2), 211-216. <https://doi.org/10.18240/ijo.2017.02.05>
- Cañas, B., Piñeiro, C., Calvo, E., López-Ferrer, D., & Gallardo, J. M. (2007). Trends in sample preparation for classical and second generation proteomics. *Journal of Chromatography A*, 1153(1), 235-258. <https://doi.org/https://doi.org/10.1016/j.chroma.2007.01.045>
- Carr, B. J., & Stell, W. K. (1995). The Science Behind Myopia. In H. Kolb, E. Fernandez, & R. Nelson (Eds.), *Webvision: The Organization of the Retina and Visual System*. University of Utah Health Sciences Center
- Copyright: © 2022 Webvision .
- Cassidy, L., Barry, P., Shaw, C., Duffy, J., & Kennedy, S. (1998). Platelet derived growth factor and fibroblast growth factor basic levels in the vitreous of patients with vitreoretinal disorders. *Br J Ophthalmol*, 82(2), 181-185. <https://doi.org/10.1136/bjo.82.2.181>
- Catherman, A. D., Skinner, O. S., & Kelleher, N. L. (2014). Top down proteomics: facts and perspectives. *Biochemical and biophysical research communications*, 445(4), 683-693.
- Cedrone, C., Nucci, C., Scuderi, G., Ricci, F., Cerulli, A., & Culasso, F. (2006). Prevalence of blindness and low vision in an Italian population: a comparison with other European studies. *Eye*, 20(6), 661-667. <https://doi.org/10.1038/sj.eye.6701934>
- Chait, B. T. (2006). Mass spectrometry: bottom-up or top-down? *Science*, 314(5796), 65-66.
- Chamberlain, P., Peixoto-de-Matos, S. C., Logan, N. S., Ngo, C., Jones, D., & Young, G. (2019). A 3-year randomized clinical trial of MiSight lenses for myopia control. *Optometry and Vision Science*, 96(8), 556-567.
- Chan, M. Y., Hoare, M., & Dunnill, P. (1986). The kinetics of protein precipitation by different reagents. *Biotechnol Bioeng*, 28(3), 387-393. <https://doi.org/10.1002/bit.260280312>
- Chan, P., Risler, J., Raguenez, G., & Salier, J. (1995). The three heavy-chain precursors for the inter- α -inhibitor family in mouse: new members of the multicopper oxidase protein group with differential transcription in liver and brain. *Biochemical Journal*, 306(2), 505-512.
- Chapman, J. D., Goodlett, D. R., & Masselon, C. D. (2014). Multiplexed and data-independent tandem mass spectrometry for global proteome profiling.

- Mass Spectrom Rev*, 33(6), 452-470.
<https://doi.org/https://doi.org/10.1002/mas.21400>
- Chen, D. Z., Koh, V., Tan, M., Tan, C. S., Nah, G., Shen, L., Bhargava, M., Cheng, C. Y., Zhao, P., Wong, T. Y., & Saw, S. M. (2018). Peripheral retinal changes in highly myopic young Asian eyes. *Acta Ophthalmol*, 96(7), e846-e851. <https://doi.org/10.1111/aos.13752>
- Chen, S. J., Lu, P., Zhang, W. F., & Lu, J. H. (2012). High myopia as a risk factor in primary open angle glaucoma. *Int J Ophthalmol*, 5(6), 750-753. <https://doi.org/10.3980/j.issn.2222-3959.2012.06.18>
- Cheung, J. K., Li, K. K., Zhou, L., To, C. H., & Lam, T. C. (2020). Data on protein changes of chick vitreous during normal eye growth using data-independent acquisition (SWATH-MS). *Data Brief*, 30, 105576. <https://doi.org/10.1016/j.dib.2020.105576>
- Chia, A., Chua, W.-H., Wen, L., Fong, A., Goon, Y. Y., & Tan, D. (2014). Atropine for the treatment of childhood myopia: changes after stopping atropine 0.01%, 0.1% and 0.5%. *American journal of ophthalmology*, 157(2), 451-457. e451.
- Chia, A., Lu, Q.-S., & Tan, D. (2016). Five-year clinical trial on atropine for the treatment of myopia 2: myopia control with atropine 0.01% eyedrops. *Ophthalmology*, 123(2), 391-399.
- Chiang, M., Kouzis, A., Pointer, R., & Repka, M. (2001). Treatment of childhood myopia with atropine eyedrops and bifocal spectacles. *Binocular Vision & Strabismus Quarterly*, 16(3), 209-215.
- Chick, H., & Martin, C. J. (1913). The Precipitation of Egg-Albumin by Ammonium Sulphate. A Contribution to the Theory of the "Salting-out" of Proteins. *Biochem J*, 7(4), 380-398. <https://doi.org/10.1042/bj0070380>
- Cho, P., & Cheung, S.-W. (2012). Retardation of Myopia in Orthokeratology (ROMIO) Study: A 2-Year Randomized Clinical Trial Retardation of Myopia in Orthokeratology Study. *Investigative Ophthalmology & Visual Science*, 53(11), 7077-7085. <https://doi.org/10.1167/iovs.12-10565>
- Choi, H., Fermin, D., & Nesvizhskii, A. I. (2008). Significance analysis of spectral count data in label-free shotgun proteomics. *Mol Cell Proteomics*, 7(12), 2373-2385. <https://doi.org/10.1074/mcp.M800203-MCP200>
- Choudhary, G., & Horvath, C. (1996). Ion-exchange chromatography. *Methods Enzymol*, 270, 47-82. [https://doi.org/10.1016/s0076-6879\(96\)70005-8](https://doi.org/10.1016/s0076-6879(96)70005-8)
- Chua, W.-H., Balakrishnan, V., Chan, Y.-H., Tong, L., Ling, Y., Quah, B.-L., & Tan, D. (2006). Atropine for the treatment of childhood myopia. *Ophthalmology*, 113(12), 2285-2291.
- Cohen, Y., Peleg, E., Belkin, M., Polat, U., & Solomon, A. S. (2012). Ambient illuminance, retinal dopamine release and refractive development in chicks. *Exp Eye Res*, 103, 33-40. <https://doi.org/10.1016/j.exer.2012.08.004>
- Collery, R. F., Veth, K. N., Dubis, A. M., Carroll, J., & Link, B. A. (2014). Rapid, accurate, and non-invasive measurement of zebrafish axial length and other eye dimensions using SD-OCT allows longitudinal analysis of myopia and emmetropization. *PLoS One*, 9(10), e110699. <https://doi.org/10.1371/journal.pone.0110699>
- Collins, B. C., Gillet, L. C., Rosenberger, G., Rost, H. L., Vichalkovski, A., Gstaiger, M., & Aebersold, R. (2013). Quantifying protein interaction dynamics by SWATH mass spectrometry: application to the 14-3-3

- system. *Nat Methods*, 10(12), 1246-1253.
<https://doi.org/10.1038/nmeth.2703>
- Collins, B. C., Gillet, L. C., Rosenberger, G., Röst, H. L., Vichalkovski, A., Gstaiger, M., & Aebersold, R. (2013). Quantifying protein interaction dynamics by SWATH mass spectrometry: application to the 14-3-3 system. *Nat Methods*, 10(12), 1246-1253.
- Cottrill, C. L., & McBrien, N. A. (1996). The M1 muscarinic antagonist pirenzepine reduces myopia and eye enlargement in the tree shrew. *Investigative Ophthalmology and Visual Science*, 37(7), 1368-1379.
- Crowell, A. M., Wall, M. J., & Doucette, A. A. (2013). Maximizing recovery of water-soluble proteins through acetone precipitation. *Anal Chim Acta*, 796, 48-54. <https://doi.org/10.1016/j.aca.2013.08.005>
- Czepita, D., Lodygowska, E., & Czepita, M. (2008). Are children with myopia more intelligent? A literature review. *Ann Acad Med Stetin*, 54(1), 13-16; discussion 16.
- D'Arcangelo, G. (2014). Reelin in the Years: Controlling Neuronal Migration and Maturation in the Mammalian Brain. *Advances in Neuroscience*, 2014, 19, Article 597395. <https://doi.org/10.1155/2014/597395>
- Davidsson, P., Westman, A., Puchades, M., Nilsson, C. L., & Blennow, K. (1999). Characterization of Proteins from Human Cerebrospinal Fluid by a Combination of Preparative Two-Dimensional Liquid-Phase Electrophoresis and Matrix-Assisted Laser Desorption/Ionization Time-of-Flight Mass Spectrometry. *Analytical Chemistry*, 71(3), 642-647. <https://doi.org/10.1021/ac980672w>
- Devin, F., Tsui, I., Morin, B., Duprat, J.-P., & Hubschman, J.-P. (2011). T-shaped scleral buckle for macular detachments in high myopes. *Retina*, 31(1), 177-180.
- Ding, X., Zhang, R., Zhang, S., Zhuang, H., & Xu, G. (2019). Differential expression of connective tissue growth factor and hepatocyte growth factor in the vitreous of patients with high myopia versus vitreomacular interface disease. *BMC Ophthalmol*, 19(1), 25. <https://doi.org/10.1186/s12886-019-1041-1>
- Dolgin, E. (2015). The myopia boom. *Nature*, 519(7543), 276-278. <https://doi.org/10.1038/519276a>
- Domon, B., & Aebersold, R. (2010). Options and considerations when selecting a quantitative proteomics strategy. *Nat Biotechnol*, 28(7), 710-721. <https://doi.org/10.1038/nbt.1661>
- Edwards, M. H. (1998). Effect of parental myopia on the development of myopia in Hong Kong Chinese. *Ophthalmic Physiol Opt*, 18(6), 477-483.
- Ehrlich, D. L., Atkinson, J., Braddick, O., Bobier, W., & Durden, K. (1995). Reduction of infant myopia: a longitudinal cycloplegic study. *Vision Res*, 35(9), 1313-1324. [https://doi.org/10.1016/0042-6989\(94\)00228-e](https://doi.org/10.1016/0042-6989(94)00228-e)
- Elliott, M. H., Smith, D. S., Parker, C. E., & Borchers, C. (2009). Current trends in quantitative proteomics. *Journal of Mass Spectrometry*, 44(12), 1637-1660.
- Engel, M., Maurel, P., Margolis, R. U., & Margolis, R. K. (1996). Chondroitin sulfate proteoglycans in the developing central nervous system. I. cellular sites of synthesis of neurocan and phosphacan. *J Comp Neurol*, 366(1), 34-43. [https://doi.org/10.1002/\(SICI\)1096-9861\(19960226\)366:1<34::AID-CNE3>3.0.CO;2-L](https://doi.org/10.1002/(SICI)1096-9861(19960226)366:1<34::AID-CNE3>3.0.CO;2-L)

- Engvall, E., & Perlmann, P. (1971). Enzyme-linked immunosorbent assay (ELISA) quantitative assay of immunoglobulin G. *Immunochemistry*, 8(9), 871-874. [https://doi.org/https://doi.org/10.1016/0019-2791\(71\)90454-X](https://doi.org/https://doi.org/10.1016/0019-2791(71)90454-X)
- Escher, C., Reiter, L., MacLean, B., Ossola, R., Herzog, F., Chilton, J., MacCoss, M. J., & Rinner, O. (2012). Using iRT, a normalized retention time for more targeted measurement of peptides. *Proteomics*, 12(8), 1111-1121. <https://doi.org/10.1002/pmic.201100463>
- Feldkaemper, M., Diether, S., Kleine, G., & Schaeffel, F. (1999). Interactions of spatial and luminance information in the retina of chickens during myopia development. *Exp Eye Res*, 68(1), 105-115. <https://doi.org/10.1006/exer.1998.0590>
- Feldkaemper, M. P., Neacsu, I., & Schaeffel, F. (2009). Insulin Acts as a Powerful Stimulator of Axial Myopia in Chicks. *Investigative Ophthalmology & Visual Science*, 50(1), 13-23. <https://doi.org/10.1167/iovs.08-1702>
- Fenn, J. B., Mann, M., Meng, C. K., Wong, S. F., & Whitehouse, C. M. (1989). Electrospray ionization for mass spectrometry of large biomolecules. *Science*, 246(4926), 64-71. <https://doi.org/10.1126/science.2675315>
- Fischer, A. J., McGuire, J. J., Schaeffel, F., & Stell, W. K. (1999). Light- and focus-dependent expression of the transcription factor ZENK in the chick retina. *Nat Neurosci*, 2(8), 706-712. <https://doi.org/10.1038/11167>
- Fishman, G. A. (1990). The Vitreous: Structure, Function, and Pathobiology. *Retina*, 10(2), 161-162. http://journals.lww.com/retinajournal/Fulltext/1990/04000/The_Vitreous_Structure_Function_and.18.aspx
- Flitcroft, D. I., He, M., Jonas, J. B., Jong, M., Naidoo, K., Ohno-Matsui, K., Rahi, J., Resnikoff, S., Vitale, S., & Yannuzzi, L. (2019). IMI - Defining and Classifying Myopia: A Proposed Set of Standards for Clinical and Epidemiologic Studies. *Invest Ophthalmol Vis Sci*, 60(3), M20-m30. <https://doi.org/10.1167/iovs.18-25957>
- Foos, R. Y. (1972). Vitreoretinal juncture; topographical variations. *Invest Ophthalmol*, 11(10), 801-808.
- Foster, P. J., & Jiang, Y. (2014). Epidemiology of myopia. *Eye (Lond)*, 28(2), 202-208. <https://doi.org/10.1038/eye.2013.280>
- Foulds, W. S. (1987). Is your vitreous really necessary? *Eye*, 1(6), 641-664. <https://doi.org/10.1038/eye.1987.107>
- French, A. N., Ashby, R. S., Morgan, I. G., & Rose, K. A. (2013). Time outdoors and the prevention of myopia. *Experimental Eye Research*, 114, 58-68. <https://doi.org/https://doi.org/10.1016/j.exer.2013.04.018>
- Frotscher, M. (2010). Role for Reelin in stabilizing cortical architecture. *Trends Neurosci*, 33(9), 407-414. <https://doi.org/10.1016/j.tins.2010.06.001>
- Furley, A. J., Morton, S. B., Manalo, D., Karagogeos, D., Dodd, J., & Jessell, T. M. (1990). The axonal glycoprotein TAG-1 is an immunoglobulin superfamily member with neurite outgrowth-promoting activity. *Cell*, 61(1), 157-170. [https://doi.org/10.1016/0092-8674\(90\)90223-2](https://doi.org/10.1016/0092-8674(90)90223-2)
- Fushimi, D., Arndt, K., Takeichi, M., & Redies, C. (1997). Cloning and expression analysis of cadherin-10 in the CNS of the chicken embryo. *Dev Dyn*, 209(3), 269-285. [https://doi.org/10.1002/\(SICI\)1097-0177\(199707\)209:3<269::AID-AJA3>3.0.CO;2-G](https://doi.org/10.1002/(SICI)1097-0177(199707)209:3<269::AID-AJA3>3.0.CO;2-G)
- Galvis, V., López-Jaramillo, P., Tello, A., Castellanos-Castellanos, Y. A., Camacho, P. A., Cohen, D. D., Gómez-Arbeláez, D., & Merayo-Llodes, J.

- (2016). Is myopia another clinical manifestation of insulin resistance? *Medical Hypotheses*, *90*, 32-40.
- Gao, B. B., Chen, X., Timothy, N., Aiello, L. P., & Feener, E. P. (2008). Characterization of the vitreous proteome in diabetes without diabetic retinopathy and diabetes with proliferative diabetic retinopathy. *J Proteome Res*, *7*(6), 2516-2525. <https://doi.org/10.1021/pr800112g>
- García-Ramírez, M., Canals, F., Hernández, C., Colomé, N., Ferrer, C., Carrasco, E., García-Arumí, J., & Simó, R. (2007). Proteomic analysis of human vitreous fluid by fluorescence-based difference gel electrophoresis (DIGE): a new strategy for identifying potential candidates in the pathogenesis of proliferative diabetic retinopathy. *Diabetologia*, *50*(6), 1294-1303. <https://doi.org/10.1007/s00125-007-0627-y>
- García-Rodríguez, S., Castilla, S. A., Machado, A., & Ayala, A. (2003). Comparison of methods for sample preparation of individual rat cerebrospinal fluid samples prior to two-dimensional polyacrylamide gel electrophoresis. *Biotechnol Lett*, *25*(22), 1899-1903. <https://doi.org/10.1023/b:bile.0000003979.92664.11>
- Gerber, S. A., Rush, J., Stemman, O., Kirschner, M. W., & Gygi, S. P. (2003). Absolute quantification of proteins and phosphoproteins from cell lysates by tandem MS. *Proceedings of the National Academy of Sciences*, *100*(12), 6940-6945.
- Geyer, P. E., Holdt, L. M., Teupser, D., & Mann, M. (2017). Revisiting biomarker discovery by plasma proteomics. *Molecular Systems Biology*, *13*(9), 942. <https://doi.org/https://doi.org/10.15252/msb.20156297>
- Gibson, U. E., Heid, C. A., & Williams, P. M. (1996). A novel method for real time quantitative RT-PCR. *Genome Res*, *6*(10), 995-1001. <https://doi.org/10.1101/gr.6.10.995>
- Gillespie, J. R., & Uversky, V. N. (2000). Structure and function of alpha-fetoprotein: a biophysical overview. *Biochim Biophys Acta*, *1480*(1-2), 41-56. [https://doi.org/10.1016/s0167-4838\(00\)00104-7](https://doi.org/10.1016/s0167-4838(00)00104-7)
- Gillet, L. C., Navarro, P., Tate, S., Rost, H., Selevsek, N., Reiter, L., Bonner, R., & Aebersold, R. (2012). Targeted data extraction of the MS/MS spectra generated by data-independent acquisition: a new concept for consistent and accurate proteome analysis. *Mol Cell Proteomics*, *11*(6), O111016717. <https://doi.org/10.1074/mcp.O111.016717>
- Glasser, A., & Howland, H. C. (1995). In vitro changes in back vertex distance of chick and pigeon lenses: species differences and the effects of aging. *Vision Res*, *35*(13), 1813-1824. [https://doi.org/10.1016/0042-6989\(94\)00292-t](https://doi.org/10.1016/0042-6989(94)00292-t)
- Goedhart, J., & Luijsterburg, M. S. (2020). VolcanoNoseR is a web app for creating, exploring, labeling and sharing volcano plots. *Sci Rep*, *10*(1), 20560. <https://doi.org/10.1038/s41598-020-76603-3>
- Gogate, P., Mukhopadhyaya, D., Mahadik, A., Naduvilath, T. J., Sane, S., Shinde, A., & Holden, B. (2013). Spectacle compliance amongst rural secondary school children in Pune district, India. *Indian journal of ophthalmology*, *61*(1), 8.
- Gong, B., Liu, X., Zhang, D., Wang, P., Huang, L., Lin, Y., Lu, F., Ma, S., Cheng, J., Chen, R., Li, X., Lin, H., Zeng, G., Zhu, X., Hu, J., Yang, Z., & Shi, Y. (2013). Evaluation of MMP2 as a candidate gene for high myopia. *Mol Vis*, *19*, 121-127. <https://www.ncbi.nlm.nih.gov/pubmed/23378725>

- Govaert, E., Van Steendam, K., Willems, S., Vossaert, L., Dhaenens, M., & Deforce, D. (2017). Comparison of fractionation proteomics for local SWATH library building. *Proteomics*, *17*(15-16). <https://doi.org/10.1002/pmic.201700052>
- Green, A. A., & Hughes, W. L. (1955). [10] Protein fractionation on the basis of solubility in aqueous solutions of salts and organic solvents.
- Gregorich, Z. R., Chang, Y.-H., & Ge, Y. (2014). Proteomics in heart failure: top-down or bottom-up? *Pflugers Archiv : European journal of physiology*, *466*(6), 1199-1209. <https://doi.org/10.1007/s00424-014-1471-9>
- Griffin, N. M., & Schnitzer, J. E. (2011). Overcoming Key Technological Challenges in Using Mass Spectrometry for Mapping Cell Surfaces in Tissues. *Molecular & Cellular Proteomics*, *10*.
- Grotendorst, G. R. (1997). Connective tissue growth factor: a mediator of TGF- β action on fibroblasts. *Cytokine & growth factor reviews*, *8*(3), 171-179.
- Guell, J. L., & Muller, A. (1996). Laser in situ keratomileusis (LASIK) for myopia from -7 to -18 diopters. *J Refract Surg*, *12*(2), 222-228. <http://www.ncbi.nlm.nih.gov/pubmed/8653524>
- Guo, J., & Huan, T. (2020). Comparison of Full-Scan, Data-Dependent, and Data-Independent Acquisition Modes in Liquid Chromatography–Mass Spectrometry Based Untargeted Metabolomics. *Analytical Chemistry*, *92*(12), 8072-8080. <https://doi.org/10.1021/acs.analchem.9b05135>
- Guo, X., & Kristal, B. S. (2012). The use of underloaded C(18) solid-phase extraction plates increases reproducibility of analysis of tryptic peptides from unfractionated human plasma. *Analytical Biochemistry*, *426*(1), 86-90. <https://doi.org/10.1016/j.ab.2012.04.003>
- Halbleib, J. M., & Nelson, W. J. (2006). Cadherins in development: cell adhesion, sorting, and tissue morphogenesis. *Genes Dev*, *20*(23), 3199-3214. <https://doi.org/10.1101/gad.1486806>
- Halfter, W., Dong, S., Dong, A., Eller, A. W., & Nischt, R. (2008). Origin and turnover of ECM proteins from the inner limiting membrane and vitreous body. *Eye (Lond)*, *22*(10), 1207-1213. <https://doi.org/10.1038/eye.2008.19>
- Halfter, W., Dong, S., Schurer, B., Ring, C., Cole, G. J., & Eller, A. (2005). Embryonic synthesis of the inner limiting membrane and vitreous body. *Invest Ophthalmol Vis Sci*, *46*(6), 2202-2209. <https://doi.org/10.1167/iovs.04-1419>
- Hammond, D. S., Wallman, J., & Wildsoet, C. F. (2013). Dynamics of active emmetropisation in young chicks – influence of sign and magnitude of imposed defocus. *Ophthalmic and Physiological Optics*, *33*(3), 215-226. <https://doi.org/https://doi.org/10.1111/opo.12056>
- Hao, C., & March, R. E. (2001). Electrospray ionization tandem mass spectrometric study of salt cluster ions: Part 2 — Salts of polyatomic acid groups and of multivalent metals. *Journal of Mass Spectrometry*, *36*(5), 509-521. <https://doi.org/10.1002/jms.150>
- Hernández, C., García-Ramírez, M., Colomé, N., Villarroel, M., Corraliza, L., García-Pacual, L., Casado, J., Canals, F., & Simó, R. (2010). New Pathogenic Candidates for Diabetic Macular Edema Detected By Proteomic Analysis. *Diabetes Care*, *33*(7), e92-e92. <https://doi.org/10.2337/dc10-0232>
- Hernández, C., Lecube, A., Segura, R. M., Sararols, L., & Simó, R. (2002). Nitric oxide and vascular endothelial growth factor concentrations are increased

- but not related in vitreous fluid of patients with proliferative diabetic retinopathy. *Diabetic Medicine*, 19(8), 655-660.
<https://doi.org/https://doi.org/10.1046/j.1464-5491.2002.00768.x>
- Hiesberger, T., Trommsdorff, M., Howell, B. W., Goffinet, A., Mumby, M. C., Cooper, J. A., & Herz, J. (1999). Direct binding of Reelin to VLDL receptor and ApoE receptor 2 induces tyrosine phosphorylation of disabled-1 and modulates tau phosphorylation. *Neuron*, 24(2), 481-489.
<https://www.ncbi.nlm.nih.gov/pubmed/10571241>
- Hindson, V. J., Gallagher, J. T., Halfter, W., & Bishop, P. N. (2005). Opticin binds to heparan and chondroitin sulfate proteoglycans. *Invest Ophthalmol Vis Sci*, 46(12), 4417-4423. <https://doi.org/10.1167/iovs.05-0883>
- Holden, A. L., Hodos, W., Hayes, B. P., & Fitzke, F. W. (1988). Myopia: induced, normal and clinical. *Eye (Lond)*, 2 Suppl, S242-256.
<https://doi.org/10.1038/eye.1988.148>
- Holden, B. A., Fricke, T. R., Wilson, D. A., Jong, M., Naidoo, K. S., Sankaridurg, P., Wong, T. Y., Naduvilath, T. J., & Resnikoff, S. (2016). Global Prevalence of Myopia and High Myopia and Temporal Trends from 2000 through 2050. *Ophthalmology*, 123(5), 1036-1042.
<https://doi.org/10.1016/j.ophtha.2016.01.006>
- Holekamp, N. M., Shui, Y. B., & Beebe, D. C. (2005). Vitrectomy surgery increases oxygen exposure to the lens: a possible mechanism for nuclear cataract formation. *Am J Ophthalmol*, 139(2), 302-310.
<https://doi.org/10.1016/j.ajo.2004.09.046>
- Holguin, A. M. C., Congdon, N., Patel, N., Ratcliffe, A., Estes, P., Flores, S. T., Gilbert, D., Rito, M. A. P., & Munoz, B. (2006). Factors Associated with Spectacle-Wear Compliance in School-Aged Mexican Children. *Investigative Ophthalmology & Visual Science*, 47(3), 925-928.
<https://doi.org/10.1167/iovs.05-0895>
- Holmes, S., Downs, A. M., Fosberry, A., Hayes, P., Michalovich, D., Murdoch, P., Moores, K., Fox, J., Deen, K., & Pettman, G. (2002). Sema7A is a potent monocyte stimulator. *Scandinavian journal of immunology*, 56(3), 270-275.
- Holy, C., Kulkarni, K., & Brennan, N. A. (2019). Predicting Costs and Disability from the Myopia Epidemic – A Worldwide Economic and Social Model. *Investigative Ophthalmology & Visual Science*, 60(9), 5466-5466.
- Howlett, M. H., & McFadden, S. A. (2006). Form-deprivation myopia in the guinea pig (*Cavia porcellus*). *Vision Res*, 46(1-2), 267-283.
<https://doi.org/10.1016/j.visres.2005.06.036>
- Howlett, M. H., & McFadden, S. A. (2007). Emmetropization and schematic eye models in developing pigmented guinea pigs. *Vision Res*, 47(9), 1178-1190. <https://doi.org/10.1016/j.visres.2006.12.019>
- Howlett, M. H. C., & McFadden, S. A. (2009). Spectacle lens compensation in the pigmented guinea pig. *Vision Research*, 49(2), 219-227.
<https://doi.org/https://doi.org/10.1016/j.visres.2008.10.008>
- Hu, A., Noble, W. S., & Wolf-Yadlin, A. (2016). Technical advances in proteomics: new developments in data-independent acquisition. *F1000Res*, 5. <https://doi.org/10.12688/f1000research.7042.1>
- Hu, A., Noble, W. S., & Wolf-Yadlin, A. (2016). Technical advances in proteomics: new developments in data-independent acquisition. *F1000Res*, 5.

- Huang, Q., Yang, L., Luo, J., Guo, L., Wang, Z., Yang, X., Jin, W., Fang, Y., Ye, J., Shan, B., & Zhang, Y. (2015). SWATH enables precise label-free quantification on proteome scale. *Proteomics*, *15*(7), 1215-1223. <https://doi.org/10.1002/pmic.201400270>
- Hughes, C., Ma, B., & Lajoie, G. A. (2010). De novo sequencing methods in proteomics. In *Proteome Bioinformatics* (pp. 105-121). Springer.
- Ibrahim, H. K., El-Leithy, I. S., & Makky, A. A. (2010). Mucoadhesive nanoparticles as carrier systems for prolonged ocular delivery of gatifloxacin/prednisolone bitherapy. *Mol Pharm*, *7*(2), 576-585. <https://doi.org/10.1021/mp900279c>
- Ignjatovic, V., Mertyn, E., & Monagle, P. (2011). The Coagulation System in Children: Developmental and Pathophysiological Considerations. *Semin Thromb Hemost*, *37*(07), 723-729.
- Inatani, M., Tanihara, H., Oohira, A., Honjo, M., & Honda, Y. (1999). Identification of a nervous tissue-specific chondroitin sulfate proteoglycan, neurocan, in developing rat retina. *Invest Ophthalmol Vis Sci*, *40*(10), 2350-2359. <https://www.ncbi.nlm.nih.gov/pubmed/10476802>
- Ip, J. M., Huynh, S. C., Robaei, D., Rose, K. A., Morgan, I. G., Smith, W., Kifley, A., & Mitchell, P. (2007). Ethnic Differences in the Impact of Parental Myopia: Findings from a Population-Based Study of 12-Year-Old Australian Children. *Investigative Ophthalmology & Visual Science*, *48*(6), 2520-2528. <https://doi.org/10.1167/iovs.06-0716>
- Irving, E. L., Sivak, J. G., & Callender, M. G. (1992). Refractive plasticity of the developing chick eye. *Ophthalmic Physiol Opt*, *12*(4), 448-456. <https://www.ncbi.nlm.nih.gov/pubmed/1293533>
- Iwasaki, M., Akiba, Y., & Kaunitz, J. D. (2019). Recent advances in vasoactive intestinal peptide physiology and pathophysiology: focus on the gastrointestinal system. *F1000Res*, *8*. <https://doi.org/10.12688/f1000research.18039.1>
- J, S. (1989). *The Vitreous: Structure, Function, and Pathobiology*. New York, Springer-Verlag.
- Jobling, A. I., Wan, R., Gentle, A., Bui, B. V., & McBrien, N. A. (2009). Retinal and choroidal TGF-beta in the tree shrew model of myopia: isoform expression, activation and effects on function. *Exp Eye Res*, *88*(3), 458-466. <https://doi.org/10.1016/j.exer.2008.10.022>
- Johnson, B. H., & Hecht, M. H. (1994). Recombinant proteins can be isolated from *E. coli* cells by repeated cycles of freezing and thawing. *Biotechnology (N Y)*, *12*(13), 1357-1360. <https://doi.org/10.1038/nbt1294-1357>
- Kachuk, C., Faulkner, M., Liu, F., & Doucette, A. A. (2016). Automated SDS Depletion for Mass Spectrometry of Intact Membrane Proteins through Transmembrane Electrophoresis. *J Proteome Res*, *15*(8), 2634-2642. <https://doi.org/10.1021/acs.jproteome.6b00199>
- Kanemaki, N., Meguro, A., Yamane, T., Takeuchi, M., Okada, E., Iijima, Y., & Mizuki, N. (2015). Study of association of PAX6 polymorphisms with susceptibility to high myopia in a Japanese population. *Clin Ophthalmol*, *9*, 2005-2011. <https://doi.org/10.2147/ophth.S95167>
- Kang, B. S., Lam, T. C., Cheung, J. K., Li, K. K., & Kee, C. S. (2019). Data on corneal proteome and differentially expressed corneal proteins in highly

- myopic chicks using a data independent quantification approach. *Data Brief*, 26, 104478. <https://doi.org/10.1016/j.dib.2019.104478>
- Kapp, E. A., Schütz, F., Connolly, L. M., Chakel, J. A., Meza, J. E., Miller, C. A., Fenyo, D., Eng, J. K., Adkins, J. N., Omenn, G. S., & Simpson, R. J. (2005). An evaluation, comparison, and accurate benchmarking of several publicly available MS/MS search algorithms: sensitivity and specificity analysis. *Proteomics*, 5(13), 3475-3490. <https://doi.org/10.1002/pmic.200500126>
- Karagozeos, D., Morton, S. B., Casano, F., Dodd, J., & Jessell, T. M. (1991). Developmental expression of the axonal glycoprotein TAG-1: differential regulation by central and peripheral neurons in vitro. *Development*, 112(1), 51-67. <https://www.ncbi.nlm.nih.gov/pubmed/1769341>
- Karas, M., & Hillenkamp, F. (1988). Laser desorption ionization of proteins with molecular masses exceeding 10,000 daltons. *Anal Chem*, 60(20), 2299-2301. <https://doi.org/10.1021/ac00171a028>
- Keay, L., Zeng, Y., Munoz, B., He, M., & Friedman, D. S. (2010). Predictors of early acceptance of free spectacles provided to junior high school students in China. *Archives of Ophthalmology*, 128(10), 1328-1334.
- Kee, C. S., Marzani, D., & Wallman, J. (2001). Differences in time course and visual requirements of ocular responses to lenses and diffusers. *Invest Ophthalmol Vis Sci*, 42(3), 575-583. <https://www.ncbi.nlm.nih.gov/pubmed/11222513>
- Kim, B., De La Monte, S., Hovanesian, V., Patra, A., Chen, X., Chen, R. H., Miller, M. C., Pinar, M. H., Lim, Y. P., & Stopa, E. G. (2020). Ontogeny of inter-alpha inhibitor protein (IAIP) expression in human brain. *Journal of neuroscience research*, 98(5), 869-887.
- Kim, T., Kim, S. J., Kim, K., Kang, U. B., Lee, C., Park, K. S., Yu, H. G., & Kim, Y. (2007). Profiling of vitreous proteomes from proliferative diabetic retinopathy and nondiabetic patients. *Proteomics*, 7(22), 4203-4215. <https://doi.org/10.1002/pmic.200700745>
- Kisilak, M. L., Campbell, M. C., Hunter, J. J., Irving, E. L., & Huang, L. (2006). Aberrations of chick eyes during normal growth and lens induction of myopia. *J Comp Physiol A Neuroethol Sens Neural Behav Physiol*, 192(8), 845-855. <https://doi.org/10.1007/s00359-006-0122-9>
- Kiyonami, R., & Domon, B. (2010). Selected reaction monitoring applied to quantitative proteomics. *Methods Mol Biol*, 658, 155-166. https://doi.org/10.1007/978-1-60761-780-8_9
- Köcher, T., Pichler, P., Swart, R., & Mechtler, K. (2012). Analysis of protein mixtures from whole-cell extracts by single-run nanoLC-MS/MS using ultralong gradients. *Nat Protoc*, 7(5), 882-890. <https://doi.org/10.1038/nprot.2012.036>
- Koh, V., Yang, A., Saw, S. M., Chan, Y. H., Lin, S. T., Tan, M. M., Tey, F., Nah, G., & Ikram, M. K. (2014). Differences in prevalence of refractive errors in young Asian males in Singapore between 1996-1997 and 2009-2010. *Ophthalmic Epidemiol*, 21(4), 247-255. <https://doi.org/10.3109/09286586.2014.928824>
- Kohfeldt, E., Sasaki, T., Gohring, W., & Timpl, R. (1998). Nidogen-2: a new basement membrane protein with diverse binding properties. *J Mol Biol*, 282(1), 99-109. <https://doi.org/10.1006/jmbi.1998.2004>

- Kondrat, R. W., McClusky, G. A., & Cooks, R. G. (1978). Multiple reaction monitoring in mass spectrometry/mass spectrometry for direct analysis of complex mixtures. *Analytical Chemistry*, 50(14), 2017-2021. <https://doi.org/10.1021/ac50036a020>
- Kong, R. P., Siu, S. O., Lee, S. S., Lo, C., & Chu, I. K. (2011). Development of online high-/low-pH reversed-phase-reversed-phase two-dimensional liquid chromatography for shotgun proteomics: a reversed-phase-strong cation exchange-reversed-phase approach. *J Chromatogr A*, 1218(23), 3681-3688. <https://doi.org/10.1016/j.chroma.2011.04.022>
- Konigsberg, W. (1972). [13] Reduction of disulfide bonds in proteins with dithiothreitol. In *Methods in enzymology* (Vol. 25, pp. 185-188). Elsevier.
- Koss, M. J., Hoffmann, J., Nguyen, N., Pfister, M., Mischak, H., Mullen, W., Husi, H., Rejdak, R., Koch, F., Jankowski, J., Krueger, K., Bertelmann, T., Klein, J., Schanstra, J. P., & Siwy, J. (2014). Proteomics of vitreous humor of patients with exudative age-related macular degeneration. *PLoS One*, 9(5), e96895. <https://doi.org/10.1371/journal.pone.0096895>
- Kuzyk, M. A., Smith, D., Yang, J., Cross, T. J., Jackson, A. M., Hardie, D. B., Anderson, N. L., & Borchers, C. H. (2009). Multiple Reaction Monitoring-based, Multiplexed, Absolute Quantitation of 45 Proteins in Human Plasma*. *Molecular & Cellular Proteomics*, 8(8), 1860-1877. <https://doi.org/https://doi.org/10.1074/mcp.M800540-MCP200>
- Laicine, E. M., & Haddad, A. (1994). Transferrin, one of the major vitreous proteins, is produced within the eye. *Exp Eye Res*, 59(4), 441-445. <https://doi.org/10.1006/exer.1994.1129>
- Lam, C. S. Y., Tang, W. C., Tse, D. Y.-y., Lee, R. P. K., Chun, R. K. M., Hasegawa, K., Qi, H., Hatanaka, T., & To, C. H. (2020). Defocus Incorporated Multiple Segments (DIMS) spectacle lenses slow myopia progression: a 2-year randomised clinical trial. *British Journal of Ophthalmology*, 104(3), 363-368. <https://doi.org/10.1136/bjophthalmol-2018-313739>
- Lam, T. C., Li, K. K., Lo, S. C., Guggenheim, J. A., & To, C. H. (2006). A chick retinal proteome database and differential retinal protein expressions during early ocular development. *J Proteome Res*, 5(4), 771-784. <https://doi.org/10.1021/pr050280n>
- Lam, T. C., Li, K. K., Lo, S. C., Guggenheim, J. A., & To, C. H. (2007). Application of fluorescence difference gel electrophoresis technology in searching for protein biomarkers in chick myopia. *J Proteome Res*, 6(11), 4135-4149. <https://doi.org/10.1021/pr0701097>
- Lambert, J. P., Ivosev, G., Couzens, A. L., Larsen, B., Taipale, M., Lin, Z. Y., Zhong, Q., Lindquist, S., Vidal, M., Aebersold, R., Pawson, T., Bonner, R., Tate, S., & Gingras, A. C. (2013). Mapping differential interactomes by affinity purification coupled with data-independent mass spectrometry acquisition. *Nat Methods*, 10(12), 1239-1245. <https://doi.org/10.1038/nmeth.2702>
- Larsson, L. I., Fahrenkrug, J., Schaffalitzky De Muckadell, O., Sundler, F., Håkanson, R., & Rehfeld, J. R. (1976). Localization of vasoactive intestinal polypeptide (VIP) to central and peripheral neurons. *Proc Natl Acad Sci U S A*, 73(9), 3197-3200. <https://doi.org/10.1073/pnas.73.9.3197>

- Lathe, G. H., & Ruthven, C. R. (1955). The separation of substances on the basis of their molecular weights, using columns of starch and water. *Biochem J*, 60(4), xxxiv.
- Le Goff, M. M., & Bishop, P. N. (2008). Adult vitreous structure and postnatal changes. *Eye (Lond)*, 22(10), 1214-1222. <https://doi.org/10.1038/eye.2008.21>
- Lee, B., Litt, M., & Buchsbaum, G. (1992). Rheology of the vitreous body. Part I: Viscoelasticity of human vitreous. *Biorheology*, 29(5-6), 521-533. <https://doi.org/10.3233/bir-1992-295-612>
- Leemhuis, J., Bouche, E., Frotscher, M., Henle, F., Hein, L., Herz, J., Meyer, D. K., Pichler, M., Roth, G., Schwan, C., & Bock, H. H. (2010). Reelin signals through apolipoprotein E receptor 2 and Cdc42 to increase growth cone motility and filopodia formation. *J Neurosci*, 30(44), 14759-14772. <https://doi.org/10.1523/jneurosci.4036-10.2010>
- Leo, S. W., & Young, T. L. (2011). An evidence-based update on myopia and interventions to retard its progression. *J AAPOS*, 15(2), 181-189. <https://doi.org/10.1016/j.jaapos.2010.09.020>
- Lezoualc'h, F., Engert, S., Berning, B., & Behl, C. (2000). Corticotropin-Releasing Hormone-Mediated Neuroprotection against Oxidative Stress Is Associated with the Increased Release of Non-amyloidogenic Amyloid β Precursor Protein and with the Suppression of Nuclear Factor- κ B. *Molecular Endocrinology*, 14(1), 147-159. <https://doi.org/10.1210/mend.14.1.0403>
- Liang, C.-L., Yen, E., Su, J.-Y., Liu, C., Chang, T.-Y., Park, N., Wu, M.-J., Lee, S., Flynn, J. T., & Juo, S.-H. H. (2004). Impact of Family History of High Myopia on Level and Onset of Myopia. *Investigative Ophthalmology & Visual Science*, 45(10), 3446-3452. <https://doi.org/10.1167/iovs.03-1058>
- Liang, C. L., Wang, H. S., Hung, K. S., Hsi, E., Sun, A., Kuo, Y. H., & Juo, S. H. (2006). Evaluation of MMP3 and TIMP1 as candidate genes for high myopia in young Taiwanese men. *Am J Ophthalmol*, 142(3), 518-520. <https://doi.org/10.1016/j.ajo.2006.03.063>
- Lim, R., Mitchell, P., & Cumming, R. G. (1999). Refractive Associations with Cataract: the Blue Mountains Eye Study. *Investigative Ophthalmology & Visual Science*, 40(12), 3021-3026.
- Lin, H. J., Kung, Y. J., Lin, Y. J., Sheu, J. J., Chen, B. H., Lan, Y. C., Lai, C. H., Hsu, Y. A., Wan, L., & Tsai, F. J. (2010). Association of the lumican gene functional 3'-UTR polymorphism with high myopia. *Invest Ophthalmol Vis Sci*, 51(1), 96-102. <https://doi.org/10.1167/iovs.09-3612>
- Lin, H. J., Wan, L., Tsai, Y., Chen, W. C., Tsai, S. W., & Tsai, F. J. (2010). The association between lumican gene polymorphisms and high myopia. *Eye (Lond)*, 24(6), 1093-1101. <https://doi.org/10.1038/eye.2009.254>
- Lin, H. J., Wan, L., Tsai, Y., Tsai, Y. Y., Fan, S. S., Tsai, C. H., & Tsai, F. J. (2006). The TGFbeta1 gene codon 10 polymorphism contributes to the genetic predisposition to high myopia. *Mol Vis*, 12, 698-703. <https://www.ncbi.nlm.nih.gov/pubmed/16807529>
- <http://www.molvis.org/molvis/v12/a78/v12a78-lin.pdf>
- Lin, L. L., Shih, Y. F., Hsiao, C. K., Chen, C. J., Lee, L. A., & Hung, P. T. (2001). Epidemiologic study of the prevalence and severity of myopia among

- schoolchildren in Taiwan in 2000. *J Formos Med Assoc*, 100(10), 684-691.
- Lin, L. L., Shih, Y. F., Tsai, C. B., Chen, C. J., Lee, L. A., Hung, P. T., & Hou, P. K. (1999). Epidemiologic study of ocular refraction among schoolchildren in Taiwan in 1995. *Optom Vis Sci*, 76(5), 275-281.
<http://www.ncbi.nlm.nih.gov/pubmed/10375241>
- Lin, Y., Zhou, J., Bi, D., Chen, P., Wang, X., & Liang, S. (2008). Sodium-deoxycholate-assisted tryptic digestion and identification of proteolytically resistant proteins. *Anal Biochem*, 377(2), 259-266.
<https://doi.org/10.1016/j.ab.2008.03.009>
- Lindstrom, R. L., Hardten, D. R., & Chu, Y. R. (1997). Laser In Situ keratomileusis (LASIK) for the treatment of low moderate, and high myopia. *Trans Am Ophthalmol Soc*, 95, 285-296; discussion 296-306.
- Link, A. J., Eng, J., Schieltz, D. M., Carmack, E., Mize, G. J., Morris, D. R., Garvik, B. M., & Yates, J. R., 3rd. (1999). Direct analysis of protein complexes using mass spectrometry. *Nat Biotechnol*, 17(7), 676-682.
<https://doi.org/10.1038/10890>
- Liu, H., Sadygov, R. G., & Yates, J. R., 3rd. (2004). A model for random sampling and estimation of relative protein abundance in shotgun proteomics. *Anal Chem*, 76(14), 4193-4201.
<https://doi.org/10.1021/ac0498563>
- Liu, Q., Duff, R. J., Liu, B., Wilson, A. L., Babb-Clendenon, S. G., Francl, J., & Marrs, J. A. (2006). Expression of cadherin10, a type II classic cadherin gene, in the nervous system of the embryonic zebrafish. *Gene Expr Patterns*, 6(7), 703-710. <https://doi.org/10.1016/j.modgep.2005.12.009>
- Liu, S. Z., Wang, H., Jiang, J. J., Wang, P. B., Wu, X. Y., Tan, X. P., & Xia, Z. H. (2005). [Dynamic expression of VIPR2 in form deprivation myopia]. *Zhong Nan Da Xue Xue Bao Yi Xue Ban*, 30(4), 456-459.
<https://www.ncbi.nlm.nih.gov/pubmed/16190398>
- Liu, Y., Bouhenni, R. A., Dufresne, C. P., Semba, R. D., & Edward, D. P. (2016). Differential Expression of Vitreous Proteins in Young and Mature New Zealand White Rabbits. *PLoS One*, 11(4), e0153560.
<https://doi.org/10.1371/journal.pone.0153560>
- Liu, Y., Hüttenhain, R., Surinova, S., Gillet, L. C., Mouritsen, J., Brunner, R., Navarro, P., & Aebersold, R. (2013). Quantitative measurements of N-linked glycoproteins in human plasma by SWATH-MS. *Proteomics*, 13(8), 1247-1256.
- Lord, M. S., Melrose, J., Day, A. J., & Whitelock, J. M. (2020). The Inter- α -Trypsin Inhibitor Family: Versatile Molecules in Biology and Pathology. *Journal of Histochemistry & Cytochemistry*, 68(12), 907-927.
<https://doi.org/10.1369/0022155420940067>
- Loukovaara, S., Nurkkala, H., Tamene, F., Gucciardo, E., Liu, X., Repo, P., Lehti, K., & Varjosalo, M. (2015). Quantitative Proteomics Analysis of Vitreous Humor from Diabetic Retinopathy Patients. *J Proteome Res*, 14(12), 5131-5143. <https://doi.org/10.1021/acs.jproteome.5b00900>
- Lui, W. O., & Edwards, M. H. (2000). Orthokeratology in low myopia. Part 1: efficacy and predictability. *Cont Lens Anterior Eye*, 23(3), 77-89.
<http://www.ncbi.nlm.nih.gov/pubmed/16303436>
- Luo, S., Xu, H., Yang, L., Gong, X., Shen, J., Chen, X., & Wu, Z. (2022). Quantitative proteomics analysis of human vitreous in rhegmatogenous

- retinal detachment associated with choroidal detachment by data-independent acquisition mass spectrometry. *Molecular and Cellular Biochemistry*. <https://doi.org/10.1007/s11010-022-04409-0>
- Luo, Y., Huang, K., Zheng, J., Zhang, J., & Zhang, L. (2019). TGF-beta1 promotes cell migration in hepatocellular carcinoma by suppressing reelin expression. *Gene*, 688, 19-25. <https://doi.org/10.1016/j.gene.2018.11.033>
- Luong, T. Q., Shu, Y.-H., Modjtahedi, B. S., Fong, D. S., Choudry, N., Tanaka, Y., & Nau, C. L. (2020). Racial and Ethnic Differences in Myopia Progression in a Large, Diverse Cohort of Pediatric Patients. *Investigative Ophthalmology & Visual Science*, 61(13), 20-20. <https://doi.org/10.1167/iovs.61.13.20>
- MacLean, B., Tomazela, D. M., Shulman, N., Chambers, M., Finney, G. L., Frewen, B., Kern, R., Tabb, D. L., Liebler, D. C., & MacCoss, M. J. (2010). Skyline: an open source document editor for creating and analyzing targeted proteomics experiments. *Bioinformatics*, 26(7), 966-968. <https://doi.org/10.1093/bioinformatics/btq054>
- Mahajan, V. B., & Skeie, J. M. (2014). Translational vitreous proteomics. *Proteomics Clin Appl*, 8(3-4), 204-208. <https://doi.org/10.1002/prca.201300062>
- Manadas, B., Mendes, V. M., English, J., & Dunn, M. J. (2010). Peptide fractionation in proteomics approaches. *Expert Rev Proteomics*, 7(5), 655-663. <https://doi.org/10.1586/epr.10.46>
- Mandal, N., Lewis, G. P., Fisher, S. K., Heegaard, S., Prause, J. U., la Cour, M., Vorum, H., & Honore, B. (2015). Proteomic Analysis of the Vitreous following Experimental Retinal Detachment in Rabbits. *J Ophthalmol*, 2015, 583040. <https://doi.org/10.1155/2015/583040>
- Margolis, R. K., Rauch, U., Maurel, P., & Margolis, R. U. (1996). Neurocan and phosphacan: two major nervous tissue-specific chondroitin sulfate proteoglycans. *Perspect Dev Neurobiol*, 3(4), 273-290. <https://www.ncbi.nlm.nih.gov/pubmed/9117260>
- Mathis, U., & Schaeffel, F. (2007). Glucagon-related peptides in the mouse retina and the effects of deprivation of form vision. *Graefes Arch Clin Exp Ophthalmol*, 245(2), 267-275. <https://doi.org/10.1007/s00417-006-0282-x>
- McBrien, N. A. (2013). Regulation of scleral metabolism in myopia and the role of transforming growth factor-beta. *Exp Eye Res*, 114, 128-140. <https://doi.org/10.1016/j.exer.2013.01.014>
- McDonald, W. H., & Yates, J. R., 3rd. (2002). Shotgun proteomics and biomarker discovery. *Dis Markers*, 18(2), 99-105. <https://doi.org/10.1155/2002/505397>
- McGlinn, A. M., Baldwin, D. A., Tobias, J. W., Budak, M. T., Khurana, T. S., & Stone, R. A. (2007). Form-deprivation myopia in chick induces limited changes in retinal gene expression. *Investigative Ophthalmology & Visual Science*, 48(8), 3430-3436. <https://doi.org/10.1167/iovs.06-1538>
- Megaw, P. L., Morgan, I. G., & Boelen, M. K. (1997). Dopaminergic behaviour in chicken retina and the effect of form deprivation. *Aust N Z J Ophthalmol*, 25 Suppl 1, S76-78. <http://www.ncbi.nlm.nih.gov/pubmed/9267633>
- Meyer-Puttlitz, B., Junker, E., Margolis, R. U., & Margolis, R. K. (1996). Chondroitin sulfate proteoglycans in the developing central nervous system. II. Immunocytochemical localization of neurocan and phosphacan.

- J Comp Neurol*, 366(1), 44-54. [https://doi.org/10.1002/\(SICI\)1096-9861\(19960226\)366:1<44::AID-CNE4>3.0.CO;2-K](https://doi.org/10.1002/(SICI)1096-9861(19960226)366:1<44::AID-CNE4>3.0.CO;2-K)
- Meyer, K., & Palmer, J. W. THE POLYSACCHARIDE OF THE VITREOUS HUMOR.
- Mi, H., Muruganujan, A., Ebert, D., Huang, X., & Thomas, P. D. (2019). PANTHER version 14: more genomes, a new PANTHER GO-slim and improvements in enrichment analysis tools. *Nucleic Acids Res*, 47(D1), D419-D426. <https://doi.org/10.1093/nar/gky1038>
- Milev, P., Maurel, P., Haring, M., Margolis, R. K., & Margolis, R. U. (1996). TAG-1/axonin-1 is a high-affinity ligand of neurocan, phosphacan/protein-tyrosine phosphatase-zeta/beta, and N-CAM. *J Biol Chem*, 271(26), 15716-15723. <https://doi.org/10.1074/jbc.271.26.15716>
- Mirakaj, V., Brown, S., Laucher, S., Steinl, C., Klein, G., Köhler, D., Skutella, T., Meisel, C., Brommer, B., & Rosenberger, P. (2011). Repulsive guidance molecule-A (RGM-A) inhibits leukocyte migration and mitigates inflammation. *Proceedings of the National Academy of Sciences*, 108(16), 6555-6560.
- Mirshahi, A., Ponto, K. A., Hoehn, R., Zwiener, I., Zeller, T., Lackner, K., Beutel, M. E., & Pfeiffer, N. (2014). Myopia and level of education: results from the Gutenberg Health Study. *Ophthalmology*, 121(10), 2047-2052. <https://doi.org/10.1016/j.ophtha.2014.04.017>
- Mirza, S. P., Halligan, B. D., Greene, A. S., & Olivier, M. (2007). Improved method for the analysis of membrane proteins by mass spectrometry. *Physiol Genomics*, 30(1), 89-94. <https://doi.org/10.1152/physiolgenomics.00279.2006>
- Montemurro, N., Orfanoti, A., Manasfi, R., Thomaidis, N. S., & Pérez, S. (2020). Comparison of high resolution mrm and sequential window acquisition of all theoretical fragment-ion acquisition modes for the quantitation of 48 wastewater-borne pollutants in lettuce. *Journal of Chromatography A*, 1631, 461566. <https://doi.org/https://doi.org/10.1016/j.chroma.2020.461566>
- Moon, S. H., Lee, J. H., Ahn, D. U., & Paik, H. D. (2015). In vitro antioxidant and mineral-chelating properties of natural and autocleaved ovotransferrin. *J Sci Food Agric*, 95(10), 2065-2070. <https://doi.org/10.1002/jsfa.6921>
- Morgan, I., & Rose, K. (2005). How genetic is school myopia? *Prog Retin Eye Res*, 24(1), 1-38. <https://doi.org/10.1016/j.preteyeres.2004.06.004>
- Morgan, I. G., Ashby, R. S., & Nickla, D. L. (2013). Form deprivation and lens-induced myopia: are they different? *Ophthalmic & physiological optics : the journal of the British College of Ophthalmic Opticians (Optometrists)*, 33(3), 355-361. <https://doi.org/10.1111/opo.12059>
- Morgan, I. G., Ohno-Matsui, K., & Saw, S. M. (2012). Myopia. *Lancet*, 379(9827), 1739-1748. [https://doi.org/10.1016/S0140-6736\(12\)60272-4](https://doi.org/10.1016/S0140-6736(12)60272-4)
- Morote-Garcia, J. C., Napiwotzky, D., Köhler, D., & Rosenberger, P. (2012). Endothelial Semaphorin 7A promotes neutrophil migration during hypoxia. *Proceedings of the National Academy of Sciences*, 109(35), 14146-14151. <https://doi.org/doi:10.1073/pnas.1202165109>
- Mulla, A., Massey, K. L., & Kalra, J. (2005). Vitreous humor biochemical constituents: evaluation of between-eye differences. *Am J Forensic Med Pathol*, 26(2), 146-149.

- Muralidharan, A. R., Low, S. W. Y., Lee, Y. C., Barathi, V. A., Saw, S. M., Milea, D., & Najjar, R. P. (2022). Recovery From Form-Deprivation Myopia in Chicks Is Dependent Upon the Fullness and Correlated Color Temperature of the Light Spectrum. *Invest Ophthalmol Vis Sci*, *63*(2), 16. <https://doi.org/10.1167/iovs.63.2.16>
- Murthy, K. R., Goel, R., Subbannayya, Y., Jacob, H. K., Murthy, P. R., Manda, S. S., Patil, A. H., Sharma, R., Sahasrabuddhe, N. A., Parashar, A., Nair, B. G., Krishna, V., Prasad, T. K., Gowda, H., & Pandey, A. (2014). Proteomic analysis of human vitreous humor. *Clin Proteomics*, *11*(1), 29. <https://doi.org/10.1186/1559-0275-11-29>
- Murthy, K. R., Goel, R., Subbannayya, Y., Jacob, H. K., Murthy, P. R., Manda, S. S., Patil, A. H., Sharma, R., Sahasrabuddhe, N. A., Parashar, A., Nair, B. G., Krishna, V., Prasad Ts, K., Gowda, H., & Pandey, A. (2014). Proteomic analysis of human vitreous humor. *Clin Proteomics*, *11*(1), 29. <https://doi.org/10.1186/1559-0275-11-29>
- Mutti, D. O., Cooper, M. E., O'Brien, S., Jones, L. A., Marazita, M. L., Murray, J. C., & Zadnik, K. (2007). Candidate gene and locus analysis of myopia. *Mol Vis*, *13*, 1012-1019.
- Mutti, D. O., Mitchell, G. L., Moeschberger, M. L., Jones, L. A., & Zadnik, K. (2002). Parental Myopia, Near Work, School Achievement, and Children's Refractive Error. *Investigative Ophthalmology & Visual Science*, *43*(12), 3633-3640.
- Mutti, D. O., & Zadnik, K. (2009). Has Near Work's Star Fallen? *Optometry and Vision Science*, *86*(2), 76-78. <https://doi.org/10.1097/OPX.0b013e31819974ae>
- Nagarwal, R. C., Kumar, R., & Pandit, J. K. (2012). Chitosan coated sodium alginate-chitosan nanoparticles loaded with 5-FU for ocular delivery: in vitro characterization and in vivo study in rabbit eye. *Eur J Pharm Sci*, *47*(4), 678-685. <https://doi.org/10.1016/j.ejps.2012.08.008>
- Natarajan, J. V., Chattopadhyay, S., Ang, M., Darwitan, A., Foo, S., Zhen, M., Koo, M., Wong, T. T., & Venkatraman, S. S. (2011). Sustained release of an anti-glaucoma drug: demonstration of efficacy of a liposomal formulation in the rabbit eye. *PLoS One*, *6*(9), e24513. <https://doi.org/10.1371/journal.pone.0024513>
- Nayak, N. C., & Mital, I. (1977). The dynamics of alpha-fetoprotein and albumin synthesis in human and rat liver during normal ontogeny. *Am J Pathol*, *86*(2), 359-374. <https://www.ncbi.nlm.nih.gov/pubmed/65131>
- Nesvizhskii, A. I., & Aebersold, R. (2005). Interpretation of shotgun proteomic data. *Molecular & Cellular Proteomics*, *4*(10), 1419-1440.
- Nickerson, J. L., & Doucette, A. A. (2020). Rapid and Quantitative Protein Precipitation for Proteome Analysis by Mass Spectrometry. *Journal of Proteome Research*, *19*(5), 2035-2042. <https://doi.org/10.1021/acs.jproteome.9b00867>
- Niessen, C. M., Leckband, D., & Yap, A. S. (2011). Tissue organization by cadherin adhesion molecules: dynamic molecular and cellular mechanisms of morphogenetic regulation. *Physiol Rev*, *91*(2), 691-731. <https://doi.org/10.1152/physrev.00004.2010>
- Norton, T. T., & McBrien, N. A. (1992). Normal development of refractive state and ocular component dimensions in the tree shrew (*Tupaia belangeri*). *Vision Res*, *32*(5), 833-842. [https://doi.org/10.1016/0042-6989\(92\)90026-f](https://doi.org/10.1016/0042-6989(92)90026-f)

- Odedra, N., Wedner, S. H., Shigongo, Z. S., Nyalali, K., & Gilbert, C. (2008). Barriers to spectacle use in Tanzanian secondary school students. *Ophthalmic epidemiology*, *15*(6), 410-417.
- Olsen, J. V., Ong, S. E., & Mann, M. (2004). Trypsin cleaves exclusively C-terminal to arginine and lysine residues. *Mol Cell Proteomics*, *3*(6), 608-614. <https://doi.org/10.1074/mcp.T400003-MCP200>
- Oohira, A., Matsui, F., Tokita, Y., Yamauchi, S., & Aono, S. (2000). Molecular interactions of neural chondroitin sulfate proteoglycans in the brain development. *Arch Biochem Biophys*, *374*(1), 24-34. <https://doi.org/10.1006/abbi.1999.1598>
- Orth, D. N., & Mount, C. D. (1987). Specific high-affinity binding protein for human corticotropin-releasing hormone in normal human plasma. *Biochem Biophys Res Commun*, *143*(2), 411-417. [https://doi.org/10.1016/0006-291x\(87\)91369-6](https://doi.org/10.1016/0006-291x(87)91369-6)
- Ötles, S., & Kartal, C. (2016). Solid-Phase Extraction (SPE): Principles and Applications in Food Samples. *Acta Sci Pol Technol Aliment*, *15*(1), 5-15. <https://doi.org/10.17306/j.Afs.2016.1.1>
- Ouchi, M., West, K., Crabb, J. W., Kinoshita, S., & Kamei, M. (2005). Proteomic analysis of vitreous from diabetic macular edema. *Exp Eye Res*, *81*(2), 176-182. <https://doi.org/10.1016/j.exer.2005.01.020>
- Pan, C.-W., Ramamurthy, D., & Saw, S.-M. (2012). Worldwide prevalence and risk factors for myopia. *Ophthalmic and Physiological Optics*, *32*(1), 3-16. <https://doi.org/https://doi.org/10.1111/j.1475-1313.2011.00884.x>
- Pan, C. W., Ramamurthy, D., & Saw, S. M. (2012). Worldwide prevalence and risk factors for myopia. *Ophthalmic Physiol Opt*, *32*(1), 3-16. <https://doi.org/10.1111/j.1475-1313.2011.00884.x>
- Panova, I. G., Tatikolov, A. S., Poltavtseva, R. A., & Sukhikh, G. T. (2011). alpha-Fetoprotein in human fetal vitreous body. *Bull Exp Biol Med*, *150*(4), 420-421. <https://www.ncbi.nlm.nih.gov/pubmed/22268032>
- Passemard, S., Sokolowska, P., Schwendimann, L., & Gressens, P. (2011). VIP-induced neuroprotection of the developing brain. *Curr Pharm Des*, *17*(10), 1036-1039. <https://www.ncbi.nlm.nih.gov/pubmed/21524251>
- Peterson, A. C., Russell, J. D., Bailey, D. J., Westphall, M. S., & Coon, J. J. (2012). Parallel reaction monitoring for high resolution and high mass accuracy quantitative, targeted proteomics. *Mol Cell Proteomics*, *11*(11), 1475-1488. <https://doi.org/10.1074/mcp.O112.020131>
- Peterson, G. L. (1977). A simplification of the protein assay method of Lowry et al. which is more generally applicable. *Analytical Biochemistry*, *83*(2), 346-356. [https://doi.org/https://doi.org/10.1016/0003-2697\(77\)90043-4](https://doi.org/https://doi.org/10.1016/0003-2697(77)90043-4)
- Peti, A. P. F., Locachevic, G. A., Prado, M. K. B., de Moraes, L. A. B., & Faccioli, L. H. (2018). High-resolution multiple reaction monitoring method for quantification of steroidal hormones in plasma. *J Mass Spectrom*, *53*(5), 423-431. <https://doi.org/10.1002/jms.4075>
- Pickett-Seltner, R. L., Doughty, M. J., Pasternak, J. J., & Sivak, J. G. (1992). Proteins of the vitreous humor during experimentally induced myopia. *Invest Ophthalmol Vis Sci*, *33*(12), 3424-3429. <https://www.ncbi.nlm.nih.gov/pubmed/1428715>
- Pickett-Seltner, R. L., Sivak, J. G., & Pasternak, J. J. (1988). Experimentally induced myopia in chicks: morphometric and biochemical analysis during

- the first 14 days after hatching. *Vision Res*, 28(2), 323-328.
[https://doi.org/10.1016/0042-6989\(88\)90160-5](https://doi.org/10.1016/0042-6989(88)90160-5)
- Picotti, P., Bodenmiller, B., & Aebersold, R. (2013). Proteomics meets the scientific method. *Nat Methods*, 10(1), 24-27.
- Pierro, L., Camesasca, F. I., Mischi, M., & Brancato, R. (1992). Peripheral retinal changes and axial myopia. *Retina*, 12(1), 12-17.
<https://doi.org/10.1097/00006982-199212010-00003>
- Płotka-Wasyłka, J., Szczepańska, N., de la Guardia, M., & Namieśnik, J. (2016). Modern trends in solid phase extraction: New sorbent media. *TrAC Trends in Analytical Chemistry*, 77, 23-43.
<https://doi.org/https://doi.org/10.1016/j.trac.2015.10.010>
- Pounder, D. J., Carson, D. O., Johnston, K., & Orihara, Y. (1998). Electrolyte concentration differences between left and right vitreous humor samples. *J Forensic Sci*, 43(3), 604-607.
- Qiao-Grider, Y., Hung, L. F., Kee, C. S., Ramamirtham, R., & Smith, E. L., 3rd. (2007). A comparison of refractive development between two subspecies of infant rhesus monkeys (*Macaca mulatta*). *Vision Res*, 47(12), 1668-1681. <https://doi.org/10.1016/j.visres.2007.03.002>
- Racay, P., & Kollarova, M. (1996). Purification and partial characterization of Ca(2+)-dependent ribonucleotide reductase from *Streptomyces aureofaciens*. *Biochem Mol Biol Int*, 38(3), 493-500.
<https://www.ncbi.nlm.nih.gov/pubmed/8829608>
- Rada, J. A., Huang, Y., & Rada, K. G. (2001). Identification of choroidal ovotransferrin as a potential ocular growth regulator. *Curr Eye Res*, 22(2), 121-132. <https://www.ncbi.nlm.nih.gov/pubmed/11402389>
- Raetz, M., Duchoslav, E., Bonner, R., & Hopfgartner, G. (2019). Hybrid SWATH/MS and HR-SRM/MS acquisition for phospholipidomics using QUAL/QUANT data processing. *Anal Bioanal Chem*, 411(22), 5681-5690. <https://doi.org/10.1007/s00216-019-01946-4>
- Rahi, J. S., Cumberland, P. M., & Peckham, C. S. (2011). Myopia over the lifecourse: prevalence and early life influences in the 1958 British birth cohort. *Ophthalmology*, 118(5), 797-804.
<https://doi.org/10.1016/j.ophtha.2010.09.025>
- Rauch, U., Gao, P., Janetzko, A., Flaccus, A., Hilgenberg, L., Tekotte, H., Margolis, R. K., & Margolis, R. U. (1991). Isolation and characterization of developmentally regulated chondroitin sulfate and chondroitin/keratan sulfate proteoglycans of brain identified with monoclonal antibodies. *J Biol Chem*, 266(22), 14785-14801.
<https://www.ncbi.nlm.nih.gov/pubmed/1907283>
- Rengstorff, R., & Doughty, C. B. (1982). Mydriatic and cycloplegic drugs: a review of ocular and systemic complications. *American journal of optometry and physiological optics*, 59(2), 162-177.
- Resing, K. A., & Ahn, N. G. (2005). Proteomics strategies for protein identification. *FEBS letters*, 579(4), 885-889.
- Reynolds, J. A., & Tanford, C. (1970). Binding of dodecyl sulfate to proteins at high binding ratios. Possible implications for the state of proteins in biological membranes. *Proc Natl Acad Sci U S A*, 66(3), 1002-1007.
<https://doi.org/10.1073/pnas.66.3.1002>
- Rose, K. A., Morgan, I. G., Ip, J., Kifley, A., Huynh, S., Smith, W., & Mitchell, P. (2008). Outdoor activity reduces the prevalence of myopia in children.

- Ophthalmology*, 115(8), 1279-1285.
<https://doi.org/10.1016/j.ophtla.2007.12.019>
- Rudnicka, A. R., Kapetanakis, V. V., Wathern, A. K., Logan, N. S., Gilmartin, B., Whincup, P. H., Cook, D. G., & Owen, C. G. (2016). Global variations and time trends in the prevalence of childhood myopia, a systematic review and quantitative meta-analysis: implications for aetiology and early prevention. *British Journal of Ophthalmology*, 100(7), 882.
<https://doi.org/10.1136/bjophthalmol-2015-307724>
- Rudnicka, A. R., Owen, C. G., Nightingale, C. M., Cook, D. G., & Whincup, P. H. (2010). Ethnic differences in the prevalence of myopia and ocular biometry in 10- and 11-year-old children: the Child Heart and Health Study in England (CHASE). *Invest Ophthalmol Vis Sci*, 51(12), 6270-6276. <https://doi.org/10.1167/iovs.10-5528>
- Sajic, T., Liu, Y., & Aebersold, R. (2015). Using data-independent, high-resolution mass spectrometry in protein biomarker research: perspectives and clinical applications. *Proteomics Clin Appl*, 9(3-4), 307-321.
<https://doi.org/10.1002/prca.201400117>
- Sanders, E. J., Walter, M. A., Parker, E., Aramburo, C., & Harvey, S. (2003). Opticin binds retinal growth hormone in the embryonic vitreous. *Invest Ophthalmol Vis Sci*, 44(12), 5404-5409.
<https://www.ncbi.nlm.nih.gov/pubmed/14638744>
- Sasoh, M., Yoshida, S., Ito, Y., Matsui, K., Osawa, S., & Uji, Y. (2000). Macular buckling for retinal detachment due to macular hole in highly myopic eyes with posterior staphyloma. *Retina (Philadelphia, Pa.)*, 20(5), 445-449.
- Saw, S. M., Gazzard, G., Shih-Yen, E. C., & Chua, W. H. (2005). Myopia and associated pathological complications. *Ophthalmic Physiol Opt*, 25(5), 381-391. <https://doi.org/10.1111/j.1475-1313.2005.00298.x>
- Saw, S. M., Hong, R. Z., Zhang, M. Z., Fu, Z. F., Ye, M., Tan, D., & Chew, S. J. (2001). Near-work activity and myopia in rural and urban schoolchildren in China. *J Pediatr Ophthalmol Strabismus*, 38(3), 149-155.
<http://www.ncbi.nlm.nih.gov/pubmed/11386647>
- Schaeffel, F., Glasser, A., & Howland, H. C. (1988). Accommodation, refractive error and eye growth in chickens. *Vision Res*, 28(5), 639-657.
<http://www.ncbi.nlm.nih.gov/pubmed/3195068>
- Schaeffel, F., & Howland, H. C. (1987). Corneal accommodation in chick and pigeon. *J Comp Physiol A*, 160(3), 375-384.
<https://doi.org/10.1007/bf00613027>
- Schaeffel, F., & Howland, H. C. (1991). Properties of the feedback loops controlling eye growth and refractive state in the chicken. *Vision Res*, 31(4), 717-734. [https://doi.org/10.1016/0042-6989\(91\)90011-s](https://doi.org/10.1016/0042-6989(91)90011-s)
- Schilling, B., MacLean, B., Held, J. M., Sahu, A. K., Rardin, M. J., Sorensen, D. J., Peters, T., Wolfe, A. J., Hunter, C. L., MacCoss, M. J., & Gibson, B. W. (2015). Multiplexed, Scheduled, High-Resolution Parallel Reaction Monitoring on a Full Scan QqTOF Instrument with Integrated Data-Dependent and Targeted Mass Spectrometric Workflows. *Anal Chem*, 87(20), 10222-10229. <https://doi.org/10.1021/acs.analchem.5b02983>
- Schippert, R., Brand, C., Schaeffel, F., & Feldkaemper, M. P. (2006). Changes in scleral MMP-2, TIMP-2 and TGFbeta-2 mRNA expression after imposed myopic and hyperopic defocus in chickens. *Exp Eye Res*, 82(4), 710-719.
<https://doi.org/10.1016/j.exer.2005.09.010>

- Schlotterbeck, J., Chatterjee, M., Gawaz, M., & Lämmerhofer, M. (2019). Comprehensive MS/MS profiling by UHPLC-ESI-QTOF-MS/MS using SWATH data-independent acquisition for the study of platelet lipidomes in coronary artery disease. *Analytica chimica acta*, *1046*, 1-15.
- Sebag, J. (2014). Vitreous. in *Health and Disease*. <https://doi.org/10.1007/978-1-4939-1086-1>
- Sebag, J., & Balazs, E. A. (1989). Morphology and ultrastructure of human vitreous fibers. *Invest Ophthalmol Vis Sci*, *30*(8), 1867-1871. <http://www.ncbi.nlm.nih.gov/pubmed/2759801>
- Sechi, S., & Chait, B. T. (1998). Modification of cysteine residues by alkylation. A tool in peptide mapping and protein identification. *Anal Chem*, *70*(24), 5150-5158. <https://doi.org/10.1021/ac9806005>
- Sekundo, W., Kunert, K. S., & Blum, M. (2011). Small incision corneal refractive surgery using the small incision lenticule extraction (SMILE) procedure for the correction of myopia and myopic astigmatism: results of a 6 month prospective study. *British Journal of Ophthalmology*, *95*(3), 335-339. <https://doi.org/10.1136/bjo.2009.174284>
- Sell, S., & Becker, F. F. (1978). alpha-Fetoprotein. *J Natl Cancer Inst*, *60*(1), 19-26. <https://doi.org/10.1093/jnci/60.1.19>
- Seltner, R. L., & Sivak, J. G. (1987). A role for the vitreous humor in experimentally-induced myopia. *Am J Optom Physiol Opt*, *64*(12), 953-957. <https://doi.org/10.1097/00006324-198712000-00013>
- Seltner, R. L., & Stell, W. K. (1995). The effect of vasoactive intestinal peptide on development of form deprivation myopia in the chick: a pharmacological and immunocytochemical study. *Vision Res*, *35*(9), 1265-1270. <https://www.ncbi.nlm.nih.gov/pubmed/7610586>
- https://ac.els-cdn.com/004269899400244G/1-s2.0-004269899400244G-main.pdf?_tid=46deb2fc-63a9-4ca8-b64b-9f4d316f1e5c&acdnat=1550545419_4bd6a900594b304dc23669ce7c83fac0
- Shan, S. S., Wang, P. F., Cheung, J. K., Yu, F., Zheng, H., Luo, S., Yip, S. P., To, C. H., & Chuen, L. (2022). Transcriptional profiling of the chick retina identifies down-regulation of VIP and UTS2B genes during early lens-induced myopia. *Molecular Omics*.
- Shan, S. W., Tse, D. Y.-y., Zuo, B., To, C. H., Liu, Q., McFadden, S. A., Chun, R. K.-M., Bian, J., Li, K. K., & Lam, T. C. (2018). Integrated SWATH-based and targeted-based proteomics provide insights into the retinal emmetropization process in guinea pig. *J Proteomics*, *181*, 1-15.
- Shan, S. W., Tse, D. Y., Zuo, B., To, C. H., Liu, Q., McFadden, S. A., Chun, R. K., Bian, J., Li, K. K., & Lam, T. C. (2018). Integrated SWATH-based and targeted-based proteomics provide insights into the retinal emmetropization process in guinea pig. *J Proteomics*, *181*, 1-15. <https://doi.org/10.1016/j.jprot.2018.03.023>
- Sherman, S. M., Norton, T. T., & Casagrande, V. A. (1977). Myopia in the lid-sutured tree shrew (*Tupaia glis*). *Brain Res*, *124*(1), 154-157. <http://www.ncbi.nlm.nih.gov/pubmed/843938>
- <https://www.sciencedirect.com/science/article/abs/pii/0006899377908721?via%3Dihub>

- Shi, T., Song, E., Nie, S., Rodland, K. D., Liu, T., Qian, W. J., & Smith, R. D. (2016). Advances in targeted proteomics and applications to biomedical research. *Proteomics*, *16*(15-16), 2160-2182.
- Shitama, T., Hayashi, H., Noge, S., Uchio, E., Oshima, K., Haniu, H., Takemori, N., Komori, N., & Matsumoto, H. (2008). Proteome Profiling of Vitreoretinal Diseases by Cluster Analysis. *Proteomics Clin Appl*, *2*(9), 1265-1280. <https://doi.org/10.1002/prca.200800017>
- Siatkowski, R. M., Cotter, S. A., Crockett, R., Miller, J. M., Novack, G. D., Zadnik, K., & Group, U. P. S. (2008). Two-year multicenter, randomized, double-masked, placebo-controlled, parallel safety and efficacy study of 2% pirenzepine ophthalmic gel in children with myopia. *Journal of American Association for Pediatric Ophthalmology and Strabismus*, *12*(4), 332-339.
- Simo, R., Lecube, A., Segura, R. M., Garcia Arumi, J., & Hernandez, C. (2002). Free insulin growth factor-I and vascular endothelial growth factor in the vitreous fluid of patients with proliferative diabetic retinopathy. *Am J Ophthalmol*, *134*(3), 376-382. [https://doi.org/10.1016/s0002-9394\(02\)01538-6](https://doi.org/10.1016/s0002-9394(02)01538-6)
- Siuti, N., & Kelleher, N. L. (2007). Decoding protein modifications using top-down mass spectrometry. *Nat Methods*, *4*(10), 817-821.
- Skeie, J. M., & Mahajan, V. B. (2011). Dissection of human vitreous body elements for proteomic analysis. *J Vis Exp*(47). <https://doi.org/10.3791/2455>
- Skeie, J. M., Roybal, C. N., & Mahajan, V. B. (2015). Proteomic insight into the molecular function of the vitreous. *PLoS One*, *10*(5), e0127567. <https://doi.org/10.1371/journal.pone.0127567>
- Smith, T. S., Frick, K. D., Holden, B. A., Fricke, T. R., & Naidoo, K. S. (2009). Potential lost productivity resulting from the global burden of uncorrected refractive error. *Bull World Health Organ*, *87*(6), 431-437. <http://www.ncbi.nlm.nih.gov/pubmed/19565121>
- Snowden, J. M., Eyre, D. R., & Swann, D. A. (1982). Vitreous structure. VI. Age-related changes in the thermal stability and crosslinks of vitreous, articular cartilage and tendon collagens. *Biochim Biophys Acta*, *706*(2), 153-157. <https://www.ncbi.nlm.nih.gov/pubmed/7126595>
- Spasova, M. S., Sadowska, G. B., Threlkeld, S. W., Lim, Y.-P., & Stonestreet, B. S. (2014). Ontogeny of inter-alpha inhibitor proteins in ovine brain and somatic tissues. *Experimental Biology and Medicine*, *239*(6), 724-736.
- Stacher, G., Havlik, E., Bergmann, H., Schmierer, G., & Winklehner, S. (1982). Effects of oral pirenzepine on gastric emptying and antral motor activity in healthy man. *Scandinavian Journal of gastroenterology. Supplement*, *72*, 153-158.
- Steely, H. T., Jr., & Clark, A. F. (2000). The use of proteomics in ophthalmic research. *Pharmacogenomics*, *1*(3), 267-280. <https://doi.org/10.1517/14622416.1.3.267>
- Stone, R. A., Cohen, Y., McGlenn, A. M., Davison, S., Casavant, S., Shaffer, J., Khurana, T. S., Pardue, M. T., & Iuvone, P. M. (2016). Development of Experimental Myopia in Chicks in a Natural Environment. *Invest Ophthalmol Vis Sci*, *57*(11), 4779-4789. <https://doi.org/10.1167/iovs.16-19310>

- Stone, R. A., Laties, A. M., Raviola, E., & Wiesel, T. N. (1988). Increase in retinal vasoactive intestinal polypeptide after eyelid fusion in primates. *Proc Natl Acad Sci U S A*, *85*(1), 257-260. <https://www.ncbi.nlm.nih.gov/pubmed/2448769>
- Stone, R. A., Lin, T., Laties, A. M., & Iuvone, P. M. (1989). Retinal dopamine and form-deprivation myopia. *Proc Natl Acad Sci U S A*, *86*(2), 704-706. <http://www.ncbi.nlm.nih.gov/pubmed/2911600>
- Sun, D., Wang, N., & Li, L. (2012). Integrated SDS removal and peptide separation by strong-cation exchange liquid chromatography for SDS-assisted shotgun proteome analysis. *J Proteome Res*, *11*(2), 818-828. <https://doi.org/10.1021/pr200676v>
- Suzuki, K., Okuno, T., Yamamoto, M., Pasterkamp, R. J., Takegahara, N., Takamatsu, H., Kitao, T., Takagi, J., Rennert, P. D., & Kolodkin, A. L. (2007). Semaphorin 7A initiates T-cell-mediated inflammatory responses through $\alpha 1\beta 1$ integrin. *Nature*, *446*(7136), 680-684.
- Szklarczyk, D., Franceschini, A., Wyder, S., Forslund, K., Heller, D., Huerta-Cepas, J., Simonovic, M., Roth, A., Santos, A., Tsafou, K. P., Kuhn, M., Bork, P., Jensen, L. J., & von Mering, C. (2015). STRING v10: protein-protein interaction networks, integrated over the tree of life. *Nucleic Acids Res*, *43*(Database issue), D447-452. <https://doi.org/10.1093/nar/gku1003>
- Tabb, D. L., Vega-Montoto, L., Rudnick, P. A., Variyath, A. M., Ham, A. J., Bunk, D. M., Kilpatrick, L. E., Billheimer, D. D., Blackman, R. K., Cardasis, H. L., Carr, S. A., Clauser, K. R., Jaffe, J. D., Kowalski, K. A., Neubert, T. A., Regnier, F. E., Schilling, B., Tegeler, T. J., Wang, M., . . . Spiegelman, C. (2010). Repeatability and reproducibility in proteomic identifications by liquid chromatography-tandem mass spectrometry. *J Proteome Res*, *9*(2), 761-776. <https://doi.org/10.1021/pr9006365>
- Taketa, K. (1990). Alpha-fetoprotein: reevaluation in hepatology. *Hepatology*, *12*(6), 1420-1432. <https://www.ncbi.nlm.nih.gov/pubmed/1701754>
- Tan, D. T., Lam, D. S., Chua, W. H., Shu-Ping, D. F., & Crockett, R. S. (2005). One-year multicenter, double-masked, placebo-controlled, parallel safety and efficacy study of 2% pirenzepine ophthalmic gel in children with myopia. *Ophthalmology*, *112*(1), 84-91. <https://doi.org/10.1016/j.ophtha.2004.06.038>
- Tanaka, K., Waki, H., Ido, Y., Akita, S., Yoshida, Y., Yoshida, T., & Matsuo, T. (1988). Protein and polymer analyses up to m/z 100 000 by laser ionization time-of-flight mass spectrometry. *Rapid Communications in Mass Spectrometry*, *2*(8), 151-153. <https://doi.org/https://doi.org/10.1002/rcm.1290020802>
- Tang, S. M., Ma, L., Lu, S. Y., Wang, Y. M., Kam, K. W., Tam, P. O. S., Young, A. L., Pang, C. P., Yam, J. C. S., & Chen, L. J. (2018). Association of the PAX6 gene with extreme myopia rather than lower grade myopias. *British Journal of Ophthalmology*, *102*(4), 570. <https://doi.org/10.1136/bjophthalmol-2017-311327>
- Tang, S. M., Rong, S. S., Young, A. L., Tam, P. O. S., Pang, C. P., & Chen, L. J. (2014). PAX6 Gene Associated with High Myopia: A Meta-analysis. *Optometry and Vision Science*, *91*(4), 419-429. <https://doi.org/10.1097/opx.0000000000000224>

- Tejedor, J., & de la Villa, P. (2003). Refractive changes induced by form deprivation in the mouse eye. *Invest Ophthalmol Vis Sci*, *44*(1), 32-36. <https://doi.org/10.1167/iovs.01-1171>
- Theocharis, A. D., Papageorgakopoulou, N., Feretis, E., & Theocharis, D. A. (2002). Occurrence and structural characterization of versican-like proteoglycan in human vitreous. *Biochimie*, *84*(12), 1237-1243. <http://www.ncbi.nlm.nih.gov/pubmed/12628301>
- Theocharis, D. A., Skandalis, S. S., Noulas, A. V., Papageorgakopoulou, N., Theocharis, A. D., & Karamanos, N. K. (2008). Hyaluronan and chondroitin sulfate proteoglycans in the supramolecular organization of the mammalian vitreous body. *Connect Tissue Res*, *49*(3), 124-128. <https://doi.org/10.1080/03008200802148496>
- Thomsen, M. S., Routhe, L. J., & Moos, T. (2017). The vascular basement membrane in the healthy and pathological brain. *J Cereb Blood Flow Metab*, *37*(10), 3300-3317. <https://doi.org/10.1177/0271678X17722436>
- Thomson, K., Morgan, I., Karouta, C., & Ashby, R. (2020). Levodopa inhibits the development of lens-induced myopia in chicks. *Sci Rep*, *10*(1), 13242. <https://doi.org/10.1038/s41598-020-70271-z>
- Tigges, M., Iuvone, P. M., Fernandes, A., Sugrue, M. F., Mallorga, P. J., Laties, A. M., & Stone, R. A. (1999). Effects of muscarinic cholinergic receptor antagonists on postnatal eye growth of rhesus monkeys. *Optometry and vision science: official publication of the American Academy of Optometry*, *76*(6), 397-407.
- Timp, W., & Timp, G. (2020). Beyond mass spectrometry, the next step in proteomics. *Sci Adv*, *6*(2), eaax8978. <https://doi.org/10.1126/sciadv.aax8978>
- Tkatchenko, A. V., Walsh, P. A., Tkatchenko, T. V., Gustincich, S., & Raviola, E. (2006). Form deprivation modulates retinal neurogenesis in primate experimental myopia. *Proc Natl Acad Sci U S A*, *103*(12), 4681-4686. <https://doi.org/10.1073/pnas.0600589103>
- Tkatchenko, T. V., & Tkatchenko, A. V. (2019). Pharmacogenomic Approach to Antimyopia Drug Development: Pathways Lead the Way. *Trends Pharmacol Sci*, *40*(11), 833-852. <https://doi.org/10.1016/j.tips.2019.09.009>
- Tong, L., Huang, X. L., Koh, A. L., Zhang, X., Tan, D. T., & Chua, W.-H. (2009). Atropine for the treatment of childhood myopia: effect on myopia progression after cessation of atropine. *Ophthalmology*, *116*(3), 572-579.
- Trier, K., Munk Ribel-Madsen, S., Cui, D., & Brøgger Christensen, S. (2008). Systemic 7-methylxanthine in retarding axial eye growth and myopia progression: a 36-month pilot study. *J Ocul Biol Dis Infor*, *1*(2-4), 85-93. <https://doi.org/10.1007/s12177-008-9013-3>
- Trier, K., Olsen, E. B., Kobayashi, T., & Ribel-Madsen, S. M. (1999). Biochemical and ultrastructural changes in rabbit sclera after treatment with 7-methylxanthine, theobromine, acetazolamide, or L-ornithine. *Br J Ophthalmol*, *83*(12), 1370-1375. <https://doi.org/10.1136/bjo.83.12.1370>
- Troger, J., Kieselbach, G., Teuchner, B., Kralinger, M., Nguyen, Q. A., Haas, G., Yayan, J., Göttinger, W., & Schmid, E. (2007). Peptidergic nerves in the eye, their source and potential pathophysiological relevance. *Brain Research Reviews*, *53*(1), 39-62.

- Troilo, D., Gottlieb, M. D., & Wallman, J. (1987). Visual deprivation causes myopia in chicks with optic nerve section. *Curr Eye Res*, 6(8), 993-999. <https://doi.org/10.3109/02713688709034870>
- Troilo, D., Nickla, D. L., & Wildsoet, C. F. (2000). Choroidal Thickness Changes during Altered Eye Growth and Refractive State in a Primate. *Investigative Ophthalmology & Visual Science*, 41(6), 1249-1258.
- Troilo, D., Smith, E. L., III, Nickla, D. L., Ashby, R., Tkatchenko, A. V., Ostrin, L. A., Gawne, T. J., Pardue, M. T., Summers, J. A., Kee, C.-s., Schroedl, F., Wahl, S., & Jones, L. (2019). IMI – Report on Experimental Models of Emmetropization and Myopia. *Investigative Ophthalmology & Visual Science*, 60(3), M31-M88. <https://doi.org/10.1167/iovs.18-25967>
- Troilo, D., & Wallman, J. (1991). The regulation of eye growth and refractive state: an experimental study of emmetropization. *Vision Res*, 31(7-8), 1237-1250. <http://www.ncbi.nlm.nih.gov/pubmed/1891815>
- Tyers, M., & Mann, M. (2003). From genomics to proteomics. *Nature*, 422(6928), 193-197. <https://doi.org/10.1038/nature01510>
- Uddman, R., Alumets, J., Ehinger, B., Håkanson, R., Lorén, I., & Sundler, F. (1980). Vasoactive intestinal peptide nerves in ocular and orbital structures of the cat. *Investigative Ophthalmology & Visual Science*, 19(8), 878-885.
- Unger, W. G., Butler, J. M., Cole, D. F., Bloom, S. R., & McGregor, G. P. (1981). Substance P, vasoactive intestinal polypeptide (VIP) and somatostatin levels in ocular tissue of normal and sensorily denervated rabbit eyes. *Exp Eye Res*, 32(6), 797-801. [https://doi.org/10.1016/0014-4835\(81\)90030-0](https://doi.org/10.1016/0014-4835(81)90030-0)
- UniProt, C. (2019). UniProt: a worldwide hub of protein knowledge. *Nucleic Acids Res*, 47(D1), D506-D515. <https://doi.org/10.1093/nar/gky1049>
- Uzma, N., Kumar, B. S., Khaja Mohinuddin Salar, B. M., Zafar, M. A., & Reddy, V. D. (2009). A comparative clinical survey of the prevalence of refractive errors and eye diseases in urban and rural school children. *Can J Ophthalmol*, 44(3), 328-333. <https://doi.org/10.3129/i09-030>
- Välikangas, T., Suomi, T., & Elo, L. L. (2016). A systematic evaluation of normalization methods in quantitative label-free proteomics. *Briefings in Bioinformatics*, 19(1), 1-11. <https://doi.org/10.1093/bib/bbw095>
- van Bentum, M., & Selbach, M. (2021). An Introduction to Advanced Targeted Acquisition Methods. *Molecular & Cellular Proteomics*, 20. <https://doi.org/10.1016/j.mcpro.2021.100165>
- Van Bockxmeer, F. M., Martin, C. E., & Constable, I. J. (1983). Iron-binding proteins in vitreous humour. *Biochim Biophys Acta*, 758(1), 17-23. [https://doi.org/10.1016/0304-4165\(83\)90004-1](https://doi.org/10.1016/0304-4165(83)90004-1)
- van Midwoud, P. M., Rieux, L., Bischoff, R., Verpoorte, E., & Niederländer, H. A. G. (2007). Improvement of Recovery and Repeatability in Liquid Chromatography–Mass Spectrometry Analysis of Peptides. *Journal of Proteome Research*, 6(2), 781-791. <https://doi.org/10.1021/pr0604099>
- van Setten, G. B., Trost, A., Schrödl, F., Kaser-Eichberger, A., Bogner, B., van Setten, M., Heindl, L. M., Grabner, G., & Reitsamer, H. A. (2016). Immunohistochemical detection of CTGF in the human eye. *Current Eye Research*, 41(12), 1571-1579.
- Vandamme, T. F. (2002). Microemulsions as ocular drug delivery systems: recent developments and future challenges. *Prog Retin Eye Res*, 21(1), 15-34. [https://doi.org/10.1016/s1350-9462\(01\)00017-9](https://doi.org/10.1016/s1350-9462(01)00017-9)

- Vaudry, D., Falluel-Morel, A., Bourgault, S., Basille, M., Burel, D., Wurtz, O., Fournier, A., Chow, B. K., Hashimoto, H., Galas, L., & Vaudry, H. (2009). Pituitary adenylate cyclase-activating polypeptide and its receptors: 20 years after the discovery. *Pharmacol Rev*, *61*(3), 283-357. <https://doi.org/10.1124/pr.109.001370>
- Vessey, K. A., Rushforth, D. A., & Stell, W. K. (2005). Glucagon- and secretin-related peptides differentially alter ocular growth and the development of form-deprivation myopia in chicks. *Invest Ophthalmol Vis Sci*, *46*(11), 3932-3942. <https://doi.org/10.1167/iovs.04-1027>
- Vidova, V., & Spacil, Z. (2017). A review on mass spectrometry-based quantitative proteomics: Targeted and data independent acquisition. *Analytica chimica acta*, *964*, 7-23.
- Vitale, S., Sperduto, R. D., & Ferris, F. L., 3rd. (2009). Increased prevalence of myopia in the United States between 1971-1972 and 1999-2004. *Arch Ophthalmol*, *127*(12), 1632-1639. <https://doi.org/10.1001/archophthalmol.2009.303>
- Waldvogel, J. A. (1990). The bird's eye view. *American scientist*, *78*(4), 342-353.
- Wallman, J., & Adams, J. I. (1987). Developmental aspects of experimental myopia in chicks: susceptibility, recovery and relation to emmetropization. *Vision Res*, *27*(7), 1139-1163. [https://doi.org/10.1016/0042-6989\(87\)90027-7](https://doi.org/10.1016/0042-6989(87)90027-7)
- Wallman, J., Adams, J. I., & Trachtman, J. N. (1981). The eyes of young chickens grow toward emmetropia. *Invest Ophthalmol Vis Sci*, *20*(4), 557-561. <http://www.ncbi.nlm.nih.gov/pubmed/7216672>
- Wallman, J., Turkel, J., & Trachtman, J. (1978). Extreme myopia produced by modest change in early visual experience. *Science*, *201*(4362), 1249-1251. <https://www.ncbi.nlm.nih.gov/pubmed/694514>
- Wallman, J., Wildsoet, C., Xu, A., Gottlieb, M. D., Nickla, D. L., Marran, L., Krebs, W., & Christensen, A. M. (1995). Moving the retina: Choroidal modulation of refractive state. *Vision Research*, *35*(1), 37-50. [https://doi.org/https://doi.org/10.1016/0042-6989\(94\)E0049-Q](https://doi.org/https://doi.org/10.1016/0042-6989(94)E0049-Q)
- Wallman, J., & Winawer, J. (2004). Homeostasis of eye growth and the question of myopia. *Neuron*, *43*(4), 447-468. <https://doi.org/10.1016/j.neuron.2004.08.008>
- Wang, Y., Yang, F., Gritsenko, M. A., Wang, Y., Clauss, T., Liu, T., Shen, Y., Monroe, M. E., Lopez-Ferrer, D., & Reno, T. (2011). Reversed-phase chromatography with multiple fraction concatenation strategy for proteome profiling of human MCF10A cells. *Proteomics*, *11*(10), 2019-2026.
- Weeber, E. J., Beffert, U., Jones, C., Christian, J. M., Forster, E., Sweatt, J. D., & Herz, J. (2002). Reelin and ApoE receptors cooperate to enhance hippocampal synaptic plasticity and learning. *J Biol Chem*, *277*(42), 39944-39952. <https://doi.org/10.1074/jbc.M205147200>
- Wei, Q., Zhang, T., Jiang, R., Chang, Q., Zhang, Y., Huang, X., Gao, X., Jin, H., & Xu, G. (2017). Vitreous Fibronectin and Fibrinogen Expression Increased in Eyes With Proliferative Diabetic Retinopathy After Intravitreal Anti-VEGF Therapy. *Invest Ophthalmol Vis Sci*, *58*(13), 5783-5791. <https://doi.org/10.1167/iovs.17-22345>

- Wessel, D., & Flugge, U. I. (1984). A method for the quantitative recovery of protein in dilute solution in the presence of detergents and lipids. *Anal Biochem*, *138*(1), 141-143. [https://doi.org/10.1016/0003-2697\(84\)90782-6](https://doi.org/10.1016/0003-2697(84)90782-6)
- Westphal, N. J., & Seasholtz, A. F. (2006). CRH-BP: the regulation and function of a phylogenetically conserved binding protein. *Front Biosci*, *11*, 1878-1891. <https://doi.org/10.2741/1931>
- Wiesel, T. N., & Raviola, E. (1977). Myopia and eye enlargement after neonatal lid fusion in monkeys. *Nature*, *266*(5597), 66-68. <http://www.ncbi.nlm.nih.gov/pubmed/402582>
- Wildsoet, C. F., Chia, A., Cho, P., Guggenheim, J. A., Polling, J. R., Read, S., Sankaridurg, P., Saw, S.-M., Trier, K., & Walline, J. J. (2019). IMI—interventions for controlling myopia onset and progression report. *Investigative Ophthalmology & Visual Science*, *60*(3), M106-M131.
- Wildsoet, C. F., & Pettigrew, J. D. (1988). Kainic acid-induced eye enlargement in chickens: differential effects on anterior and posterior segments. *Invest Ophthalmol Vis Sci*, *29*(2), 311-319.
- Williams, J. (1968). A comparison of glycopeptides from the ovotransferrin and serum transferrin of the hen. *Biochem J*, *108*(1), 57-67. <https://doi.org/10.1042/bj1080057>
- Williams, K., & Hammond, C. (2019). High myopia and its risks. *Community Eye Health*, *32*(105), 5-6.
- Wingfield, P. (2001). Protein precipitation using ammonium sulfate. *Curr Protoc Protein Sci*, Appendix 3, Appendix 3F. <https://doi.org/10.1002/0471140864.psa03fs13>
- Wöhlbrand, L., Rabus, R., Blasius, B., & Feenders, C. (2017). Influence of NanoLC Column and Gradient Length as well as MS/MS Frequency and Sample Complexity on Shotgun Protein Identification of Marine Bacteria. *Microbial Physiology*, *27*(3), 199-212. <https://doi.org/10.1159/000478907>
- Wolf-Yadlin, A., Hautaniemi, S., Lauffenburger, D. A., & White, F. M. (2007). Multiple reaction monitoring for robust quantitative proteomic analysis of cellular signaling networks. *Proc Natl Acad Sci U S A*, *104*(14), 5860-5865. <https://doi.org/10.1073/pnas.0608638104>
- Wolman, M. A., Sittaramane, V. K., Essner, J. J., Yost, H. J., Chandrasekhar, A., & Halloran, M. C. (2008). Transient axonal glycoprotein-1 (TAG-1) and laminin-alpha1 regulate dynamic growth cone behaviors and initial axon direction in vivo. *Neural Dev*, *3*, 6. <https://doi.org/10.1186/1749-8104-3-6>
- Wu, H., Chen, W., Zhao, F., Zhou, Q., Reinach, P. S., Deng, L., Ma, L., Luo, S., Srinivasalu, N., Pan, M., Hu, Y., Pei, X., Sun, J., Ren, R., Xiong, Y., Zhou, Z., Zhang, S., Tian, G., Fang, J., . . . Zhou, X. (2018). Scleral hypoxia is a target for myopia control. *Proc Natl Acad Sci U S A*, *115*(30), E7091-e7100. <https://doi.org/10.1073/pnas.1721443115>
- Wu, J. Y., Feng, L., Park, H.-T., Havlioglu, N., Wen, L., Tang, H., Bacon, K. B., Jiang, Z.-h., Zhang, X.-c., & Rao, Y. (2001). The neuronal repellent Slit inhibits leukocyte chemotaxis induced by chemotactic factors. *Nature*, *410*(6831), 948-952.
- Wu, X., Gao, G., Jin, J., Hua, W., Tao, L., Xu, S., & Tao, F. (2016). Housing type and myopia: the mediating role of parental myopia. *BMC Ophthalmol*, *16*(1), 151. <https://doi.org/10.1186/s12886-016-0324-z>
- Wu, Y., Liu, Q., Ho To, C., Li, K.-K., KM Chun, R., FJ Yu, J., & C Lam, T. (2014). Differential Retinal Protein Expressions During form Deprivation

- Myopia in Albino Guinea Pigs. *Current Proteomics*, 11(1), 37-47.
<https://doi.org/10.2174/1570164610666140109002531>
- Xiang, F., He, M., & Morgan, I. G. (2012). The Impact of Parental Myopia on Myopia in Chinese Children: Population-Based Evidence. *Optometry and Vision Science*, 89(10), 1487-1496.
<https://doi.org/10.1097/OPX.0b013e31826912e0>
- Xiong, S., Sankaridurg, P., Naduvilath, T., Zang, J., Zou, H., Zhu, J., Lv, M., He, X., & Xu, X. (2017). Time spent in outdoor activities in relation to myopia prevention and control: a meta-analysis and systematic review. *Acta Ophthalmol*, 95(6), 551-566. <https://doi.org/10.1111/aos.13403>
- Xu, L., Wang, Y., Li, Y., Wang, Y., Cui, T., Li, J., & Jonas, J. B. (2006). Causes of blindness and visual impairment in urban and rural areas in Beijing: the Beijing Eye Study. *Ophthalmology*, 113(7), 1134.e1131-1111.
<https://doi.org/10.1016/j.ophtha.2006.01.035>
- Xu, P., Duong, D. M., & Peng, J. (2009). Systematical optimization of reverse-phase chromatography for shotgun proteomics. *J Proteome Res*, 8(8), 3944-3950. <https://doi.org/10.1021/pr900251d>
- Yamane, K., Minamoto, A., Yamashita, H., Takamura, H., Miyamoto-Myoken, Y., Yoshizato, K., Nabetani, T., Tsugita, A., & Mishima, H. K. (2003). Proteome analysis of human vitreous proteins. *Mol Cell Proteomics*, 2(11), 1177-1187. <https://doi.org/10.1074/mcp.M300038-MCP200>
- Yang, F., Shen, Y., Camp, D. G., & Smith, R. D. (2012). High-pH reversed-phase chromatography with fraction concatenation for 2D proteomic analysis. *Expert Rev Proteomics*, 9(2), 129-134.
- Yates, J. R., 3rd. (1998). Mass spectrometry and the age of the proteome. *J Mass Spectrom*, 33(1), 1-19. [https://doi.org/10.1002/\(sici\)1096-9888\(199801\)33:1<1::Aid-jms624>3.0.Co;2-9](https://doi.org/10.1002/(sici)1096-9888(199801)33:1<1::Aid-jms624>3.0.Co;2-9)
- Yates, J. R., 3rd. (2004). Mass spectral analysis in proteomics. *Annu Rev Biophys Biomol Struct*, 33, 297-316.
<https://doi.org/10.1146/annurev.biophys.33.111502.082538>
- Yee, K. M., Feener, E. P., Madigan, M., Jackson, N. J., Gao, B. B., Ross-Cisneros, F. N., Provis, J., Aiello, L. P., Sadun, A. A., & Sebag, J. (2015). Proteomic Analysis of Embryonic and Young Human Vitreous. *Invest Ophthalmol Vis Sci*, 56(12), 7036-7042. <https://doi.org/10.1167/iovs.15-16809>
- Young, F. A. (1965). The effect of atropine on the development of myopia in monkeys. *Optometry and Vision Science*, 42(8), 439-449.
- Yu, F. J., Lam, T. C., Liu, L. Q., Chun, R. K., Cheung, J. K., Li, K. K., & To, C. H. (2017). Isotope-coded protein label based quantitative proteomic analysis reveals significant up-regulation of apolipoprotein A1 and ovotransferrin in the myopic chick vitreous. *Sci Rep*, 7(1), 12649.
<https://doi.org/10.1038/s41598-017-12650-7>
- Yu, F. J., Lam, T. C., Sze, A. Y., Li, K. K., Chun, R. K., Shan, S. W., & To, C. H. (2020). Alteration of retinal metabolism and oxidative stress may implicate myopic eye growth: Evidence from discovery and targeted proteomics in an animal model. *J Proteomics*, 221, 103684.
<https://doi.org/10.1016/j.jprot.2020.103684>
- Zha, Y., Leung, K. H., Lo, K. K., Fung, W. Y., Ng, P. W., Shi, M. G., Yap, M. K., & Yip, S. P. (2009). TGFB1 as a susceptibility gene for high myopia: a

- replication study with new findings. *Arch Ophthalmol*, 127(4), 541-548.
<https://doi.org/10.1001/archophthalmol.2008.623>
- Zhang, F., Zhu, T., Zhou, Z., Wu, Y., & Li, Y. (2009). Association of lumican gene with susceptibility to pathological myopia in the northern han ethnic chinese. *J Ophthalmol*, 2009, 514306.
<https://doi.org/10.1155/2009/514306>
- Zhang, Y., Bilbao, A., Bruderer, T., Luban, J., Strambio-De-Castillia, C., Lisacek, F., Hopfgartner, G., & Varesio, E. (2015). The Use of Variable Q1 Isolation Windows Improves Selectivity in LC-SWATH-MS Acquisition. *J Proteome Res*, 14(10), 4359-4371.
<https://doi.org/10.1021/acs.jproteome.5b00543>
- Zhang, Y., Fonslow, B. R., Shan, B., Baek, M.-C., & Yates, J. R. (2013). Protein Analysis by Shotgun/Bottom-up Proteomics. *Chemical Reviews*, 113(4), 2343-2394. <https://doi.org/10.1021/cr3003533>
- Zhao, F., Zhou, Q., Reinach, P. S., Yang, J., Ma, L., Wang, X., Wen, Y., Srinivasalu, N., Qu, J., & Zhou, X. (2018). Cause and Effect Relationship between Changes in Scleral Matrix Metalloproteinase-2 Expression and Myopia Development in Mice. *Am J Pathol*, 188(8), 1754-1767.
<https://doi.org/10.1016/j.ajpath.2018.04.011>
- Zhou, Q., Friedman, D. S., Lu, H., Duan, X., Liang, Y., Yang, X., Wang, F., & Wang, N. (2007). The epidemiology of age-related eye diseases in Mainland China. *Ophthalmic Epidemiol*, 14(6), 399-407.
<https://doi.org/10.1080/09286580701331974>
- Zhu, W., Smith, J. W., & Huang, C. M. (2010). Mass spectrometry-based label-free quantitative proteomics. *J Biomed Biotechnol*, 2010, 840518.
<https://doi.org/10.1155/2010/840518>
- Zhu, X., & Wallman, J. (2009). Opposite effects of glucagon and insulin on compensation for spectacle lenses in chicks. *Invest Ophthalmol Vis Sci*, 50(1), 24-36. <https://doi.org/10.1167/iovs.08-1708>

Appendices

Appendix 1 Optimization of vitreous proteomics workflow

Appendix 1.1 ANOVA testing for homogenization methods comparison

Protein concentration (µg/ul)

Univariate Analysis of Variance

Between-Subjects Factors

		N
Homo_Method	Homo	9
	Sonic	9
Buffer_Ratio	1:0.5	6
	1:0.67	6
	1:1	6

Descriptive Statistics

Dependent Variable: Protein_Conc

Homo_Method	Buffer_Ratio	Mean	Std. Deviation	N
Homo	1:0.5	.18000	.039038	3
	1:0.67	.14033	.012342	3
	1:1	.15733	.052691	3
	Total	.15922	.037553	9
Sonic	1:0.5	.18967	.071038	3
	1:0.67	.17833	.049136	3
	1:1	.12700	.011269	3
	Total	.16500	.052280	9
Total	1:0.5	.18483	.051538	6
	1:0.67	.15933	.038208	6
	1:1	.14217	.037913	6
	Total	.16211	.044257	18

Levene's Test of Equality of Error Variances^{a,b}

		Levene Statistic	df1	df2	Sig.
Protein_Conc	Based on Mean	1.818	5	12	.184
	Based on Median	.701	5	12	.633
	Based on Median and with adjusted df	.701	5	7.166	.640
	Based on trimmed mean	1.728	5	12	.203

Tests the null hypothesis that the error variance of the dependent variable is equal across groups.

a. Dependent variable: Protein_Conc

b. Design: Intercept + Homo_Method + Buffer_Ratio + Homo_Method * Buffer_Ratio

Tests of Between-Subjects Effects

Dependent Variable: Protein_Conc

Source	Type III Sum of Squares	df	Mean Square	F	Sig.	Partial Eta Squared
Corrected Model	.009 ^a	5	.002	.919	.501	.277
Intercept	.473	1	.473	235.728	.000	.952
Homo_Method	.000	1	.000	.075	.789	.006
Buffer_Ratio	.006	2	.003	1.378	.289	.187
Homo_Method * Buffer_Ratio	.004	2	.002	.881	.440	.128
Error	.024	12	.002			
Total	.506	18				
Corrected Total	.033	17				

a. R Squared = .277 (Adjusted R Squared = -.025)

Sample Volume (µl)

Univariate Analysis of Variance

Between-Subjects Factors

		N
Homo_Method	Homo	9
	Sonic	9
Buffer_Ratio	1:0.5	6
	1:0.67	6
	1:1	6

Descriptive Statistics

Dependent Variable: Protein_Conc

Homo_Method	Buffer_Ratio	Mean	Std. Deviation	N
Homo	1:0.5	123.33333	5.773503	3
	1:0.67	130.00000	17.320508	3
	1:1	210.00000	36.055513	3
	Total	154.44444	46.398036	9
Sonic	1:0.5	83.33333	23.094011	3
	1:0.67	110.00000	26.457513	3
	1:1	123.33333	5.773503	3
	Total	105.55556	25.055494	9
Total	1:0.5	103.33333	26.583203	6
	1:0.67	120.00000	22.803509	6
	1:1	166.66667	52.788888	6
	Total	130.00000	44.058784	18

Levene's Test of Equality of Error Variances^{a,b}

		Levene Statistic	df1	df2	Sig.
Protein_Conc	Based on Mean	3.262	5	12	.043
	Based on Median	.559	5	12	.729
	Based on Median and with adjusted df	.559	5	8.012	.729
	Based on trimmed mean	2.883	5	12	.062

Tests the null hypothesis that the error variance of the dependent variable is equal across groups.

a. Dependent variable: Protein_Conc

b. Design: Intercept + Homo_Method + Buffer_Ratio + Homo_Method * Buffer_Ratio

Tests of Between-Subjects Effects

Dependent Variable: Protein_Conc

Source	Type III Sum of Squares	df	Mean Square	F	Sig.	Partial Eta Squared
Corrected Model	27200.000 ^a	5	5440.000	11.255	.000	.824
Intercept	304200.000	1	304200.000	629.379	.000	.981
Homo_Method	10755.556	1	10755.556	22.253	.000	.650
Buffer_Ratio	12933.333	2	6466.667	13.379	.001	.690
Homo_Method * Buffer_Ratio	3511.111	2	1755.556	3.632	.058	.377
Error	5800.000	12	483.333			
Total	337200.000	18				
Corrected Total	33000.000	17				

a. R Squared = .824 (Adjusted R Squared = .751)

Post Hoc Tests

Buffer_Ratio

Multiple Comparisons

Dependent Variable: Protein_Conc

Tukey HSD

(I)	(J)	Mean Difference (I-J)	Std. Error	Sig.	95% Confidence Interval	
					Lower Bound	Upper Bound
Buffer_Ratio	Buffer_Ratio					

1:0.5	1:0.67	-16.66667	12.69295	.415	-50.52974	17.19641
			5			
	1:1	-63.33333*	12.69295	.001	-97.19641	-29.47026
			5			
1:0.67	1:0.5	16.66667	12.69295	.415	-17.19641	50.52974
			5			
	1:1	-46.66667*	12.69295	.008	-80.52974	-12.80359
			5			
1:1	1:0.5	63.33333*	12.69295	.001	29.47026	97.19641
			5			
	1:0.67	46.66667*	12.69295	.008	12.80359	80.52974
			5			

Based on observed means.

The error term is Mean Square(Error) = 483.333.

*. The mean difference is significant at the .05 level.

Homogeneous Subsets

Protein_Conc

Tukey HSD^{a,b}

Buffer_Ratio	N	Subset	
		1	2
1:0.5	6	103.33333	
1:0.67	6	120.00000	
1:1	6		166.66667
Sig.		.415	1.000

Means for groups in homogeneous subsets are displayed.

Based on observed means.

The error term is Mean Square(Error) = 483.333.

a. Uses Harmonic Mean Sample Size = 6.000.

b. Alpha = .05.

Total protein concentration

Univariate Analysis of Variance

Between-Subjects Factors

		N
Homo_Method	Homo	9
	Sonic	9
Buffer_Ratio	1:0.5	6
	1:0.67	6
	1:1	6

Descriptive Statistics

Dependent Variable: Protein_Conc

Homo_Method	Buffer_Ratio	Mean	Std. Deviation	N
Homo	1:0.5	22.03833	4.014000	3
	1:0.67	18.38000	4.049278	3
	1:1	32.69367	10.117166	3
	Total	24.37067	8.671306	9
Sonic	1:0.5	16.77000	10.695836	3
	1:0.67	20.30000	9.617297	3
	1:1	15.70667	2.160123	3
	Total	17.59222	7.564796	9
Total	1:0.5	19.40417	7.780221	6
	1:0.67	19.34000	6.682929	6
	1:1	24.20017	11.374389	6
	Total	20.98144	8.629990	18

Levene's Test of Equality of Error Variances^{a,b}

		Levene Statistic	df1	df2	Sig.
Protein_Conc	Based on Mean	1.867	5	12	.174
	Based on Median	.695	5	12	.637

Based on Median and with adjusted df	.695	5	7.244	.643
Based on trimmed mean	1.765	5	12	.195

Tests the null hypothesis that the error variance of the dependent variable is equal across groups.

a. Dependent variable: Protein_Conc

b. Design: Intercept + Homo_Method + Buffer_Ratio + Homo_Method * Buffer_Ratio

Tests of Between-Subjects Effects

Dependent Variable: Protein_Conc

Source	Type III Sum of Squares	df	Mean Square	F	Sig.	Partial Eta Squared
Corrected Model	573.254 ^a	5	114.651	1.986	.153	.453
Intercept	7923.978	1	7923.978	137.241	.000	.920
Homo_Method	206.763	1	206.763	3.581	.083	.230
Buffer_Ratio	93.254	2	46.627	.808	.469	.119
Homo_Method * Buffer_Ratio	273.237	2	136.618	2.366	.136	.283
Error	692.851	12	57.738			
Total	9190.083	18				
Corrected Total	1266.104	17				

a. R Squared = .453 (Adjusted R Squared = .225)

Appendix 1.2 ANOVA testing for protein precipitation methods

Protein recovery

Oneway

Descriptives

P_recovery

		N	Mean	Std. Deviation	Std. Error	95% Confidence Interval for Mean		Minimum	Maximum	Between-Component Variance
						Lower Bound	Upper Bound			
Acetone		3	42.24077	3.676174	2.122440	33.10865	51.37289	38.972	46.220	
Chloroform/methanol		3	29.03856	2.417743	1.395884	23.03255	35.04456	27.033	31.723	
TCA/acetone		3	20.92140	2.146102	1.239053	15.59019	26.25262	18.932	23.195	
Total		9	30.73358	9.634787	3.211596	23.32762	38.13953	18.932	46.220	
Model	Fixed Effects			2.826393	.942131	28.42827	33.03889			
	Random Effects				6.212452	4.00356	57.46360			113.120834

ANOVA

P_recovery

	Sum of Squares	df	Mean Square	F	Sig.
Between Groups	694.702	2	347.351	43.481	.000
Within Groups	47.931	6	7.988		
Total	742.633	8			

Robust Tests of Equality of Means

P_recovery

	Statistic ^a	df1	df2	Sig.
Welch	33.082	2	3.855	.004

a. Asymptotically F distributed.

Post Hoc Tests

Multiple Comparisons

Dependent Variable: P_recovery

Tukey HSD

(I) Sample	(J) Sample	Mean Difference (I-J)	Std. Error	Sig.	95% Confidence Interval	
					Lower Bound	Upper Bound
Acetone	Chloroform/methanol	13.202215*	2.307740	.003	6.12143	20.28300
	TCA/acetone	21.319366*	2.307740	.000	14.23859	28.40015
Chloroform/methanol	Acetone	-13.202215*	2.307740	.003	-20.28300	-6.12143
	TCA/acetone	8.117151*	2.307740	.029	1.03637	15.19793
TCA/acetone	Acetone	-21.319366*	2.307740	.000	-28.40015	-14.23859
	Chloroform/methanol	-8.117151*	2.307740	.029	-15.19793	-1.03637

*. The mean difference is significant at the 0.05 level.

Homogeneous Subsets

P_recovery

Tukey HSD^a

Sample	N	Subset for alpha = 0.05		
		1	2	3
TCA/acetone	3	20.92140		
Chloroform/methanol	3		29.03856	
Acetone	3			42.24077
Sig.		1.000	1.000	1.000

Means for groups in homogeneous subsets are displayed.

a. Uses Harmonic Mean Sample Size = 3.000.

Protein concentration

Oneway

Descriptives

P_Conc

	N	Mean	Std. Deviation	Std. Error	95% Confidence Interval for Mean		Minimum	Maximum	Between-Component Variance
					Lower Bound	Upper Bound			
Acetone	3	.20324	.017688	.010212	.15930	.24718	.188	.222	
Chloroform/methanol	3	.13645	.014120	.008152	.10138	.17153	.127	.153	
TCA/acetone	3	.11161	.028722	.016583	.04026	.18295	.091	.144	
Total	9	.15043	.044930	.014977	.11590	.18497	.091	.222	
Model									
Fixed Effects			.021112	.007037	.13321	.16765			
Random Effects				.027361	.03271	.26816			.002097

ANOVA

P_Conc

	Sum of Squares	df	Mean Square	F	Sig.
Between Groups	.013	2	.007	15.116	.005
Within Groups	.003	6	.000		
Total	.016	8			

Robust Tests of Equality of Means

P_Conc

	Statistic ^a	df1	df2	Sig.
Welch	14.580	2	3.770	.017

a. Asymptotically F distributed.

Post Hoc Tests

Multiple Comparisons

Dependent Variable: P_Conc

Tukey HSD

(I) Sample	(J) Sample	Mean Difference (I-J)	Std. Error	Sig.	95% Confidence Interval	
					Lower Bound	Upper Bound
Acetone	Chloroform/methanol	.066790*	.017238	.019	.01390	.11968
	TCA/acetone	.091636*	.017238	.004	.03875	.14453
Chloroform/methanol	Acetone	-.066790*	.017238	.019	-.11968	-.01390
	TCA/acetone	.024847	.017238	.380	-.02804	.07774
TCA/acetone	Acetone	-.091636*	.017238	.004	-.14453	-.03875
	Chloroform/methanol	-.024847	.017238	.380	-.07774	.02804

*. The mean difference is significant at the 0.05 level.

Homogeneous Subsets

P_Conc

Tukey HSD^a

Sample	N	Subset for alpha = 0.05	
		1	2
Acetone	3	.11161	
Chloroform/methanol	3	.13645	
TCA/acetone	3		.20324
Sig.		.380	1.000

Means for groups in homogeneous subsets are displayed.

a. Uses Harmonic Mean Sample Size = 3.000.

Appendix 1.3 ANOVA testing for clean-up methods

Oneway

Descriptives

P_conc

	N	Mean	Std. Deviation	Std. Error	95% Confidence Interval for Mean		Minimum	Maximum	Between-Component Variance
					Lower Bound	Upper Bound			
ZipTip	3	.14769	.042346	.024449	.04249	.25288	.111	.194	
SPE HLB	3	.20368	.035541	.020519	.11539	.29197	.163	.228	
C-18 spin column	3	.13954	.012455	.007191	.10860	.17048	.129	.153	
Total	9	.16363	.041440	.013813	.13178	.19549	.111	.228	
Model									
Fixed Effects			.032718	.010906	.13695	.19032			
Random Effects				.020160	.07689	.25037			.000862

Test of Homogeneity of Variances

		Levene Statistic	df1	df2	Sig.
P_conc	Based on Mean	2.192	2	6	.193
	Based on Median	.506	2	6	.626
	Based on Median and with adjusted df	.506	2	4.253	.635
	Based on trimmed mean	2.001	2	6	.216

ANOVA

P_conc

	Sum of Squares	df	Mean Square	F	Sig.
Between Groups	.007	2	.004	3.417	.102
Within Groups	.006	6	.001		
Total	.014	8			

Robust Tests of Equality of Means

P_conc

	Statistic ^a	df1	df2	Sig.
Welch	3.590	2	3.139	.154

a. Asymptotically F distributed.

Post Hoc Tests

Multiple Comparisons

Dependent Variable: P_conc

Tukey HSD

(I) P_method_no	(J) P_method_no	Mean Difference (I-J)	Std. Error	Sig.	95% Confidence Interval	
					Lower Bound	Upper Bound
ZipTip	SPE HLB	-.055988	.026715	.171	-.13796	.02598
	C-18 spin column	.008154	.026715	.950	-.07381	.09012
SPE HLB	ZipTip	.055988	.026715	.171	-.02598	.13796
	C-18 spin column	.064142	.026715	.116	-.01783	.14611
C-18 spin column	ZipTip	-.008154	.026715	.950	-.09012	.07381
	SPE HLB	-.064142	.026715	.116	-.14611	.01783

Homogeneous Subsets

P_conc

Tukey HSD^a

P_method_no	N	Subset for alpha = 0.05
C-18 spin column	3	1
ZipTip	3	.13954
SPE HLB	3	.14769
Sig.		.20368
		.116

Means for groups in homogeneous subsets are displayed.

a. Uses Harmonic Mean Sample Size = 3.000.

Oneway

Resources	Processor Time	00:00:00.02
	Elapsed Time	00:00:00.02

Descriptives

P_recov

	N	Mean	Std. Deviation	Std. Error	95% Confidence Interval for Mean		Minimum	Maximum	Between-Component Variance
					Lower Bound	Upper Bound			
ZipTip	3	31.08135	8.911870	5.145270	8.94304	53.21966	23.302	40.805	
SPE HLB	3	42.86412	7.479599	4.318349	24.28377	61.44448	34.284	48.012	
C-18 spin column	3	29.36541	2.621138	1.513315	22.85415	35.87668	27.077	32.225	
Total	9	34.43696	8.721136	2.907045	27.73331	41.14062	23.302	48.012	
Model									
Fixed Effects			6.885642	2.295214	28.82078	40.05315			
Random Effects				4.242597	16.18254	52.69139			38.194870

Test of Homogeneity of Variances

		Levene Statistic	df1	df2	Sig.
P_recov	Based on Mean	2.192	2	6	.193
	Based on Median	.506	2	6	.626
	Based on Median and with adjusted df	.506	2	4.253	.635
	Based on trimmed mean	2.001	2	6	.216

ANOVA

P_recov

	Sum of Squares	df	Mean Square	F	Sig.
Between Groups	323.993	2	161.997	3.417	.102
Within Groups	284.472	6	47.412		
Total	608.466	8			

Robust Tests of Equality of Means

P_recov

	Statistic ^a	df1	df2	Sig.
Welch	3.590	2	3.139	.154

a. Asymptotically F distributed.

Post Hoc Tests

Multiple Comparisons

Dependent Variable: P_recov

Tukey HSD

(I) P_method_no	(J) P_method_no	Mean Difference (I-J)	Std. Error	Sig.	95% Confidence Interval	
					Lower Bound	Upper Bound
ZipTip	SPE HLB	-11.782773	5.622103	.171	-29.03293	5.46738
	C-18 spin column	1.715938	5.622103	.950	-15.53422	18.96609
SPE HLB	ZipTip	11.782773	5.622103	.171	-5.46738	29.03293
	C-18 spin column	13.498710	5.622103	.116	-3.75145	30.74887
C-18 spin column	ZipTip	-1.715938	5.622103	.950	-18.96609	15.53422
	SPE HLB	-13.498710	5.622103	.116	-30.74887	3.75145

Homogeneous Subsets

P_recov

Tukey HSD^a

P_method_no	N	Subset for alpha = 0.05
		1
ZipTip	3	29.36541
SPE HLB	3	31.08135
C-18 spin column	3	42.86412
Sig.		.116

Means for groups in homogeneous subsets are displayed.

a. Uses Harmonic Mean Sample Size = 3.000.

Appendix 1.4 Distinct proteins (at 1 % FDR) identified from each cleanup

Found in:	UniProt ID	Protein name	Gene name	Length	Mass
ZT only	F1NXQ4	5,6-dihydroxyindole-2-carboxylic acid oxidase	TYRP1	536	60740
	F1P010	Actin-related protein 2/3 complex subunit 4	ARPC4	168	19706
	A0A1D5P521	Activated RNA polymerase II transcriptional coactivator p15 (SUB1 homolog)	LOC1N/A7N/A55444	126	14307
	A0A1D5NV71	Activin beta-A chain (Inhibin beta A chain)	INHBA	424	47601
	P05081	Adenylate kinase isoenzyme 1 (AK 1) (EC 2.7.4.3) (EC 2.7.4.6) (ATP-AMP transphosphorylase 1) (ATP:AMP phosphotransferase) (Adenylate monophosphate kinase) (Myokinase)	AK1	194	21683
	A0A1D5PHC7	Agrin	AGRN	2061	222661
	R4GG24	Aldo_ket_red domain-containing protein	AKR1E2	316	35808
	E1BT44	Alpha-galactosidase (EC 3.2.1.-)	GLA	409	45943
	A0A1D5PZZ8	Alpha-mannosidase (EC 3.2.1.-)	MAN2A2	1164	131015
	E1C866	AP-2 complex subunit alpha	AP2A2	938	104147
	Q5ZMW3	Apoptosis inhibitor 5 (API-5)	API5 RCJMBN/A4_1a12	523	58609
	Q05706	Beta-tropomyosin (Tropomyosin beta chain)	BRT-1 TPM2	283	32800
	F1NXH7	BRICHOS domain-containing protein	LECT1	347	38680
	F1P1D4	Cadherin-7	CDH7	785	87148
	A0A1D5PQL8	Calcium regulated heat stable protein 1	CARHSP1	152	16485
	F1P011	Calcium/calmodulin-dependent protein kinase (EC 2.7.11.17)	CAMK2A	478	54077
	P07630	Carbonic anhydrase 2 (EC 4.2.1.1) (Carbonate dehydratase II) (Carbonic anhydrase II) (CA-II)	CA2	260	29008
	F1N8Y3	Carbonyl reductase (NADPH) (EC 1.1.1.184)	CBR3	276	30326
	A0A1L1RNM1	Cellular retinoic acid-binding protein 1	CRABP1	110	12653
	Q5ZHR7	Clathrin light chain	CLTA RCJMBN/A4_33p3	215	23760
	E1C3J7	CN hydrolase domain-containing protein	BTD	521	59330
	A0A1D5PEU7	CN hydrolase domain-containing protein	VNN1	491	54664
	P25155	Coagulation factor X (EC 3.4.21.6) (Stuart factor) (Virus-activating protease) (VAP) [Cleaved into: Factor X light chain; Factor X heavy chain; Activated factor Xa heavy chain]	F1N/A FX	475	53142
	Q5ZLU8	Cold-inducible RNA-binding protein	RBM3 RCJMBN/A4_4m1	190	20974

F1NX22	Collagen alpha-1(XII) chain	COL12A1	3065	333515
F1NZ30	Creatine kinase B-type	CKB	381	42871
F1NHH1	Cystatin domain-containing protein	CSTB	98	11160
A0A1D5PE17	Cytosolic malate dehydrogenase (EC 1.1.1.37) (Malate dehydrogenase, cytoplasmic)	MDH1	527	56428
A0A1L1RRY4	Elongation factor 1-alpha	EEF1A1	415	45245
Q9PUJ4	Ephrin-B2	EFNB2	333	36761
A0A1D5P900	Erythrocyte membrane protein band 4.1 like 2	N/A	1061	118915
A0A1L1RQA1	Eukaryotic translation initiation factor 5A	N/A	133	14708
Q5ZIR7	FABP domain-containing protein	RCJMBN/A4_23p16	134	15079
A0A1D5PXF8	FERM domain-containing protein	EPB41L3	1202	133635
P08267	Ferritin heavy chain (Ferritin H subunit) (EC 1.16.3.1)	FTH	180	21092
A0A1D5PJ69	Glutamate receptor	GRIA4	902	100923
P20136	Glutathione S-transferase 2 (EC 2.5.1.18) (GST class-mu) (GST-CL2) (GSTM1-1)	GSTM2	220	25893
A0A1D5NT70	Glutathione transferase (EC 2.5.1.18)	LOC395611	221	25347
Q9W6U9	Glycoprotein 130	gp13N/A IL6ST	918	102496
R4GGM5	GOLD domain-containing protein	TMED7	330	36749
F1P3F0	Growth arrest specific 6	GAS6	666	74860
E1C453	Heterogeneous nuclear ribonucleoprotein K	HNRNPK	427	47154
A0A1L1RNY8	Histone H2A	H2AFX	143	15045
F1P2A1	HMA domain-containing protein	ATOX1	71	7984
A0A1D5PW77	Ig-like domain-containing protein	LOC776376	310	34987
F1NTY3	Ig-like domain-containing protein	LRRC4C	638	71705
F1P4S8	Interleukin-1 receptor accessory protein-like 1 (X-linked interleukin-1 receptor accessory protein-like 1)	IL1RL1	485	56450
Q5ZKH9	Kinesin-like protein	RCJMBN/A4_1N/A113	881	99196
A0A1L1RNM2	Low molecular weight phosphotyrosine protein phosphatase	ACP1	67	7927
E1C4H4	LRRNT domain-containing protein	PODN	583	65879
A0A1D5PW25	L-type lectin-like domain-containing protein	LMAN2	337	37539
A0A1D5PER0	Melanocyte protein PMEL	PMEL	740	74997
A0A1D5PMU9	Melanoma cell adhesion molecule	MCAM	583	64291
E1C6D1	Microtubule-associated protein	MAP2	504	53319
Q8UWG6	Mitogen-activated protein kinase (EC 2.7.11.24)	N/A	368	41942

A0A1D5NZ30	Nucleolin	NCL	691	75400
F1NSM1	Nudix hydrolase domain-containing protein	NUDT9	357	40085
F1NUG0	P/Homo B domain-containing protein	PCSK2	582	64655
A0A1D5PIZ1	Peptidase_M3 domain-containing protein	THOP1	685	78309
R4GL78	Platelet-activating factor acetylhydrolase IB subunit beta	PAFAH1B2	241	26807
Q5ZJL1	Polypeptide N-acetylgalactosaminyltransferase (EC 2.4.1.-) (Protein-UDP acetylgalactosaminyltransferase)	GALNT1 RCJMBN/A4_17f16	559	64073
F1NMD3	Polypeptide N-acetylgalactosaminyltransferase (EC 2.4.1.-) (Protein-UDP acetylgalactosaminyltransferase)	GALNT12	587	67444
F1NZW7	PPase cyclophilin-type domain-containing protein	PPIC	359	38074
F1NQ49	Protein-tyrosine-phosphatase (EC 3.1.3.48)	PTPRD	1960	219464
F1N897	Protein-tyrosine-phosphatase (EC 3.1.3.48)	PTPRF	1921	214714
Q5ZKU5	Ras-related protein Rab-14	RAB14 RCJMBN/A4_9b24	215	23897
A0AIL1RMJ5	Receptor of-activated protein C kinase 1	RACK1	282	31207
P22329	Red-sensitive opsin (Iodopsin) (Red cone photoreceptor pigment)	N/A	362	40326
A0A1L1RXR7	Reticulon	RTN4	199	22307
F1NI89	S-(hydroxymethyl)glutathione dehydrogenase (EC 1.1.1.284)	ADH4	374	39605
E1BWU6	Sema domain-containing protein	PLXNB3	1916	214936
A0A1D5NYA7	Sema domain-containing protein	PLXNB2	1519	171531
A0A1D5PMF8	Sema domain-containing protein	SEMA6D	1088	121520
F1NPN5	SERPIN domain-containing protein	SPIA3	419	47580
F1NF68	Solute carrier family 2, facilitated glucose transporter member 1	SLC2A1	488	53537
Q5ZHZ0	Spliceosome RNA helicase DDX39B (EC 3.6.4.13) (56 kDa U2AF65-associated protein) (DEAD box protein UAP56)	DDX39B BAT1 UAP56 RCJMBN/A4_32b9	428	49003
F1NH21	STI1 domain-containing protein	ST13P5	361	40188
E1C3P2	Thrombospondin-2	THBS2	1155	129182
Q90998	Transforming growth factor-beta type III receptor	TGFBR3	841	93313
P00940	Triosephosphate isomerase (TIM) (EC 5.3.1.1) (Methylglyoxal synthase) (EC 4.2.3.3) (Triose-phosphate isomerase)	TPI1	248	26620
A0A1D5P198	Tubulin alpha chain	LOC1N/AN/A859737	466	51693
G1K338	Tubulin beta chain	TUBB2A	445	49923
P09206	Tubulin beta-3 chain (Beta-tubulin class-IV)	N/A	445	49861

A0A1L1RIX9	Tudor-interacting repair regulator protein	NUDT16L1	233	24015
Q98T89	Twisted gastrulation protein homolog 1	TWSG1 TSG	224	24904
A0A1L1RSW4	Ubiquitin-conjugating enzyme E2 variant 1	UBE2V1	147	16488
A0A1D5P5P6	Uncharacterized protein	N/A	177	19796
F1NSC8	Uncharacterized protein	IGLL1	104	10706
A0A1L1RNR2	Uncharacterized protein	LOC107056878	202	22443
H9KYZ6	Uncharacterized protein	N/A	763	83722
A0A1D5P8H4	Uncharacterized protein	ITIH3	892	100257
F1NGV0	Uncharacterized protein	TMEM132D	1098	122402
F1NR30	Uncharacterized protein	ROBO1	1542	168766
A0A1D5PZ45	Uncharacterized protein	GNAT2	354	40040
A0A1D5P3C1	Uncharacterized protein	B4GALT3	435	48571
E1BZE6	Uncharacterized protein	HNRNPA3	378	39541
F1NFW6	Uncharacterized protein	TMEM132C	1104	122199
F1P3P3	Uncharacterized protein	ARHGDI A	204	23262
A0A1D5P1Z5	Uncharacterized protein	HTRA3	456	49223
A0A1D5PY27	Uncharacterized protein	HMCN1	5417	586234
A0A1D5NU88	Uncharacterized protein	DDX31	495	55340
F1NEY5	Uncharacterized protein	TNFRSF21	651	71034
F1NF64	Uncharacterized protein	CFI	596	67214
A0A1D5NZ77	Uncharacterized protein	TMEM132A	577	62758
E1C5F2	Uncharacterized protein	RNASET2	266	31198
Q5F3D2	Uncharacterized protein	HNRNPH3 RCJMBN/A4_21b18	342	36656
R4GIN9	Uncharacterized protein	LRTM2	460	50513
E1C6U2	Uncharacterized protein	C7	834	93016
F1NNI0	Uncharacterized protein	RGMB	406	44244
A0A1D5PF08	Uncharacterized protein	CANX	601	68369
F1P4H4	Uncharacterized protein	TXNDC5	414	46422
F1NZF1	Uncharacterized protein	CLN5	339	39278
E1C3N9	Uncharacterized protein	GOLM1	376	43043
A0A1D5PYZ2	Uncharacterized protein	NRN1	144	15556
Q5ZKQ2	Uncharacterized protein	QDPR RCJMBN/A4_915	238	24894
F1NLV4	Uncharacterized protein	GNB1	340	37290
A0A1D5P946	Uncharacterized protein	SMPD1	669	70986

	R4GJU7	Uncharacterized protein	MXRA7	80	9454
	F1NHI6	Uncharacterized protein	LOC395991	307	34723
	A0A1D5PLJ7	Uncharacterized protein	LOC1N/A7N/A54133	886	96646
	A0A1D5PD11	Uncharacterized protein	LOC426N/A23	366	38769
	A0A1D5PIN9	VWFA domain-containing protein	CACNA2D2	1119	126438
	A0A1D6UPS2	Fascin actin-bundling protein 1	FSCN1	490	54,172
	P10042-2	Isoform A1 of Beta-crystallin A3	CRYBA1	215	24,749
SPIN only	A0A1L1RU07	Actin, alpha cardiac muscle 1	ACTC1	377	41999
	A0A1D5P630	Actin, cytoplasmic 2	ACTG1	379	42184
	A0A1D5PPA8	AdoHcyase_NAD domain-containing protein	AHCY	433	47736
	A0A1D5PZ27	Annexin A2	ANXA2	139	15081
	F1NZ38	Arrestin-C (Cone arrestin)	ARR3	395	44266
	A0A1D5PJG9	ATP synthase subunit alpha	ATP5A1W	543	59257
	Q90864	Beta-H globin	HBE1	147	16365
	A0A1D5PG99	Cellular retinoic acid-binding protein 1	CRABP1	99	11224
	A0A1L1RM27	Dipeptidyl peptidase 7	DPP7	329	36167
	F1NPA9	DNA-(apurinic or apyrimidinic site) lyase (EC 4.2.99.18)	RPS3	243	26719
	F1N9H4	Elongation factor 1-alpha	EEF1A2	463	50498
	A0A1L1RRV4	Ermin (Juxtanodin)	ERMN	252	26711
	A0A1L1RR56	Fatty acid-binding protein, brain	FABP7	150	16679
	A0A1D5NTY2	Golgi apparatus protein 1	GLG1	1194	134860
	R4GI40	LDLR chaperone MESD (LRP chaperone MESD) (Mesoderm development candidate 2) (Mesoderm development protein)	MESDC2	219	24564
	A0A1L1RLN6	Myosin light polypeptide 6	MYL6	150	16838
	A0A1I7Q438	Nucleoside diphosphate kinase	NME2	153	17314
	P19179	Plastin-1 (Fimbrin)	PLS1	630	70939
	F1NXB0	Procollagen-lysine 5-dioxygenase (EC 1.14.11.4)	PLOD2	703	81273
	P37042	Progonadoliberein-1 (Progonadoliberein I) [Cleaved into: Gonadoliberein-1 (Gonadoliberein I) (Gonadotropin-releasing hormone I) (GnRH-I) (Luliberin I) (Luteinizing hormone-releasing hormone I) (LH-RH I); GnRH-associated peptide 1 (GnRH-associated peptide I)]	GNRH1	92	10206
E1C8J9	Ras-related protein Rab-3	RAB3B	226	25997	

	A0A1D5PQS8	Repulsive guidance molecule A	RGMA	420	46353
	A0A1D5PS44	Sulfatase domain-containing protein	ARSA	506	54952
	Q90661	Synaptophysin IIa	SYP	268	29413
	A0A1D5PFU9	Syntaxin-binding protein 1	STXBP1	603	68585
	A0A1L1RK76	Tubulin alpha chain	TUBA1C	441	49061
	A0A1D5P6L2	Tubulin alpha chain	TUBA1C	423	47239
	A0A1D5P4N6	Tubulin beta chain	TUBB6	448	49950
	P09203	Tubulin beta-1 chain (Beta-tubulin class-I)	N/A	445	49909
	A0A1D5PM53	Uncharacterized protein	MYH1E	1823	209592
	A0A1D5PLW1	Uncharacterized protein	LOC107050926	356	38194
	A0A1L1RSL1	Uncharacterized protein	N/A	128	13928
	A0A1L1RQS4	Uncharacterized protein	N/A	1620	172335
	A0A1D5P671	Uncharacterized protein	SNED1	1444	157419
	A0A1D5P382	Uncharacterized protein	NRCAM	1178	130274
	A0A1D5NW03	Uncharacterized protein	NTNG1	483	54741
	A0A1D5P5X1	Uncharacterized protein	RCN2	303	35711
	A0A1L1RJ69	Uncharacterized protein	HSPG2	3717	395043
	F1NWX6	Uncharacterized protein	NELL2	816	90903
	A0A1D5P2G7	Uncharacterized protein	CHL1	1209	134117
	E1BQD1	Uncharacterized protein	GATD3AL1	280	30107
	A0A1D5PYQ9	VWFA domain-containing protein	COL22A1	1599	159942
SPE only	F1NMY1	14-3-3 protein gamma	YWHAG	247	28303
	A0A1L1RKQ5	60S ribosomal protein L7	RPL7	117	13616
	Q5ZMQ2	Actin, cytoplasmic 2 (Gamma-actin) [Cleaved into: Actin, cytoplasmic 2, N-terminally processed]	ACTG1 RCJMBN/A4_1h13	375	41793
	F1NJ10	ADP/ATP translocase (ADP,ATP carrier protein)	SLC25A5	389	42355
	F1NT57	Aldo_ket_red domain-containing protein	AKR1B1	331	37058
	Q5ZK84	Aldo-keto reductase family 1 member A1 (EC 1.1.1.2) (Alcohol dehydrogenase [NADP(+)] (Aldehyde reductase))	AKR1A1 RCJMBN/A4_12g8	327	37077
	E1BSF5	Branched-chain-amino-acid aminotransferase (EC 2.6.1.42)	BCAT1	389	43615
	A0A1D5PMJ9	Dihydropyrimidinase like 4	DPYSL4	643	68411
	F1NKG5	Dimethylargininase (EC 3.5.3.18)	DDAH1	322	34323

A0A1L1S0Z9	Elongation factor 1-alpha	EEF1A2	463	50,498
F1N9N4	Epididymal secretory protein E1 (NPC intracellular cholesterol transporter 2)	NPC2	148	16206
A0A1D5PX10	Glutamate receptor	GRIA4	933	105388
P42558	GTP-binding nuclear protein Ran (GTPase Ran) (Ras-like protein TC4) (Ras-related nuclear protein)	RAN	216	24427
F1NVX0	Hexosyltransferase (EC 2.4.1.-)	B3GALNT2	497	56517
A0A1L1RZ04	IF rod domain-containing protein	N/A	556	58033
F1NSY7	Interphotoreceptor matrix proteoglycan 2	IMPG2	1420	157189
A0A1D5P7D9	Lymphocyte antigen 6E	LY6E	126	12977
R4GHN2	Meteorin-like protein	METRNL	292	32235
R4GG19	Neurexophilin	NXPH2	265	30158
A0A1D5NY88	Neurofascin	NFASC	1069	119914
P35331	Neuronal cell adhesion molecule (Nr-CAM) (Neuronal surface protein Bravo) (gBravo) (NgCAM-related cell adhesion molecule) (Ng-CAM-related)	NRCAM	1284	141852
Q8UWC5	Nuclear protein matrin 3	MATR3	902	100713
E1BUB7	Olfactomedin-like domain-containing protein	OLFM3	458	52740
A0A1D5PAD4	Peroxidase (EC 1.11.1.7)	PXDNL	1399	156708
F1NHT3	Spectrin alpha chain, non-erythrocytic 1	SPTAN1	2477	285326
A0A1D5PJY1	Spectrin beta chain	SPTBN1	2362	274111
Q5ZJE4	SREBP regulating gene protein	SPRING; RCJMBN/A4_18o22	205	23565
Q90634	TOP AP	SLMAP	359	41425
A0A1L1S0Y8	Transaldolase	TALDO1	275	31039
P09653	Tubulin beta-5 chain (Beta-tubulin class-V)	N/A	446	49971
A0A1D5P4K6	Uncharacterized protein	N/A	185	20218
F1NIE3	Uncharacterized protein	ITIH3	882	99115
A0A1D5P7C2	Uncharacterized protein	N/A	198	21693
A0A1D5PNE6	Uncharacterized protein	N/A	212	23656
F1NQI0	Uncharacterized protein	AGA	345	36605
A0A1D5NV17	Uncharacterized protein	ACTBL2	377	42014
E1C235	Uncharacterized protein	CDH12	794	88405
F1P201	Uncharacterized protein	VCAM1	541	59890
F1NIV5	Uncharacterized protein	NTM	346	38070
A0A1D5P4J8	Uncharacterized protein	NCAN	1290	138912

A0A1D5PE33	Uncharacterized protein	RAB1B	228	25114
F1NWA7	Uncharacterized protein	ADGRL3	1470	163960
R4GI13	Uncharacterized protein	CPLX3	157	17757
E1BRJ2	Uncharacterized protein	STC2	306	33294
A0A1D5PPW3	Uncharacterized protein	SLC12A5	1111	123323
E1BYN7	Voltage-dependent anion-selective channel protein 1	VDAC1	283	30707

Appendix 1.5 Distinct proteins (at 1% FDR) found from each loading quantity (0.5, 1, and 2 µg load)

Found in:	Uniprot ID	Protein names	Gene Names	Length	Mass
0.5 µg load only	C5H3Z3	Phospholipid transfer protein	PLTP	503	56096
	E1C5M1	BOC cell adhesion associated, oncogene regulated	BOC	1107	121099
	A0A1D5NXY4	Barrier to autointegration factor 1	BANF1	90	10058
	F1NK32	Zinc finger protein 521	ZNF521	1398	157311
	Q05705	Beta-tropomyosin	BRT-2	248	28672
	Q5ZJN6	CANT1 nucleotidase	RCJMB04_16o7	311	34216
	F1NCV8	Endoplasmic reticulum lectin 1	ERLEC1	452	51177
	Q3MQ70	Ovocalysin-32 protein	OCX32	118	12976
	Q2XP57	TASK-1 potassium channel	KCNK3	389	43407
	Q90WA6	Heat shock protein 108	N/A	795	91253
	A2N888	VH1 protein	VH1	120	12547
	Q804W9	Coagulation factor X (EC 3.4.21.6)	F10	475	53774
	Q6WEB3	Thymosin beta	N/A	45	5181
	Q5ZIJ5	Carboxypeptidase (EC 3.4.16.-)	RCJMB04_25I7	471	53155
	F1NPJ2	H15 domain-containing protein	N/A	305	31876
	Q9W6J3	Glutathione transferase (EC 2.5.1.18)	N/A	186	21340
	Q5F3C9	SH3 domain-binding glutamic acid-rich-like protein	SH3BGRL RCJMB04_21c16	114	12795
	Q5F4C5	RAB35, member RAS oncogene family	RAB35 RCJMB04_1b12	201	23125
	A0A1L1RZ04	IF rod domain-containing protein	N/A	556	58033
	Q90Z41	Roundabout2 protein	ROBO2	333	37689
	A0A1D5PPB3	PCDGA protein	N/A	850	91601
	A0A1D5PN37	Adhesion G protein-coupled receptor L3	ADGRL3	1497	166579
	O57484	Laminin beta 2-like chain	N/A	1792	195724
A0A1D5P198	Tubulin alpha chain	LOC100859737	466	51693	
1 µg load only	A0A1D5PQI8	Shroom family member 2	SHROOM2	1755	196264
	Q5ZIR7	FABP domain-containing protein	RCJMB04_23p16	134	15079
	A0A1D5PDE6	Myristoylated alanine-rich C-kinase substrate	MARCKS	281	27643
	A0A1L1RY04	ATP synthase subunit beta (EC 7.1.2.2)	ATP5B	649	68410
	Q789A6	Myosin, heavy chain 10, non-muscle (Nonmuscle myosin heavy chain)	MYH10	1976	229038
	A0A1D5PEA7	Gastric intrinsic factor	GIF	301	32298
	F1NKX8	ArfGAP with SH3 domain, ankyrin repeat and PH domain 2	ASAP2	1130	125005
	F1NFH0	Growth arrest-specific 1	GAS1	159	17128
	A0A1D5PKQ4	Collagen alpha-1(III) chain	COL3A1	1384	132445
	E1C6Y2	Membrane bound transcription factor peptidase, site 1	MBTPS1	1060	118783
	A0A1L1RZ85	Protein transport protein Sec31A	SEC31A	1260	136836

F1ND57	Rearranged L-myc fusion	RLF	1797	205659
C4PFJ9	Cathelicidin-3 (Fowlicidin-3)	CATHL3 CATH-3 CathL3	151	16281
Q5ZHU8	DUF1716 domain-containing protein	RCJMB04_33b20	177	20830
Q6R0I8	Cadherin-related neuronal receptor 3	CNRv3	1000	104822
Q5ZIB1	Lysosomal acid phosphatase	RCJMB04_28i17	421	48214
A0A1D5NUQ7	Insulin like growth factor binding protein 7	IGFBP7	327	33925
F1NQI7	Neurexophilin	NXPH1	271	31036
Q90626	Ribonucleoprotein	N/A	285	32293
E1BY40	ATP binding cassette subfamily A member 5	ABCA5	1647	186427
Q2ACD0	Mesotocin-neurophysin I	MST	107	11302
E1BS74	G protein subunit alpha L	GNAL	379	44310
Q8UWC1	Fucosyltransferase (EC 2.4.1.-)	cFuc-TIX FUT9	359	42077
A0A1D5NTY2	Golgi apparatus protein 1	GLG1	1194	134860
A0A1L1RPC8	Glycosylated lysosomal membrane protein	GLMP	366	38789
Q5ZKC7	GOLD domain-containing protein	RCJMB04_11m5	115	13054
F1NHC7	Receptor protein-tyrosine kinase (EC 2.7.10.1)	EPHB2	995	111034
A0A1D5P8P3	Collagen type IV alpha 1 chain	COL4A1	1669	160770
F1NKQ2	Multiple EGF like domains 11	MEGF11	1001	108688
D2X2H4	Neuroigin 3	nlg3	764	85869
E1C1Y0	RNA 3'-terminal-phosphate cyclase (ATP) (EC 6.5.1.4) (RNA terminal phosphate cyclase domain-containing protein 1)	RTCA	365	39223
E1BSM6	von Willebrand factor C domain containing protein 2 like	VWC2L	229	25599
F1NU53	Protein xylosyltransferase (EC 2.4.2.26)	XYLT2	858	97102
F1P027	Glypican 6	N/A	263	29559
E1C6G2	Leucine rich repeat and fibronectin type III domain containing 2	LRFN2	763	84620
A0A1D5NW27	Tubulin alpha chain	TUBA1A	451	50136
Q5ZHQ3	Flotillin	FLOT2 RCJMB04_34i9	330	36204
F1NMT5	Ras-related protein Rab-10	RAB10	200	22583
I6XMD4	ST3 beta-galactoside alpha-2,3-sialyltransferase 1	ST3GAL1	342	39570
Q8QG56	Chemokine ah221	N/A	91	9898
F1NQ49	Protein-tyrosine-phosphatase (EC 3.1.3.48)	PTPRD	1960	219464
A0A1D5NX16	ADAM metalloproteinase with thrombospondin type 1 motif 1	ADAMTS1	924	100612
F1NRI4	Dynein light chain	DYNLL2	89	10350
F1NPH3	von Willebrand factor A domain-containing protein 1	VWA1	499	54790
Q6LBV3	Calcitonin/CGRP gene exon 3	N/A	43	4824
F1N8B4	Transmembrane protein 132B	TMEM132B	1086	121382

	Q5ZIM7	Protein disulfide-isomerase (EC 5.3.4.1)	RCJMB04_24o2	414	46481
	A0A1D5PFK3	Dystroglycan 1 (Dystroglycan) (Dystrophin-associated glycoprotein 1)	DAG1	896	97710
	Q804X5	Anticoagulant protein C (EC 3.4.21.69)	PROC	433	48689
	F1NW11	Protocadherin 18	PCDH18	1141	126496
	Q5ZKZ7	LisH domain-containing protein	RCJMB04_8j10	473	51441
	B8YK79	Lysozyme C (EC 3.2.1.17) (1,4-beta-N-acetylmuramidase C) (Allergen Gal d IV) (allergen Gal d 4)	LYZ	147	16239
	Q5F497	Stress-70 protein chaperone microsome-associated 60 kDa protein	RCJMB04_1o11	468	51746
	Q5ZKN8	Transaldolase (EC 2.2.1.2)	RCJMB04_9n21	337	37611
	F1NX10	Fraser extracellular matrix complex subunit 1	FRAS1	3989	439595
	E1BVG7	Patatin like phospholipase domain containing 8	PNPLA8	803	90698
	Q6PVZ3	Type II alpha-keratin IIC	N/A	521	56904
	Q5ZHY1	Elongation factor 1-beta	RCJMB04_32c11	227	25005
	A0A1L1S0C3	Cystatin C	CST3	131	13710
	Q90ZG0	Peptidylprolyl isomerase (EC 5.2.1.8)	FKBP12 FKBP1A	108	11973
	F1NQT4	NPC intracellular cholesterol transporter 1	NPC1	1286	143165
	Q90Z42	Roundabout1 protein	ROBO1	330	36725
	E1C004	Carbonic anhydrase 4 (EC 4.2.1.1) (Carbonate dehydratase IV) (Carbonic anhydrase IV)	CA4	316	36159
	A9CDT6	C-type natriuretic peptide (C-type natriuretic peptide 3)	CNP3 NPPC	130	14508
	A0A1D5P6K3	Retinol binding protein 1	RBP1	135	15755
	Q5F3R8	RAB11B, member RAS oncogene family	RAB11B RCJMB04_8i9	218	24521
	F1NKB6	ATP-dependent 6-phosphofructokinase (ATP-PFK) (Phosphofructokinase) (EC 2.7.1.11) (Phosphohexokinase)	PFKL	780	85146
	F1NUQ3	Fatty acid binding protein 3 (Heart fatty acid binding protein)	FABP3	133	14844
	E1BXM9	Zinc finger and BTB domain containing 40	ZBTB40	1069	118943
	A0A1D5PEA9	Cerebellin 3 precursor	CBLN3 RCJMB04_31n19	196	21325
	A0A1P7XK06	SPIG2-A	N/A	846	95692
	F1NE64	RING-type E3 ubiquitin transferase (EC 2.3.2.27)	TRIM36	724	81524
	Q5ZL50	Profilin	PFN2 RCJMB04_7m18	140	15046
2 µg load only	A0A1D5PJW3	EH domain binding protein 1	EHBP1	1167	132339
	F1NPS6	Glycoprotein nmb	GNPMB	559	62012
	A0A1L1RNK7	PCDBG protein	N/A	792	84494
	A0A1D5PZB7	Nitric oxide synthase (EC 1.14.13.39)	NOS2	1136	129628
	Q7T2X3	Low-density lipoprotein receptor	LDLR	891	93987

Q7SX63	Heat shock protein 70 (Heat shock protein Hsp70)	HSP70 hsp70	634	69913
Q5ZME1	Heterogeneous nuclear ribonucleoprotein A2/B1	HNRNPA2B1 RCJMB04_2g17	349	36985
A0A1D5PVF8	Tartrate-resistant acid phosphatase type 5 (EC 3.1.3.2)	ACP5	321	34961
A0A1D5PAE8	Leukotriene A(4) hydrolase (LTA-4 hydrolase) (EC 3.3.2.6)	LTA4H	680	76640
Q9PUF7	Platelet-derived growth factor A-chain	N/A	211	24349
F1NMN7	Aldehyde dehydrogenase 9 family member A1	ALDH9A1	579	63674
E1BV78	Fibrinogen gamma chain	FGG	438	49955
E1C5F3	Sulfotransferase (EC 2.8.2.-)	CHST6	393	45323
Q68BG0	NAD-dependent deacetylase SIRT1	sirt1	756	82632
E1BT21	Crumbs cell polarity complex component 1	N/A	807	89034
Q5ZKJ2	Tyrosine 3-monooxygenase/tryptophan 5-monooxygenase activation protein eta	YWHAH RCJMB04_10g10	247	28342
F1NZV0	Semaphorin 4B	SEMA4B	861	95441
A0A1D5PJE0	Polypeptide N-acetylgalactosaminyltransferase (EC 2.4.1.-) (Protein-UDP acetylgalactosaminyltransferase)	GALNT7	654	75142
Q4F9K2	Tumor necrosis factor receptor superfamily member 11B (Osteoprotegerin)	N/A	402	45931
F1NN44	Alkaline phosphatase (EC 3.1.3.1)	ALPL	519	56797
E1BSF5	Branched-chain-amino-acid aminotransferase (EC 2.6.1.42)	BCAT1	389	43615
Q5QSI1	HspB5 protein	cryab	45	5182
A0A1D5PR80	Protocadherin 7	PCDH7	1267	137478
R4GG19	Neurexophilin	NXP2	265	30158
F1NNS8	Peroxiredoxin 4	PRDX4	265	29634
F1P110	Insulin-like growth factor-binding protein 2	IGFBP2	311	33543
F1N8G6	Tubulointerstitial nephritis antigen like 1	TINAGL1	464	51681
B8XA33	Disintegrin and metalloprotease 23	N/A	758	84430
E1BSH4	C1GALT1 specific chaperone 1	C1GALT1C1	318	36044
E1BWQ8	Protein phosphatase 2 regulatory subunit B"beta	PPP2R3B	584	67765
A0A1D5PNB0	Calcium/calmodulin-dependent protein kinase (EC 2.7.11.17)	CAMK2D	478	54206
A0A1D5PHE2	Inositol-1-monophosphatase (EC 3.1.3.25)	IMPA1	278	30142
F1NP45	Tetratricopeptide repeat, ankyrin repeat and coiled-coil containing 2	TANC2	2067	228068
R4GIL3	Heparan-sulfate 6-O-sulfotransferase (EC 2.8.2.-)	N/A	239	28682
E1C482	Endothelin-2 (Preproendothelin-2)	EDN2	179	19751
Q5ZLP9	TACC_C domain-containing protein	RCJMB04_5e11	890	99485

A7LAP2	SPIG1-A	N/A	840	94683
E1BX97	Immunoglobulin superfamily DCC subclass member 3	IGDCC3	773	84613
A0A1D5P0D7	Growth differentiation factor 6	GDF6	398	44341
Q9I9H0	Gamma-synuclein	SNCG1 SNCG	128	12966
A0A1D5P7Z5	Prolyl 3-hydroxylase 3	P3H3	340	37272
Q805B0	Tumor necrosis factor receptor- II	TNFR-II	462	50142
Q4PLA5	Receptor protein-tyrosine kinase (EC 2.7.10.1)	ERBB4	1292	145119
A6N8N6	Insulin-like growth factor- binding protein 3	N/A	282	31174
A0A1D5P5B4	Integral membrane protein 2	ITM2C	264	29985
A0A1N8XHL8	Neuroblastoma suppressor of tumorigenicity 1	NBL1	194	21277
F1NKL4	Dynein cytoplasmic 1 heavy chain 1	DYNC1H1	4652	533178
F1NIS8	Receptor protein-tyrosine kinase (EC 2.7.10.1)	EPHB3	971	107962
F1P4H4	Protein disulfide-isomerase (EC 5.3.4.1)	TXNDC5	414	46422
A0A1D5PE33	RAB1B, member RAS oncogene family	RAB1B	228	25114
A0A1D5PTG3	Elastin (Tropoelastin)	ELN	777	66444
E1BU03	Arylsulfatase G	ARSG	533	57251
Q5ZMT1	GDIR1 inhibitor	RCJMB04_1d23	204	23274
Q5ZK81	S-(hydroxymethyl)glutathione dehydrogenase (EC 1.1.1.284)	RCJMB04_12i19	374	39591
Q5ZMK0	Cathepsin O	CTSO RCJMB04_1m17	320	35028
F1NL38	Histidine rich glycoprotein	HRG	1078	123032
D8UWD9	Colony-stimulating factor 1	CSF1	490	52479
F1N9F8	Alcohol dehydrogenase (NADP(+)) (EC 1.1.1.2)	AKR1A1	365	41373
Q5ZHR1	NUCB2 protein	RCJMB04_34c21	455	53766
A0A1D5PZ45	G protein subunit alpha transducin 2	GNAT2	354	40040
F1NIV5	Neurotrimin	NTM	346	38070
F1NIF9	PPR_long domain-containing protein	PTCD1	715	80575
Q4ADJ7	Ovotransferrin	TFEW	705	77832
E1BSP7	Sorbin and SH3 domain containing 2	SORBS2	1170	131560
Q8QFQ7	Leptin receptor (OB receptor)	LIFR	1083	120864
E1C200	Protein-tyrosine sulfotransferase (EC 2.8.2.20)	TPST1	370	42040
R4GG24	Aldo-keto reductase family 1 member E2	AKR1E2	316	35808
E1C633	KIAA0319 like	KIAA0319L	1141	125685
F1P476	Actin, aortic smooth muscle	ACTA2	377	42009
E1BZ05	Desmin	DES	464	53513
Q5ZJV8	Adenosine deaminase (EC 3.5.4.4)	RCJMB04_15f15	479	53883
F1NLT8	Rho GDP dissociation inhibitor beta	ARHGDI3	200	22886
F1NJ43	Nyctalopin	N/A	475	53944
E1BV71	Extracellular matrix protein 2	ECM2	704	80235

A0A1D5PMV8	Reticulon 4 receptor-like 2	RTN4RL2	353	38523
A0A1D5P986	Lipase G, endothelial type	LIPG	483	53769
F1NY83	Carbohydrate sulfotransferase (EC 2.8.2.-)	LOC101747844	316	37214
A0A1D5PE52	Glutamate receptor	GRIA4	902	100949
A0A1D5PEE8	Semaphorin-3E	SEMA3E	779	90166
E1C7M0	Carboxypeptidase N subunit 1	CPN1	453	51206
E1BVD1	Aldo-keto reductase family 1 member B10-like	LOC418170	314	35663
E1C2A2	PR/SET domain 11	PRDM11	1114	127939
Q5ZK02	GM2 ganglioside activator	RCJMB04_14a17	118	12770
A0A1D5PNU2	Beta-2-glycoprotein 1 (Apolipoprotein H) (Beta-2-glycoprotein I)	APOH	374	41093
A0A1D5PPY3	Myosin IXA	MYO9A	2537	290944
A0A1D5P4L2	Laminin, beta 2 (laminin S)	LAMB2	1802	196107
A0A1D5PW77	C-reactive protein, pentraxin-related	LOC776376	310	34987
A0A1D5PUP4	Reversion-inducing cysteine-rich protein with Kazal motifs	RECK	963	105701
F1NAU1	Glypican 4	GPC4	508	56814
Q2YHU4	Triggering receptor expressed on myeloid cells (Triggering receptor expressed on myeloid cells 2)	TREM-A1 TREM2	221	24922
Q5F366	Iduronidase, alpha-L-	IDUA RCJMB04_31123	630	71564
A0A1D5PU63	Transmembrane protein 132B	TMEM132B	1101	123283
A0A1D5PIX0	Alpha-actinin-4	ACTN4	1045	118420
F1NGB8	Exostosin like glycosyltransferase 3	EXTL3	919	105146
Q2XP49	Deoxyribonuclease II (EC 3.1.22.1)	DNASE2 DNASE2B	363	40883
A0A1D5P0U5	Calreticulin	CALR	416	48107
Q5ZL93	ADA17 protein	RCJMB04_7b18	829	93606
A1IMF0	Ubiquitin carboxyl-terminal hydrolase (EC 3.4.19.12)	UCH-L1 UCHL1	224	25111
Q7LZA0	Beta-crystallin B3 (Beta-B3 crystallin)	N/A	139	15812
F1NXX9	Bactericidal permeability-increasing protein (BPI)	LBP	481	52780
E1BVK1	Protocadherin 11 X-linked	PCDH11X	1026	113163
E1C206	Serpin peptidase inhibitor, clade A (alpha-1 antiproteinase, antitrypsin), member 5	SPIA5	423	48140
Q90X55	Fatty acid-binding protein, adipocyte (Adipocyte-type fatty acid-binding protein) (Fatty acid-binding protein 4)	AFABP	132	14894
F1N8A2	Protein-tyrosine-phosphatase (EC 3.1.3.48)	PTPRB	1848	206933
E1C4X1	Filamin binding LIM protein 1	FBLIM1	338	36743
A0A1L1RQQ1	NAD(P)H-hydrate epimerase (EC 5.1.99.6) (Apolipoprotein A-I-binding protein) (AI-BP) (NAD(P)HX epimerase)	APOA1BP AIBP	240	25939
F1NW32	Neogenin 1	NEO1	1407	154210
F1NSK8	ADP-ribosylarginine hydrolase	ADPRH	384	42136

F1N9H8	Protein PRRC1	PRRC1	442	45957
F1NX22	Collagen alpha-1(XII) chain	COL12A1	3065	333515
R4GHQ6	ST8 alpha-N-acetyl-neuraminide alpha-2,8-sialyltransferase 4	ST8SIA4	359	41230
Q5ZM23	Ectonucleoside triphosphate diphosphohydrolase 6	RCJMB04_3g1	307	33542
R4GGM5	Transmembrane p24 trafficking protein 7	TMED7	330	36749
Q8AYP9	ATP-dependent 6-phosphofructokinase (ATP-PFK) (Phosphofructokinase) (EC 2.7.1.11) (Phosphohexokinase)	pfk	770	83966
F1NWX7	SIL1 nucleotide exchange factor	SIL1	461	51551
Q91000	Furin, paired basic amino acid cleaving enzyme (Trans Golgi network protease furin)	FURIN	789	86631
A0A1D5P3C1	Beta-1,4-galactosyltransferase (Beta-1,4-GalTase) (EC 2.4.1.-)	B4GALT3	435	48571
F1NFR1	Family with sequence similarity 19 member A2, C-C motif chemokine like	FAM19A2	131	14608
E1BTB7	C1q domain-containing protein	N/A	582	66760
A0A146F0A0	Keratin, type II cytoskeletal cochlear	otokeratin	492	53749
A0A1D5P4W8	Stabilin 1	STAB1	2650	286241
F1P0J8	Thrombospondin 1	THBS1	1175	129556
A0A1D5NX54	Proprotein convertase subtilisin/kexin type 6	PCSK6	1024	112158
I6ZIP5	Aminopeptidase (EC 3.4.11.-)	N/A	967	108606
E9KFA0	Neuroigin 3 (Neuroigin 3 isoform A1A2)	NLGN3	853	95213
F1NIF0	Carbonic anhydrase (EC 4.2.1.1)	CA9	397	43823
R4GM14	Dual specificity phosphatase 16	DUSP16	664	73255
F1NWX9	Contactin-associated protein-like 5	CNTNAP5	1306	145713
Q801D7	Insulin-like growth factor-binding protein 4	IGFBP4	260	27726

Appendix 1.6 Distinct proteins (at 1% FDR) found in each gradient (90 mins and 155 mins)

Found in:	Uniprot ID	Protein name	Gene name	Length	Mass
Found only in 90 mins gradient	Q5ZKJ9	ATPase H+ transporting V1 subunit E1	ATP6V1E1 RCJMB04_10e23	226	26118
	B3Y932	DNA-(apurinic or apyrimidinic site) endonuclease (EC 3.1.-.-)	chApex1	300	33458
	Q5ZK20	Protein disulfide-isomerase A4 (EC 5.3.4.1)	RCJMB04_13I7	627	70987
	Q6EE62	Ribosomal protein	N/A	184	20798
	F1P5J7	Alkylglycerone-phosphate synthase (Alkyl-DHAP synthase) (EC 2.5.1.26)	AGPS	636	70750
	E1C7J1	Carbonic anhydrase-related protein 10	CA10	328	37595
	A0A1L1RSA3	Fibulin 7	FBLN7	444	47808
	Q4ADJ7	Ovotransferrin	TFEW	705	77832
	Q98923	HEMCAM	N/A	504	55540
	E1BZS2	Nucleosome assembly protein 1 like 1	NAP1L1	393	45359
	R4GHQ6	ST8 alpha-N-acetyl-neuraminide alpha-2,8-sialyltransferase 4	ST8SIA4	359	41230
	E1C4H7	HECT and RLD domain containing E3 ubiquitin protein ligase family member 1	HERC1	4861	533113
	R4GH61	Complement C1q like 1	C1QL1	245	25075
	F1NA27	Protein-tyrosine-phosphatase (EC 3.1.3.48)	PTPRG	1387	154682
	F1P331	Aldo-keto reductase family 7, member A2 (aflatoxin aldehyde reductase)	AKR7A2	326	36625
	A0A1L1RJ79	Adrenomedullin	ADM	73	8106
	A0A1D5PQ92	Keratin, type II cytoskeletal 4-like	LOC112529929	550	58643
	A0A0K2TBI7	Pecanex-like protein	PCNX	1737	194098
	I6LLZ9	Glutathione peroxidase	N/A	138	16119
	A0A1D5P4Y0	Tubulin polymerization promoting protein	TPPP	219	23956
	G1K338	Tubulin beta chain	TUBB2A	445	49923
	F1NNP2	Transforming growth factor beta	TGFB2	412	47623
	F1P1Y1	Rho guanine nucleotide exchange factor 12	ARHGEF12	1544	172603
	E1C125	SLIT and NTRK like family member 4	SLITRK4	870	98146
	A0A1D5PFR7	Microtubule associated protein 1 light chain 3 alpha	MAP1LC3A	121	14374
	Q5ZKQ0	LANC1 protein	RCJMB04_9I13	343	38605
	E1C043	Cytochrome c oxidase subunit 5A, mitochondrial (Cytochrome c oxidase polypeptide Va)	COX5A	140	15968
	F1NPJ1	Tenascin-R	TNR	1308	143214
	F1DQG4	Complement component 7	C7	834	93013
	F1NIU3	Inter-alpha-trypsin inhibitor heavy chain 2	ITI2	946	106511
	Q8QGD7	Vascular endothelial growth factor D	N/A	252	28768
	A0A1D5P363	Cerebellin 1 precursor	CBLN1	194	21085

F6SG96	Heterogeneous nuclear ribonucleoprotein R	HNRNPR	654	73062
E1C038	Guanylate kinase (EC 2.7.4.8)	GUK1	213	24002
Q8AYG7	Galactosylgalactosylxylosylprotein 3-beta-glucuronosyltransferase (EC 2.4.1.135)	N/A	159	18287
F1NGI6	N-sulfoglucosamine sulfohydrolase	SGSH	575	63514
A0A1D5PEA7	Gastric intrinsic factor	GIF	301	32298
A0A1D5PE52	Glutamate receptor	GRIA4	902	100949
F1NP60	Mannose receptor C type 2	MRC2	1389	157874
E1C633	KIAA0319 like	KIAA0319L	1141	125685
F1NDT9	Acid phosphatase 2, lysosomal	ACP2	421	48193
A0A1D5P6T7	Cadherin-11	CDH11	792	87587
A0A1L1RZK6	Promyelocytic leukemia-like	PMLL	464	51935
F1NQ20	Collagen alpha-1(IX) chain	COL9A1	920	91597
A0A1D5P6K3	Retinol binding protein 1	RBP1	135	15755
A0A1D5NU78	N-acetylglucosaminidase, alpha	NAGLU	751	83916
F1NIN5	Collectin-12	COLEC12	892	97129
F1NMY1	14-3-3 protein gamma	YWHAG	247	28303
A0A1D5P2G7	Cell adhesion molecule L1 like	CHL1	1209	134117
Q5ZKC7	GOLD domain-containing protein	RCJMB04_11m5	115	13054
E1C8A1	Macrophage stimulating 1 (hepatocyte growth factor-like)	MST1	704	79380
Q5ZIA4	Beta-glucuronidase	RCJMB04_28I23	657	74569
Q90796	Alpha-1 type XI collagen	N/A	888	86409
A0A1D5NW86	Fibrillin 3	FBN3	3009	324632
A0A1D5PZQ2	Ephrin-A5	EFNA5	223	25508
Q2EJU6	Pentaxin (Pentraxin)	CRP	227	25660
E1BX24	Parvalbumin	LOC427654	129	13844
A0A1D5NXG6	Adhesion G protein-coupled receptor B1	ADGRB1	1622	180798
A0A1D5PW72	Protein-tyrosine-phosphatase (EC 3.1.3.48)	PTPRD	1917	214981
A0A1L1RIY1	RING finger protein 17	N/A	587	66497
E1BQD1	Putative glutamine amidotransferase like class 1 domain containing 3A-like1	GATD3AL1	280	30107
Q5ZIM7	Protein disulfide-isomerase (EC 5.3.4.1)	RCJMB04_24o2	414	46481
A0A1D5PAK0	ADAM metalloproteinase with thrombospondin type 1 motif 2	ADAMTS2	1166	132571
E1C6D1	Microtubule-associated protein	MAP2	504	53319
A0A0K2U7W2	Zinc finger protein 277 [Gallus gallus]	ZNF277	467	54987
Q5ZI86	Nucleosome assembly protein 1-like 4	RCJMB04_29e19	376	42831
A0A1D5PWR7	Hemicentin 1	HMCN1	5360	580024
A0A1D5PVG8	Prolylcarboxypeptidase	PRCP	483	54687
A0A1D5PAD4	Peroxidasin like	PXDNL	1399	156708
E1C2F2	Pinin	PNN	691	78127

A0A1D5P3C1	Beta-1,4-galactosyltransferase (Beta-1,4-GalTase) (EC 2.4.1.-)	B4GALT3	435	48571
F1NJ12	ST8 alpha-N-acetyl-neuraminide alpha-2,8-sialyltransferase 6	ST8SIA6	378	42546
A9DAB9	Midkine	N/A	142	15579
Q5ZKU9	Keratinocyte-associated transmembrane protein 2	RCJMB04_9b14	251	28153
A0A1D5PKQ4	Collagen alpha-1(III) chain	COL3A1	1384	132445
Q5F3J8	HS74L protein	RCJMB04_15d24	843	94812
A0A1D5PR80	Protocadherin 7	PCDH7	1267	137478
A0A1D5P806	Heparan sulfate proteoglycan 2	HSPG2	3907	414834
Q5ZMU3	Glucose-6-phosphate isomerase (EC 5.3.1.9)	RCJMB04_1c14	553	62216
A0A1L1RSF6	Ectonucleoside triphosphate diphosphohydrolase 2	ENTPD2	536	59210
E1BTB7	C1q domain-containing protein	N/A	582	66760
A0A1L1RVU7	Tropomyosin 3	TPM3	248	29023
R4GGZ2	NDUFA4, mitochondrial complex associated	NDUFA4	82	9497
F1NCV8	Endoplasmic reticulum lectin 1	ERLEC1	452	51177
R4GIP8	SR-related CTD-associated factor 11	SCAF11	1344	151131
Q703P0	Corticotropin releasing hormone	CRH	167	18222
F1NMD3	Polypeptide N-acetylgalactosaminyltransferase (EC 2.4.1.-) (Protein-UDP acetylgalactosaminyltransferase)	GALNT12	587	67444
F1NBF1	Beta-mannosidase (EC 3.2.1.25) (Lysosomal beta A mannosidase) (Mannanase)	MANBA	883	100867
F1NC51	Complex III subunit 9	UQCR10	62	7126
Q90602	Single stranded D box binding factor	N/A	302	31861
Q9PW67	Ubiquitin carboxyl-terminal hydrolase (EC 3.4.19.12)	UCH-6	230	26315
A0A1D5PQJ8	Shroom family member 2	SHROOM2	1755	196264
A0A1D5PBP6	Ceruloplasmin	CP	1143	130815
E1BYQ4	[Heparan sulfate]-glucosamine N-sulfotransferase (EC 2.8.2.8)	NDST2	879	101416
E1C1Y0	RNA 3'-terminal-phosphate cyclase (ATP) (EC 6.5.1.4) (RNA terminal phosphate cyclase domain-containing protein 1)	RTCA	365	39223
A0A024B7I3	Roundabout-like protein 2	ROBO2	1206	132704
E1BXI3	Programmed cell death 5	PDCD5	126	14219
F1NGS7	ADP-ribosylation factor	ARF4 RCJMB04_9i5	180	20529
F1P593	Heat shock protein beta-1 (Heat shock 27 kDa protein)	HSPB1	194	21827
A0A1D5NT90	Lectin, mannose binding 1 like	LMAN1L	598	66468
F1NC02	Proteasome subunit alpha type	PSMA4	261	29498
Q5ZMI0	Serine and arginine rich splicing factor 7	SRSF7 RCJMB04_1p22	223	26001
Q9I895	Stathmin	N/A	111	12875

E1BV45	RNA binding protein with serine rich domain 1	RNPS1	284	31851
Q5F497	Stress-70 protein chaperone microsome-associated 60 kDa protein	RCJMB04_1o11	468	51746
C1L370	Parvalbumin	pvalb1 PVALB	110	12073
A0A1L1RZ04	IF rod domain-containing protein	N/A	556	58033
A0A1D5P1E1	Tripeptidyl-peptidase 1 (EC 3.4.14.9) (Tripeptidyl aminopeptidase) (Tripeptidyl-peptidase I)	TPP1	575	62885
Q6YDP0	Tenomodulin	N/A	319	36486
F1NW97	Tubulin alpha chain	TUBA4B	448	50012
D3WGL1	Neuroigin 1 (Neuroigin 1 isoform B)	NLGN1	823	92233
Q5ZKQ9	RNA binding motif protein, X-linked	RBMX RCJMB04_9j22	385	41452
A0A1L1RUE7	Proteasome subunit beta	LOC107049719	204	21314
F1NXQ4	5,6-dihydroxyindole-2-carboxylic acid oxidase	TYRP1	536	60740
E1BVE9	Polypeptide N-acetylgalactosaminyltransferase (EC 2.4.1.-) (Protein-UDP acetylgalactosaminyltransferase)	WBSCR17	662	74206
O93568	Fibrinogen gamma chain	N/A	435	49642
Q5ZMI7	Prolyl endopeptidase (EC 3.4.21.-)	RCJMB04_1o16	710	80791
A0A1D5PS29	Elongation factor 2	EEF2	858	95360
F1P011	Calcium/calmodulin-dependent protein kinase (EC 2.7.11.17)	CAMK2A	478	54077
A0A1D5PS69	Protocadherin gamma-A7-like	LOC427618	830	88912
F1NUQ6	Laminin subunit beta 4	LAMB4	1773	195350
F1NH21	Suppression of tumorigenicity 13 (colon carcinoma) (Hsp70 interacting protein) pseudogene 5	ST13P5	361	40188
F1NIP5	Ribose-phosphate diphosphokinase (EC 2.7.6.1)	PRPS1L1	318	34747
Q5F3S5	Exostosin glycosyltransferase 2	RCJMB04_7p22	567	64290
F6T168	Calsyntenin 1	CLSTN1	948	106667
F1P5E3	Serp family E member 3	SERPINE3	428	47619
Q6EE33	S-(hydroxymethyl)glutathione dehydrogenase (EC 1.1.1.284)	N/A	371	39124
F1NJT3	Fibronectin (FN)	FN1	2483	273248
A0A1L1RLH6	Voltage-dependent anion-selective channel protein 2	VDAC2	283	30198
Q8AWW2	Cadherin-7	N/A	551	60862
F1NF81	Acyl-CoA-binding protein	DBI	86	9643
Q802T1	Insulin-like growth factor binding protein 2	IGFBP2	209	23304
E1C200	Protein-tyrosine sulfotransferase (EC 2.8.2.20)	TPST1	370	42040
A0A1D5PRI6	NEDD8 (Neddylin) (Ubiquitin-like protein Nedd8)	NEDD8	85	9591
Q5ZJJ6	Leukotriene A(4) hydrolase (LTA-4 hydrolase) (EC 3.3.2.6)	RCJMB04_17k12	612	69324
E1C1K8	Oligodendrocyte myelin glycoprotein	OMG	434	48422
E1C0K5	Milk fat globule-EGF factor 8 protein	MFGE8	474	53146

	E1C6W9	WAP, follistatin/kazal, immunoglobulin, kunitz and netrin domain containing 2	WFIKKN2	570	64039
Found only in 155 mins gradient	A0A1I7Q417	Serine/threonine-protein kinase receptor (EC 2.7.11.30)	TGFBR2	671	76255
	Q9PSF3	Opsin CHK-2	CHK-2	51	5576
	A0A1D5P996	NDRG family member 4	NDRG4	528	57270
	F1NS31	Low-density lipoprotein receptor-related protein 8	LRP8	917	101357
	R9PXQ3	Tyrosinase	TYR	537	61237
	F1NKR1	Alpha-mannosidase (EC 3.2.1.-)	MAN2A1	1095	125162
	A0A1D5PEI3	ST8 alpha-N-acetyl-neuraminide alpha-2,8-sialyltransferase 6	ST8SIA6	398	44779
	A0A1D5PU31	Phospholipase A2 group XV	PLA2G15	388	44129
	F1P053	DnaJ homolog subfamily C member 3	DNAJC3	504	57398
	A0A1D5PY27	Hemicentin 1	HMCN1	5417	586234
	F1NXX9	Bactericidal permeability-increasing protein (BPI)	LBP	481	52780
	F1NQ49	Protein-tyrosine-phosphatase (EC 3.1.3.48)	PTPRD	1960	219464
	F6QGM9	Heterogeneous nuclear ribonucleoprotein D	HNRNPD RCJMB04_26e18	257	29355
	Q5ZII4	Prostaglandin reductase 1 (EC 1.3.1.48) (EC 1.3.1.74) (15-oxoprostaglandin 13-reductase) (Dithiolethione-inducible gene 1 protein) (Leukotriene B4 12-hydroxydehydrogenase) (NAD(P)H-dependent alkenal/one oxidoreductase)	RCJMB04_25o1	329	35908
	E1C341	Discoidin, CUB and LCCL domain containing 2	DCBLD2	676	74186
	F1NE81	Extracellular leucine rich repeat and fibronectin type III domain containing 2	ELFN2	808	90224
	Q5ZLJ7	Tropomyosin 3	TPM3 RCJMB04_5n23	248	28761
	R4GGJ0	Ribosomal protein S16	RPS16	146	16413
	Q5ZLX6	ENTH domain-containing protein	RCJMB04_4i4	723	75418
	Q5ZIO1	Cerebellin 3 precursor	CBLN3 RCJMB04_31n19	196	21325
	E1BT43	KIAA0355	KIAA0355	1058	116527
	Q5ZMF5	CALX protein	RCJMB04_2d15	599	68109
	F1NL84	Contactin 3	CNTN3	928	101654
	A0A1D5NTA0	Ubiquitin thioesterase (EC 3.4.19.12)	OTUB1	270	31176
	I6ZIP5	Aminopeptidase (EC 3.4.11.-)	N/A	967	108606
	A0A1D5PNH7	Collagen triple helix repeat containing 1	N/A	236	25704
	A0A1D5PSS5	Vascular endothelial growth factor D	VEGFD	378	43264
	A0A1D5NTM8	Protein-tyrosine-phosphatase (EC 3.1.3.48)	PTPRG	1422	159797
	F1NVG0	Immunoglobulin superfamily containing leucine rich repeat	ISLR	422	45354
	F5CSS8	Transporter associated with antigen presentation 1	TAP1	583	62665

F1P170	Prolactin-like protein	LOC417800	225	24908
F1NY09	Chromosome 1 open reading frame, human C11orf54	C1H11ORF54	316	34680
F1NQI7	Neurexophilin	NXPH1	271	31036
A0A1D5PIW9	Ankyrin 3	ANK3	4335	475907
Q90626	Ribonucleoprotein	N/A	285	32293
Q9DDD3	Calsyntenin-1 protein	calsyntenin-1	948	106615
A0A1D5PPA8	Adenosylhomocysteinase	AHCY	433	47736
A0A1D5PBN9	Purine rich element binding protein A	PURA	327	34388
Q5F3R9	Protein SET	RCJMB04_8c13	277	32151
E1BXA7	Myosin IH	MYO1H	1042	120367
R4GFR0	Carbohydrate sulfotransferase (EC 2.8.2.-)	CHST10	380	44827
Q90634	Sarcolemma associated protein (TOP AP)	SLMAP	359	41425
F1P1D4	Cadherin-7	CDH7	785	87148
E1BUN0	Hyaluronan and proteoglycan link protein 3	HAPLN3	359	41002
A0A1D5PZC7	Transmembrane anterior posterior transformation protein 1 homolog	TAPT1	657	73574
Q5ZM93	SEP15 protein	RCJMB04_2n3	90	9675
F1NWI5	Mannosidase endo-alpha	MANEA	457	52810
F1P4C0	Netrin 4	NTN4	626	68249
B3VE14	Inter-alpha inhibitor heavy chain 2	ITIH2	948	106768
F1P4H4	Protein disulfide-isomerase (EC 5.3.4.1)	TXNDC5	414	46422
F1NZF1	Ceroid-lipofuscinosis, neuronal 5	CLN5	339	39278
A0A1D5P959	Collagen alpha-1(III) chain	COL3A1	1449	138168
E1C4P4	Protein kinase C and casein kinase substrate in neurons protein 1	PACSIN1	403	46207
O93560	Calcium/calmodulin-dependent protein kinase (EC 2.7.11.17)	N/A	540	60181
F1NNV6	ATPase H+ transporting accessory protein 1	ATP6AP1	455	50531
A0A1D5NTY7	Fibromodulin (Keratan sulfate proteoglycan fibromodulin)	FMOD	380	43854
A0A1D5PMT8	60S acidic ribosomal protein P2	RPLP2	115	11842
F1NZH0	SLIT and NTRK like family member 1	SLITRK1	692	77557
E1AWU3	BMP and activin membrane-bound inhibitor homolog	BAMBI	259	29027
A0A1D5NU01	Activating transcription factor 6 beta	ATF6B	671	74292
Q90865	Hepatocyte growth factor-like/macrophage stimulating protein	HGF1 MSP	704	79342
A0A1L1RQ04	Stathmin	STMN1	172	19623
F1NAE5	Contactin associated protein 1	CNTNAP1	1306	147347
Q8UWH4	CALII (Lipocalin 15)	LCN15	195	22098
A0A1D5P4W8	Stabilin 1	STAB1	2650	286241
F1NYA2	Eukaryotic translation initiation factor 4H	EIF4H	254	27635
A0A1D5P2Z6	Protein kinase domain containing, cytoplasmic a	PKDCCA	496	55613

F1NIJ6	Glucose-6-phosphate isomerase (EC 5.3.1.9)	GPI	525	59227
Q6J4Y8	FUS/TLS	N/A	504	52360
Q5ZK81	S-(hydroxymethyl)glutathione dehydrogenase (EC 1.1.1.284)	RCJMB04_12i19	374	39591
Q90ZK7	Peptidylprolyl isomerase (EC 5.2.1.8)	FKBP25	227	25032
F1NCF9	Semaphorin-4D	SEMA4D	855	96323
A0A1D5PP46	Adhesion G-protein coupled receptor G1 (G-protein coupled receptor 56)	ADGRG1	667	74875
A0A1D5PN26	Exostosin glycosyltransferase 1	EXT1	458	52857
Q5ZHW5	Proteasome subunit alpha type	RCJMB04_32j6	85	9135
Q9PS17	Puromycin-sensitive aminopeptidase isozyme II	N/A	19	2159
F1N8G6	Tubulointerstitial nephritis antigen like 1	TINAGL1	464	51681
E1BV78	Fibrinogen gamma chain	FGG	438	49955
A0A1D5PPB3	PCDGA protein	N/A	850	91601
A0A1L1RV09	Tenascin-R	TNR	1353	148227
Q5ZLV5	M20_dimer domain-containing protein	RCJMB04_4i9	475	53079
E1BYS4	Carboxypeptidase D (EC 3.4.17.22) (Metalloprotease D)	CPD	1360	150773
E1C6V1	Cytidine deaminase (EC 3.5.4.5) (Cytidine aminohydrolase)	CDA	191	20770
F1NE64	RING-type E3 ubiquitin transferase (EC 2.3.2.27)	TRIM36	724	81524
A0A1D5PUZ0	Meiosis regulator and mRNA stability factor 1 (Limkain-b1)	KIAA0430	1635	182393
F1NFK3	Leucine rich repeat and Ig domain containing 2	N/A	632	70698
A0A1D5PM19	Myosin-9	MYH9	1960	226638
F1NYG2	Protein arginine methyltransferase 3	PRMT3	526	59449
F1NVH2	Tubulin-specific chaperone A	TBCA	108	12707
F1P458	Sulfhydryl oxidase (EC 1.8.3.2)	QSOX2	670	76079
R4GI13	Complexin 3	CPLX3	157	17757
A0A0K2TVV5	3',5'-cyclic-AMP phosphodiesterase (EC 3.1.4.53)	PDE8B	942	104369
E9KFA0	Neurologin 3 (Neurologin 3 isoform A1A2)	NLGN3	853	95213
F1NZ04	Bridging integrator 1	BIN1	442	48701
F1NW23	Clathrin heavy chain	CLTC	1675	191611
A0A1L1RNI7	Fibrillar collagen NC1 domain-containing protein	N/A	888	86389
Q6EE30	Eukaryotic translation elongation factor 1	N/A	436	49843
Q9PUF7	Platelet-derived growth factor A-chain	N/A	211	24349
Q5ZM75	Serine--tRNA ligase (EC 6.1.1.11) (Seryl-tRNA synthetase)	RCJMB04_2o24	514	58304
A0A1D5PA22	Phosducin	PDC	249	28639
A0A1D5PIZ1	Thimet oligopeptidase 1	THOP1	685	78309
A0A1D5P2Y6	PBX homeobox interacting protein 1	PBXIP1	622	67263

Q6WNG8	Heterogeneous nuclear ribonucleoprotein H1-like protein (Heterogeneous nuclear ribonucleoprotein H2 (H'))	HNRNPH2	519	56566
A0A1D5PPM4	Development and differentiation enhancing factor-like 1	DDEFL1	940	105197
A0A1D5PJ79	Lysosome-associated membrane glycoprotein 1	LAMP1	406	43864
A0A1L1RPC8	Glycosylated lysosomal membrane protein	GLMP	366	38789
Q5ZLD1	Fumarate hydratase, mitochondrial (EC 4.2.1.2)	FH RCJMB04_6k20	507	54299
Q5ZJK6	Signal-regulatory protein beta-1	RCJMB04_17h6	368	39649
Q4ADJ6	Ovotransferrin	TFEW	705	77801
Q5ZJT4	Peptidylprolyl isomerase (EC 5.2.1.8)	RCJMB04_15n8	442	50431
E1BVK1	Protocadherin 11 X-linked	PCDH11X	1026	113163
F1NEP4	Dipeptidyl peptidase like 10	DPP10	786	88896
A0A1D5P9V0	Pyruvate kinase (EC 2.7.1.40)	PKLR	550	60379
A0A1D5PPL7	Eukaryotic translation elongation factor 1 delta	EEF1D	291	32325
A0A146F0A0	Keratin, type II cytoskeletal cochlear	otokeratin	492	53749
A0A1L1RU28	Fibulin-1	FBLN1	684	75654
A5YW27	Somatostatin	N/A	116	12675
F1NAB7	Complement subcomponent C1r (EC 3.4.21.41)	C1R	712	80507
A0A1D5P382	Neuronal cell adhesion molecule	NRCAM	1178	130274
E1C3B9	Calsyntenin 3	CLSTN3	1024	113036
Q5ZM59	FXD domain-containing ion transport regulator	FXD6 RCJMB04_3a16	95	10212
Q7SX63	Heat shock protein 70 (Heat shock protein Hsp70)	HSP70 hsp70	634	69913
E1C1K5	Vang-like protein	VANGL1	522	59292
A0A1D5PYX8	Dipeptidyl peptidase like 6	DPP6	797	90914
E1BZ13	C-type lectin domain family 3 member A	CLEC3A	193	22010
F1P110	Insulin-like growth factor-binding protein 2	IGFBP2	311	33543
Q8UWC1	Fucosyltransferase (EC 2.4.1.-)	cFuc-TIX FUT9	359	42077
F1NH19	Complement C1q B chain	C1QB	244	26286
E1BXW7	ARMD4 protein	N/A	618	64120
Q5F3E6	L-type lectin-like domain-containing protein	RCJMB04_19g16	503	56520
A0A1L1S0S2	Matrilin 2	MATN2	1297	146404
E1C2A1	Acidic nuclear phosphoprotein 32 family member A	ANP32A	291	32910
Q5F3D2	Heterogeneous nuclear ribonucleoprotein H3	HNRNPH3 RCJMB04_21b18	342	36656
A0A1D5PKN8	Sulfurtransferase	MPST	297	33223
F1P3Y2	Rhodopsin	RHO	351	39299
Q98922	HEMCAM	N/A	626	69105
A0A1D5P4I1	Cell adhesion molecule L1 like	CHL1	1171	129688

A0A1L1S0S0	Voltage-dependent anion-selective channel protein 2	VDAC2	283	30198
Q8AY28	Fast myosin heavy chain HCIII	N127	1940	222972
F1P1G6	Hyaluronoglucosaminidase (EC 3.2.1.35)	CEMIP	1357	152782
A0A1D5PQ85	Complement component 3	C3	1682	186792
A0A1D5P7V6	Growth differentiation factor 11	GDF11	368	41977
Q9PUK2	Caronte	CAR	272	31202
F1NR90	E2F transcription factor 3	E2F3	341	37830
F1NSK8	ADP-ribosylarginine hydrolase	ADPRH	384	42136
F1NKK8	Nectin cell adhesion molecule 3	NECTIN3	559	62363
E1C0E3	ADAM metalloproteinase with thrombospondin type 1 motif, 19	ADAMTS19	1195	133026
A0A1D5PT55	Adhesion G protein-coupled receptor L2	ADGRL2	1488	166844
E1C6G2	Leucine rich repeat and fibronectin type III domain containing 2	LRFN2	763	84620
Q5ZKQ2	Quinoid dihydropteridine reductase	QDPR RCJMB04_9J5	238	24894
Q90858	Glutamate receptor	GluR4 D	902	100824
A0A1D5PK05	Complement C1q like 3	C1QL3	255	26659
A0A1D5PW77	C-reactive protein, pentraxin-related	LOC776376	310	34987
D5LPR1	Fascin	FSCN1	490	54172
F1P0Z3	Phospholipase B-like (EC 3.1.1.-)	PLBD2	557	62001
F1N9A3	ADP ribosylation factor like GTPase 3	ARL3	182	20409
R4GIC2	Guanylate cyclase activator 2B (uroguanylin)	GUCA2B	110	12110
F1NPH3	von Willebrand factor A domain-containing protein 1	VWA1	499	54790
F1NW79	Contactin-associated protein-like 5	CNTNAP5	1306	145713
Q670N5	Mx	Mx	705	79529
F1NIF0	Carbonic anhydrase (EC 4.2.1.1)	CA9	397	43823
F1P195	Transmembrane protein 132E	TMEM132E	1053	115850
A0A1D5PZT0	alpha-1,2-Mannosidase (EC 3.2.1.-)	MAN1A2	643	73075
A0A1L1RLN6	Myosin light polypeptide 6	MYL6	150	16838
Q90864	Beta-H globin (Hemoglobin subunit epsilon 1)	HBE1	147	16365
Q90642	Cell division cycle control protein 37	cdc37	246	29307
F1N8B4	Transmembrane protein 132B	TMEM132B	1086	121382
O42486	Beta catenin	Bcat	781	85439
Q5ZHY1	Elongation factor 1-beta	RCJMB04_32c11	227	25005
A0A1D5P9X0	Ephrin-B1	EFNB1	334	36873
F1NRX4	Ragulator complex protein LAMTOR5 (Late endosomal/lysosomal adaptor and MAPK and MTOR activator 5)	LAMTOR5	91	9516
F1NN49	Delta-aminolevulinic acid dehydratase (EC 4.2.1.24)	ALAD	502	55254
F1NQS2	Glutathione transferase (EC 2.5.1.18)	LOC396380	229	26340
F1NPS6	Glycoprotein nmb	GNPMB	559	62012
F1NVB2	T-cell leukemia homeobox protein 3	TLX3	296	32213

R4GKL8	C1q and tumor necrosis factor related protein 3	C1QTNF3	314	34498
A0A1D5PXU4	Family with sequence similarity 179 member B	FAM179B	1580	170039
A0A1D5PJW3	EH domain binding protein 1	EHBP1	1167	132339
F1NT44	Translin (Component 3 of promoter of RISC)	TSN	229	25977
Q90681	Cation-independent mannose-6-phosphate receptor	N/A	2470	275647
Q92007	Fructose-bisphosphate aldolase (EC 4.1.2.13)	aldolase C	42	4384

Appendix 2 SWATH window parameters for calculation (15Da, 20Da, 25Da and variable window 100)

2.1 SWATH window parameters for calculation (15 Da)

Experiment Type:	TOF MS (CE=10)		Experiment Type:	TOF MS ² (CE=16.297)
Num. Cycles:	2980		Num. Cycles:	2980
Polarity:	Positive		Polarity:	Positive
Period Cycle Time:	3008 ms		Product:	350.00 to 365.00
Pulser Frequency:	16.113 kHz		Period Cycle Time:	3008 ms
Accumulation Time:	50.0 ms		Pulser Frequency:	16.113 kHz
			Accumulation Time:	30.0 ms
TOF	Cycle time	3008		
	Acc time	50		
MS/MS	Cycle time	3008		
	Acc time	50		
MS/msec		msec		Cycle time (msec)
59.16	x	50	=	2958
				Cycle time (sec)
				2.958

2.2 SWATH window parameters for calculation (20 Da)

Experiment Type:	TOF MS (CE=10)		Experiment Type:	TOF MS ² (CE=16.344)
Num. Cycles:	2980		Num. Cycles:	2980
Polarity:	Positive		Polarity:	Positive
Period Cycle Time:	3032 ms		Product:	350.00 to 370.00
Pulser Frequency:	16.113 kHz		Period Cycle Time:	3032 ms
Accumulation Time:	50.0 ms		Pulser Frequency:	16.113 kHz
			Accumulation Time:	50.0 ms
TOF	Cycle time	3032		
	Acc time	50		
MS/MS	Cycle time	3032		
	Acc time	50		
MS/msec		msec		Cycle time (msec)
59.64	x	50	=	2982
				Cycle time (sec)
				2.982

2.3 SWATH window parameters for calculation (25 Da)

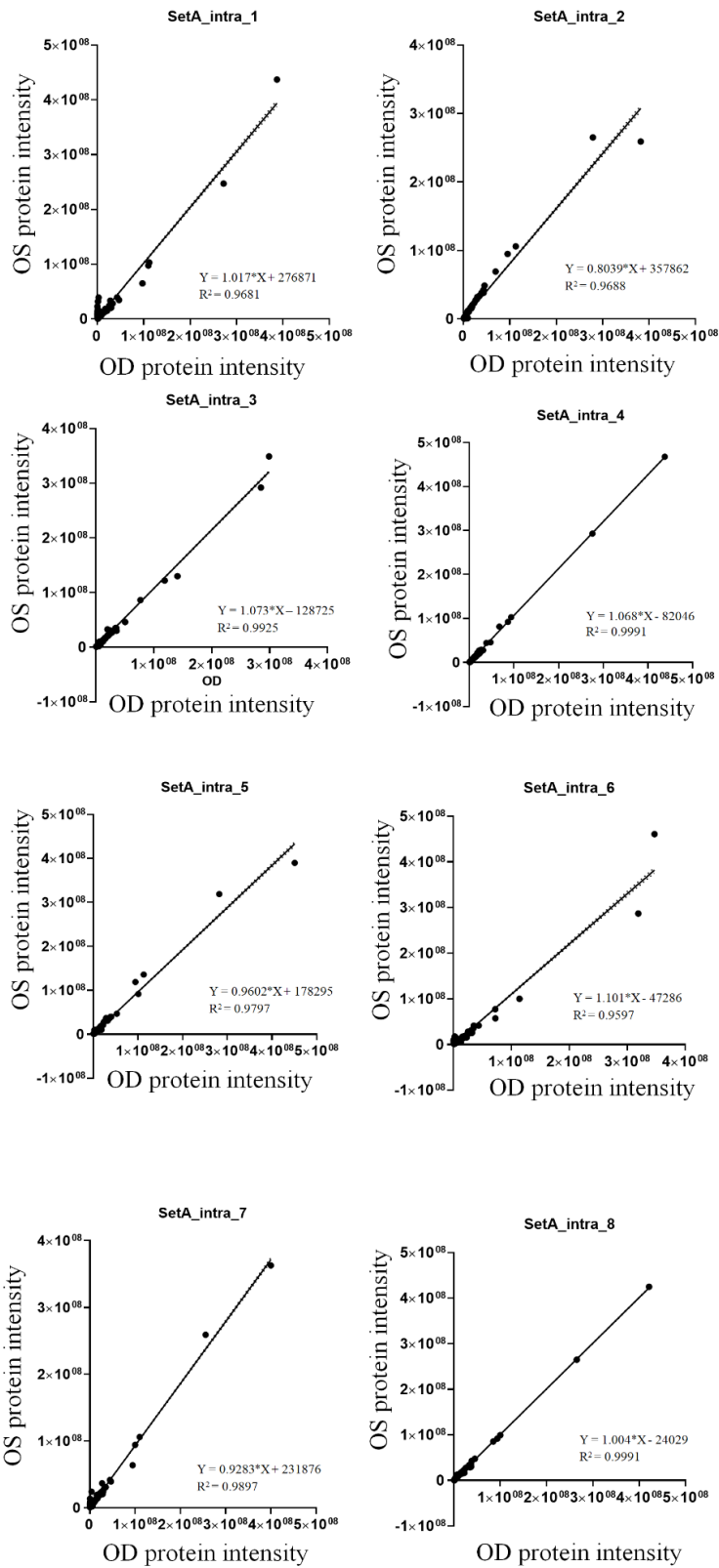
Experiment Type:	TOF MS (CE=10)		Experiment Type:	TOF MS ² (CE=16.39)
Num. Cycles:	3019		Num. Cycles:	3019
Polarity:	Positive		Polarity:	Positive
Period Cycle Time:	3001 ms		Product:	350.00 to 375.00
Pulser Frequency:	16.113 kHz		Period Cycle Time:	3001 ms
Accumulation Time:	50.0 ms		Pulser Frequency:	16.113 kHz
			Accumulation Time:	50.0 ms
TOF	Cycle time	3001		
	Acc time	50		
MS/MS	Cycle time	3001		
	Acc time	50		
MS/msec		msec		Cycle time (msec)
59.02	x	50	=	2951
				Cycle time (sec)
				2.951

2.4 SWATH window parameters for calculation (VW 100)

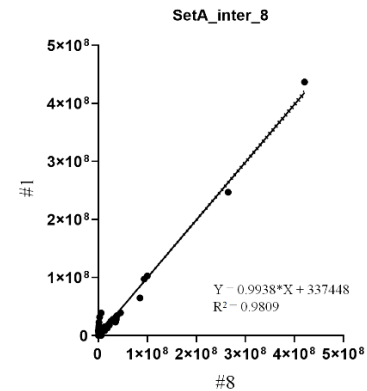
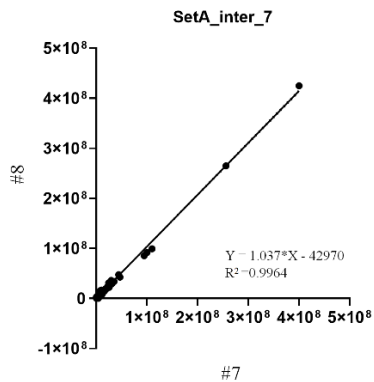
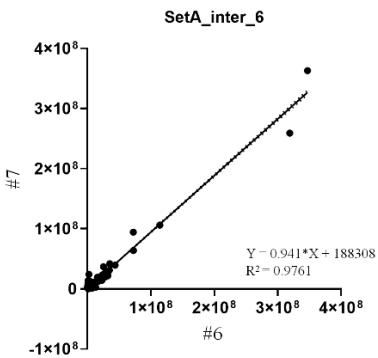
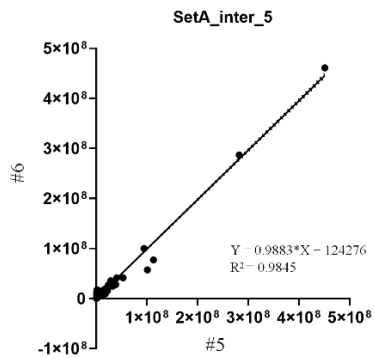
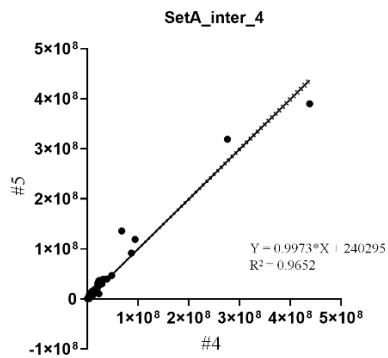
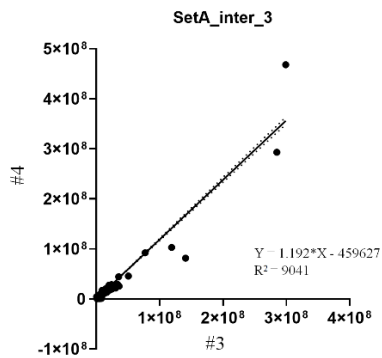
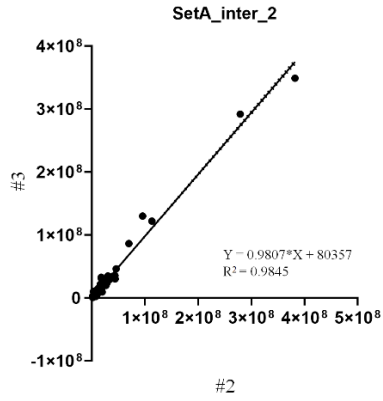
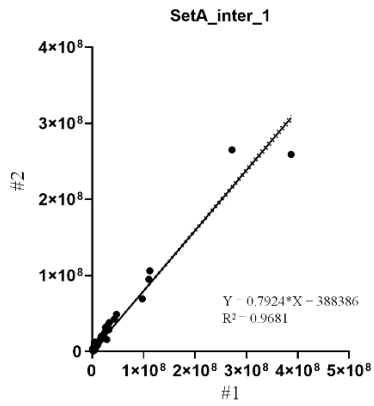
Experiment Type:	TOF MS (CE=10)		Experiment Type:	TOF MS ² (CE=16.525)
Num. Cycles:	2933		Num. Cycles:	2933
Polarity:	Positive		Polarity:	Positive
Period Cycle Time:	3048 ms		Product:	349.50 to 392.60
Pulser Frequency:	16.113 kHz		Period Cycle Time:	3048 ms
Accumulation Time:	50.0 ms		Pulser Frequency:	16.113 kHz
			Accumulation Time:	29.5 ms
TOF	Cycle time	3048		
	Acc time	50		
MS/MS	Cycle time	3048		
	Acc time	29.5		
MS/msec		msec		Cycle time (msec)
101.6271186	x	29.5	=	2998
				Cycle time (sec)
				2.998

Appendix 3 Intraocular and interocular comparison fo set A and set B

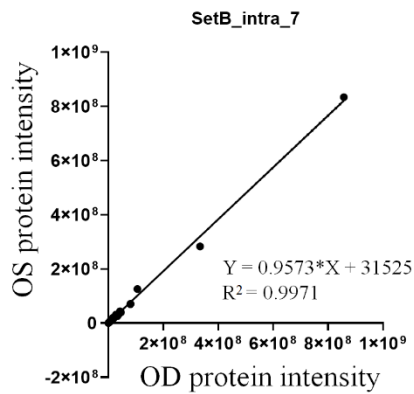
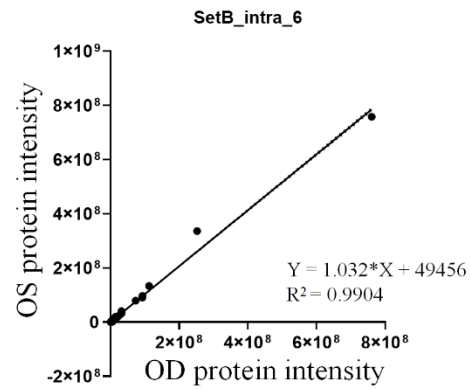
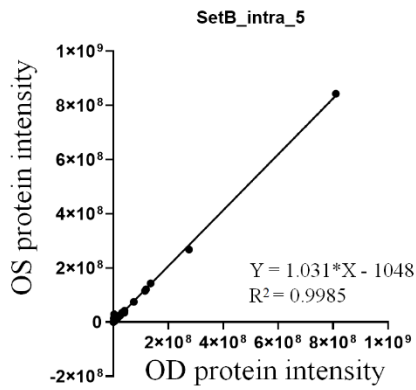
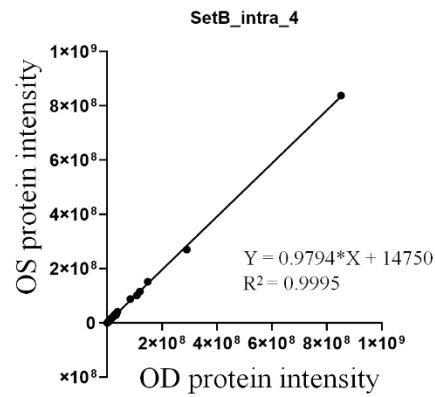
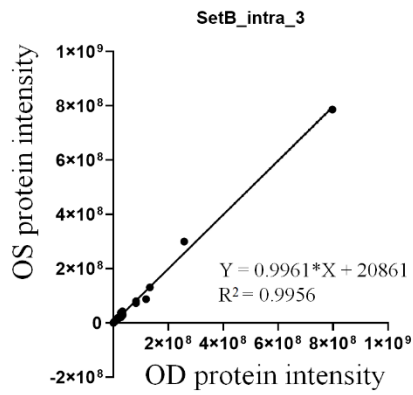
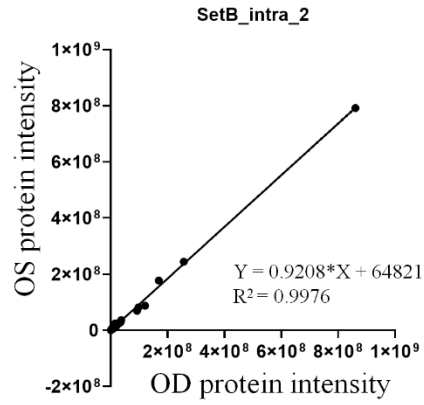
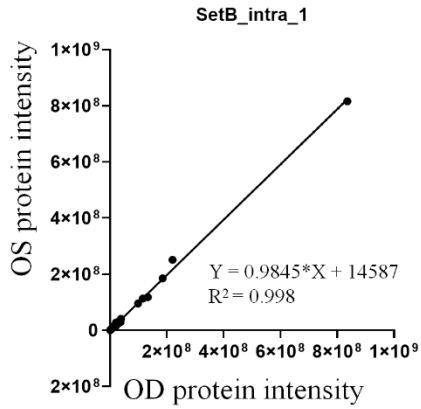
Set A intraocular comparison



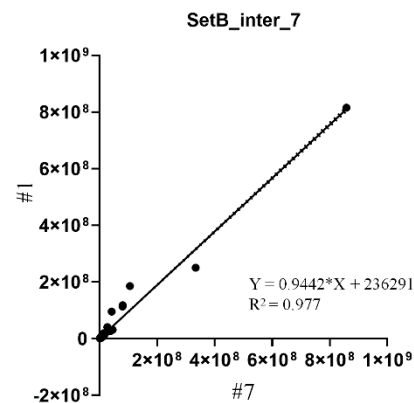
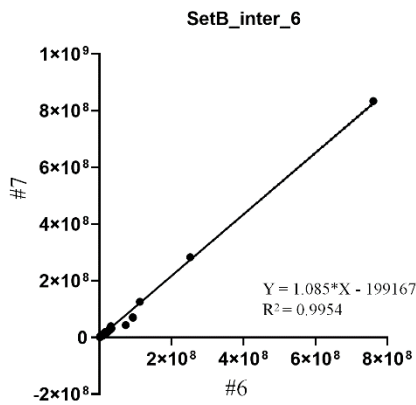
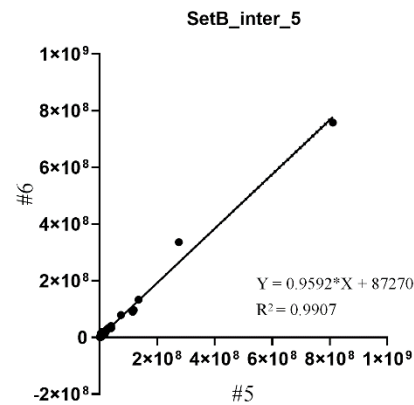
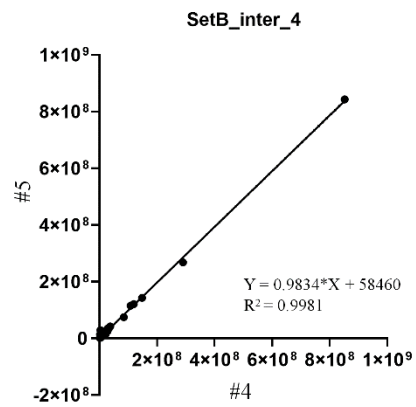
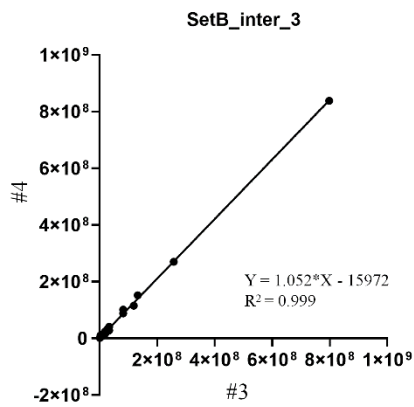
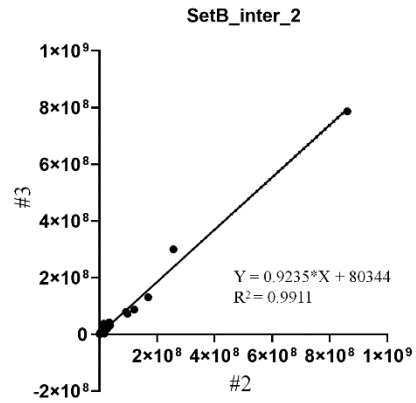
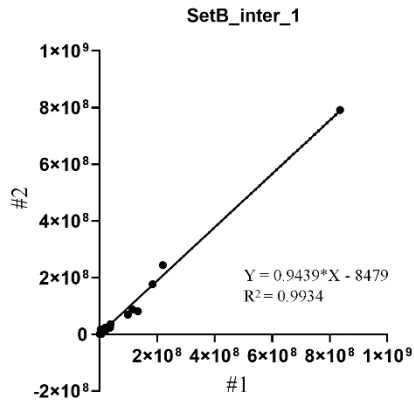
Set A interocular comparison



Set B intraocular comparison



Set B interocular comparison



Appendix 4 Refractive error and ocular parameters for normal growth study

4.1 Refractive error and weight of chicks at baseline for normal growth study

Baseline	OD			OS				
Sample ID	Horizontal axis	Vertical axis	SE	Sample ID	Horizontal axis	Vertical axis	SE	Weight
189R	5.50	5.50	5.50	190L	5.50	5.50	5.50	46.40
191R	6.00	6.50	6.25	192L	6.50	6.50	6.50	44.80
193R	6.50	6.00	6.25	194L	5.00	5.00	5.00	46.80
195R	6.50	6.00	6.25	196L	6.00	6.50	6.25	45.50
197R	6.00	5.50	5.75	198L	6.00	6.00	6.00	44.60
199R	6.00	6.00	6.00	200L	6.00	6.00	6.00	44.20
140R	5.00	5.50	5.25	141L	5.50	5.50	5.50	48.50
142R	4.50	4.00	4.25	143L	5.00	5.50	5.25	49.70
103R	6.00	6.00	6.00	104L	6.00	6.50	6.25	47.60
105R	4.50	5.00	4.75	106L	5.50	5.50	5.50	47.00
107R	5.50	6.00	5.75	108L	5.50	5.50	5.50	44.00
21R	4.50	4.50	4.50	22L	5.00	4.50	4.75	51.00
177R	5.50	5.50	5.50	178L	6.00	6.50	6.25	43.90
179R	6.50	6.00	6.25	180L	6.50	6.00	6.25	47.20
181R	5.50	5.50	5.50	182L	6.50	5.00	5.75	43.10
183R	6.00	5.50	5.75	184L	5.50	5.00	5.25	42.70
185R	6.50	5.50	6.00	186L	6.00	5.50	5.75	42.20
187R	5.00	4.50	4.75	188L	5.00	5.50	5.25	42.90
209R	5.00	5.00	5.00	210L	5.00	4.00	4.50	48.00
211R	6.00	6.50	6.25	212L	6.00	5.00	5.50	42.20
213R	6.00	6.00	6.00	214L	5.50	6.00	5.75	47.80
215R	6.50	6.00	6.25	216L	6.50	6.00	6.25	48.20
217R	5.50	5.50	5.50	218L	6.50	6.00	6.25	44.20
223R	6.50	6.00	6.25	224L	5.50	5.00	5.25	50.60

AVE			5.65				5.67	45.96
SD			0.61				0.53	2.64
T-test	(OD vs OS)		0.856					

4.2 Refractive error and weight of chicks at day 7, 14, 21, and 28 for normal growth study

		OD			OS				
Day 7	Sample ID	Horizontal axis	Vertical axis	SE	Sample ID	Horizontal axis	Vertical axis	SE	Weight
	189R	4.50	4.00	4.25	190L	5.00	5.00	5.00	56.20
	191R	4.00	4.00	4.00	192L	4.00	4.00	4.00	55.20
	193R	4.50	4.00	4.25	194L	4.50	4.50	4.50	61.80
	195R	4.50	4.50	4.50	196L	4.00	4.00	4.00	57.40
	197R	4.00	4.00	4.00	198L	4.00	4.50	4.25	53.70
	199R	5.00	5.00	5.00	200L	5.00	5.50	5.25	52.40
AVE				4.33				4.5	56.12
SD				0.38				0.52	3.30
T-test	(OD vs OS)			0.363					

		OD			OS				
Day 14	Sample ID	Horizontal axis	Vertical axis	SE	Sample ID	Horizontal axis	Vertical axis	SE	Weight
	140R	4.00	3.00	3.50	141L	4.00	3.50	3.75	123.00
	142R	4.00	3.00	3.50	143L	3.50	3.00	3.25	126.00
	103R	4.50	4.50	4.50	104L	4.00	4.50	4.25	113.00
	105R	4.00	4.00	4.00	106L	5.00	4.50	4.75	110.00
	107R	4.50	4.00	4.25	108L	4.00	4.00	4.00	113.00
	21R	4.00	4.50	4.25	22L	4.50	4.00	4.25	109.00
AVE				4.00				4.04	115.67
SD				0.42				0.51	7.09
T-test	(OD vs OS)			0.809					

		OD			OS				
Day 21	Sample ID	Horizontal axis	Vertical axis	SE	Sample ID	Horizontal axis	Vertical axis	SE	Weight
	177R	3.50	3.50	3.50	178L	3.50	3.50	3.50	140.00
	179R	3.50	3.00	3.25	180L	3.00	2.50	2.75	160.00
	181R	3.50	3.50	3.50	182L	3.00	3.00	3.00	160.00
	183R	3.50	3.50	3.50	184L	3.50	3.00	3.25	140.00
	185R	3.00	3.50	3.25	186L	3.50	3.50	3.50	160.00
	187R	2.00	2.50	2.25	188L	3.00	2.50	2.75	160.00
AVE				3.21				3.13	153.33
SD				0.49				0.34	10.33
T-test	(OD vs OS)			0.638					

		OD			OS				
Day 28	Sample ID	Horizontal axis	Vertical axis	SE	Sample ID	Horizontal axis	Vertical axis	SE	Weight
	209R	3.50	3.50	3.50	210L	2.50	3.00	2.75	320.00
	211R	3.50	3.50	3.50	212L	3.00	3.00	3.00	280.00
	213R	3.50	3.00	3.25	214L	3.50	3.50	3.50	280.00
	215R	2.50	2.50	2.50	216L	3.00	2.50	2.75	280.00
	217R	2.50	2.50	2.50	218L	3.00	3.00	3.00	260.00
	223R	3.00	3.00	3.00	224L	3.00	2.00	2.50	260.00
AVE				3.04				2.92	280.00
SD				0.46				0.34	21.91
T-test	(OD vs OS)			0.580					

4.3 The axial length (AXL) and vitreous chamber depth (VCD) at baseline for normal growth study

Baseline	OD			OS	
Sample ID	VCD (mm)	AXL (mm)	Sample ID	VCD (mm)	AXL (mm)
189R	5.376	8.513	190L	5.275	8.440
191R	5.332	8.458	192L	5.311	8.450
193R	5.379	8.495	194L	5.337	8.486
195R	5.137	8.249	196L	5.224	8.343
197R	5.332	8.571	198L	5.241	8.439
199R	5.312	8.434	200L	5.283	8.405
140R	5.007	8.269	141L	5.091	8.309
142R	5.278	8.538	143L	5.324	8.575
103R	5.035	8.243	104L	4.933	8.112
105R	5.269	8.343	106L	5.228	8.270
107R	5.302	8.416	108L	5.246	8.399
21R	5.258	8.470	22L	5.232	8.422
177R	5.331	8.517	178L	5.313	8.470
179R	5.361	8.476	180L	5.155	8.300
181R	5.240	8.417	182L	5.193	8.334
183R	5.261	8.344	184L	5.218	8.340
185R	5.226	8.421	186L	5.165	8.381
187R	4.906	8.046	188L	5.272	8.411
209R	5.331	8.525	210L	5.223	8.381
211R	5.358	8.492	212L	5.306	8.435
213R	5.269	8.325	214L	5.227	8.281
215R	5.564	8.829	216L	5.503	8.768
217R	5.434	8.589	218L	5.786	8.586
223R	5.327	8.523	224L	5.273	8.480
AVE	5.276	8.438		5.265	8.409
SD	0.140	0.151		0.151	0.127
T-test	(OD vs OS) VCD	0.675			
	(OD vs OS) AXL	0.191			

4.4 The axial length (AXL) and vitreous chamber depth (VCD) at day 7, 14, 21, and 28 for normal growth study.

Day 7			OS		
Sample ID	VCD (mm)	AXL (mm)	Sample ID	VCD (mm)	AXL (mm)
189R	5.345	8.675	190L	5.248	8.598
191R	5.345	8.621	192L	5.322	8.623
193R	5.304	8.608	194L	5.236	8.552
195R	5.207	8.493	196L	5.229	8.448
197R	5.341	8.750	198L	5.219	8.599
199R	5.158	8.454	200L	5.168	8.449
AVE	5.283	8.600		5.237	8.545
SD	0.081	0.111		0.050	0.078
T-test	(OD vs OS) VCD	0.110			
	(OD vs OS) AXL	0.059			

Day 14			OS		
Sample ID	VCD (mm)	AXL (mm)	Sample ID	VCD (mm)	AXL (mm)
140R	5.718	9.487	141L	5.706	9.445
142R	5.714	9.596	143L	5.730	9.583
103R	5.448	9.183	104L	5.393	9.156
105R	5.696	9.350	106L	5.823	9.443
107R	5.709	9.353	108L	5.624	9.275
21R	5.349	9.122	22L	5.425	9.225
AVE	5.606	9.348		5.617	9.354
SD	0.164	0.178		0.173	0.162
T-test	(OD vs OS) VCD	0.749			
	(OD vs OS) AXL	0.850			

Day 21			OS		
Sample ID	VCD (mm)	AXL (mm)	Sample ID	VCD (mm)	AXL (mm)
177R	5.913	10.013	178L	5.878	10.009
179R	5.883	9.899	180L	5.912	9.935
181R	6.040	10.047	182L	6.067	10.064
183R	5.742	9.765	184L	5.835	9.808
185R	6.002	9.902	186L	5.934	9.858
187R	5.940	10.040	188L	6.082	10.022
AVE	5.920	9.944		5.951	9.949
SD	0.105	0.110		0.101	0.100
T-test	(OD vs OS) VCD	0.372			
	(OD vs OS) AXL	0.733			

Day 28	OD			OS	
Sample ID	VCD (mm)	AXL (mm)	Sample ID	VCD (mm)	AXL (mm)
209R	6.737	11.182	210L	6.582	11.039
211R	6.500	10.989	212L	6.500	10.993
213R	6.342	10.519	214L	6.377	10.467
215R	6.759	11.315	216L	6.704	11.254
217R	6.434	10.814	218L	6.475	10.863
223R	6.401	10.845	224L	6.444	10.885
AVE	6.529	10.944		6.514	10.917
SD	0.177	0.284		0.115	0.261
T-test	(OD vs OS) VCD	0.651			
	(OD vs OS) AXL	0.405			

Appendix 5 The differential expressed proteins (DEPs) quantified across all time points (Day 7, 14, 21 and 28) during normal growth study.

5.1 A total of 27 up regulated DEPs were quantified across all time points (Day 7, 14, 21 and 28) during normal growth study.

Uniprot ID	Protein name	Gene name	(14/7) Fold Change		(21/7) Fold Change		(28/7) Fold Change	
			OD14/OD7	OS14/OS7	OD21/OD7	OS21/OS7	OD28/OD7	OS28/OS7
A0A1D5P6B0	Procollagen C- endopeptidase enhancer	N/A	1.71	1.83	1.75	1.56	1.83	2.10
A0A1D5PEU7	CN hydrolase domain- containing protein	VNN1	2.60	1.77	2.29	2.36	4.27	2.84
A0A3Q2TRX4	Spondin domain- containing protein	SPON2	2.96	2.42	3.00	2.20	4.04	3.41
A0A3Q2U0X6	Sema domain- containing protein	LOC112530215	2.47	1.98	1.68	1.62	2.22	1.89
A0A3Q2U5R1	Uncharacterized protein	N/A	1.74	1.72	1.73	1.74	2.02	1.90
A0A3Q2U7Y1	Peptidase_M14 domain-containing protein	N/A	1.91	1.95	2.01	1.87	2.45	2.68
A0A3Q2UAZ7	LAM_G_DOMAIN domain-containing protein	N/A	2.64	1.97	1.97	2.50	2.20	2.75
ALBU	Serum albumin (Alpha- livetin) (allergen Gal d 5)	ALB	9.20	2.71	3.96	2.17	13.58	3.45

E1BXK3	Glycogen [starch] synthase (EC 2.4.1.11)	GYS2	2.01	1.52	1.52	3.52	1.86	3.79
E1C1R3	Corticotropin-releasing factor-binding protein (CRF-BP)	CRHBP	3.07	3.54	3.78	4.43	3.44	3.89
E1C4M3	Pept_C1 domain-containing protein	CTSZ	2.13	1.62	2.16	1.74	2.36	2.00
F1N9I4	Uncharacterized protein	LTBP1	1.53	1.58	1.71	1.68	2.37	2.65
F1NEL5	Uncharacterized protein	MGAT5	2.65	2.07	2.01	2.56	3.26	2.56
F1NLB5	Uncharacterized protein	KAZALD1	1.75	2.62	1.70	1.97	2.62	3.45
F1NM17	Integral membrane protein 2B	ITM2B	2.62	1.63	1.71	1.63	3.14	1.67
F1NNV6	Uncharacterized protein	ATP6AP1	5.60	2.61	2.81	2.11	9.51	3.80
F1NYJ1	Uncharacterized protein	CTSV	1.93	1.58	1.87	1.67	2.33	2.20
F1NYP8	F5/8 type C domain-containing protein	N/A	1.89	1.81	1.86	1.51	2.05	2.04
F1PIG6	G8 domain-containing protein	CEMIP	2.27	1.70	1.52	1.50	2.54	2.13
O42397	Crescent	N/A	8.41	3.16	15.52	6.46	19.76	6.02

Q4ADJ6	Ovotransferrin	TFEW	4.09	2.30	1.81	2.26	9.39	5.11
Q5F3I1	Fibrinogen C-terminal domain-containing protein	FGL2 RCJMB04_16g14	2.59	2.22	2.92	1.91	2.22	2.28
R4GH41	Uncharacterized protein	ASAH1	1.83	1.54	1.99	1.67	2.41	2.18
R4GKL8	C1q domain-containing protein	C1QTNF3	1.73	2.63	2.45	2.85	3.45	5.32
R4GLH0	IGFBP N-terminal domain-containing protein	ESM1	4.08	3.02	4.53	3.51	6.73	5.09
R4GM86	EGF-like domain-containing protein	CCBE1	3.12	2.14	3.74	2.10	4.33	2.62
TENA	Tenascin (TN)	TNC	4.53	2.07	2.40	1.56	3.39	2.26

5.2 A total of 37 down regulated DEPs were quantified across all time points (Day 7, 14, 21 and 28) during normal growth study.

Uniprot ID	Protein name	Gene name	(14/7) Fold Change		(21/7) Fold Change		(28/7) Fold Change	
			OD14/OD7	OS14/OS7	OD21/OD7	OS21/OS7	OD28/OD7	OS28/OS7
A0A1D5P0F4	Collagen alpha-1(XIV) chain	COL14A1	0.16	0.27	0.11	0.13	0.07	0.08
A0A1D5P363	C1q domain-containing protein	CBLN1	0.56	0.55	0.53	0.61	0.57	0.67
A0A1D5P6T7	Cadherin-11	CDH11	0.39	0.36	0.40	0.34	0.35	0.33
A0A1D5P8I3	Uncharacterized protein	SFPQ	0.34	0.26	0.21	0.34	0.24	0.35
A0A1D5PYV2	Cadherin-10	CDH10	0.46	0.12	0.43	0.39	0.40	0.35
A0A1L1RRN4	Peptidyl-prolyl cis-trans isomerase (PPIase) (EC 5.2.1.8)	PPIB	0.04	0.02	0.33	0.33	0.04	0.34
A0A2H4Y833	OVA (Fragment)	OVA	0.17	0.28	0.18	0.09	0.19	0.11
A0A3Q2U1A2	Ig-like domain-containing protein	N/A	0.50	0.31	0.31	0.32	0.63	0.57
A0A3Q2U471	Uncharacterized protein	ROBO1	0.58	0.10	0.66	0.63	0.62	0.65
A0A3Q2UAA5	Ig-like domain-containing protein	LOC107051274	0.21	0.34	0.25	0.27	0.31	0.43
A0A3Q3ACG0	Cadherin-4	CDH4	0.31	0.32	0.34	0.43	0.37	0.40
A0A3Q3B2L3	Uncharacterized protein	N/A	0.09	0.36	0.12	0.34	0.11	0.31
ACES	Acetylcholinesterase (AChE) (EC 3.1.1.7)	ACHE	0.29	0.63	0.55	0.28	0.22	0.35

B8YK79	Lysozyme (EC 3.2.1.17)	LYZ	0.40	0.31	0.33	0.24	0.33	0.18
CSPG2	Versican core protein (Chondroitin sulfate proteoglycan core protein 2) (Chondroitin sulfate proteoglycan 2) (Large fibroblast proteoglycan) (PG-M)	VCAN CSPG2	0.33	0.59	0.20	0.25	0.19	0.19
E1BRK7	Fibrinogen C-terminal domain-containing protein	ANGPTL7	0.56	0.32	0.35	0.32	0.19	0.13
E1BUN0	Uncharacterized protein	HAPLN3	0.24	0.48	0.27	0.43	0.22	0.27
E1C3A7	Uncharacterized protein	CDH22	0.41	0.14	0.34	0.41	0.33	0.30
E1C836	Ig-like domain-containing protein	PDGFRL	0.52	0.48	0.41	0.44	0.38	0.39
F1NE63	Reelin	RELN	0.41	0.58	0.45	0.48	0.42	0.47
F1NEQ4	A2M_recep domain-containing protein	N/A	0.23	0.16	0.33	0.32	0.45	0.36
F1NM47	Uncharacterized protein	LAMA1	0.41	0.25	0.37	0.39	0.45	0.45
F1NSJ1	Contactin-2	CNTN2	0.51	0.23	0.44	0.46	0.52	0.52
F1NZH0	Uncharacterized protein	SLITRK1	0.52	0.25	0.60	0.66	0.50	0.61
F1NZZ6	Uncharacterized protein	CDH8	0.33	0.48	0.35	0.32	0.35	0.24
FETA	Alpha-fetoprotein (Alpha-1-fetoprotein) (Alpha-fetoglobulin)	AFP	0.01	0.40	0.01	0.01	0.01	0.02

HPLN1	Hyaluronan and proteoglycan link protein 1 (Cartilage-linking protein 1) (Cartilage-link protein) (Proteoglycan link protein)	HAPLN1 CRTL1	0.55	0.52	0.45	0.57	0.47	0.62
NEO1	Neogenin (Fragment)	N/A	0.65	0.39	0.54	0.55	0.67	0.62
NRCAM	Neuronal cell adhesion molecule (Nr-CAM) (Neuronal surface protein Bravo) (gBravo) (NgCAM-related cell adhesion molecule) (Ng-CAM-related)	N/A	0.32	0.57	0.59	0.56	0.67	0.50
Q197X2	Apolipoprotein B	APOB	0.12	0.38	0.12	0.12	0.18	0.10
Q8AWW2	Cadherin-7	N/A	0.33	0.38	0.39	0.32	0.32	0.34
Q90800	Collagen-alpha-3 type IX	N/A	0.34	0.47	0.47	0.47	0.24	0.39
Q90864	Beta-H globin	HBE1	0.24	0.35	0.42	0.14	0.06	0.06
Q9W6E1	Neurocan core protein	N/A	0.23	0.48	0.21	0.20	0.17	0.19
R9PXM5	Ig-like domain-containing protein	N/A	0.23	0.47	0.29	0.28	0.27	0.31
R9PXP7	Cadherin-20	CDH20	0.47	0.61	0.44	0.44	0.45	0.53
SDK2	Protein sidekick-2	SDK2	0.58	0.58	0.63	0.59	0.52	0.59

Appendix 6 Refractive error and ocular parameters at baseline (day 7) and after 3 days and 7 days LIM

6.1 Refractive error at baseline and after 3 days LIM for myopia study (LIM3)

Baseline	Treated eye			Control eye				
Sample ID	Horizontal axis	Vertical axis	SE	Sample ID	Horizontal axis	Vertical axis	SE	Weight
255R	4.50	4.50	4.50	256L	4.50	4.50	4.50	52.30
257R	4.00	4.00	4.00	260L	5.50	5.00	5.25	53.30
264L	4.00	4.00	4.00	261R	5.50	5.00	5.25	52.90
266L	4.50	4.25	4.38	263R	4.50	5.00	4.75	46.00
268L	5.50	5.50	5.50	265R	4.50	4.50	4.50	46.80
270L	4.00	4.25	4.13	269R	5.00	5.00	5.00	49.00
273R	5.50	5.50	5.50	272L	5.00	5.00	5.00	47.40
AVE			4.57				4.89	49.67
SD			0.66				0.32	3.10
T-test	(LIM vs control)		0.268811					

Day 10 (3-day LIM)	Treated eye			Control eye				
Sample ID	Horizontal axis	Vertical axis	SE	Sample ID	Horizontal axis	Vertical axis	SE	Weight
255R	-4	-5.5	-4.75	256L	4.5	4.5	4.5	76.3
257R	-5	-4.5	-4.75	260L	4	3.5	3.75	70.4
264L	-4.5	-5.5	-5	261R	4.5	4.5	4.5	76.2
266L	-4.5	-4.5	-4.5	263R	4	4	4	73
268L	-0.5	-1.5	-1	265R	5.5	5.5	5.5	79.2
270L	-4	-6	-5.00	269R	5	4	4.5	72.6
273R	0	-2	-1.00	272L	3.5	3	3.25	66.7
AVE			-3.71				4.29	73.49
SD			1.86				0.71	4.17
T-test	(LIM vs control)		0.000					

6.2 Refractive error at baseline and after 7 days LIM for myopia study (LIM7)

Baseline	Treated eye			Control eye				
Sample ID	Horizontal axis	Vertical axis	SE	Sample ID	Horizontal axis	Vertical axis	SE	Weight
245R	5	5	5.00	244L	4.5	4.5	4.50	54.80
247R	5.5	5.5	5.50	248L	6	5.5	5.75	50.60
250L	5.5	5.5	5.50	253R	6.5	6.5	6.50	50.10
254L	5	5	5.00	275R	4.5	4	4.25	54.00
280L	5.5	5	5.25	277R	4.5	4.5	4.50	48.30
281R	4	4.5	4.25	279R	5	5	5.00	47.70
288L	4	4.5	4.25	284L	4.5	4	4.25	45.80
AVE			4.96				4.96	50.19
SD			0.53				0.86	3.29
T-test	(LIM vs control)		1					

Day 14 (7-day LIM)	Treated eye			Control eye				
Sample ID	Horizontal axis	Vertical axis	SE	Sample ID	Horizontal axis	Vertical axis	SE	Weight
245R	-6.5	-7	- 6.75	244L	4.5	4	4.25	109.3
247R	-6.5	-7	- 6.75	248L	3.5	4.5	4	128.7
250L	-7	-7.5	- 7.25	253R	4.5	5	4.75	113
254L	-6.5	-6	- 6.25	275R	5	5	5	105.1
280L	-5.5	-8.5	-7	277R	4.5	4.5	4.5	107.4
281R	-7.5	-5.5	- 6.50	279R	4.5	4.5	4.5	128.8
288L	-5.5	-6.5	- 6.00	284L	4.5	4.5	4.5	105.4
AVE			- 6.64				4.50	113.96
SD			0.43				0.32	10.45
T-test	(LIM vs control)		0.00					

6.3 The axial length (AXL) and vitreous chamber depth (VCD) at baseline and after 3 days LIM for myopia study (LIM3)

VCD (mm)	Treated eye			Control eye	
Sample ID	Baseline	LIM3	Sample ID	Baseline	LIM3
255R	5.244	5.697	256L	5.260	5.247
257R	5.049	5.435	260L	5.250	5.274
264L	5.049	5.382	261R	5.351	5.335
266L	4.989	5.298	263R	5.080	4.984
268L	5.183	5.355	265R	5.223	5.088
270L	5.119	5.281	269R	5.038	4.983
273R	5.061	5.391	272L	4.906	4.743
AVE	5.099	5.405		5.158	5.094
SD	0.088	0.139		0.155	0.209
T-test	0.000			0.048	

AXL	Treated eye			Control eye	
Sample ID	Baseline	LIM3	Sample ID	Baseline	LIM3
255R	8.677	9.274	256L	8.627	8.762
257R	8.459	8.944	260L	8.689	8.773
264L	8.399	8.800	261R	8.744	8.866
266L	8.489	8.908	263R	8.413	8.461
268L	8.528	8.789	265R	8.670	8.673
270L	8.489	8.821	269R	8.517	8.562
273R	8.492	8.964	272L	8.290	8.224
AVE	8.505	8.929		8.564	8.617
SD	0.086	0.168		0.165	0.221
T-test	0.000			0.091	

6.4 The axial length (AXL) and vitreous chamber depth (VCD) at baseline and after 7 days LIM for myopia study (LIM7)

VCD (mm)	Treated eye			Control eye	
Sample ID	Baseline	LIM7	Sample ID	Baseline	LIM7
245R	5.095	5.757	244L	5.284	5.499
247R	5.364	5.931	248L	5.296	5.440
250L	5.166	5.892	253R	5.288	5.567
254L	5.223	6.077	275R	5.348	5.682
280L	5.381	6.143	277R	5.177	5.474
281R	5.151	5.855	279R	5.479	5.667
288L	5.102	6.085	284L	5.277	5.533
AVE	5.212	5.963		5.307	5.552
SD	0.118	0.142		0.091	0.093
T-test	0.000			0.000	

AXL	Treated eye			Control eye	
Sample ID	Baseline	LIM7	Sample ID	Baseline	LIM7
245R	8.439	9.503	244L	8.655	9.191
247R	8.826	9.891	248L	8.786	9.271
250L	8.541	9.789	253R	8.738	9.362
254L	8.640	9.859	275R	8.784	9.454
280L	8.666	9.919	277R	8.420	9.139
281R	8.436	9.624	279R	8.755	9.429
288L	8.471	9.869	284L	8.673	9.310
AVE	8.574	9.779		8.687	9.308
SD	0.144	0.156		0.128	0.117
T-test	0.000			0.000	

Appendix 7 Transitions and peptide sequence used in MRM^{HR} experiments

7.1 Transitions and peptide sequences used in MRM^{HR} experiments for normal growth study

Uniprot ID	Protein name	Gene name	Peptide sequence	Transitions
Q4ADJ6	Ovotransferrin	TF	GDVAFVK	+2y5, +2y4, +2y3
			FFSASC[CAM]V PGATIEQK	+2y11, +2y8, +3y8
			AQSDFGVDTK	+2y8, +2y7, +2y6
FINE63	Reelin	RELN	VPSLVSVVISPD LQTPATK	+2y12, +2y10, +3y9
			DFIQAQR	+2y5, +2y4, +2b3
			FSYSDPSITVSYS K	+2y11, +2y10, +2y9
FINSJ1	Contactin 2	CNTN2	LVAGDLVISNPV K	+2y11, +2y10, +2y6
			FSQLSLAAEDA R	+2y9, +2y8, +2y6
			GPPGPPGGVVV R	+2y10, +2y9, +2y8
FETA	Alphafeto protein	AFP	NDC[CAM]FLSL K	+2y7, +2y6, +2y5
			GDMLEC[CAM] MR	+2y5, +2y4, +2y3
			GYEDLLDEC[CA M]C[CAM]K	+2y6, +2y5, +2y4
CADH7	Cadherin-7	CDH7	LTNKPVEPESEF VIK	+3y11, +3y8, +3y6
			FLSLGPFSDMTT VK	+2y12, +2y10, +2y9
			IIVEDVDEPPVF TSR	+2y12, +2y9, +2y7
A0A1D5PYV 2	Cadherin-10	CDH10	TALPNMNR	+2y6, +2y5
			EQYQVVIQAK	+2y8, +2y6, +2y5
			VPVYVR	+2y5, +2y4, +2y3
Q9W6E1	Neurocan core protein	N/A	EDVPILVAK	+2y8, +2y7, +2y6
			YFQLQQQSR	+2y6, +2y5, +2y4
			YQC[CAM]JEEGF TQR	+2y8, +2y7, +2y6

7.2 Transitions and peptide sequence used in MRM^{HR} experiments for myopia (LIM3) study

Uniprot ID	Protein name	Gene name	Peptide sequence	Transitions
A0A1D5NXA6	Inter-alpha-trypsin inhibitor heavy chain 3	ITIH3	DINQNSLTVDVK	+2y10
			GEGANDVLSFTTQQDK	+2y9
			HFYDGSEIVVAGR	+3b7
E1C1R3	Corticotropin-releasing factor-binding protein	CRHBP	VFDGWILK	+2y6
F1NWT5	Vasoactive intestinal polypeptide	VIP	SESDILQNTLPENEK	+2y10, +2y5, +2y8

7.3 Transitions and peptide sequences used in MRM^{HR} experiments for myopia (LIM7) study.

Uniprot ID	Protein name	Gene name	Peptide sequence	Transitions
A0A1D5NUV0	Secretogranin II	SCG2	EHLSQLGPQEAAR	+3y7, +3b7, +3y6
			QYLDEEDMLAK	+2y6, +2y8, +2y7
			VLEYLK	+2y3, +2y4, +2y5
A0A1D5PCF5	Insulin like growth factor binding protein 7	IGFBP7	C[CAM]AAGLEC[CAM]VK	+2y8, +2y6, +2y7
			GAC[CAM]EQGPSIVTPPK	+2y10, +2y8, +2y9
			HEVTGWVLISPLSK	+3b6, +3y6, +3y7
A0A1D5PSQ1	A2M_N_2 domain-containing protein	N/A	MITIEDK	+2y5, +2y6, +2y3
			SVLLMKPEDELSPESSVYNLLPVK	+3y11, +3b12, +3y7
			VNLSFVPK	+2y7, +2y6
A0A3Q2TWJ9	MG2 domain-containing protein	N/A	IVSLDEDFHPLNEK	+3y10, +3y7, +3y5
			SLIDVVTEK	+2y5, +2y6, +2y7
A0A3Q2TZA4	A2M_recep domain-containing protein	N/A	MLSGFIPVK	+2y6, +2y8, +2y7
			SVSNMVIIDVK	+2y6, +2y5, +2y9
			GC[CAM]VYLQTSR	+2y5, +2y8, +2y7
A0A3Q2UCH2	A2M domain-containing protein	N/A	ASAF[CAM]MSPDTGFGLSPTVSLR	+2y15, +2y14
			ATVFNYLTAC[CAM]JIR	+2y5, +2y6, +2y9
			GEAFTLK	+2y3, +2y4, +2y5
E1BQW4	EGF like, fibronectin type III and laminin G domains	EGFLAM	EIQMESMVLK	+2y8, +2y7
			VSVGAYGWAGK	+2y8
F1NIZ9	Sema domain-containing protein	SEMA7A	VEPLAPTR	+2y6
			WTTFLK	+2y5
			NFITLIAK	+2b3
F1NWT5	Vasoactive intestinal polypeptide	VIP	GAAFPVPR	+2y5
			SESDILQNTLPENK	+2y5
			FYFDLSR	+2y5